Charles University in Prague, Faculty of Science
Department of Inorganic Chemistry

PORPHYRIN-LAYERED DOUBLE HYDROXIDE HYBRIDS AS NOVEL PHOTOFUNCTIONAL MATERIALS

Ph.D. Thesis

Ing. Eva Káfuňková

Supervisor: Ing. Kamil Lang, CSc.
Supervisor consultant: Doc. Jiří Mosinger, PhD.

Prague 2010

Declaration

Prohlašuji, že jsem tuto práci, ani její podstatnou část, nepředložila k získání jiného nebo stejného titulu. Prohlašuji, že jsem pracovala na disertaci sama a používala jsem jen citované zdroje.

I hereby declare that neither this thesis nor its part I used previously to obtain an equivalent or another academic degree. I declare that the this thesis I submit for the Ph. D. degree at the Charles University in Prague is my own and I used only sources cited in the list of references. This work was elaborated in the Institute of Inorganic Chemistry of the ASCR, v.v.i., and in the Department of Inorganic Chemistry of the Faculty of Science, Charles University in Prague

Prague, September 20, 2010 Eva Káfuňková

Acknowledgment

First and foremost, I would like to thank my supervisor Ing. Kamil Lang, CSc., who gave me the opportunity to work on this challenging project. The guidance I received from him was invaluable. I also greatly appreciate all his contributions of time, idea and funding to make my Ph.D. experience productive and stimulating. The joy and enthusiasm he has for his research was contagious and motivational for me, even during tough times in the Ph.D. pursuit.

Secondly, I am very grateful to Dr. Christine Taviot-Guého for her supervision during my doctoral internship in France. I also thank for taking her dear time and providing great input into this work. I am also thankful for the excellent example she has provided as a successful woman scientist.

My sincerest gratitude is extended to Doc., RNDr. Jiří Mosinger, PhD. and RNDr. Dana Wagnerová, DrSc. for valuable advices and help during the completion of thesis.

I would also like to acknowledge all my colleagues from the Institute of Inorganic Chemistry. I appreciate their helpful support, listening, and having wonderful time during my years in this Institute.

Lastly, I would like to thank my family, my sisters and my friends who motivated, encouraged and supported me in difficult times, for being there for me.

Table of contents

List of figures

List of tables

List of abbreviations

AEC	Anion exchange capacity
ATP	Adenosine triphophate
DNA	Deoxyribonucleic acid
EDX	Energy Dispersive X-ray Analysis
EXAFS	Extended X-ray absorption fine structure
FTIR	Fourier transform infrared spectroscopy
HT-XRD	High temperature x-ray diffraction
HR-TEM	High resolution transmission electron microscopy
IC	Internal conversion
ISC	Intersystem crossing
LDH	Layered double hydroxides
PBS	Polybutylene succinate
PDT	Photodynamic therapy of cancer
PdTPPC	Pd(II)-5,10,15,20-tetrakis(carboxyphenyl)porphyrin
PU	Polyurethane
RNA	Ribonucleic acid
S_0	The ground state of sensitizer
S_1	The singlet state of sensitizer
SAXS	Small-angle X-ray scattering
SEM	Scanning electron microscopy
Sens	Sensitizer
TEM	Transmission electron microscopy
TEM/BF	Transmission electron microscopy/bright field
TDL	Time-dependent near-infrared luminescence
TPPC	5,10,15,20-tetrakis(4-carboxylphenyl)porphyrin
TPPS	5,10,15,20-tetrakis(4-sulfonatophenyl)porphyrin
TGA/DTA	Thermogravimetry and differential thermal analysis
UV-vis	Ultraviolet-visible
XRD	X-ray diffraction
ZnTPPS	Zn (II)-5,10,15,20-tetrakis(sulfonatophenyl)porphyrin
ZnTPPC	Zn (II)-5,10,15,20-tetrakis(carboxyphenyl)porphyrin
$M^{2+}{}_RM^{3+}$ LDH	Composition of LDH: M^{2+} and M^{3+} represent divalent and trivalent cations, respectively and R = (1-x)/x is the M^{2+}/M^{3+} molar ratio
M^{2+} M^{3+} LDH	General formula of the LDH composition (M^{2+} M^{3+}) without signification of R
A-$M^{2+}{}_RM^{3+}$	Abbreviations used throughout the text: the layers are composed of M^{2+} and M^{3+} ions in the ratio R and the intercalated anions are A

1 Abstract

This Ph.D. Thesis is based on publications to which the author contributed considerably. The list of the publications is attached at the end of this text.

This work describes preparation and photophysical properties of hybrid materials derived from layered double hydroxides (LDH) containing Zn^{2+}/Al^{3+} or Mg^{2+}/Al^{3+} cations. The materials were prepared in the form of powders or thin films. In the first part of my work, photosensitizing porphyrins have been intercalated into Zn_RAl and Mg_RAl LDH (R = 2, 3, 4) using anion-exchange, rehydration, and coprecipitation procedures. According to the obtained results of X-ray analysis, the orientation of the equatorial plain of the porphyrin molecules is nearly perpendicular to LDH layers and fosters the photosensitizing properties of the hybrid materials. Furthermore, the porphyrin-LDH hybrids were used as nanofillers and nanocontainers in eco-friendly polymers, polyurethane (PU) and poly(butylene succinate) (PBS). The porphyrin-LDH material is well dispersed in PU polymer (nanofiller function) to form transparent colored films while porphyrins remain intercalated between LDH layers (nanocontainer function). The polymers allow oxygen diffusion.

The second part has been dedicated to investigation of photophysical properties of the porphyrin-LDH powders and the porphyrin-LDH/polymer films. Upon irradiation with visible light, porphyrins embedded in the materials retain their photosensitizing properties with sufficiently long lifetimes of the triplet states to produce singlet oxygen ($^1O_2$). Singlet oxygen is known as a reactive species with cytotoxic effects. The porphyrin-LDH hybrid materials are suitable for the preparation of novel photoactive surfaces with controlled photoactivity of the porphyrin molecules anchored between the inorganic LDH layers. Such materials are readily suitable for construction of surfaces with photooxidative and bactericidal properties.

Tato disertační práce je koncipována jako soubor publikovaných článků, na nichž se autorka během studia spolupodílela. Jejich seznam je zařazen na konci doktorské práci.

Předkládaná práce se zabývá přípravou a fyzikálně chemickou charakterizací fotoaktivních hybridních materiálů. Tyto materiály jsou složeny z porfyrinových sensitizátorů produkujících singletový kyslík, které jsou interkalovány do vrstevnatých podvojných hydroxidů (LDH) obsahujících Zn^{2+}/Al^{3+} nebo Mg^{2+}/Al^{3+} kationty. V první části práce byly porfyriny interkalovány do LDH aniontovou výměnou, rehydratací nebo koprecipitací. Materiály byly připraveny ve formě prášků a polymerních filmů. Ze studií vyplývá, že orientace rovin porfyrinových molekul je téměř kolmá k rovině hydroxidových vrstev, nedochází k nežádoucí agregaci porfyrinů a tím se zachovává jejich fotosensitizační schopnost. Práškový materiál byl rovněž využit jako plnivo do polyuretanu (PU) a polybutylen sukcinátu (PBS). Polyuretanový film s porfyriny interkalovanými mezi LDH vrstvami, které jsou dispergovány v polymeru, je transparentní. Použité polymery umožňují difúzi kyslíku.

V druhé části práce byl výzkum zaměřen na popis fotofyzikálních vlastností porfyrin-LDH prášků a porfyrin-LDH/polymer filmů. Fotofyzikální experimenty ukazují, že interkalované porfyriny v LDH si zachovávají fotoaktivní vlastnosti jako např. produkci tripletových stavů, které dále interagují s kyslíkem za vzniku singletového kyslíku ($^1O_2$). Singletový kyslík je reaktivní, energeticky bohatší forma molekulárního kyslíku, která vykazuje cytotoxické vlastnosti. Z výsledků plyne, že získané hybridní materiály jsou účinnými producenty $^1O_2$. Bylo rovněž prokázáno, že LDH jsou vhodnými anorganickými nosiči pro fotoaktivní látky. Z těchto důvodů mohou být připravené hybridní materiály považovány za použitelné zdroje singletového kyslíku např. pro přípravu baktericidních povrchů.

2 Aims of this work

To the best of our knowledge, this thesis newly addresses photoactive properties of intercalated porphyrin molecules in LDH as possible carriers for $^1O_2$ photosensitizers. The aim of the work is to put forward hybrid materials derived from LDH loaded with porphyrin for possible applications in the area of oxidation reactions and bactericidal materials. Attention was focused on synthesis, characterization of the role of LDH structure on organization of incorporated photoactive porphyrins, evaluation and control of photofunctions, characterization of the structure-photofunction relation, and description of the hybrid structure. The thesis contributes to detailed understanding of the behavior of porphyrinoid compounds confined in LDH-based hybrid materials. The objectives of the thesis are formulated as follows:

1. Intercalation of porphyrins into LDH hosts having different charge density in order to avoid porphyrin aggregation: specification whether LDH materials are suitable carriers of porphyrinoid sensitizers, determination of the arrangement of the porphyrin molecules in the interlayer space, characterization of hybrids, morphology, and thermal stability.

2. Preparation of LDH-porphyrin/polymer films: combination of two aspects of LDH chemistry; nanocontainer and nanofiller function to design photoactive surfaces based on porphyrin-LDH/polymer composites.

3. Elucidation of photophysical and photochemical properties, production of $^1O_2$, its reactivity with contiguous substances, evaluation of the key photophysical characteristics including the formation of the triplet states and of singlet oxygen and specification of the effects of a molecular organization.

3 Introduction

Numerous hybrid materials originate in nature, not in a chemical laboratory. Many natural materials consist of inorganic and organic building blocks with molecular or nanoscale distribution. Current examples of such materials are crustacean carapaces or mollusc shells and bones. As far as man-made materials are concerned, the possibility to mix inorganic and organic components in materials design is an old challenge started ages ago. Typical examples of ancient hybrid materials are Egyptian inks, bodies of china ceramics, or Maya fresco paintings.[1] Hybrid inorganic-organic materials are not simple physical mixtures. They can be defined as nanocomposites in which inorganic and organic components are intimately mixed. Hybrids are either homogeneous systems derived from miscible organic and inorganic components or heterogeneous systems (nanocomposites) where at least one of the components has a size ranging from several to hundreds of nanometers. Usually, a nanocomposite is formed from building blocks such as carbon nanotubes or galleries of clays minerals, which are incorporated into an organic polymer. Hybrid materials favorably combine different properties of organic and inorganic components. Interactions together binding inorganic and organic species can be divided into two distinct classes. *Class I* hybrid materials are distinguished by noncovalent interactions between the two phases, namely by hydrogen bonding, weak electrostatic interactions, or dispersion (London) forces. In *Class II* materials two phases are linked together by chemical bonds, covalent, or iono-covalent.

Hybrids based on layered materials represent one of the most fascinating developments in materials chemistry. They can form multifunctional materials with specific optical, electronic, magnetic, or photoactive properties.[2] The guest species confined in layered hosts are due to noncovalent interactions, geometrically constrained and consequently their properties generally differ from those of the free guest species. In our case, the host matrices are layered double hydroxides (LDH) with intercalated porphyrin guests. These hybrids belong to C*lass I* materials.[1,3]

Porphyrins are characterized by photoactivity that can be preserved by intercalation into LDH matrix. It has shown that the relatively long-lived excited states of intercalated porphyrin molecules in LDH can be involved in photochemical reactions.[4,5] Indeed, the LDH host with an interlayer space of a flexible height and variable layer charge density,

allows incorporation of large guest molecules such as porphyrins together with control of their distribution and orientation.[6] In addition, the dispersed LDH fillers in polymers improve thermal, mechanical, barrier, even flame-retardant properties of polymer matrix.[7] LDH fillers can also bring additional functionalities such as optical and antioxidant properties depending on interlayer anions. It leads to multifunctional polymer composites and opens novel interesting application fields.[8,9,1011] Porphyrin-LDH hybrids are an object of interest not only from the photophysical point of view but offer potential applications in catalysis,[12,13] as electrochemical microsensors,[14,15] and handy sources of singlet oxygen.[16,17,18] The immobilization of porphyrin by polymers has already been proposed to create solid surfaces with potential applications in water disinfection,[19] sensing of toxic gases,[20] and fabrication of photobactericidal surfaces.[21,22,23]

3.1 Layered structures as host materials

Layered materials represent a special class in which the units are built by stacking of layers bound together by weak forces. Layered materials comprise clay minerals and a number of inorganic species such as layered phosphates, phosphonates, niobates, oxoantimonates, arsenates, titanates, and sulfides. The layered structures are also denoted as 2D in contrast to 1D chain structures and 3D porous frameworks. Layered materials act as hosts keeping guest molecules separated from the bulk and offering a two-dimensional expandable interlayer space for their organizing.[4,24] Clays are two-dimensional structured minerals, with particle sizes of less than 2 μm and different chemical compositions. Clay minerals can be divided into three classes by their ion properties: cationic, non-ionic, and anionic. The difference between these classes is in the layer charge; layers are either negatively (cationic) or positively (anionic) charged or neutral (non-ionic). The interlayer region of clays contains cations or anions compensating the layer charge. Cationic clays with cation exchange capacity include numerous alumino-silicate materials. Non-ionic ones without ion-exchange capacity are, e.g., kaolinite and serpentine.[25] Layered double hydroxides (LDH) belong to the class with anionic exchange capacity (AEC).

LDH compare favorably with other layered hosts in the production of hybrid materials for several reasons: (i) LDH are practically the only class of lamellar hosts with positive charge layers balanced by exchangeable anions. (ii) These hosts can be used for

intercalation of organic or organo-metallic species with anionic groups (carboxylic, sulfonic, phosphonic) which, in general, are much more numerous than those with cationic groups. (iii) It is possible to modulate LDH properties by changing nature of the divalent and/or trivalent cations in layers. (iv) LDH have low or null toxicity. (v) LDH are biocompatible.[26,27]

3.1.1 Layered double hydroxides

Historical background

Natural layered hydroxides are denoted as hydrotalcites. The first was discovered in Sweden in 1842 as a white-colored mineral that could be easily crushed to a powder similar to talc. The correct chemical composition of hydrotalcite, $Mg_6Al_2(OH)_{16}(CO_3)\cdot 4H_2O$, was first suggested by Manasse, who also recognized that carbonate anions are an essential component of the mineral.[24] Hydrotalcite is found in deposits from ground water or as a weathering product of primary oxides.[28] Unlike cationic clays, hydrotalcite is rare and is found in small quantities in a limited number of geographic places, e.g., Norway and the Ural area. Hydrotalcite is also a reference name for many isomorphous LDH materials (anionic clays).[29]

Synthetic LDH were first prepared by coprecipitation in the 20th century. Their stability and structure were described by Feitknecht who called these compounds "Doppelschichtstrukturen" - double sheet structures. Feitknecht assumed that layers composed of cations and anions make an LDH structure.[30,31] This hypothesis was later corrected on the basis of single-crystal XRD analysis.[26] The study proved that all the cations are localized in the same layer, while the anions and water molecules are placed in the interlayer region.

LDH structure and composition

LDH are rare in nature but can be easily synthesized. LDH are nanostructured materials, which can be described by the general chemical formula $[M^{2+}_{1-x}M^{3+}_{x}(OH)_2]A^{m-}_{x/m}\cdot nH_2O$, abbreviated hereafter as $M^{2+}_{R}M^{3+}$ LDH, where M^{2+} and M^{3+} represent divalent and trivalent cations, respectively, A^{m-} is an interlayer anion of the valence *m,* and R = (1-x)/x is the M^{2+}/M^{3+} molar ratio. The structure of LDH is shown in Figure 1. The basic layer

structure is related to the structure of brucite ($Mg(OH)_2$), where hydroxyl ions are hexagonally closely packed and Mg^{2+} cations occupy the centres of octahedral sites. These octahedra share edges to form an infinite sheet. The LDH structure is made up by a partial replacement of divalent cations, e.g., (Mg^{2+}) with trivalent cations, e.g., (Al^{3+}). This isomorphous substitution results in a net positive charge on the LDH layer. The interlayer space accommodates anions, which maintain the charge balance.[32] The water molecules in the interlayer space are either hydrogen bonded to interlayer anions or to the hydroxyl groups of the surface on the LDH layers. The water molecules are free to move by breaking and forming new bonds.[33,34]

LDH are characteristic by their two-dimensional structure which results from the electrostatic and hydrogen bonds between the layers and the interlayer region. The sheets are stacked one on the top of the other and are held together by hydrogen bonds. The surface areas are usually lower than 100 m^2 g^{-1} and the layer thickness is approximately 4.8 Å.[24,32]

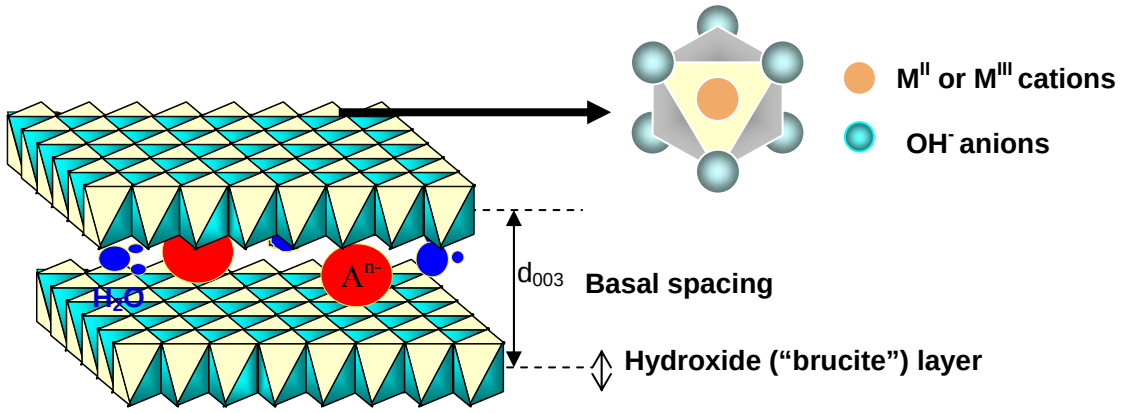

Figure 1. Structure of LDH.

Most LDH are based on magnesium and aluminum. However, a large number of M^{II}/M^{III}, M^{I}/M^{III}, and M^{II}/M^{IV} cation pairs can be combined to form the LDH layers:

Divalent metals M^{II}: Mg, Zn, Ni, Cu, Co, Fe, Ca, Mn
Trivalent metals M^{III}: Al, Ga, Cr, Fe, Co, Mn, V, and Y
Monovalent metal M^{I}: Li
Tetravalent metals M^{IV}: Ti, Mn, Zr, Sn, Pd

LDH are not limited by a binary combination of metal cations, multimetal LDH can be synthesized as well. The structural arrangement of layers differs depending on the composition and size of cation pairs, e.g., the hydroxide layers of MgAl LDH have the brucite structure, while LiAl LDH has the structure of gibbsite.

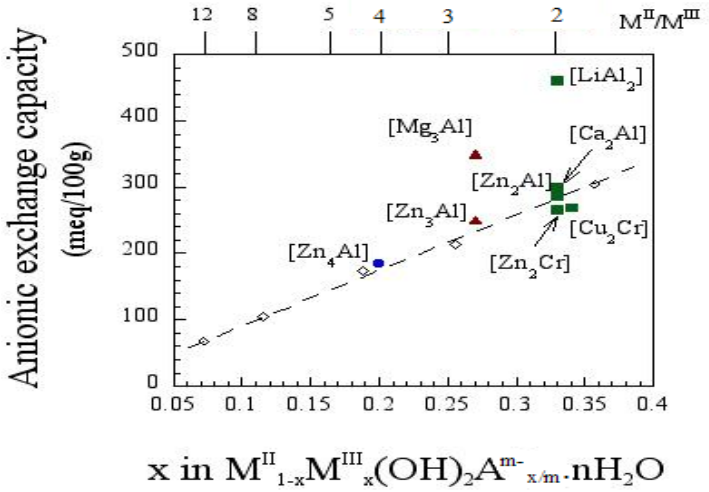

Figure 2. Variation of the AEC as a function of the amount of trivalent cation. [35]

M^{II} and M^{III} ions should have an ionic radius close to that of Mg^{2+} (0.065 nm) to enable the M^{II}/M^{III} isomorphous substitution in the octahedral positions of the hydroxide layers. The charge density and stability of the LDH layers depends on the M^{II}/M^{III} molar ratio. LDH exist in a relative wide range of the M^{II}/M^{III} molar ratios. In general, it is agreed that pure LDH phases can be formed with stoichiometries in the range of $0.20 < x < 0.33$, where $x = M^{III}/(M^{II} + M^{III})$. The upper limit is generally given by the electrostatic repulsion between the neighboring trivalent cations in the hydroxide layers and can cause the formation of others phases (e.g., basic magnesium carbonates). The lower limit is generally displayed by the disorder of layers. The anionic exchange capacity (AEC) for some LDH compositions is demonstrated in Figure 2.

A variety of charge-balancing anions can be incorporated into the interlayer gallery. Relatively weak bonding between interlayer ions and the host sheets results in expanding the exchange properties of LDH. Anions may vary in a geometry, size, and charge, giving rise to an extensive class of isostructural materials with different physico-chemical properties. Some of the anions are listed below:

Simple anions: CO_3^{2-}, OH^-, F^-, Cl^-, Br^-, I^-, NO_3^-, ClO_4^-

Halocomplexes: $[NiCl_4]^-$, $[CoCl_4]^{2-}$, $[IrCl_6]^{2-}$

Cyanocomplexes: $[Fe(CN)_6]^{4-}$, $[Co(CN)_6]^{4-}$, $[Mo(CN)_8]^{4-}$

Oxocomplexes: $[MoO_2(O_2CC(S)Ph_2)_2]^{2-}$, $[MoO_2(O_2)_4C_4H_2O_6]^{4-}$

Macrocyclic ligands: porphyrins, metaloporphyrins, phthalocyanines

Heteropolyoxometals: $(PM_{12}O_{40})^{3-}$, $(PW_{12}O_{40})^{3-}$

Organic anions or polymers: carboxylates and alkyl sulfates, organometallic complexes, polyvinyl siloxane (PVS), poly(styrene sulfonic acid) (PSS), deoxyribonucleic acid (DNA), ribonucleic acid (RNA).

Practically, there is no limitation to the nature of interlayer anions, which only must not form strong complexes with the hydroxide cations. Selective anion exchange of LDH leads to the preferential incorporation of carbonate anions. The high affinity of LDH for carbonate anions is due to strong hydrogen bonds and, therefore, it is important to eliminate contamination by CO_2 during the synthesis of LDH.[24,32, 36]

The number, length, orientation, and strength of the bonds between the anions and the hydroxyl groups of the hydroxide sheets determine the width of the interlayer space. Depending on the arrangement of the octahedral sheets in brucite-like layers and interlayer space two polytypes can be derived. The first (hydrotalcite) has a rhombohedral unit cell containing three stacked repeat units; the second (manasseite) has a hexagonal unit cell with two stacked repeat units.[37] In some cases of synthetic LDH, the stacking sequence can be changed from the three-layer polytype at ambient temperature to the two layer polytype at higher temperature.[29]

Preparation of LDH

A broad variety of methods is available for the synthesis of LDH. Their use depends on the purpose for which the particular LDH is to be used. The most common methods are coprecipitation, anion exchange, and reconstruction (calcination-rehydration procedure).

1) Coprecipitation in aqueous solution is the most frequently used method for LDH synthesis. Since the carbonate anions have a high affinity toward LDH layers, their replacement by anion exchange is difficult. Therefore, the synthesis of LDH containing specific anions requires carbonate and CO_2-free conditions. This synthetic route is often

chosen for the preparation of organic anion-containing LDH, which are otherwise difficult to obtain.[38] Coprecipitation is based on the slow addition of mixed solutions of metal salts in a given ratio into a reactor containing an aqueous solution of desired interlayer anion. A second solution of alkali is added simultaneously into the reactor in order to maintain pH at a selected value leading to coprecipitation of metallic salts in a ratio fixed by the starting solutions. The resulting precipitate is aged under stirring, then centrifuged, washed, and dried. It is necessary to optimize the experimental conditions for each system in order to obtain well-crystallized LDH phases. The nitrate or chloride forms are prepared by this procedure because the interlayer chloride or nitrate anions are good precursors for anion exchange.[48,39,40] In order to improve the crystallinity of the solids, a post-synthesis hydrothermal treatment in the presence of water vapour is performed at temperatures, which do not exceed the decomposition temperature of LDH.[41,42]

2) Anion exchange is useful when the coprecipitation method is inapplicable, e.g., when the layer metal cations or the interlayer anions are unstable in alkaline solution, or when a direct reaction between the metal ions and the guest anions is favorable.[43,44] Under standard conditions, the anion-exchange method can be carried out in two ways: (i) A precursor containing univalent anions such as chloride or nitrate with weak electrostatic interactions with the layers can easily be exchanged for desired anions. (ii) LDH precursor contains anions, especially carbonates or carboxylates susceptible to acid attack (Equation 1).[45,46]

$$LDH\cdot A^{m-} + X^{n-} + mH^{+} \rightarrow LDH\cdot (X^{n-})_{m/n} + H_m A \qquad (1)$$

3) An alternative procedure is rehydration using a structural memory effect. LDH are able to regenerate the layered structure collapsed by calcination at high temperatures by swelling in an aqueous solution. Calcination of LDH removes interlayer water, anions, and hydroxyl group, and leads to mixed metal oxides. The main advantage is avoiding the competitive intercalation of inorganic anions arising from metal salts. However, amorphous phases are often produced simultaneously. This method can also be employed for intercalation of bulky guests.[29, 44,47]

The described methods are the main intercalation strategies and their application for anionic porphyrin intercalation will be given in Chapter 4. It is relevant to shortly recall other methods for the preparation of LDH such as urea coprecipitation, salt-oxide methods,

and sol-gel technique. The detailed description of these synthetic routes has been reported in numerous reviews.[29,44,48]

4) A special case of the LDH synthesis proceeds *via* thermally induced urea hydrolysis.[49,50] This method is basically a modification of the coprecipitation method where a precipitating agent is urea. The advantage of this method is the production of well crystallized LDH (large hexagonal plates) with a narrow distribution of particle size.[51,52] The conversion of carbonate anions for other anions can be carried out by anion exchange, but this process is difficult. The anion exchange of carbonate by other anions, e.g., chloride, nitrate, and sulfate occurs in acid media.[45,46,53]

5) The salt-oxide method consists in the reaction of $M^{II}O$ oxide with a solution containing M^{III} cations and desired anions. Boehn et al[54] proposed the preparation of ZnAl or CrAl LDH using salts and oxides as metal sources. It can be also used for the preparation of ZnCr or CuCr LDH, which are difficult to obtain by coprecipitation.[44,55]

6). The sol-gel technique consists in hydrolysis of alkoxides or acetylacetonates of M(II) and M(III) metals, consisting of a fast nucleation process followed by a separate aging step at elevated temperatures.[44,56,57] Mg/M(III) (M=Al, Ga, In) LDH were synthesized in this way and provided lower crystallite dimensions and high surface areas compared with coprecipitated samples prepared from the aqueous solution of magnesium and aluminum or gallium or indium nitrates.[58] The sol-gel technique can be used for the preparation of pure phases.

3.1.2 LDH/polymer composites

The effort for obtaining polymers with improved functionalities led to the development of LDH/polymer hybrids. The properties of LDH/polymer composites depend not only on the properties of their individual components (polymer, LDH), but also on their morphology and interfacial characteristics. The polymer composites can be considered as either intercalated compounds, where an organic component such as polymer is incorporated into layered materials or materials where LDH is a nanofiller and is dispersed in the polymeric matrix. Depending on the nature of the components used (layered materials, AEC, polymeric matrix) and the method of preparation, significant differences in final properties of the product may occur. There are three types of LDH/polymer composites (Figure 3): (i) Tactoid structures are obtained when the filler is surrounded by

the polymer. (ii) Intercalated structures undergo interlayer expansion. In this case, a well-ordered stacked multilayer structure appears as a result of affinity between the polymer and LDH. The interlayer space of LDH is expanded as polymer chains penetrate interspace, but the shape of the layered stack is maintained. (iii) Exfoliation: LDH layers are completely and uniformly dispersed in a continuous polymer matrix. All the three LDH/polymer structures can be present separately or combined in one sample.

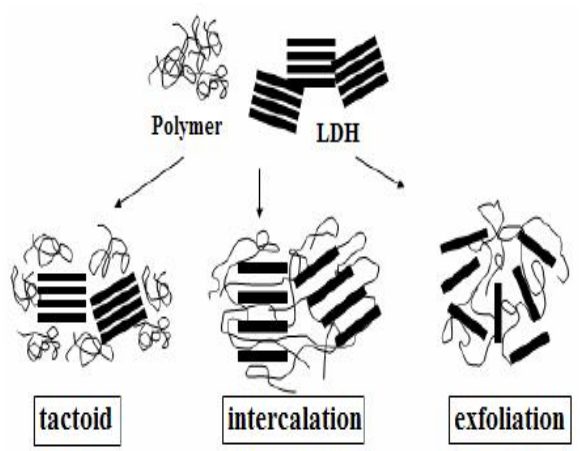

Figure 3. Three types of the composite structure.

The exfoliation of LDH is difficult to achieve due to strong electrostatic interactions between highly charged hydroxide layers and interlayer anions. The LDH/polymer composites are both partially exfoliated and combined with tactoids. It was observed that the hybrids possess enhanced mechanical, thermal, gas-barrier, and flame-retardant properties compared with the pristine polymer, leading to potential applications in materials science.[9,59, 60]

Bio-hybrids based on LDH may provide new opportunities as reservoirs and delivery carriers of functional groups. For example, nanofillers based on biocompatible LDH intercalated with photoactive molecules or drugs dispersed into a polymer lead to polymeric composites in the form of films with useful photophysical[61] or biomedical properties.[8,35,59]

3.1.3 Applications of LDH

LDH have already found numerous applications due to their ability to vary chemical composition and their chemical and physical properties as was demonstrated in the previous sections. The summary of current applications is shown in Figure 4.

LDH are used in polymer industry to produce nanocomposite materials with defined chemical and physical properties.[52,60] Employing LDH in the preparation of nanocomposites results in materials with increased tensile and thermal properties, reduced permeability, solvent uptake, and lower flammability.[62,28] Nanocomposites based on PVC and modified by LDH manifest improved thermal stability.[63,64]

LDH have also attracted attention in catalysis because of a small particle size and versatility of chemical compositions. LDH are often used as efficient catalysts for different chemical reactions, e.g., aldol condensation of aldehydes and ketones.[65]

LDH have excellent adsorption ability. Inorganic contaminants such as oxoanions (e.g., NO_3^-, SO_4^{2-}, CrO_4^{2-}) and anions (e.g., F^-, Cl^-) can be removed by uncalcined and calcined LDH.[65] It offers a way for the disposal of radioactive wastes[66] and for removing heavy metals from contaminated waters.[67] LDH can be used in separation processes for the removal of environmentally hazardous acid mine drainage or as scavengers of soil contaminants.

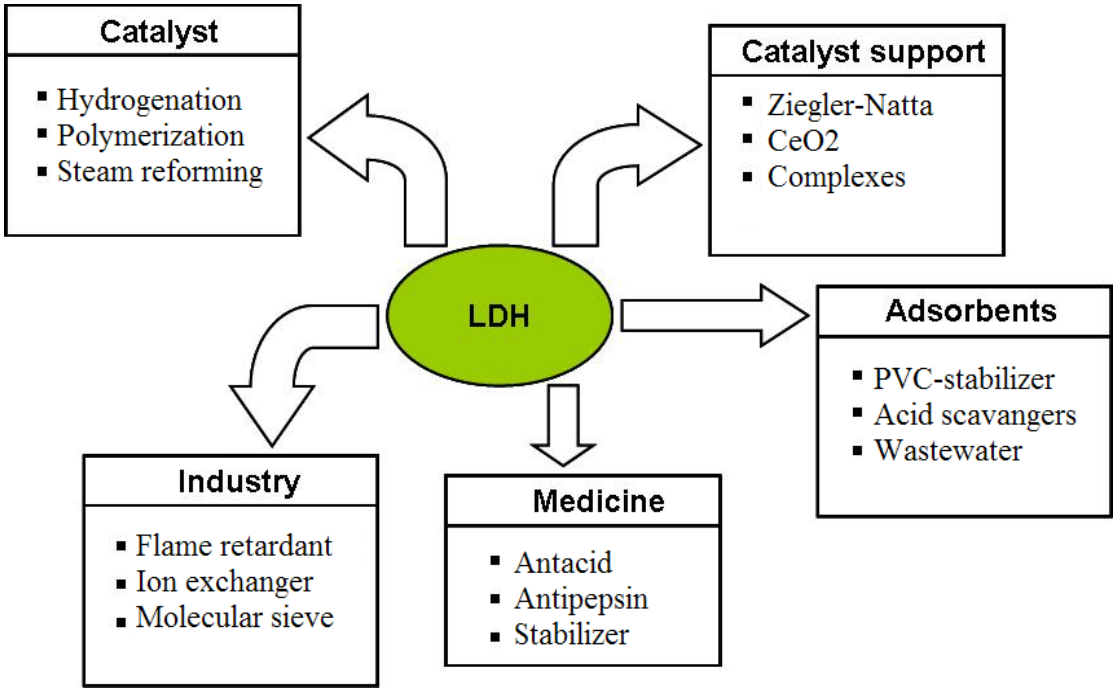

Figure 4. Main industrial applications of LDH.[26]

It is also worth to note many applications in medicine and biology. The earliest medical applications of LDH were as antacid and antipepsin agents. These agents were also suggested for the removal of phosphate anions from the gastrointestinal fluid to prevent hyperphosphatemia. In the last decade, LDH have found potential applications as pharmaceuticals. The recent research has focused on intercalation and controlled release of pharmaceutically active compounds from LDH carriers. The main aim of the pharmaceutical technology is to maintain pharmacologically active drug levels for long periods, avoiding repeated administration, and/or, to localize the drug release at a target site. The interlayer space of LDH may be considered as a microvessel where the anionic drugs are stored while maintaining their integrity, and are protected from oxidation or photolysis. Many molecules of biological interest have been intercalated into LDH, including sorbic acid, vitamins, amino acids, single or double stranded DNA, oligomers, adenosine triphosphate (ATP), and porphyrins.

Other practical applications are in the cosmetic field mainly for removal of skin exudates, encapsulation of skin-sensitive coloring, and as UV-screening agents.[25,26,68] Intensive research activity in recent years has been dedicated to the preparation of tailored materials with magnetic, photochemical, and optical properties with the aim of immobilizing these compounds on a solid support and/ or modifying their properties by

confining them in a medium. For example, the insertion of dyes produces materials for tunable lasers, fluorescent, and non-linear optics devices.

3.2 Porphyrins as guest species

3.2.1 Porphyrins

Porphyrins are a plentiful class of aromatic, naturally occurring macrocycles. The porphyrin ring system is a tetrapyrrole macrocycle where the four pyrrole rings are linked together by four methine bridges (Figure 5). Porphyrins are aromatic owing to the presence of a conjugated 18 π-electron system in each macrocycle. Their conjugated double bond system tends to form closely stacked aggregates, in which absorbed excitation energy is dissipated through decay channels competing with desired photoinitiated reactions. This macrocycle plays important roles in vital biological processes as oxygen storage and transport, enzymatic redox reactions, and light harvesting. The porphyrin macrocycle is a versatile platform for substitution of the peripheral sites by various groups, modifying its properties. Synthetic porphyrins are typically substituted in the meso-positions. Porphyrins exist as free ligands or can coordinate almost all metals of the periodic table *via* the four pyrrolic nitrogens at the core and typically form square planar or octahedral structures. The metalloporphyrins are usually very stable and can bind a variety of small molecules (known as ligands) to the central metal atom. Several porphyrins with selected peripheral substitution and metal (Fe, Cu, Mg, Co) coordination catalyse important biochemical processes in living organisms such as active sites of enzymes and respiratory pigments. Synthetic porphyrins have unique coordination, electronic, and chemical properties leading to many applications in catalysis, advanced materials, optical data storage, and in electrochromic materials.[4,69]

In the context of this work, the main attention was devoted to the photosensitizing properties of porphyrins. Porphyrins are photosensitizers with rich fluorescence properties and the ability to produce singlet oxygen (see next chapter).

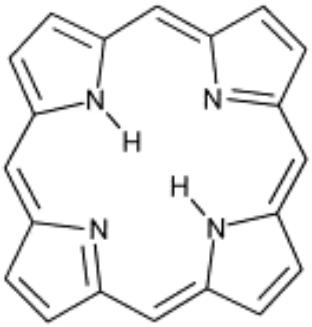

Figure 5. Structure of porphyrin macrocycle.

3.2.2 Singlet oxygen

Singlet oxygen, ($^1O_2$), is a metastable excited state of the ground state molecular oxygen $^3O_2$. The ground state of oxygen is the triplet state ($^3\sum_g^-$) with two unpaired electrons localized in the highest occupied antibonding pπ*orbitals. The rearrangement of the electron spins results in two possible singlet excited states. The energy difference between the ground and first singlet state of oxygen ($^1\Delta_g$) is 94 kJ mol^{-1}. Both electrons paired in a single orbital characterize this state. In the higher singlet state ($^1\sum_g^+$) the energy difference is 157 kJ mol^{-1}. This state is characterized by spin pairing electrons in two pπ* orbitals. The energy level diagram and transitions between electronic states of oxygen are shown in Figure 6. Singlet oxygen ($^1\sum_g^+$) has very short lifetime, therefore, singlet oxygen in the ($^1\Delta_g$) state is the most important species from the chemical point of view. In the following context, $^1O_2$ means singlet oxygen $^1O_2$ ($^1\Delta_g$). The lifetime of $^1O_2$ depends on the nature of the solvent (Table 1).

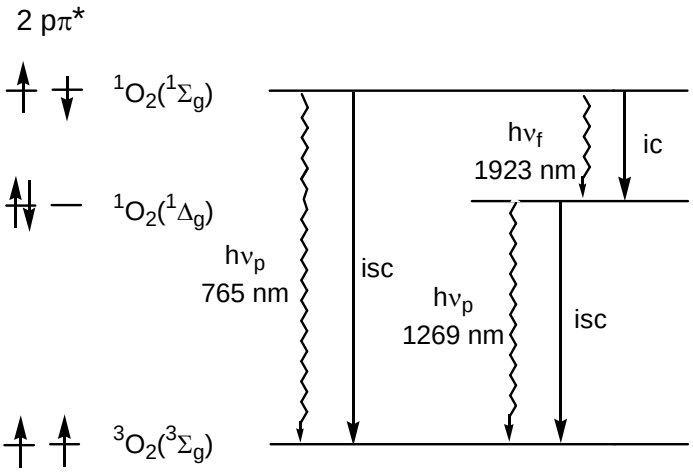

Figure 6. Transitions between electronic states of oxygen.[70]

Table 1. Lifetime (τ) of singlet oxygen in various solvents.[71]

Solvent	t/μs
H_2O	3,8
D_2O	62
CH_3OH	10
$CDCl_3$	740
CCl_4	700

Singlet oxygen can be generated by physical, chemical, and biological methods. Photosensitization reactions, microwave or radiofrequency discharge belong to physical methods. Several chemical methods include thermolysis of endoperoxides, reactions of ozone and some organic ozonides, decomposition of peroxochromate or peroxomolybdate, and reaction of hydrogen peroxide with hypochlorite. The last route is also biologically relevant. Hyprochlorite ions ClO^- are formed by myeloperoxidase during phagocytosis and react with hydrogen peroxide in the tissues.[72]

Singlet oxygen is a dangerous initiator of detrimental biological oxidations due to its high reactivity and oxidation potential, e.g., $^1O_2$ causes membrane damage by oxidizing amino acids, unsaturated fatty acids, and cholesterol.[73] Scavengers of $^1O_2$ such as carotenes, ascorbic acid, or thiols can prevent these harmful effects. On the other hand, the

same effect is utilized for oxidative degradation of neoplastic tissue during photodynamic therapy of cancer (PDT)[74] and for the inactivation of microorganisms.[75,76,77]

The most reliable spectroscopic determination of $^1O_2$ is by its luminescence at 1270 nm.[71]

3.2.3 Photosensitized generation of singlet oxygen

The most feasible method of the $^1O_2$ production is a photosensitized reaction. The principle of photosensitized oxygen reaction rests in excitation of the sensitizer into a higher electronic state (Equation 2) by absorption of light (UV-vis, NIR) followed by energy transfer to an oxygen molecule, which is thus excited from the ground triplet state to the singlet state (Equation 3). During formation of $^1O_2$ (Equation 3), the sensitizer is regenerated so that many singlet oxygen molecules are formed by a single molecule of the sensitizer, so long as light and molecular oxygen are present.

$$^1\text{Sens} \xrightarrow{h\nu} {}^1\text{Sens}^* \longrightarrow {}^3\text{Sens}^* \qquad (2)$$

$$^3\text{Sens}^* + {}^3O_2 \longrightarrow {}^1\text{Sens} + {}^1O_2 \qquad (3)$$

The process of energy transfer and subsequent transition is also visualized in Figure 7. The sensitizer is excited from the ground state S_0 to the singlet state S_1. The lifetimes of S_1 states of the most sensitizers are in the nanosecond range, which is too short to allow significant quenching by oxygen to yield $^1O_2$. The S_1 states spontaneously deactivate *via* radiative processes fluorescence ($h\nu_f$) and phosphorescence ($h\nu_p$), or by non-radiative processes intersystem crossing (*isc*) and internal conversion (*ic*). Fluorescence and internal conversion are transitions between energy levels of the same spin multiplicity and are spin allowed. Deactivation of the excited sensitizer to a lower lying triplet state T_1 proceeds by intersystem crossing. Transitions between states of different spin multiplicity are spin forbidden. Because the deactivation of T_1 to S_0 is forbidden the triplet state T_1 has a relatively long lifetime (up to hundreds of μs). This is long enough for a variety of quenching processes to compete favorably with the phosphorescence. The most probable process is quenching by oxygen, the quenching rate being of the order of $10^8 – 10^9$ M^{-1} s^{-1}.

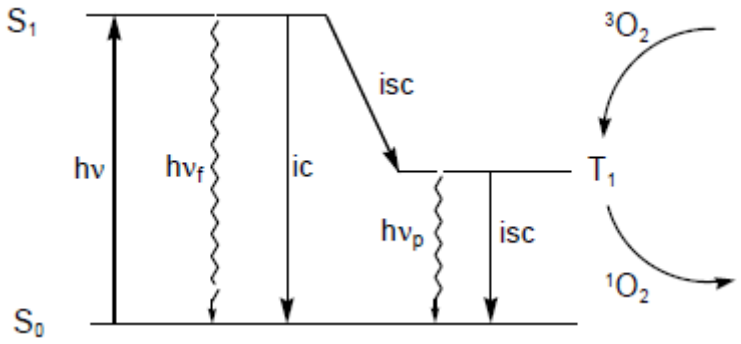

Figure 7. Mechanism of photosensitized production of $^1O_2$, *ic* – internal conversion, *isc* - intersystem crossing, $h\nu_f$ – fluorescence, $h\nu_p$ – phosphorescence.

Photosensitized oxygen reactions are classified as Type I and Type II according to the nature of quencher. Quenching of the excited sensitizer by molecular oxygen (Type II reactions) involve energy transfer yielding $^1O_2$ or electron transfer process yielding superoxide anion radical O_2^- (Equation 4, 5, 6). These mechanisms are considered to be main routes destroying cells. Type I reaction is quenching by a substrate or solvent molecules and yields corresponding radicals.[70,71]

$$\text{Sens}(T_1) + {}^3O_2 \rightarrow \text{Sens}^+ + O_2^- \quad (4)$$

$$\text{Sens}(T_1) + {}^3O_2 \rightarrow \text{Sens}(S_0) + {}^1O_2 \quad (5)$$

$$\text{Sens}(T_1) + {}^3O_2 \rightarrow \text{Sens}(S_0) + {}^3O_2 + \text{heat} \quad (6)$$

Numerous free porphyrins and their complexes with non-transition metals possess photosensitizing properties. Sensitizers appropriate for PDT must not be toxic in the absence of light. In contrast, phototoxicity is essential for photo-bactericidal materials and pharmaceuticals for PDT.[73,77,78] Due to strong ππ interactions, the porphyrin molecules tend to form closely stacked assemblies. Porphyrin molecules in solution and adsorbed on solids are prone to aggregate.[79] The aggregation is an undesired process because of fast dissipation of the absorbed energy, mediated by exciton coupling between the stacked porphyrin units. The competitive relaxation reduces the fluorescence lifetimes and quantum yields, and suppresses the generation of the porphyrin triplet states. The suppression of the aggregation can be achieved by the immobilization of the individual molecules in inorganic layered hosts of ordered structure such as LDH.[4] In addition, the main advantages are the well-defined microscopic structures of the host matrices, specific

organization, variability, enhanced stability, and preservation of photoactivity of the porphyrin molecules.[80,81,82]

3.3 Host-guest interactions: intercalation of porphyrins

Intercalation can be defined as insertion of a guest species into the interlayer gallery of a layered host, leaving the host layer structure unchanged. The intercalation is often a reversible process. Layered materials are characterized by asymmetric bonding strength and the rigidity of the layers will play an important role in the intercalation mechanism and in the overall energetics. Whereas the "in-plain" (layer) bonds are relatively strong covalent or co-ordination bonds, bonds in the direction perpendicular to the plain (interlayer) are weaker noncovalent interactions directing the interlayer distance. This arrangement enables accommodation of guests into the galleries. Furthermore, the hydrated gallery ions can be readily exchanged by other ions of the same charge sign. Layered hosts adapt to the geometry of the inserted guest species by adjusting the interlayer space, and increasing the basal spacing. The amount of the guest-intercalated species depends on charge density of the layers. The higher is the charge density of the layers, the higher is also the content of intercalated anions. Intercalation reactions are particularly important as they can dramatically change the chemical, electronic, optical, and magnetic properties of a host lattice.[83,84] It is worth noticing that the formation of a final intercalated structure is based on self-assembling of the reorganized units and that it relies on the collective effect of noncovalent bonds namely hydrogen bonds, coulombic forces, ππ interactions, and dispersion forces.[84] Intercalation into layered materials provides means to arrange an intercalated guest into well-ordered layers. The effect of the spatial confinement of the guest and/or the enforced change is reflected in the change of the guest properties.

In this respect, LDH possess relatively rigid layers, positively charged due to the isomorphous substitution of a divalent cation by a trivalent cation and contains exchangeable anions. Nanomaterials based on LDH are promising carriers of drugs because they can be hydrophilized, possess large surface areas, can penetrate into tissues, and as a rule are efficiently taken up by the cells.

When the anions are intercalated into LDH, interactions between the positively charged layers and the original interlayer anions are broken and new bonding interactions between the host and new guest anions are formed. The number of layers between

successively filled or partially filled layers defines the order of staging. In some cases the formation of the second-stage intermediates was observed, i.e., alternating galleries filled with original and exchanged anions. Co-intercalation of different anions into the same gallery has not been observed so far.[85,86]

3.3.1 Arrangement of porphyrin and intercalation strategies

The organization of porphyrins in a constrained space, their proximity, relative orientation, and chemical environment play an important role in modulating their properties. In fact, there are two different organizations of the guest species in LDH: (i) the organization on the surface of the crystals (adsorbed species), (ii) the arrangement in the interlayer region (intercalated species). Their relative populations depend on original anions of LDH and the organization of guest species is independent on the synthetic procedure. The plane of intercalated porphyrins can be arranged in space between LDH layers parallel, perpendicular or slanted with respect to the hydroxide layers. The arrangement depends on the nature and charge density of active sites and on the shape and size of a guest. Intercalation into LDH requires porphyrins functionalized with anionic groups as shown in Figure 8.[4] The general procedures of intercalation were described in Chapter 3.1.1.

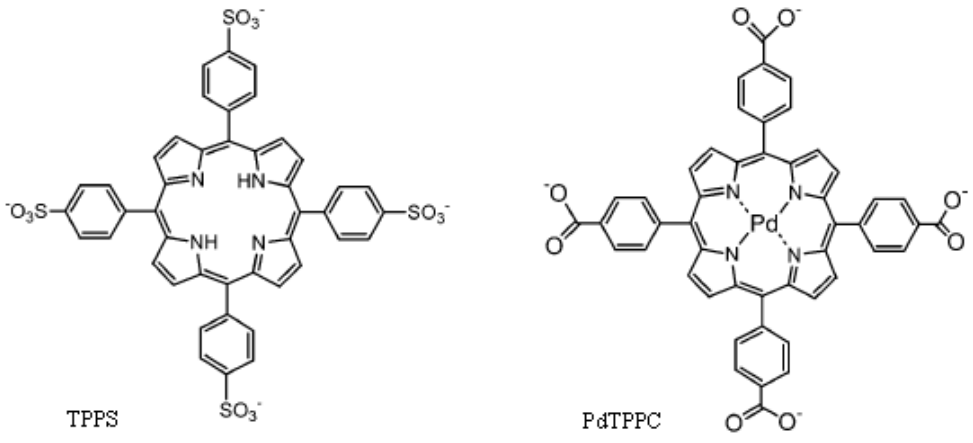

Figure 8. Structure of 5,10,15,20-tetrakis(4-sulfonatophenyl)porphyrin (TPPS) and Pd(II)-5,10,15,20-tetrakis(carboxyphenyl)porphyrin (PdTPPC).

In the anion-exchange method the guest anions are intercalated by dispersing LDH in an aqueous solution containing an excess of a desired anion (see Chapter 3.1.1). The method is also generally used for obtaining porphyrin-LDH hybrids. It was used in the pioneering work on intercalation of TPPS into MgAl LDH. [87] The interlayer spacing of the intercalate was found to be 22.4 Å, which might indicates that the arrangement of porphyrin molecules is perpendicular to the hydroxides layers. A partial exchange leads to a mixture of the starting and the fully exchanged material. Carrado[88] *et al.* reported intercalation of Cu(II) phthalocyanine into the gallery of MgAl LDH by the anion-exchange and coprecipitation methods. The orientation of intercalated Cu phthalocyanine in MgAl LDH was suggested to be perpendicular to the LDH layers independently of the used method. By contrast, phthalocyanine intercalated into LiAl LDH show a relatively small interlayer distance signifying that phthalocyanine adopts orientation parallel to the layers.[89]

The rehydration method (Chapter 3.1.1) based on "*memory effect*" is more complicated than coprecipitation or anion-exchange methods. This method is usually employed for intercalation of large guests. The advantage is the possibility of circumvention the competitive intercalation of inorganic anions arising from metal salts. Ukrainczyk[90] *et al.* used this method to intercalate Co(II) tetrasulfophthalocyanine into MgAl LDH. The orientation of Co(II) phthalocyanine was suggested to be perpendicular to the LDH layers. Barbarossa[91] *et al.* reported synthesis of MgAl LDH containing Co(II) 5,10,15,20-tetrakis(4-sulfonatophenyl)porphyrin by (i) reconstruction method and (ii) adsorption of anionic metalloporphyrin on the external surfaces of the pristine LDH. They compared the catalysis of phenol oxidation by intercalated porphyrins and porphyrins adsorbed on the surfaces of LDH.

Coprecipitation (Chapter 3.1.1) followed by a post-synthesis hydrothermal treatment is one of the methods commonly used for the preparation of LDH intercalated materials. The benefit of the method is high crystallinity and pure intercalates. Bonnet[92] *et al.* successfully intercalated porphyrins into ZnAl LDH by the coprecipitation or anion-exchange methods. They established that the coprecipitation method followed by a hydrothermal treatment leads to highly crystalline and pure materials. Halma[12] *et al.* used the coprecipitation method for intercalation of tetraanionic porphyrins between the ZnAl LDH layers. They showed that porphyrin immobilization in LDH facilitates recovery of the catalytic activity.

3.3.2 Methods of characterization used in the study

Of the rather wide spectrum of characterization methods, following techniques were used: powder X-ray diffraction (XRD), scanning electron microscopy (SEM), high-resolution transmission electron microscopy (HR-TEM), UV-vis diffuse-reflectance spectroscopy, infrared spectroscopy (FTIR), and thermogravimetric analysis (TGA/DTA). Less extensively were employed molecular modelling, extended X-ray absorption fine structure (EXAFS), and small-angle X-ray scattering (SAXS). Photophysical properties of the materials were studied by time-resolved spectroscopies, namely transient absorption spectroscopy (triplet states) and time-dependent near-infrared luminescence of $^1O_2$ at 1270 nm (TDL). The most important techniques used are discussed in the following section.

XRD is one of the most frequently employed techniques for identification of the crystalline phases, its purity, and/or structure of host-guest compounds. It is a rather fast and non-destructive technique.

The diffraction lines of an LDH fall into three groups (Figure 9):

1) A series of sharp basal 00*l* diffraction lines at low values of 2θ allows direct determination of the basal spacing normal to the (00*l*) plane. It equals to the thickness of the LDH layer and interlayer space (Figure 1). The unit cell parameter *c* is determined by the relationship $c = 3d_{003}$, where d_{003} is the *d* spacing of the *003* diffraction lines (following the $R\bar{3}m$ symmetry).

2) The relatively weak non-basal diffraction lines are at higher values of 2θ. The M^{2+}/M^{3+} ratio in the hydroxide layers can be derived from the parameter of the unit cell *a*, that is given by the relationship $a = 2d_{110}$, where d_{110} is the 110 diffraction. The dependence of d_{110} on the M^{2+}/M^{3+}ratio enables to calculate the chemical formulae of the LDH layers.

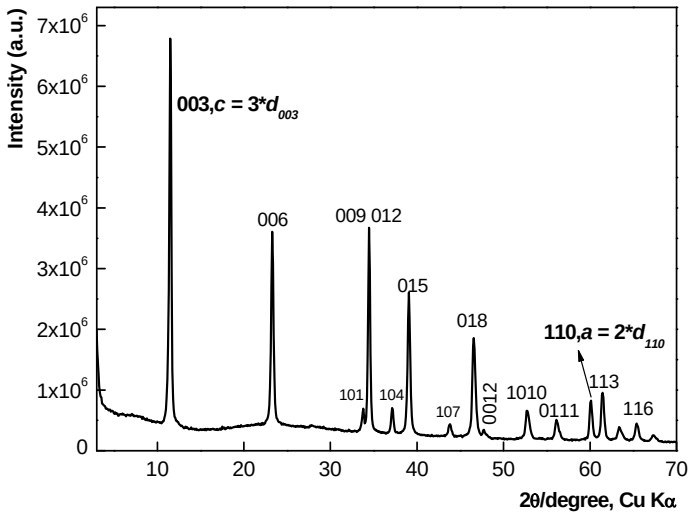

Figure 9. Diffraction pattern of CO_3-Zn_2Al.

3) Finally, the positions of the 01*l* and/or 10*l* diffraction lines at intermediate values of 2θ can be used to determinate the stacking pattern of the layers. In certain cases, the non-basal reflections are quite broad, attributed to a turbostratic disorder of the hydroxide layers.[24]

FTIR is applied to investigate the structural bonding of compounds. Incorporation of the porphyrin molecules into LDH is, for example, identified by strong antisymmetric and symmentric stretching bands of the corresponding carboxylic or sulfonic groups of porphyrins. In addition, the purity of the materials can also be confirmed because carbonate or nitrate anions are easy to observe (Figure 10).

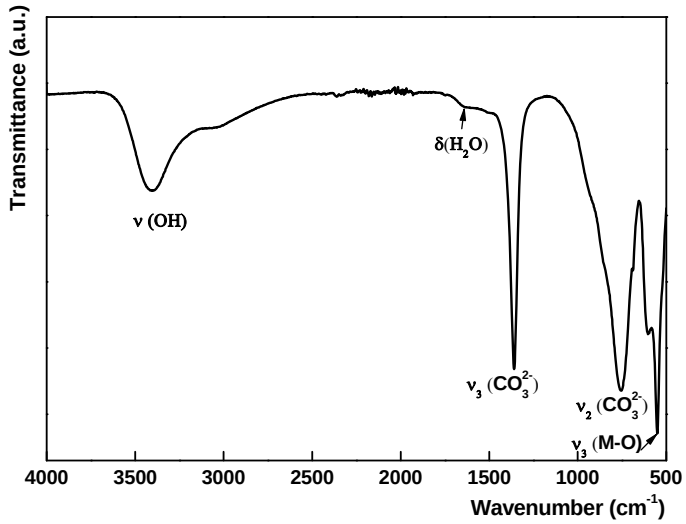

Figure 10. FTIR spectra of CO_3-Zn_2Al.

The thermal properties of porphyrin-LDH are studied by thermogravimetry and differential thermal analysis (TGA/DTA). The thermal analyses are often coupled with a mass spectral analysis, to study weight changes of samples and the nature of the evolved gases in relation to temperature changes. TGA/DTA is employed to investigate the thermal stability (degradation temperatures), the amount of inorganic component, the amount of water, and the amount of organic volatiles.

HRTEM and SEM became important techniques for study of the materials morphology and the microstructure on the nanometer scale. SEM is employed for the obtaining of the surface topography of LDH intercalates (Figure 11). The problem of HRTEM measurements is that organic components cannot be detected because they decompose and that the hydroxide layers are unstable in an electron beam.

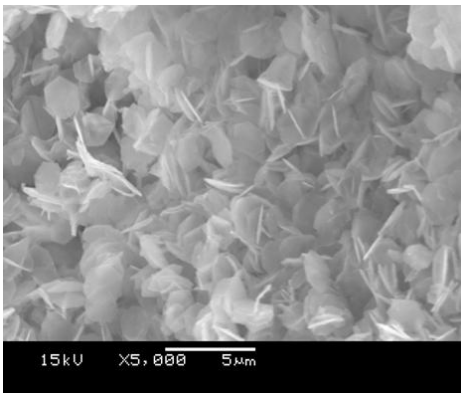

Figure 11. CO_3-Zn_2Al morphology observed by SEM.

In the study of LDH intercalates, the EXAFS and SAXS methods were employed only partly due to difficult and expensive measurements, but they bring important results in the structural characterization of hybrid materials. SAXS is a technique, in which the source of X-ray scattering is the nanometer range of inhomogeneities in the samples. It provides information about the shape and size of the inhomogeneities and their distances. The SAXS patterns are recorded at very low angles (typically <3-5°). EXAFS is employed to characterize the local structure of intercalate. The structural analysis based on the combination of the molecular mechanics and molecular dynamics simulations, quantum-chemistry calculations, XRD, and electron density measurements can solve the structure of the LDH intercalate, i.e., the arrangement of guests, the layer stacking, and the energy characteristics.

The direct measurement of $^1O_2$ is based on the monitoring of its luminescence at 1270 nm (TDL). The sample is placed in a quartz cuvette and it is excited by a laser pulse of appropriate wavelength for excitation of intercalated sensitizer. The quantum yield of phosphorescence is small, it is about 10^{-4} and 10^{-7} in dependence on solvent, and hence it has to accentuate the sensitivity of a detection system. The lifetimes of $^1O_2$ in hybrid materials were obtained by the analysis of measured luminescence curves.

4 Results and discussion

4.1 Mg_RAl LDH with intercalated porphyrins

Appendix I describes preparation, structure, and photophysical properties of powdered hybrid materials based on LDH of the Mg^{2+}/Al^{3+} type (Mg_RAl LDH) intercalated by anion exchange with the porphyrins TPPS and PdTPPC.[16] The objective was to elucidate the influence of intercalation on the photophysical parameters of the porphyrin containing hybrid, namely on lifetimes of the porphyrin triplet states and lifetime of $^1O_2$.

In the Appendix II, high-temperature powder X-ray diffraction (HT-XRD) in a combination with thermal analysis were employed as analytical tools for the determination of the intercalation degree of porphyrin-Mg_RAl hybrids. The anion-exchange and rehydration methods were used for intercalation of TPPS, TPPC, PdTPPC, and ZnTPPC porphyrins into Mg_RAl LDH hosts. [93]

The structural properties of Mg_RAl LDH containing TPPS, ZnTPPC and PdTPPC prepared by rehydration are described as well.[17] The experimental data were employed for the study of the alignment of TPPS in the Mg_RAl LDH matrix by molecular modelling.[94]

Mg_RAl LDH as a matrix was chosen because this type of LDH can be easily synthesized and modified by intercalation, has minimum absorption in the visible region, and it is environmentally friendly. In order to ascertain how the charge density of the LDH layers influences porphyrin intercalation, we used LDH with the Mg/Al molar ratios of 2, 3, and 4. The porphyrin-LDH ratio was adjusted to achieve 10% and 100% loadings with respect to the theoretical AEC of LDH. For photophysical experiments were used porphyrin-Mg_RAl LDH with the 10% exchange because of the lower optical density. On the other hand, structural characterizations were carried out with porphyrin-LDH samples with the highest loading. The following notation is used throughout the text, e.g., Mg_3Al LDH with of the formula $Mg_{0.75}Al_{0.25}(OH)_2(CO_3)_{0.5}x0.5\ H_2O$ is abbreviated as CO_3-Mg_3Al to express the type of intercalated anions.

4.1.1 Structural characterization

The Mg_RAl LDH hosts with nitrate, chloride or carbonate anions were prepared by the coprecipitation method according to Miyata.[39] The adjusted procedure is described in detail in the Supporting Information of Appendix I. Anion exchange with NO_3-Mg_RAl or Cl-Mg_RAl as precursors was used to obtain intercalated products.

The powder XRD patterns of Mg_2Al LDH intercalated with TPPS are visualized in Figure 12. Original nitrate or chloride anions in the Mg_RAl interlayer space were replaced by TPPS and PdTPPC by the ion-exchange method. The original nitrate and chloride forms of Mg_2Al LDH showed characteristic diffractions corresponding to a crystalline layered phase with basal spacing of 8.8 Å and 7.8 Å, respectively.

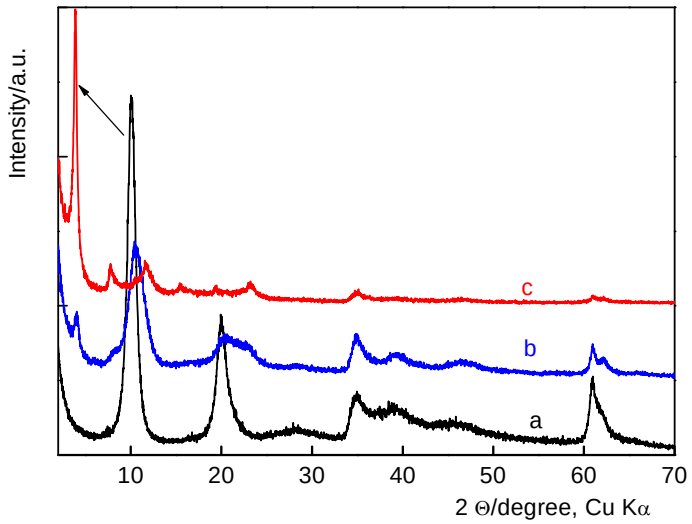

Figure 12. Powder XRD patterns of NO_3-Mg_2Al (a), TPPS-Mg_2Al (10% AEC) (b), and TPPS-Mg_2Al (100% AEC) (c). For clarity, the patterns are vertically shifted.

The samples of TPPS-Mg_2Al and PdTPPC-Mg_2Al display XRD patterns different from the precursor: basal diffraction lines shift toward lower 2θ, indicating larger interlayer spacing of 22.5 Å for the TPPS intercalates (Figure 12), and 23 Å for the PdTPPC intercalate. It confirms that the porphyrins were successfully intercalated into the interlayer galleries of Mg_2Al LDH. If we subtract the thickness of the sole LDH layer (4.8 Å), the gallery height of the TPPS-Mg_2Al intercalates is 16-18 Å. Such a distance is consistent with orientation of porphyrin anions the nearly perpendicular toward the hydroxide layers. It allows the peripheral sulfo or carboxyl groups to interact with the hydroxyl groups of the

brucite-like sheets. The 100% porphyrin loading of LDH was not achieved in the performed syntheses (max. 75 - 80 % AEC). The small residues of non-intercalated LDH particles (non-exchanged nitrate anions of LDH precursor) were always observed. Analogous results were obtained with intercalated PdTPPC and ZnTPPC.

On the basis of the above mentioned experimental results and molecular modelling, Kovář *et al.*[94] described the arrangement of the interlayer gallery of Mg_RAl LDH intercalated with TPPS. The plane of the guest porphyrin anions is titled with respect to the hydroxide layers (the angle between porphyrin plane and layer normal is ca 20º).

The tilted orientation of the porphyrin anions can be explained by the presence of interlayer water. Water molecules due to the hydrophobic character of the porphyrin ring predominantly fill the space between the hydroxide layers and the porphyrin anions.

The reference sample of TPPS-Mg_2Al containing porphyrin molecules adsorbed on the LDH external surfaces was prepared with the aim to compare photophysical properties of intercalated and adsorbed porphyrins. In this sample, the powder XRD patterns show identical diffraction lines as the parent CO_3-Mg_2Al (Figure 13). It documents that the porphyrins are not ion-exchanged with carbonate anions in the LDH gallery because of the extremely high affinity of carbonate toward the hydroxide layers. The same results were obtained with PdTPPC-Mg_2Al samples.

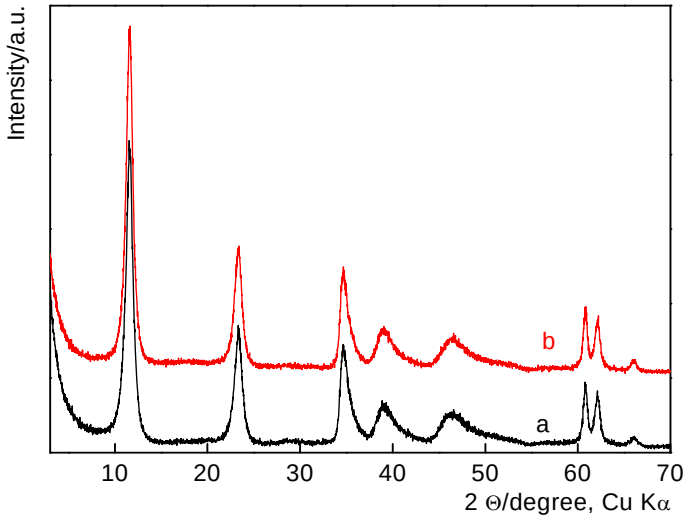

Figure 13. Powder XRD patterns of CO_3-Mg_2Al before (a) and after adsorption of TPPS (b); for clarity, the patterns are vertically shifted.

The powder XRD patterns of TPPS intercalated in LDH having different Mg/Al molar ratios are shown in Figure 14. TPPS-Mg_RAl with the molar ratios of 3 and 4 have XRD patterns similar to those of TPPS-Mg_2Al, with basal spacings (d_{003}) of 21.5 Å and 21.2 Å, respectively. The results indicate that the Mg/Al molar ratio has no specific influence on the extension of the LDH layered structure by porphyrins. However, Mg_4Al LDH exhibits remarkably lower exchange properties.

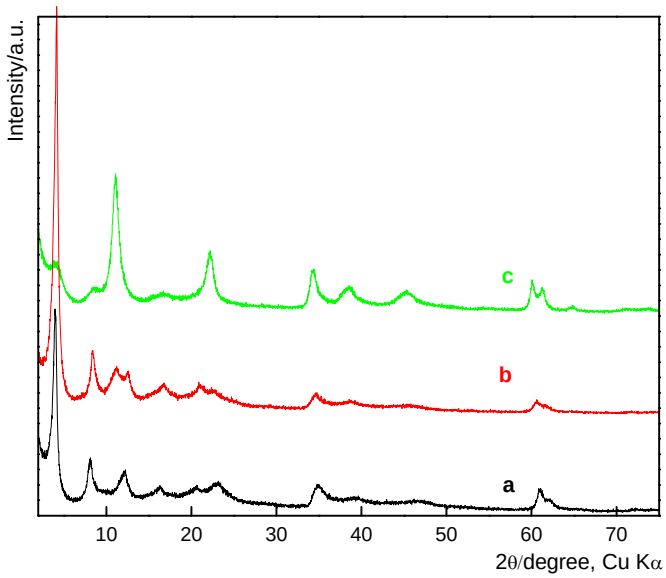

Figure 14. Powder XRD patterns of samples: TPPS-Mg_2Al (a), TPPS-Mg_3Al (b), and TPPS-Mg_4Al (c) prepared by the anion-exchange method.

The porphyrin-Mg_RAl samples obtained by rehydratation provide similar results as shown above.[17] The preparative method (anion-exchange or rehydratation) does not significantly affect the structural properties of intercalated LDH.

Thermal behaviour of LDH (Appendix II) allows identifying mixtures of intercalated and non-intercalated LDH. The analysis of porphyrin intercalates is not a trivial task, because the simple fact of "immobilization" of porphyrin in the solid product does not necessarily mean their intercalation. HT-XRD can serve as a specific tool for the ascertainment of the behavior of porphyrin anions.

The HT-XRD results show that the basal diffraction lines are shifted toward a lower *d*-spacing and the *003* line intensity increases due to the improved structural ordering after the weakly bonded interlayer water is released. Mg_2Al LDH intercalated with TPPC and

TPPS are stable up to 400ºC and 360ºC, respectively. The results were confirmed by TGA/DTA measurements.

The actual elemental composition of LDH influences their thermal stability, e. g., the lower charged Mg_4Al LDH containing nitrate, chloride, or carbonate are stable up to 300ºC, whereas the Mg_2Al with the same anions are by at least 50ºC more stable.

4.1.2 Photophysical characterization

Ground states. The ground state absorption spectra of solid porphyrin-LDH were measured using UV-vis diffuse reflectance spectroscopy. The spectra of the TPPS-Mg_2Al LDH intercalate show characteristic porphyrin absorption bands: the Soret band at 412-415 nm and the Q-bands at 520, 555, 594, and 650 nm (Supporting Information, Figures S8, S9 in Appendix I). The absence of splitting or a spectral shift of the Soret band in the TPPS-Mg_2Al LDH samples showed that neither intercalated nor adsorbed porphyrin molecules notably aggregate and mostly, as a rule, retain their photoactive monomeric form. Similar conclusions can be inferred from the comparison of the diffuse reflectance spectra of PdTPPC-Mg_2Al and PdTPPC-Mg_2Al with 10% of AEC saturation with the absorption spectrum of monomeric PdTPPC in solution (Figure 15).

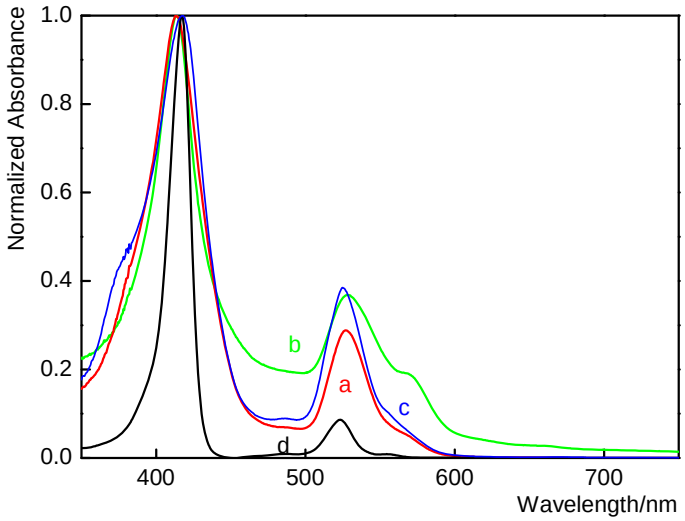

Figure 15. Normalized diffuse reflectance spectra of the PdTPPC-Mg_2Al (10% AEC) (a), PdTPPC-Mg_2Al (100% AEC) (b) and PdTPPC-Mg_2Al (10% AEC) with adsorbed PdTPPC (c) compared with the absorption spectrum of 5 μM PdTPPC in a *N,N*-dimethylformamide (d).

Although the intercalated porphyrin molecules should be more dispersed than those bound on the surface, no significant differences in the diffuse reflectance spectra of the intercalated and surface-bound porphyrins were observed.

Triplet states. The excited state dynamics of intercalated porphyrins was investigated by means of time-resolved diffuse reflectance. The triplet states of PdTPPC and TPPS in Mg_RAl LDH interact with oxygen. Figure 16 illustrates the decay of the triplet states of PdTPPC-Mg_2Al (10% AEC) and PdTPPC-Mg_2Al with adsorbed PdTPPC in nitrogen atmosphere and on air. Similar data were recorded for the TPPS intercalated samples (Supporting Information, Figure S11 in Appendix I.). The changes observed clearly demonstrate that the porphyrin molecules are accessible to oxygen even when intercalated into the solid matrix, in other words that oxygen demonstrably diffuses into the LDH matrix.

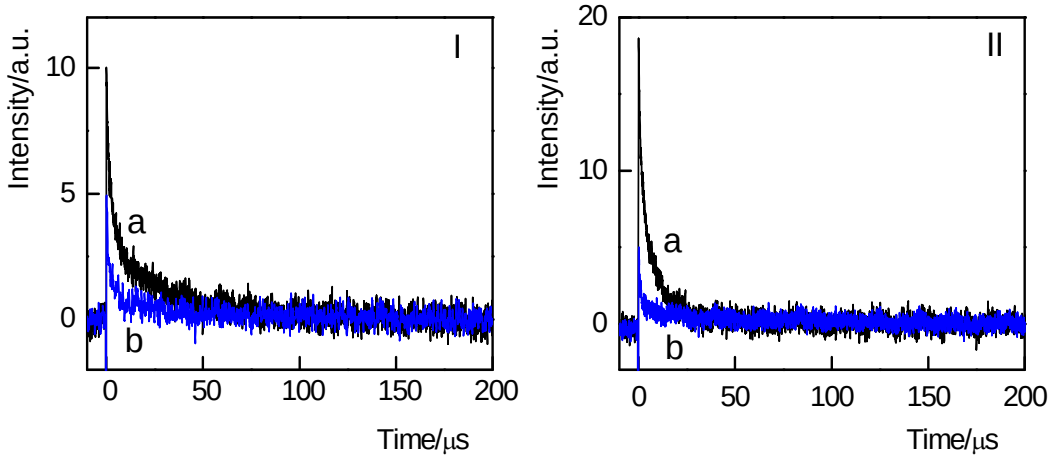

Figure 16. Decays of the triplet states of PdTPPC-Mg_2Al (10% AEC) (I) and PdTPPC-Mg_2Al with adsorbed PdTPPC (II) under N_2 (a), in air (b) (λ_{exc} = 532 nm, λ_{abs} = 480 nm).

Singlet oxygen. Photoproduction of $^1O_2$ was monitored by time-resolved measurement of its luminescence at 1270 nm. From the results plotted in Figure 17 it is evident that $^1O_2$ signals obtained for the solids containing PdTPPC are significantly larger than for those with TPPS. Evidently, PdTPPC-Mg_RAl are effective producers of $^1O_2$, regardless of whether the porphyrin molecules are intercalated or adsorbed on the surface. The measured lifetimes of $^1O_2$ lie in the 6-64 μs range, which means that the $^1O_2$ molecules

generated in the interior of LDH can diffuse out of the matrix and possible react with external substrates.

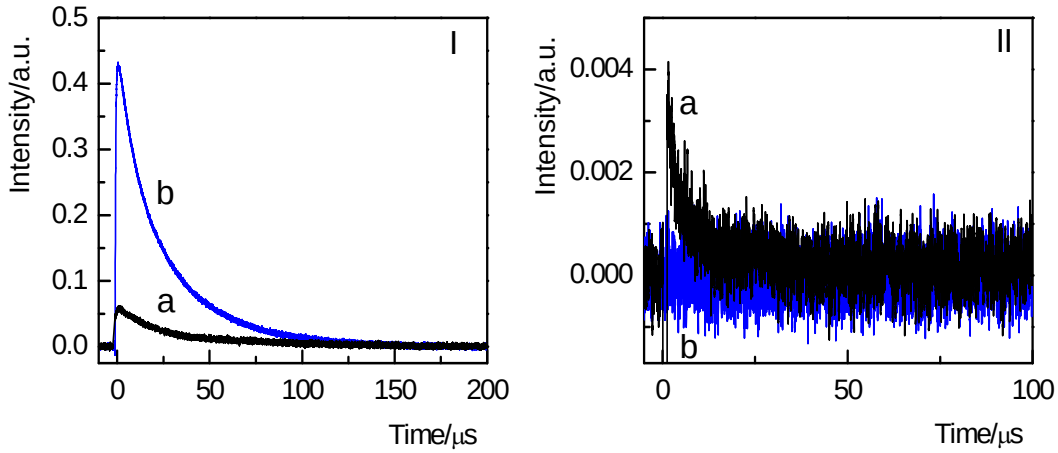

Figure 17. Time dependence of the $^1O_2$ luminescence signal at 1270 nm of PdTPPC-Mg_2Al (10% AEC) (I, a), PdTPPC-Mg_2Al with adsorbed PdTPPC (I, b), TPPS-Mg_2Al (10% AEC) (II, a), TPPS- Mg_2Al with adsorbed TPPS (II, b) in air (A: λ_{exc} = 532 nm; B: λ_{exc} = 435 nm).

Effect of subtle structural changes. In the previous paragraphs, we confirmed that the LDH host is not an inert matrix and influences the apparent lifetime of photoproduced $^1O_2$, as has already been observed for other inorganic hosts.[82,95] Hence, the structural and composition changes of the host may cause significant variations of the $^1O_2$ production. The studied systems included two Mg_2Al LDH samples with intercalated or adsorbed PdTPPC, which, after evacuation and heating (~ 70ºC) were fed with dry air or O_2. According to HT-XRD, such conditions lead to the decrease of the interlayer distance in the LDH hosts, which can be ascribed to the removal of interlayer water molecules. It was found out that the dehydration of the LDH matrices enhances the singlet oxygen quenching ability of the LDH layers and shortens the lifetime. The process can be reverted by exposing the material to ambient atmosphere. The LDH materials with intercalated PdTPPC molecules can therefore be considered as an efficient source of $^1O_2$ whose activity can be tuned by successive dehydration-rehydration of the host.

4.2 Zn_RAl LDH with intercalated porphyrins: structural arrangement

In the Appendix III, the arrangement of porphyrin molecules in the interlayer space of LDH was studied by a combination of experimental techniques and molecular dynamics simulations. Zn_RAl and Mg_RAl LDH intercalated with TPPS and ZnTPPS porphyrins were prepared as pure phases using the co-precipitation method followed by a post-synthesis hydrothermal treatment.[18] In the Zn_RAl and Mg_RAl LDH systems, the ratio can be varied from 2 to 4. Zn_RAl LDH has similar suitable properties for intercalation of porphyrin molecules as Mg_RAl LDH. Moreover, the Zn_RAl hybrids exhibit higher crystallinity than the corresponding hybrids based on Mg_RAl LDH, which allows for a more detailed structural characterization. The gain in crystallinity was accompanied with the stabilization of the Zn^{2+}/Al^{3+} ratio of 2, and with the appearance of many in-plane diffraction lines in the XRD pattern that for the first time enabled to demonstrate a structural model of the interlayer space of Zn_RAl LDH hosts. The originally used TPPS was during the hydrothermal treatment metallated to ZnTPPS.

4.2.1 Structural characterization

The porphyrin-LDH samples were prepared at constant pH using the coprecipitation technique adjusted to small quantities of materials. It is described in detail in the Appendix III. The coprecipitation method was used because it allows intercalation of bulky molecules like porphyrins and adjustment of the M^{2+}/M^{3+} ratio for a better matching between the charge density of the hydroxide layers and the charge of the intercalated porphyrins. The coprecipitation route often viewed as a self-assembly process appears to be the most suitable method for preparing pure porphyrin-LDH materials. The properties of both Zn_RAl LDH and Mg_RAl LDH hybrids were presented.

The XRD patterns of as-prepared samples (*vide infra*) were all indexed in the rhombohedral space group $R\bar{3}m$, typical for LDH systems (Figure 18). The cell parameters, shown in Table 2, were obtained from the peak profile analysis. Splitting of 00*l* (*l*=3n) basal lines of Zn_RAl hybrids indicates the presence of two phases with close interlayer distances that are both consistent with the intercalation of porphyrin. These two

distances result from intercalation of TPPS and metalated TPPS by Zn from the layers during the coprecipitation reaction as was confirmed by XRD and UV-vis measurements. Thus, TPPS-Mg_RAl (R = 2 - 4) is characterized by a single basal spacing of 21.70 Å, while the two phases containing either TPPS or ZnTPPS within the Zn_RAl (R = 2 - 4) interlayer space result in two different basal spacings of 21.44 Å and 22.95Å, respectively.

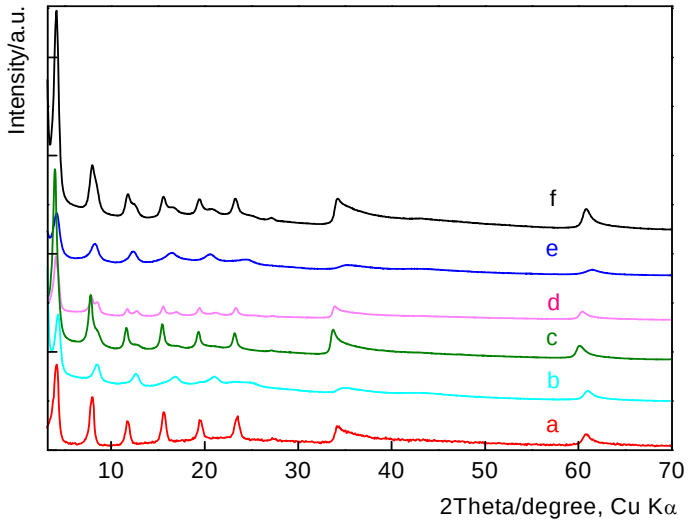

Figure 18. Powder XRD patterns of samples before the hydrothermal treatment: ZnTPPS-Zn_2Al (a), TPPS-Mg_4Al (b), TPPS-Zn_4Al (c), TPPS-Zn_3Al (d), TPPS-Mg_2Al (e), TPPS-Zn_2Al (f).

Table 2. Refined cell parameters of porphyrin-LDH intercalates and the molar M^{2+}/M^{3+} ratios obtained from XRD (R_{calc}) and elemental analysis (R_{exp}).

Samples	***a* / Å**	***c* / Å**	***d_{003}* / Å**	**R_{calc}**	**R_{exp}**
TPPS-Mg_2Al	3.0300(3)	65.093(9)	21.70	1.5	-
TPPS-Mg_2Al*	3.0351(2)	69.105(5)	23.03	1.8	1.73
TPPS-Zn_2Al	3.0548(2)	68.856(3)	22.95	1.8	1.94
	3.0548(2)	64.332(9)	21.44	-	-
(Zn)TPPS-Zn_2Al*	3.0500(1)	65.070(1)	23.01	1.7	1.90
ZnTPPS-Zn_2Al	3.0621(2)	69.215(7)	23.07	1.8	-
ZnTPPS-Zn_2Al*	3.0625(3)	69.090(1)	23.03	1.8	1.91
TPPS-Zn_3Al	3.0774(3)	68.660(1)	22.87	2.9	-
	3.0774(3)	63.440(3)	21.15	-	-
(Zn)TPPS-Zn_3Al*	3.0658(2)	68.939(8)	22.98	2.0	-
TPPS-Zn_4Al	3.0859(3)	68.909(9)	22.97	4.1	3.60
	3.0859(3)	63.740(3)	21.25	-	-
(Zn)TPPS-Zn_4Al*	3.0667(2)	69.047(4)	23.01	2.1	3.05

* stands for hydrothermally treated samples;
(Zn) indicate metalation of TPPS to ZnTPPS.

The hydrothermal treatment causes a net increase of crystallinity of all samples characterized by d_{003} values of 23 Å. The disappearance of the two-phase XRD patterns (Figure 18 and 19) and corresponding UV-vis spectra (for more detail see Appendix III) document that the originally intercalated TPPS is in the Zn_RAl LDH hosts completely metalated to ZnTPPS, while TPPS intercalated in the Mg_RAl LDH hosts remains unchanged. It is worth noting that TPPS metalation can be expected due to the high affinity of TPPS towards free Zn^{2+} in solution.

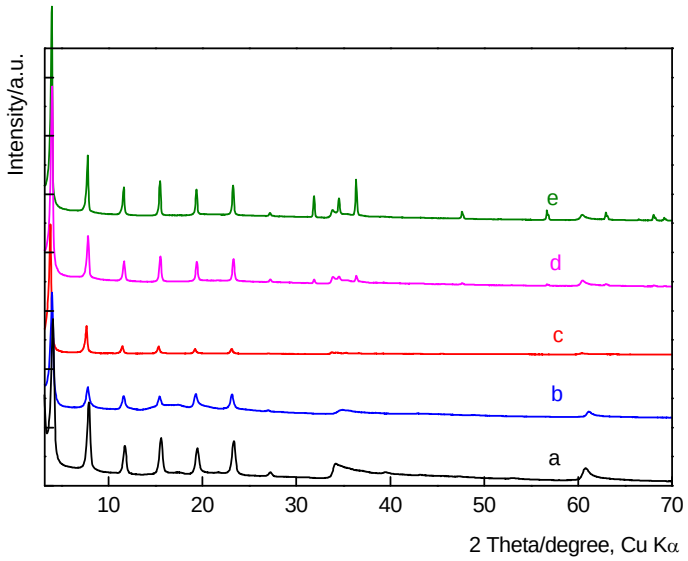

Figure 19. Powder XRD patterns of samples after the hydrothermal treatment: (Zn)TPPS-Zn_2Al (a), TPPS-Mg_2Al (b), ZnTPPS-Zn_2Al (c), (Zn)TPPS-Zn_3Al (d) and (Zn)TPPS-Zn_4Al (e).

High stability of the Zn_2Al LDH hosts under specific hydrothermal conditions indicates that the most energetically favorable host-guest charge and structure alignment is reached at this molar ratio.

Thermal stabilization of the porphyrin molecules intercalated between the hydroxide layers was investigated by DTA/TGA in conjunction with mass spectroscopy. Pure ZnTPPS starts to decompose at about 340°C and the onset is shifted to nearly 465°C after intercalation in Zn_2Al LDH. In the case of the Mg_2Al LDH hybrid, the onset is shifted from about 310 to 480°C. These results indicate that host-guest interactions between porphyrin molecules and hydroxide layers thermally stabilize the intercalated molecules.

The ZnTPPS-Zn_2Al hybrid displays very narrow 00*l* (*l*=3n) diffraction lines after the hydrothermal treatment. It is typical for high coherency materials. In addition, there is a large number of the 10*l* and 01*l* in-plane diffractions, which is quite rare in LDH-based materials (Figure 20). Indeed, these materials, especially the LDH hybrids, are known to be of low crystallinity due to anisotropic size effects (*i.e.*, platelet morphology), micro strains, and stacking faults. It can be suggested that the rigidity of the porphyrin framework has a beneficial effect on the layer ordering.

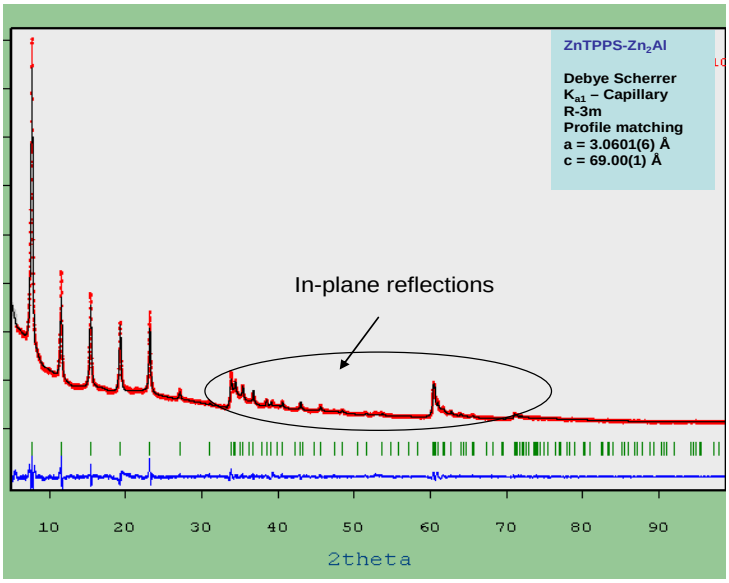

Figure 20. Profile analysis of the XRD pattern of ZnTPPS- Zn_2Al after the hydrothermal treatment recorded in the Debye-Scherrer geometry: experimental X-ray diffraction (circle), calculated (line), Bragg reflections (ticks) and difference profiles (blue).

The sstructural model was obtained by the calculation of a one-dimensional electron-density distribution along the c-stacking axis, by molecular simulations, and by HRTEM analysis. Molecular dynamic simulations were used to probe the interlayer arrangement and orientation of the intercalated ZnTPPS molecules in Zn_2Al LDH, and the obtained results are in general agreement with the experimental results. The interlayer height of 15.5 Å is fully comparable with the porphyrin size and it is in favor of titled arrangement of the porphyrin units with respect to the hydroxide layers. The porphyrin sulfonate groups are located at about 4 Å from the center of the hydroxide layers that is consistent with hydrogen bonding interactions between the sulfonate groups and OH groups of the layers. The aromatic ring system in the middle of the gallery is rather disordered. The minimized models show that the interlayer space is filled with nearly parallel porphyrin units slightly inclined with respect to the hydroxide layers (Figure 21).

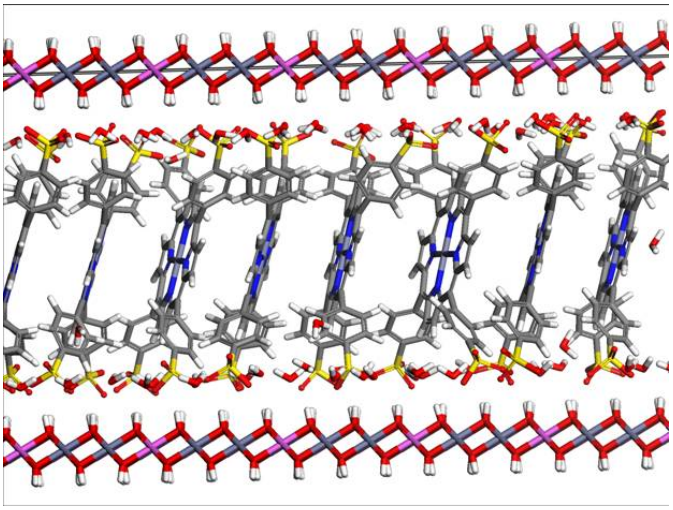

Figure 21. Molecular modeling of the interlayer space of ZnTPPS-Zn_2Al after the hydrothermal treatment.

The angle between the porphyrin plane and the layer normal is on average about 14°. The distance between two neighboring central atoms in ZnTPPS varies between 6 and 9 Å. The distance is considerably larger than the typical van der Waals separation of 3.5 Å known from the ππ stacking of aromatic compounds. The intercalation into the LDH hosts avoids extensive porphyrin aggregation.

4.2.2 Photophysical characterization

The presented results document that the LDH hosts are well-suited for accommodating porphyrin molecules. Evidently, intercalation of TPPS and ZnTPPS into the solid hosts does not significantly alter the shape of the Soret band, but only broadens it. The UV-vis spectra of intercalated porphyrins are similar to those of monomeric porphyrin solutions. Thus, extensive porphyrin aggregation, a process that often occurs in solutions and on solid templates, can be ruled out.[79]

Figure 22 depicts the $^1O_2$ luminescence recorded after the laser excitation of Mg_2Al LDH intercalated with TPPS. Since pure LDH hosts do not exhibit any $^1O_2$ luminescence, it is evident that ^1O is generated solely by the porphyrin photosensitized reaction. The effective lifetime of $^1O_2$ recovered from the monoexponential fits is 16 μs and it is comparable to the data reported in the Chapter 4.1.2. Surprisingly, the formation of $^1O_2$ was observed only for the porphyrin hybrids based on Mg_2Al LDH hosts (Figure 22),

while Zn_2Al LDH containing ZnTPPS do not produce any measurable amount of this species. The lifetimes of $^1O_2$ are evidently affected by Zn- and Al-coordinated OH groups oriented toward the interlayer space in a way leading to effective quenching of $^1O_2$. So far, there is no explanation of this effect, because both TPPS and ZnTPPS are sensitizers with high quantum yields of the $^1O_2$ formation in aqueous solutions. The hydrothermal treatment did not measurably influence the lifetime of $^1O_2$. According to the experimental results, the best photosensitizing LDH materials are based on the Mg_RAl LDH hosts.

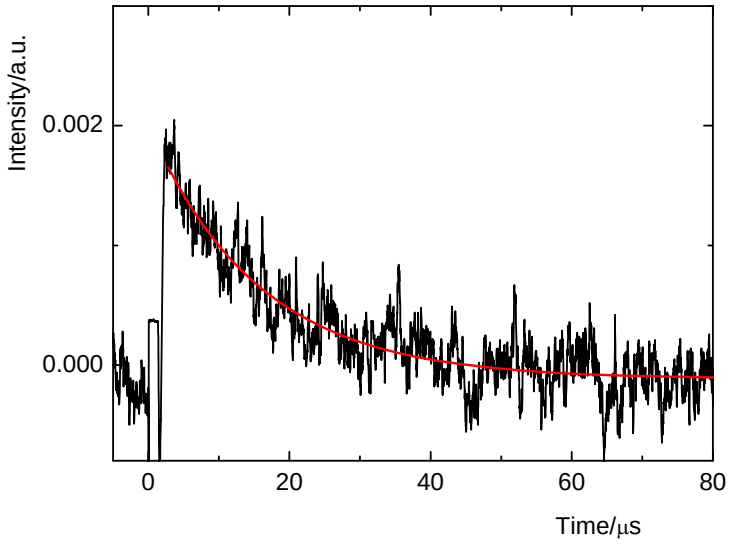

Figure 22. Time dependence of the $^1O_2$ luminescence signal at 1270 nm of Mg_2Al-TPPS (λ_{exc}= 425 nm, ~1 mJ). The smoothed line (red) is a least squares monoexponential fit.

4.3 Porphyrin-LDH /polymer composites

Appendix IV describes preparation and photophysical properties of novel composites consisting of porphyrin-LDH fillers dispersed in polyurethane (PU) or poly(butylene succinate) (PBS) polymers. The objective of this paper was to combine two aspects of the LDH chemistry, the nanocontainer and nanofiller functions, to prepare porphyrin-LDH/polymer composites for photosensitizing coatings.[61] It was established that the polymers do not significantly block diffusion of oxygen and that the triplet states of porphyrins in the films have sufficiently long lifetimes to produce singlet oxygen on irradiation by visible light. The molar ratios of employed LDH ($M^{2+} = Mg^{2+}$, Zn^{2+}) equal to 2 or 3 for which a high concentration of the intercalated porphyrin molecules can be attained. Photosensitizers PdTPPC and TPPS were chosen because they produce high amounts of $^1O_2$ upon irradiation. Owing to the softness and low gas barrier properties combined with their biodegradability, both polymers are promising materials for the above mentioned purpose.

4.3.1 Structural characterization

The first part of the Appendix IV is focused on the preparation and characterization of porphyrin-LDH reference materials, namely PdTPPC-Zn_RAl and corresponding filler materials porphyrin-Zn_RAl and porphyrin-Mg_2Al. The synthesis of these materials was carried out by coprecipitation. PdTPPC-Zn_RAl reference materials were investigated in order to get structural information on the location of the PdTPPC porphyrin molecules between LDH layers.

The PdTPPC-Zn_RAl reference samples show structural results from X-ray and HRTEM measurment similar to those presented in the Chapter 4.2.1. As usually observed, a post-synthesis hydrothermal treatment has a benifical effect on the crystallinity of the samples. The EXAFS technique allowed more detailed structural characterization of PdTPPC-Zn_2Al LDH. The Pd K-edges spectra are identical to those of pure PdTPPC indicating that PdTPPC retains its molecular structure once

intercalated into the LDH host. The results also indicate that intercalated PdTPPC molecules are spaced apart by at least ~ 6 Å.

The porphyrin-LDH fillers were characterized to get information on the extent of intercalation. In order to avoid extensive aggregation of porphyrin-LDH particles and get a good dispersion within the polymer matrix, either no aging or a short ageing time was applied for the preparation of porphyrin-LDH fillers. Accordingly, the crystallinity of porphyrin-LDH fillers (Figure 23) was found poorer than that of the porphyrin-LDH references. Yet, from the positions of the diffraction lines, the formation of porphyrin-intercalated LDH phases was confirmed in all cases.

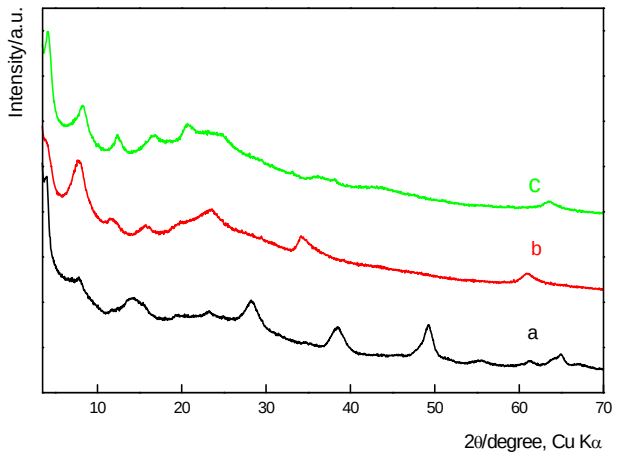

Figure 23. Powder XRD patterns of the porphyrin-LDH fillers: TPPS-Mg_2Al, no aging (a), PdTPPC-Zn_2Al, no aging (b), PdTPPC-Mg_2Al, aged for 12 h (c).

In the second part, porphyrin-LDH/polymer composites were prepared either by the solvent cast/cross-linking technique or by melt-compounding with different porphyrin-LDH filler loadings. XRD of composites (Figure 24) show poor signals partly due to the low loadings of porphyrin-LDH fillers (0.4 - 1 w/w %.). The faint diffractions at low 2θ angles can be assigned to porphyrin-LDH indicating that the intercalated structure remains in the composite. Whereas cationic clay particles easily exfoliate when dispersed into polymers, exfoliation is usually not observed with LDH. This is due to strong electrostatic interactions between the LDH hydroxide layers interlayer anions and resulting from the high layer charge density of the LDH hydroxide layers.

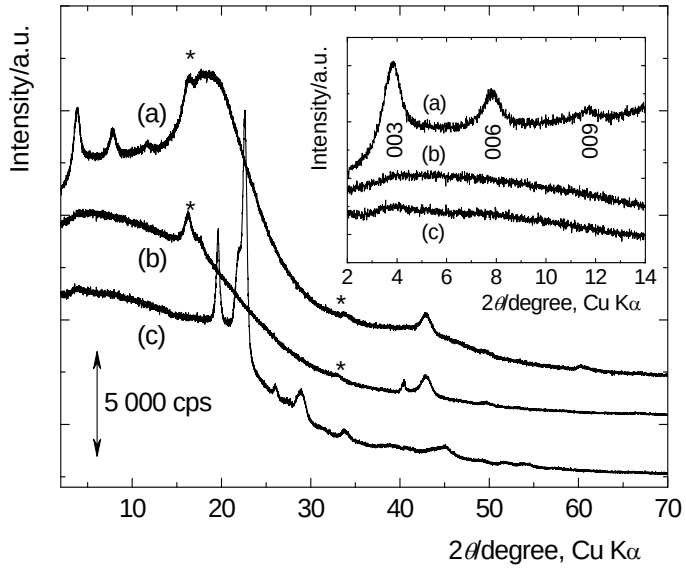

Figure 24. Powder XRD patterns of representative porphyrin-LDH/polymer composites: (a) PdTPPC-Zn_3Al/PU, (b) TPPS-Mg_2Al/PU, (c) PdTPPC-Zn_2Al/PBS. The peaks labeled as * are due to a Mylar foil used as a support. The inset shows the *00l* diffraction peaks at low *2θ* angles. The curves are shifted for clarity.

With the goal to more precisely characterize the nanostructure of the composites, were performed SAXS experiments, the fillers are present in the polymer simultaneously as isolated platelets and as particles containing more hydroxide layers (thickness of about 10-15nm). The morphology and dispersion degree of the PU composite films was investigated by TEM/BF. Although LDH fillers and PU are partially phase separated, their compatibility is quite good as the matrix tended to encapsulate single LDH particles and/or sheets, which is clearly observed at higher-magnification micrographs (Figure 25). Both XRD and TEM measurements indicate a good dispersion of porphyrin-LDH fillers into the polymer matrices and that the porphyrin molecules remain intercalated within the LDH layers.

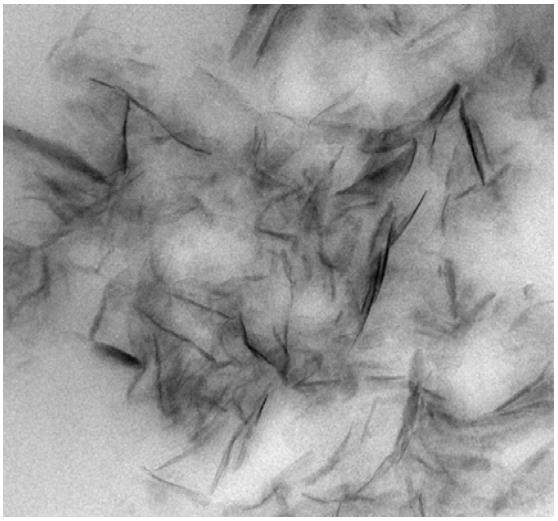

Figure 25. TEM/bright field micrographs of the PdTPPC-Zn_3Al/PU composite.

4.3.2 Photophysical characterization

Absorption spectra that exclude porphyrin aggregation are good prerequisites for the fabrication of photoactive polymer composites. The absorption spectra of the composites confirm the identity of intercalated porphyrins. The Q-bands of PdTPPC-Zn_RAl/PU (R = 2, 3) at 524 and 555 nm are slightly shifted, resolved, and narrower than those of PdTPPC-Zn_RAl reference samples (Figure 26). This can be attributed to the effect of the PU matrix because the LDH nanoparticles are partially delaminated. In contrast, PdTPPC-Zn_2Al/PBS is spectrally similar to PdTPPC-Zn_RAl which is consistent with the worse dispersion of LDH particles in PBS than in PU.

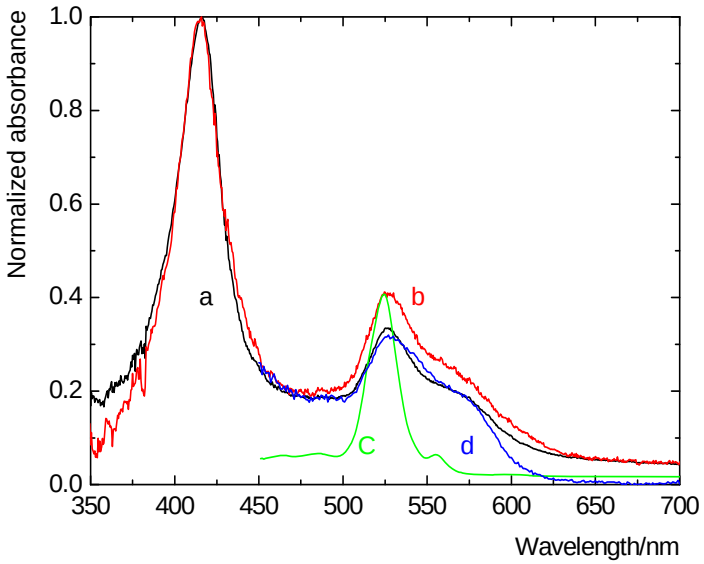

Figure 26. Normalized absorption spectra: PdTPPC-Zn_2Al (a); PdTPPC-Zn_2Al after hydrothermal treatment (b); PdTPPC-Zn_2Al/PU (c), PdTPPC-Zn_2Al/PBS (d).

As has already been described in the previous (Chapter 4.1.2 and 4.2.2.), both TPPS and PdTPPC intercalated in Mg_RAl LDH have suitable photosensitizing properties. The references PdTPPC-Zn_RAl show similar photosensitizing activity like previous powder samples. As composition and post-synthesis treatment of LDH do not appear to affect the productivity of the $^1O_2$ formation, the usage of less crystalline fillers is a good choice for obtaining well-dispersed LDH in the polymer matrix while keeping high yields $^1O_2$.

The excited state dynamics of the porphyrin molecules in polymer composites was probed by nanosecond laser flash photolysis. The triplet state lifetimes of TPPS in Mg_2Al/PU decrease from 1.4 – 3.0 ms in vacuum to 60 -100 μs in oxygen atmosphere. Similar behavior is observed for the PdTPPC-LDH/PU and PdTPPC-LDH/PBS composites, lifetimes of the triplet states in oxygen atmosphere are about 10-200 μs. The observed quenching by oxygen demonstrates that porphyrins in the triplet states are accessible to oxygen even when imbedded in the polymer matrix. The composites containing PdTPPC are better producers of $^1O_2$ than those with TPPS. It can be ascribed to the higher yield of the triplet state formation of Pd porphyrins.

The measured lifetime of $^1O_2$ in oxygen atmosphere lays between 30-80 μs for all hereinbefore composites. Summing up the results, the irradiated surface and the bulk of the composite films are filled with photoproduced $^1O_2$ molecules. The photosensitizing activity of used porphyrins is affected by the polymer matrix, however, the placement of TPPS

molecules in the LDH hosts shields the molecules from the polymer and positively affects the $^1O_2$ productivity. The polymers do not significantly block diffusion of oxygen and the triplet states of the intercalated porphyrins in the composite films have lifetimes long enough to produce $^1O_2$ upon irradiation by visible light.

5 Conclusions

New photoactive hybrids derived from LDH and porphyrins were prepared. Moreover, their structural and photophysical properties were investigated. One of the most important outcomes of this study is that LDH are convenient inorganic carriers for porphyrin sensitizers. It was also proved that LDH are good nanofillers and nanocontainers for the fabrication of functional polymer composites.

The obtained results can be summarized as follows.

1. Intercalation of porphyrins into Mg_RAl and Zn_RAl LDH hosts by the coprecipitation method followed by hydrothermal treatment is the most suitable method for obtaining pure and well crystalline intercalates.
2. The structural models indicate that the porphyrin planes are slightly inclined with respect to the hydroxide layers. The ZnTPPS porphyrin units are titled with respect to the hydroxide layer normal with an average angle of about 14°. The rigid framework of ZnTPPS has a beneficial effect on the ordering of the Zn_RA LDH hydroxide layers.
3. The porphyrin-LDH fillers are well dispersed in polymer matrices and the porphyrins remain intercalated between LDH layers.
4. Porphyrins intercalated in LDH are thermally more stable than free porphyrin molecules because the host-guest interactions stabilize the porphyrin molecules.
5. The porphyrin molecules intercalated into LDH can be effectively excited to the corresponding triplet states. These states are accessible for oxygen molecules to generate singlet oxygen. Intercalation into the LDH hosts avoids extensive porphyrin aggregation and sustains the photophysical properties of porphyrins.
6. Mg_RAl LDH with both intercalated and adsorbed PdTPPC or TPPS are efficient producers of singlet oxygen. TPPS-Mg_RAl hybrids produce $^1O_2$, while no measurable amount of singlet oxygen was found for Zn_RAl LDH-based hybrids.
7. Dehydration of the Mg_RAl LDH matrices enhances its singlet oxygen quenching capacity and inhibits the production of the $^1O_2$ molecules, a process that can be reverted by exposing the material to atmosphere humidity.
8. On account of the long lifetime of $^1O_2$ (16-80 μs) produced by the porphyrin-LDH powders and films, the singlet oxygen molecules generated in the interior of the

LDH matrix can diffuse out of the solid matrix. The cytotoxic effects of singlet oxygen on the composite surface will be predominantly governed by the $^1O_2$ molecules produced in the narrow layer of the polymer composite.

9. The presented composites allow construction of photoactive surfaces with a control of the $^1O_2$ concentration by porphyrin-LDH filler loading and by the amount of intercalated porphyrin within the LDH hosts.
10. The porphyrin-LDH/polymer composites provide a platform for the fabrication of bactericidal surfaces under visible light.

All the presented results are included in the published papers (Appendix I, II, III, IV and references 17, 94).

6 References

1. C. Sanchez, B. Julián, P. Belleville, M. Popall, *J. Mater. Chem.* **2005**, *15*, 3559-3592.
2. L. Latterini, M. Nocchetti, G. G. Aloisi, U. Constantino, F. Elisei, *Inorg. Chim. Acta* **2007**, *360*, 728-740.
3. G. Kickelbick, *Hybrid Materials*, *Synthesis, Characterization, and Applications* [online], Ed. G. Kickelbick, Wiley-VCH, **2006** [cit. 2010-08-15]. Available from: <http://books.google.cz/books?id=RPBgw0zicgMC&printsec=frontcover&dq=.+Kickelbick#v=onepage&q&f=false>
4. M. Wark, *in The Porphyrin Handbook, Pophyrins and Phthalocyanines Encapsulated in Inorganic Host Materials*, p. 247-283, Vol. 17, Eds. K. M. Kadish, K. M. Smith, R. Guilard, Elsevier Science, New York, **2003**.
5. K. Lang, P. Kubát, J. Mosinger, J. Bujdák, M. Hof, P. Janda, J. Sýkora, N. Iyi, *Phys. Chem. Chem. Phys*. **2008**, *10*, 4429-4434.
6. V. Rives, M. A. Ulibarri, *Coord. Chem. Rev*. **1999**, *181*, 61-120.
7. F. Leroux, *J. Nanosci. Nano Techn.* **2006**, *6*, 303-315.
8. U. Costantino, V. Bugatti, G. Gorrasi, F. Montanari, M. Nocchetti, L. Tamaro, V. Vittoria, *ACS Appl. Mater. Inter.* **2009***, 1*, 668-677.
9. A. L. Troutier-Thuilliez, C. Taviot-Guého, J. Cellier, H. Hintze-Bruening, F. Leroux, *Prog. Org. Coat.* **2009**, *64*, 182-192.
10. H. Hintze-Bruening, A. L. Troutier-Thuilliez, F. Leroux, *Prog. Org. Coat.* **2009**, *64*, 193-204.
11. A. Illaik, C. Taviot-Guého, J. Lavis, S. Commereuc, V. Verney, F. Leroux, *Chem. Mater.* **2008,** *20,* 4854–4860.
12. M. Halma, K. A. D de Freitas Castro, C. Taviot-Guého, V. Prévot, C. Forano, F. Wypych, S. Nakagaki, *J. Catal.* **2008**, *237*, 233-243.
13. T. J. Pinnavaia, M. Chibwe, Vera. R. L. Constantino, S. K. Yun, *Appl. Clay Sci.* **1995**, *10*, 117-129.
14. C. Mousty, *Appl. Clay Sci.* **2004**, *27*, 159-177.
15 D. Shan, S. Cosnier, C. Mousty, *Anal. Chem.* **2003**, *75*, 3872-3879.

16. K. Lang, P. Bezdička, J. L. Bourdelande, J. Hernando, I. Jirka, E. Káfuňková, F. Kovanda, P. Kubát, J. Mosinger, D. M. Wagnerová, *Chem. Mater.* **2007**, *19*, 3822-3829.
17. F. Kovanda, E. Káfuňková, T. Rojka, K. Lang, *Mater. Structure* **2008***, 15*, 28-31.
18. E. Káfuňková, C. Taviot-Guého, P. Bezdička, M. Klementová, P. Kovář, P. Kubát, J. Mosinger, M. Pospíšil, K. Lang, *Chem. Mater.* **2010**, *22*, 2481-2490.
19. R. Bonnett, M.-A. Krysteva, I.-G. Lalov , S.-V. Artarsky, *Water Research*. **2006**, *40*, 1269-1275.
20. Y. Itagaki, K. Deki, S.-I. Nakashima, Y. Sadaoka, *Sens. Actuator B: Chem.* **2005**, *108*, 393-397.
21. J. Mosinger, O. Jirsák, P. Kubát, K. Lang, B. Mosinger, *J. Mater. Chem*. **2007**, *17*, 164-166.
22. M. Krouit, R. Granet, P. Krausz, *Eur. Polymer J.* **2009**, *45*, 1250-1259.
23. M. Krouit, R. Granet, P. Branland, B. Verneuil, P. Krausz, *Bioorg. Med. Chem. Lett*. **2006**, *16*, 1651-1655.
24. D. G. Evans, R. C. T. Slade, *in Layered Double Hydroxides*, *Struct. Bond*. **2006**, *119*, p. 1-87, Eds. X. Duan, D. G. Evans, Springer-Verlag, Berlin, Heidelberg, 2005.
25. J.-H. Choy, M. Mark, *in Clays Surfaces: Fundamental and Applications, Cationic and anionic clays biological applications*, p. 404-427, Eds. F. Wypych, K. G. Satyanarayana, Elsevier Ltd., the Netherlands, 2004.
26. C. Del Hoyo, *Appl. Clay Sci.* **2007**, *36*, 103-121.
27. J.-H. Choy, S.-J. Choi, J.-M. Oh, T. Park, *Appl. Clay Sci.* **2007**, *36*, 122-132.
28. R. L. Frost, M. L. Weier, M. E. Clissold, P. A. Williams, *Spectrochim. Acta Part A* **2003**, *59*, 3313-3319.
29. F. Kovanda, K. Jirátová, R. Kalousková, *in Advances in Chemistry Research, Synthetic hydrotalcite-like compounds*, p. 89-139, Vol. 1., Ed. F. L. Gerard, Nova Sicence Publishers, Inc., New York, 2006.
30. W. Feitknecht, M. Gerber, *Helv. Chim. Acta* **1942**, *25*, 131-137.
31. F. Cavani, F. Trifiro, A. Vaccari, *Catal. Today* **1991**, *11,* 173-301.
32. F. Leroux, C. Taviot-Guého, *J. Mater. Chem*. **2005,** *15*, 3628.
33. A. Van Der Pol, B. L. Mojet, E. Van De Ven, E. De Boer, *J. Phys. Chem.* **1994**, *98,* 4050-4054.

34. S. K. Yun, T. J. Pinnavaia, *Chem. Mater.* **1995**, *7*, 348-354.
35. F. Leroux, J. P. Besse, in *Clays Surfaces Fundamental and Applications*, *Layered Double Hydroxide/Polymer Nanocomposites*, p. 459-496, Eds. F. Wypych, K. G. Satyanarayana, Elsevier Ltd., the Netherlands, **2004**.
36. F. Wypych, in *Clays Surface: Fundamental and Applications, Chemical Modification of Clay Surfaces*, p. 2-56, Eds. F. Wypych, K. G. Satyanarayana, Elsevier Ltd., the Netherlands, **2004**.
37. Hydrotalcite Mineral Data [online]. [cit. 2010-06-27]. Available from: <http://www.webmineral.com/data/Hydrotalcite.shtml>
38. S. Miyata, *Clays Clay Miner.* **1980**, *28*, 50.
39. S. Miyata, *Clays Clay Miner.* **1975**, *23*, 369-375.
40. J. Olanrewaju, B. L. Newalkar, C. Mancino, S. Komarneni, *Mater. Lett.* **2000**, *45*, 307-310.
41. F. Kovanda, D. Koloušek, Z. Cílova, V. Hulinsky, *Appl. Clay Sci.* **2005,** *28,* 101-109.
42. S. K. Sharma, P. K. Kushwaha, V. K. Srivastava, S. D. Bhatt, R. V. Jasra, *Ind. Eng. Chem. Res.* **2007**, *4*, 4856-4865.
43. M. Meyn, K. Beneke, G. Lagaly, *Inorg. Chem.* **1990**, *29*, 5201-5207.
44. D. G. Evans, R. C. T. Slade, *in Layered Double Hydroxides*, *Struct. Bond*. **2006**, *119*, p. 89-119, Eds. X. Duan, D. G. Evans, Springer-Verlag, Berlin, Heidelberg, 2005.
45. N. Iyi, T. Matsumoto, Y. Kaneko, K. Kitamura, *Chem. Mater.* **2004**, *16*, 2926-2932.
46. N. Iyi, T. Sasaki, *J. Coll. and Inter. Sci.* **2008**, *322*, 237-245.
47. F. Kovanda, E. Kovacsova, D. Kolousek, *Collect. Czech. Chem. Commun.* **1999**, *64*, 1517-1528.
48. A. de Roy, C. Forano, J. P. Besse, in Layered double hydroxides: Present and future, p. 1-41, Ed. V. Rives, Nova Science Publishers, Inc., New York **2001**.
49. U. Constantino, F. Marmottini, M. Nocchetti, R. Vivani, *Eur. J. Inorg. Chem.* **1998**, *10*, 1439-1446.
50. M. Akinc, N. Jongen, J. Lemaitre, H. Hofmann, J. *European Ceramic Society* **1998**, *18*, 1559-1564.
51. M. M. Rao, B. R. Reddy, M. Jayalakshmi, V. S. Jaya, B. Sridhar, *Mater. Res. Bull.* **2005**, *40*, 347-359.
52. M. Adachi-Pagano, C. Forano, J. P. Besse, *J. Mater. Chem.* **2003**, *13*, 1988–1993.

53. Z. Liu, R. Ma, M. Osada, N. Iyi, Y. Ebina, K. Takada, T. Sasaki, *J. Am. Chem. Soc.* **2006**, *128*, 4872-4880.
54. H. P. Boehm, J. Steinle, C. Vieweger, *Angew. Chem. Int*. **1977***, 16*, 265-269.
55. K. El. Malki, A. De Roy, J. P. Besse, *Eur. J. Solid State Inorg. Chem.* **1989**, *26,* 339-344.
56. C. Sanchez, L. Rozes, F. Ribot, C. Laberty-Robert, D. Grossso, C. Sassoye, C. Boissiere, L. Nicole, *Comptes Rendus Chimie* **2009**, *13*, 3-33.
57. J. Gopalakrishnan, *Chem. Mater.* **1995**, *7*, 1265-1275.
58. M. A. Aramendía, V. Borau, C. Jiménez, J. M. Marinas, J. R. Ruiz, F. J. Urbano*, J. Solid State Chem* .**2002**, *168*, 156-162.
59. C. Taviot-Guého, F. Leroux, *in Layered Double Hydroxides*, *Struct. Bond*. **2006**, *119*, p. 121-159, Eds. X. Duan, D. G. Evans, Springer-Verlag, Berlin, Heidelberg, 2005.
60. H. Fisher, *Mater. Sci. Eng. C* **2003**, *23*, 763-772.
61. E. Káfuňková, K. Lang, P. Kubát, M. Klementová, J. Mosinger, M. Šlouf, A. L. Troutier-Thuilliez, F. Leroux, V. Verney, C. Taviot-Guého, *J. Mater. Chem.* **2010**, DOI: 10.1039/C0JM00746C.
62. M. Zammarano, S. Bellayer, J. W. Gilman, M. Franceschi, F. L. Beyer, R. H. Harris, S Meriani, *Polymer* **2006**, *47*, 652-662.
63. Y.-J. Lin, J. Wang, D. G. Evans, D. Li. Lin, *J. Phys. Chem. Solids* **2006**, *67*, 998-1001.
64. Y.-J. Lin, D.-Q. Li, D. G. Evans, X. Duan, *Polym. Degrad. Stab.* **2005**, *88*, 286-293.
65. F. Li, X. Duan, *in Layered Double Hydroxides*, *Struct. Bond*. **2006**, *119*, p. 193-223, Eds. X. Duan, D. G. Evans, Springer-Verlag, Berlin, Heidelberg, 2005.
66. G. Fetter, E. Ramos, M. T. Olguín, P. Bosch, T. López, S. J. Bulbulian, *Radioanal. Nucl. Chem.* **1997**, *221,* 63-75.
67. M.A. Ulibarri, M. del Carmen-Hermosín, in *Layered Double Hydroxides: Present and Future*, *Layered Double Hydroxide in Water Decontamination*, p. 285-321, Ed. V. Rives, Nova Science Publishers, New York, **2001**.
68. D. G. Evans, X. Duan, *Chem. Commun*. **2006**, 485-496.
69. K. M. Kadish, K. M. Smith, R. Guilard, *The Porphyrin Handbook, Applications: Past, Present and Future,* Vol. 6, Academic Press, London, **2000**.
70. K. Lang, J. Mosinger, D. M. Wagnerová, *Coord. Chem. Rev.* **2004**, *248*, 321-350.
71. K. Lang, J. Mosinger, D. M. Wagnerová, *Chem. Listy* **2005**, *99*, 211-221.

72. Z. Juračková, in *Volné radikály a antioxidanty v medicíně (I),* p. 55-71, Ed. Z Juračková, Slovak Academic Press, Bratislava, **1998.**
73. M. C DeRosa, R. J. Crutchley, *Coord. Chem. Rev.* **2002**, *352*, 233-234.
74. I. J. MacDonald, T. J. Dougherty, *J. Porphyrins Phtalocyanines* **2001**, *5,* 105-129.
75. K. Lang, J. Mosinger, D.M. Wagnerova, *Chem. Listy* **2006**, *100*, 169-177.
76. E. A. Lukyanets, *J. Porphyrins Phthalocyanines* **1999**, *3*, 424-432.
77. S. Wang ,R. Gao, F. Zhou, M. Selke, *J. Mater. Chem.* **2004**, *14,* 487-493.
78. R. Rychtářiková, G. Kuncová, *Chem. Listy* **2009**, *103*, 800-813.
79. W. Xu, H. Guo, D. L. Akins, *J. Phys. Chem. B* **2001**, *105*, 7686-7696.
80. S. Tagaki, M. Eguchi, D. A. Tryk, H. Inoue, *J. Photochem. Photobiol. C* **2006**, *7*, 104-110.
81. V. Chirvony V. Bolotin, E. Matveeva, V. Parkhutik, *J. Photochem. Photobiol A: Chemistry* **2006**, *181*, 106-113.
82. A. Pace, E. L. Clennan, *J. Am. Chem. Soc.* **2002**, *124*, 11236-11237.
83. A.I. Khan, D. O´Hare, *J. Mater. Chem.* **2002**, *12*, 3191-3198.
84 E. Giannelis, in *Nanoporous Layered Materials in Materials Chemistry*, Eds. ACS Symp. Series 1995, *245*, 259-281.
85. Y. J. Feng, G. R. Williams, F. Leroux, C. Taviot-Guého, D. O`Hare, *Chem. Mater.* **2006**, *18*, 4312-4318.
86. D. G. Evans, R. C. T. Slade, *in Layered Double Hydroxides*, *Struct. Bond*. **2006**, *119*, p. 161-192, Eds. X. Duan, D. G. Evans, Springer-Verlag, Berlin, Heidelberg, 2005.
87. I. Y. Park, K. Kuroda, C. Kato, *Chem. Lett.* **1989**, 2057.
88. K. A. Carrado, J. E. Forman, R. E. Botto, R. E. Winans, *Chem. Mater.* **1993,** *5*, 472-478.
89. P. K. Dutta, M. Puri, *J. Phys. Chem.* **1989**, *93*, 376-380.
90. L. Ukrainczyk, M. Chibwe, T. J. Pinnavaia, S. A. Boyd, *J. Phys. Chem.* **1994**, *98*, 2668-2676.
91. C. A. S. Barbosa, A. M. D. C. Ferreira, V. R. L. Constantino, *Eur. J. Inog. Chem.* **2005**, 1577-1584.
92. S. Bonnet, C. Forano, A. de Roy, J. P. Besse, *Chem. Mater.* **1996**, *8*, 1962-1968.
93. A. Píšková, P. Bezdička, D. Hradil, E. Káfuňková, K. Lang, E. Večerníková, F. Kovanda, T. Grygar, *Appl. Clay Sci*. **2010**, *49*, 363-371.

94. P. Kovář, M. Pospíšil, E. Káfuňková, K. Lang, F. Kovanda, *J. Mol. Model.* **2010**, *16*, 213-233.

95. K. K. Iu, J. K. Thomas, *J. Am. Chem. Soc.* **1990**, *112*, 3319-3325.

7 Appendices

7.1 Publications (articles)

List of publication related to the Thesis:

Paper # I.

K. Lang, P. Bezdička, J. L. Bourdelande, J. Hernando, I. Jirka, ***E. Káfuňková****, F. Kovanda, P. Kubát, J. Mosinger, D. M. Wagnerová:*

Layered Double Hydroxides with Intercalated Porphyrins as Photofunctional Materials: Subtle Structural Changes Modify Singlet Oxygen Production

Chemistry of Materials **2007**, *19*, 3822-3829

Appendix I

Paper # II.

A. Píšková, P. Bezdička, D. Hradil, ***E. Káfuňková****, K. Lang, E. Večerníková, F. Kovanda, T. Grygar:*

High-temperature XRD as a tool for characterization of smectites, layered double hydroxides, and their intercalates with porphyrins

Applied Clay Science **2010**, *49*, 363-371

Appendix II

Paper # III.

E. Káfuňková*, C. Taviot-Guého, P. Bezdička, M. Klementová, P. Kovář, P. Kubát, J. Mosinger, M. Pospíšil, K. Lang:* Porphyrins Intercalated in Zn/Al and Mg/Al Layered Double Hydroxides: Properties and Structural Arrangement

Chemistry of Materials **2010**, *22*, 2481-2490

Appendix III

Paper # IV.

E. Káfuňková*, K. Lang, P. Kubát, M. Klementová, J. Mosinger, M. Šlouf, A. L. Troutier-Thuilliez, F. Leroux, V. Verney, C. Taviot-Guého:*

Porphyrin-Layered Double Hydroxides/Polymer Composites as Novel Ecological Photoactive Surfaces

Journal of Materials Chemistry **2010**, DOI: 10.1039/C0JM00746C

Appendix IV

Other articles:

Paper # V.

*F. Kovanda, **E. Káfuňková**, T. Rojka, K. Lang*:

Intercalation of porphyrins into Mg-Al hydrotalcite

Materials Structure in Chemistry, Biology, Physics and Technology **2008**, *15*, 28-32

Paper # VI.

*P. Kovář, M. Pospíšil, **E. Káfuňková**, K. Lang, F. Kovanda:*

Mg-Al layered double hydroxide intercalated with porphyrin anions: molecular simulations and experiments

Journal of Molecular Modeling **2010,** *16,* 213-233

My contribution to the papers:

I carried out experimental work concerning the preparation of LDH materials as well as interpretation of results related to the papers V and VI. In the papers I, II, IV, I performed the preparation of LDH samples and I significantly contributed to the structural interpretations. My contribution to the paper III was the preparation of LDH, porphyrin-LDH hybrids interpretation, and writing.

I also participated in photophysical measurements carried out in the Institute of Inorganic Chemistry of the Academy of Sciences of the Czech Republic, v.v.i. (AS CR) and J. Heyrovsky Institute of Physical Chemistry of the ASCR, v. v. i.

Appendix I

K. Lang, P. Bezdička, J. L. Bourdelande, J. Hernando, I. Jirka,

***E. Káfuňková**, F. Kovanda, P. Kubát, J. Mosinger, D. M. Wagnerová:*

Layered Double Hydroxides with Intercalated Porphyrins as Photofunctional Materials: Subtle Structural Changes Modify Singlet Oxygen Production

Chemistry of Materials **2007**, *19*, 3822-3829.

Layered Double Hydroxides with Intercalated Porphyrins as Photofunctional Materials: Subtle Structural Changes Modify Singlet Oxygen Production

Kamil Lang,*,† Petr Bezdička,† José L. Bourdelande,‡ Jordi Hernando,*,‡ Ivan Jirka,§ Eva Káfuňková,† František Kovanda,# Pavel Kubát,§ Jiří Mosinger,†,⊥ and Dana M. Wagnerová†

Institute of Inorganic Chemistry v.v.i., Academy of Sciences of the Czech Republic, 250 68 Řež, Czech Republic, Departament de Química, Universitat Autonoma de Barcelona, Bellaterra, 08193 Barcelona, Spain, J. Heyrovský Institute of Physical Chemistry v.v.i., Academy of Sciences of the Czech Republic, Dolejškova 3, 182 23 Praha 8, Czech Republic, Department of Solid State Chemistry, Institute of Chemical Technology Prague, Technická 5, 166 28 Praha 6, Czech Republic, and Faculty of Sciences, Charles University in Prague, 2030 Hlavova, 128 43 Praha 2, Czech Republic

Received February 5, 2007. Revised Manuscript Received May 11, 2007

This study presents new photofunctional materials producing singlet oxygen, $^1O_2$, and investigates the interdependence between their structural and photophysical properties. These materials consist of Mg−Al layered double hydroxides (LDH) with intercalated photosensitizers, 5,10,15,20-tetrakis(4-sulfonatophenyl)porphyrin (TPPS) or Pd(II)-5,10,15,20-tetrakis(4-carboxyphenyl)porphyrin (PdTPPC). Powder X-ray diffraction and X-ray photoelectron spectroscopies were employed to characterize the host structure and confirm intercalation of porphyrins into the interlayer space. Because the kinetic parameters of the sensitizer triplet states predetermine the formation of $^1O_2$, the excited-state kinetics of intercalated porphyrins were investigated by means of time-resolved diffuse reflectance. Comparison of the decay rates in the presence and absence of oxygen confirms that the triplet states of PdTPPC and TPPS in LDHs are quenched by oxygen. Photoproduction of $^1O_2$ was monitored by time-resolved measurement of its luminescence at 1270 nm. It was established that PdTPPC-doped LDHs are very effective producers of $^1O_2$, regardless of whether the porphyrin molecules are intercalated or adsorbed on the surface. The measured lifetimes of $^1O_2$ lie in the 6−64 μs range, which means that the $^1O_2$ molecules generated in the interior of LDHs can diffuse out of the matrix and react with a contiguous substrate. Dehydration of the LHD matrices enhances its singlet oxygen quenching capacity and inhibits the production of the long-lived $^1O_2$ molecules, a process that can be reverted by exposing the material to atmospheric humidity. Consequently, we envisage LDHs with intercalated PdTPPC as efficient $^1O_2$ sources whose oxidative activity can be modulated by successive dehydration−rehydration cycles.

Introduction

During the past decade, inorganic layered and porous materials (e.g., clays, layered double hydroxides, zeolites, sol−gel-derived matrices) have attracted attention as versatile hosts for immobilization of guest species.[1−3] Utilization of these hosts in the design of novel photofunctional materials emerged as a prospective area of research that found applications in energy storage, photocatalysis, nonlinear optics, and biology.[3−5] A feasible way of creating photofunctional layered materials is the intercalation of sensitizer molecules into the interlayer space of the host. Embedding of an active species within a solid matrix not only provides an easy-to-apply photonic material but may also minimize eventual leakage and retard degradation of sensitizer molecules. Because the guest molecules are constrained within the solid environment, their inherent photophysical and photochemical properties might be altered, and the photonic activity of the resulting composite material cannot be directly extrapolated from the known behavior of the sensitizer in solution.[6] Indeed, such properties will depend on the type and charge density of the solid host, and on the concentration, charge, and size of the intercalated sensitizer molecules.

Porphyrins and related macrocycles are well-known as photosensitizers producing singlet oxygen, $^1O_2$, a short-lived, highly reactive form of molecular oxygen. Photosensitized production of $^1O_2$ consists of excitation of the sensitizer by light to the triplet state followed by energy transfer to the ground electronic state of oxygen ($O_2(^3\Sigma_g)$) that, in turn,

* Corresponding author. E-mail: lang@iic.cas.cz (K.L.); jordi.hernando@uab.es (J.H.).
† Institute of Inorganic Chemistry v.v.i., Academy of Sciences of the Czech Republic.
‡ Universitat Autonoma de Barcelona.
§ J. Heyrovský Institute of Physical Chemistry v.v.i., Academy of Sciences of the Czech Republic.
# Institute of Chemical Technology Prague
⊥ Charles University in Prague.

(1) Rives, V.; Ulibarri, M. A. *Coord. Chem. Rev.* **1999**, *181*, 61.
(2) Evans, D. G; Duan, X. *Chem. Commun.* **2006**, 485.
(3) Ogawa, M.; Kuroda, K. *Chem. Rev.* **1995**, *95*, 399.
(4) Takagi, S.; Eguchi, M.; Tryk, D. A.; Inoue, H. *J. Photochem. Photobiol., C* **2006**, *7*, 104.
(5) Wang, S.; Gao, R.; Zhou, F.; Selke, M. *J. Mater. Chem.* **2004**, *14*, 487.
(6) Lang, K.; Mosinger, J.; Wagnerová, D. M. *Coord. Chem. Rev.* **2004**, *248*, 321.

10.1021/cm070351d CCC: $37.00
Published on Web 06/27/2007

becomes excited to the lowest singlet state ($O_2(^1\Delta_g)$). Singlet oxygen is involved in numerous oxidative processes and can cause serious damage to biological systems. On the other hand, its oxidative potential can be exploited in chemical syntheses, photodynamic treatment of cancer, and disinfection.[6−8] Therefore, the design and building of new operative singlet oxygen sources is of technological relevance.

Although most of the reported photooxygenation reactions induced by sensitizers embedded in inorganic materials involve $^1O_2$ as the oxidizing agent, the effects of the host matrix on the singlet oxygen formation, interaction of $^1O_2$ with the host, and diffusion of $^1O_2$ toward a substrate are far from being understood.[9−12] Some evidence for the crucial role of the host have already been reported. For instance, the lifetimes of $^1O_2$ produced by sensitizer-loaded zeolites vary from 2.8 μs up to 35 μs depending on the aluminum content of the matrix.[9,10] To address such host effects, we have herein thoroughly investigated the $^1O_2$ formation activity by sensitizer-loaded layered double hydroxides.

Layered double hydroxides (LDHs), also known as hydrotalcite-like compounds, exhibit a layered crystal structure consisting of positively charged hydroxide layers and interlayers composed of anions and water molecules. The chemical composition of LDHs can be represented by the general formula $[M^{II}_{1-x}M^{III}_x(OH)_2]^{x+}[A^{n-}_{x/n}\cdot yH_2O]^{x-}$ where M^{II} and M^{III} are divalent and trivalent metal cations, A^{n-} is an n-valent anion, and x usually lies between 0.20 and 0.35. The ordering of hydroxide layers in LDHs is similar to that of brucite, $Mg(OH)_2$, where each Mg^{2+} cation is octahedrally surrounded by six OH^- anions and the resulting octahedra share edges to form infinite sheets. The isomorphous substitution of M^{II} for M^{III} results in a net positive charge, which has to be neutralized by interlayer anionic species. The binding of monovalent anions in the interlayer space is relatively weak. Therefore, an anion-exchange procedure can be applied to the synthesis of LDHs intercalated with desired anions. At the same time, the use of multivalent anions increases their binding force to the LDH matrix, which would minimize the unfavorable leakage of the intercalated species.

A large number of LDHs containing various M^{II} and M^{III} cations, as well as A^{n-} anions can be synthesized,[13−15] providing suitable inorganic structures for preparation of intercalated compounds and nanocomposite materials. To date, several attempts of porphyrin intercalation into LDHs have been reported,[16−20] but possible applications of the resulting materials in photochemistry have been rarely discussed.[21] To the best of our knowledge, no photophysical properties and singlet oxygen production activity of LDH composites have been described so far, apart from a nonphotochemical $^1O_2$ generation based on the catalyzed decomposition of hydrogen peroxide by molybdate- and tungstate-LDHs.[22]

With an intent of systematic description of porphyrin-LDHs composites with tunable photophysical properties, we investigated the optical properties of 5,10,15,20-tetrakis(4-sulfonatophenyl)porphyrin (TPPS) and Pd(II)-5,10,15,20-tetrakis(4-carboxyphenyl)porphyrin (PdTPPC) in Mg−Al LDHs. The photooxygenation ability of the porphyrin composites has been studied in the solid−gas phase and in liquid suspensions to provide algorithms for the design of new photofunctional materials. The sensitizer-doped inorganic host materials developed in this work are not only of utmost interest in terms of solid-state photophysics but also offer relevant applications as photodisinfecting materials and effective sources of $^1O_2$.

Experimental Section

Materials. The tetrasodium salt of 5,10,15,20-tetrakis(4-sulfonatophenyl)porphyrin, TPPS (Aldrich), Pd(II)-5,10,15,20-tetrakis-(4-carboxyphenyl)porphyrin, PdTPPC (Frontier Scientific Europe, Ltd., UK), $Al(NO_3)_3\cdot 9H_2O$, $AlCl_3\cdot 6H_2O$, $Mg(NO_3)_2\cdot 6H_2O$, $MgCl_2\cdot 6H_2O$, NaOH, and Na_2CO_3 (all Penta, Czech Republic) were used as purchased.

Sample Preparation. The detailed procedures of the LDH preparation are described in the Supporting Information. The obtained LDHs are represented by acronyms describing the elemental composition, molar ratios of the constituents (Mg:Al), and interlayer anions, i.e., Mg4Al2-NO_3 (idealized formula is $Mg_4Al_2(OH)_{12}(NO_3)_2\cdot 4H_2O$), Mg8Al2-$NO_3$ ($Mg_8Al_2(OH)_{20}(NO_3)_2\cdot 4H_2O$), Mg4Al2-Cl ($Mg_4Al_2(OH)_{12}Cl_2\cdot 4H_2O$), and Mg4Al2-$CO_3$ ($Mg_4Al_2(OH)_{12}CO_3\cdot 4H_2O$). For the synthesis of porphyrin-doped LDHs, an anion-exchange procedure was implemented by dispersing the LDH solid in a carbonate-free aqueous solution of desired porphyrin (0.001 M, pH 9 controlled by the addition of 3 M $NaOH_{(aq)}$). The resulting suspension was sealed in a 500 mL glass bottle under N_2 and stirred for 6 days at 30 °C. Then the product was filtered off, washed with distilled water, and dried at 60 °C.

To prepare TPPS-intercalated samples, we used both nitrate and chloride LDH precursors (Mg4Al2-NO_3, Mg8Al2-NO_3, and Mg4Al2-Cl). The PdTPPC-LDHs were prepared from Mg4Al2-Cl. In both cases, the porphyrin/LDH ratio was adjusted to achieve 2, 10, and 100% exchange with respect to the theoretical anion-exchange

(7) Hamblin, M. R.; Hasan, T. *Photochem. Photobiol*. **2004**, *3*, 436.
(8) Mosinger, J.; Jirsák, O.; Kubát, P.; Lang, K.; Mosinger, B. *J. Mater. Chem*. **2007**, *17*, 164.
(9) Pace, A.; Clennan, E. L. *J. Am. Chem. Soc*. **2002**, *124*, 11236.
(10) Jockusch, S.; Sivaguru, J.; Turro, N. J.; Ramamurthy, V. *Photochem. Photobiol. Sci*. **2005**, *4*, 403.
(11) (a) Iu, K. K.; Thomas, J. K. *J. Am. Chem. Soc*. **1990**, *112*, 3319. (b) Iu, K. K.; Thomas, J. K. *J. Photochem. Photobiol., A* **1993**, *71*, 55.
(12) (a) Levin, P. P.; Costa, S. M. B. *Chem. Phys*. **2001**, *263*, 423. (b) Madhavan, D.; Pitchumani, K. *J. Photochem. Photobiol., A* **2002**, *153*, 205. (c) Hino, T.; Anzai, T.; Kuramoto, N. *Tetrahedron Lett*. **2006**, *47*, 1429. (d) Chirvony, V.; Bolotin, V.; Matveeva, E.; Parkhutik, V. *J. Photochem. Photobiol., A* **2006**, *181*, 106.
(13) Cavani, F.; Trifiro, F.; Vaccari, A. *Catal. Today* **1991**, *11*, 173.
(14) Rives, V. (Editor), *Layered Double Hydroxides: Present and Future*; Nova Science Publishers: New York, 2001; pp 251−434.
(15) Kovanda, F.; Jirátová, K.; Kalousková, R. In *Advances in Chemistry Research*; Gerard, F. L., Ed.; Nova Science Publishers: New York, 2006; Vol. 1, pp 89−139.
(16) Bonnet, S.; Forano, C.; de Roy, A.; Besse, J. P.; Maillard, P.; Momenteau, M. *Chem. Mater*. **1996**, *8*, 1962.
(17) Tong, Z.; Shichi, T.; Zhang, G.; Takagi, K. *Res. Chem. Intermed*. **2003**, *29*, 335.
(18) Barbosa, C. A. S.; Ferreira, A. M. D. C.; Constantino, V. R. L. *Eur. J. Inorg. Chem*. **2005**, 1577.
(19) Ukrainczyk, L.; Chibwe, M.; Pinnavaia, T. J.; Boyd, S. A. *J. Phys. Chem*. **1994**, *98*, 2668.
(20) Wypych, F.; Bubniak, G. A.; Halma, M.; Nakagaki, S. *J. Colloid Interface Sci*. **2003**, *264*, 203.
(21) Costantino, U.; Nocchetti, M. In *Layered Double Hydroxides: Present and Future*; Rives, V., Ed.; Nova Science Publishers, New York, 2001; pp 383−411.
(22) Sels, B. F.; De Vos, D. E.; Grobet, P. J.; Pierard, F.; Kirsch-De Mesmaeker, F.; Jacobs, P. A. *J. Phys. Chem. B* **1999**, *103*, 11114.

capacity (AEC) of the solid. Considering total anion exchange of Mg4Al2-NO_3 and Mg4Al2-Cl, these two hosts could accommodate up to 0.91 and 1.00 mmol g^{-1} of tetravalent porphyrin anions to compensate for the positive layer charge. However, 100% exchange of NO_3^- and Cl^- for porphyrins was not reached (~80% AEC was achieved at best), a result that we ascribe to the presence of competing hydroxide anions and to the limited diffusion capacity of the bulky porphyrin molecules within the LDH matrix. Resulting porphyrin-LDHs are referred to in the following way: e.g., Mg4Al2/TPPS(10) stands for the sample prepared from precursor Mg4Al2-NO3 with a Mg/Al molar ratio of 2, where 10% of NO_3^- was replaced by TPPS. Similarly, Mg4Al2/TPPS(10)-Cl indicates that Mg4Al2-Cl was used instead of Mg4Al2-NO_3. Finally, we also prepared reference samples Mg4Al2/TPPS(ads) and Mg4Al2/PdTPPC(ads) starting from Mg4Al2-CO_3 under the same procedure (stirring at 30 or 120 °C) with porphyrin/LDH molar ratios equivalent to 10% AEC. These LDHs were denoted by the suffix (ads) since CO_3^{2-} anions cannot be exchanged for porphyrins and the porphyrin molecules are adsorbed only on the LDH surface.

Characterization Techniques. The details on powder X-ray diffraction (XRD), X-ray photoelectron spectroscopy (XPS), thermal analysis TGA/DSC/DTA QMS, and diffuse reflectance UV−vis spectroscopy are described in the Supporting Information.

Diffuse Reflectance Transient Absorption Spectroscopy. Transient absorption measurements were performed by means of the diffuse reflectance accessory of a laser flash-photolysis system (LKII, Applied Photophysics) equipped with a Xe lamp, an arc pulser, a monochromator, and a photomultiplier tube (PMT, R928, Hamamatsu). The 20 ns pulsed laser beam arising from an OPO (Rainbow, Quantel) pumped by a Nd:YAG laser (Brilliant, Quantel) was used to excite solid porphyrin-LDH samples within the 400−550 nm range and a power density less than 20 mJ/cm^2. The signal from the PMT was collected in a 500 MHz oscilloscope (Agilent Infiniium) and transferred to an Acorn PCRisk station. The porphyrin-LDHs were measured in a 2 mm quartz cell equipped with a high-vacuum stopcock to ensure a controlled atmosphere during the measurements. Equilibration of the solid samples in given atmosphere was performed in two ways: (i) purging the cell with N_2, Ar, or O_2 at least for 30 min; (ii) evacuating the cell and filling it with N_2, Ar, or O_2, a treatment that was repeated three times to ensure desired atmosphere before excitation of the sample. In some experiments, the evacuated samples were heated up to 70 °C.

Singlet Oxygen Luminescence. Time-resolved near-infrared luminescence of singlet oxygen at 1270 nm was monitored using a Ge detector (Edinburgh Instruments, Ltd.) upon laser excitation of the solids with the above-mentioned laser source. The same excitation wavelengths, power densities, and sample preparation methods as in the transient absorption experiments were used. The signal from the detector was collected in a 500 MHz oscilloscope (Agilent Infiniium) and transferred to an Acorn PCRisk station for further analysis. In additional experiments, the solid porphyrin-LDHs and porphyrin-LDHs suspended in toluene or D_2O saturated with air, O_2, or Ar were excited with a Lambda Physik FL 3002 dye laser (λ_{exc} = 418−425 nm, incident energy from 0.3 to 2.1 mJ/pulse) pumped with a Lambda Physik COMPEX 102 excimer laser. In this case, the luminescence signal at 1270 nm was detected using a homemade detector unit. The signal-to-noise ratio of the signals was improved by averaging 100−500 individual traces. To eliminate the effect of laser dispersion on singlet oxygen luminescence, the signal detected under nitrogen or argon was subtracted from the signal measured for the same sample in air or in oxygen atmosphere (see the Supporting Information, Figure S13). As a result of this treatment and the limited time resolution of our detector, we cannot rely on correctness of the singlet oxygen signal during the first 5 μs after the laser pulse (see the Supporting Information for further details on data analysis).

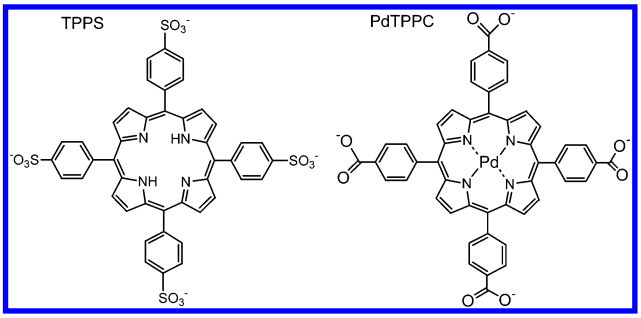

Figure 1. Molecular structures of TPPS and PdTPPC.

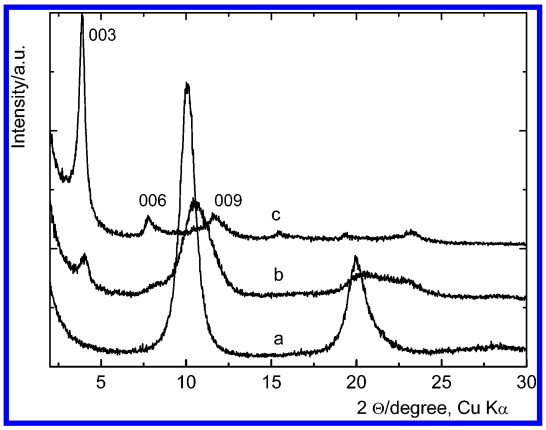

Figure 2. Powder XRD patterns of (a) Mg4Al2-NO_3, (b) Mg4Al2/TPPS-(10), and (c) Mg4Al2/TPPS(100). The patterns are shifted for clarity.

Results and Discussion

Structural Characterization. Nitrate and chloride anions intercalated into the LDH interlayer space can be replaced by a variety of anions,[23] such as tetraanionic porphyrins TPPS and PdTPPC (Figure 1). Intercalation and orientation of the porphyrin molecules within LDHs were investigated by powder X-ray diffraction (XRD).[16] The powder XRD patterns of pristine Mg4Al2-NO_3 and Mg4Al2-Cl show a well-crystallized hydrotalcite-like structure. From the position of the basal diffraction line (003) in the spectra, we estimated basal spacings to be 0.88 and 0.78 nm, respectively (Figure 2). After intercalation of bulky porphyrin molecules the diffraction lines shift toward lower 2θ°, indicating a larger basal spacing (2.08−2.30 nm) (Figure 2). Taking a 0.48 nm thickness for every hydroxide sheet, we calculated the interplanar distance between consecutive hydroxide layers to be 1.6−1.8 nm. This distance matching the size of the porphyrin anions points to a perpendicular orientation of the porphyrin plane toward the hydroxide layers and allows porphyrin peripheral sulfo or carboxy groups to interact with the hydroxyl groups of the brucite-like sheets.[16] This arrangement was not observed for Mg4Al2/TPPS(ads) and Mg4Al2/PdTPPC(ads), whose powder XRD patterns show the same diffraction lines as the Mg4Al2-CO_3 precursor with a basal spacing of 0.76 nm (see the Supporting Information, Figure S1). As already commented, CO_3^{2-} anions in Mg4Al2-CO_3 cannot be exchanged for other anions because of their

(23) Parker, L. M.; Milestone, N. B.; Newman, R. H. *Ind. Eng. Chem. Res.* **1995**, *34*, 1196.

Table 1. Mg/Al, N/Al, and S/Al Atomic Ratios Measured by XPS for Several Synthesized LDHs

composite	Mg/Al	N/Al	S/Al
Mg4Al2-NO_3	2.27	0.87,[a] 0.00[b]	0.00
Mg8Al2-NO_3	4.25	0.73,[a] 0.00[b]	0.00
Mg4Al2/TPPS(100)	2.48	0.00,[a] 0.88[b] (0.13)[c]	0.70
Mg8Al2/TPPS(100)	4.15	0.35,[a] 0.63[b] (0.06)[c]	0.54
Mg4Al2/TPPS(ads)[d]	2.18	0.00,[a] 0.11[b]	

[a] N 1s line arising from NO_3^- (and NO_2^-, see the Supporting Information). [b] N 1s line arising from TPPS. [c] Standard deviation of the N/Al ratio arising from TPPS. [d] The amount of CO_3^{2-} remains unaffected and equal to the expected stoichiometry C/Al = 0.5.

extremely high affinity toward the hydroxide layers.[23] Consequently, Mg4Al2-CO_3 behaves as a non-intercalating host with the sensitizer molecules adsorbed on the surface.

Comparison of powder XRD patterns also reports on the different anion exchange capability of LDHs with identical anions but a different Al content. The decrease in the Al content in the hydroxide layers causes a slight shrinkage of the basal spacing due to higher coulombic attraction between the layers (cf. basal spacing of 0.80 nm for Mg8Al2-NO_3 with that of 0.88 nm obtained for Mg4Al2-NO_3). As a consequence, whereas TPPS in Mg4Al2/TPPS(10) is intercalated (Figure 2), interlayer NO_3^- anions in Mg8Al2-NO_3 are not exchanged (see the Supporting Information, Figure S2). Porphyrin intercalation is partially achieved only upon heavy porphyrin loading such as in Mg8Al2/TPPS(100).

Additional insight into the arrangement of the porphyrin molecules is provided by X-ray photoelectron spectroscopy (XPS), which reports on the elemental composition of the surface region (Table 1, see the Supporting Information for detailed discussion). The Mg/Al ratios allow distinguishing LDHs matrices with the different aluminum content and are in agreement with the relative quantities of Mg^{2+} and Al^{3+} used in the synthesis. From the intensities of the N 1s, S 2p, and C 1s lines, we can determine the relative amounts of NO_3^-, porphyrin, and CO_3^{2-} ions in the solids. In the case of Mg4Al2/TPPS(100), the XPS results indicate quantitative exchange of NO_3^- by TPPS because (i) the N 1s line from NO_3^- is fully replaced by the N 1s lines from TPPS (see the Supporting Information, Figure S3), and (ii) the N(TPPS)/Al ratio of the sample is, within experimental error, close to 1. Conversely, only partial exchange of NO_3^- for the TPPS molecules occurs in Mg8Al2/TPPS(100), indicating that the capability of the hydroxide layered structure to intercalate bulky porphyrins lowers with the decreasing amount of Al^{3+} in the matrix, in agreement with the XRD results (see the Supporting Information, Figure S3). For Mg4Al2/TPPS(ads), the N 1s lines arising from TPPS are observed, whereas the C/Al ratio estimated from the C 1s line of CO_3^{2-} remains unaltered with respect to the Mg4Al2-CO_3 precursor. Hence, we postulate that only TPPS adsorption occurs in those LDH samples where the porphyrin intercalation is totally impeded.

Structural changes of LDHs provoked by external stimuli have been investigated by thermal analysis. Simultaneous TGA/DSC/DTA QMS shows the occurrence of an endothermic process up to ca. 250 °C, which is accompanied by a weight loss of 10−15% and by evolution of a gas with a mass peak $m/e = 18$. This weight loss is attributed to the release of interlayer and adsorbed water.[23−25] High-temperature XRD measurements document that assuming constant thickness of the hydroxide layer dehydration leads to a slight decrease in the interplanar distance (see the Supporting Information, Figures S4−S6). For example, the temperature increase from 25 to 125 °C induces the basal spacing (003) shift of the Mg4Al2-NO_3 host from 0.88 to 0.80 nm. A similar temperature-induced shrinkage is observed for the porphyrin-intercalated solids: e.g. the basal spacing of Mg4Al2/TPPS(100) decreases from 2.18 to 2.06 nm. It indicates that when the water content in the interlayer space is reduced, the porphyrin anions are packed more tightly to the hydroxide layers. The thermal-induced structural changes caused by the release of interlayer water are observed also after sample evacuation, as proven by XRD measurements in vacuo (see the Supporting Information, Figure S7). Evacuation of the Mg4Al2/PdTPPC(10) sample at room temperature induces a decrease in the basal spacing of the LDH phase from 0.78 to 0.76 nm, which we ascribe to the dehydration process. After heating the sample to 120 °C, a further reduction to 0.73 nm occurs along with a broadening and intensity decrease in the (006) line. These effects were attributed to an increased disorder in the layer stacking sequence.[24]

Some smaller LDH-intercalated organic anions that are perpendicularly arranged to the hydroxide layers can with the decreasing content of interlayer water adopt a parallel orientation.[26,27] In our case, however, the slight decrease in the basal spacing observed for porphyrin-intercalated LDHs indicates that the original alignment of the bulky porphyrin anions remains nearly unaltered even after dehydration of the interlayer space. Nevertheless, dehydration must affect the interaction between the intercalated sensitizer molecules and the host matrix because the contribution of water molecules to hydrogen bonding between porphyrins and the hydroxide layers is reduced.[16,28] As will be discussed below, it leads to a critical change in the photoactivity of the porphyrin-LDH composites.

Ground States. The ground state absorption spectra of solid porphyrin-LDHs have been measured using UV−vis diffuse reflectance spectroscopy. The spectra of the TPPS-LDH composites show characteristic porphyrin absorption bands: the Soret band at 412−415 nm and the Q-bands at 520, 555, 594, and 650 nm (see the Supporting Information, Figures S8 and S9). Two main features can be noticed: First, small shifts of the Soret, $Q_y(1,0)$, and $Q_y(0,0)$ bands are observed after intercalation or adsorption of TPPS, and only the maxima of the $Q_x(1,0)$ and $Q_x(0,0)$ bands vary appreciably from 578 and 633 nm in aqueous solution to 593 and 650 nm in the porphyrin-LDH samples. Second, intercalation and adsorption of TPPS to the solid hosts does not significantly alter the shape of the Soret band but only broadens it, an

(24) Yun, S. K.; Pinnavaia, T. J. *Chem. Mater*. **1995**, *7*, 348.
(25) Zhao, Y.; Li, F.; Zhang, R.; Evans, D. G.; Duan, X. *Chem. Mater*. **2002**, *14*, 4286.
(26) Kooli, F.; Chisem, I. C.; Vucelic, M.; Jones, W. *Chem. Mater*. **1996**, *8*, 1969.
(27) Reinholdt, M. X.; Kirkpatrick, R. J. *Chem. Mater*. **2006**, *18*, 2567.
(28) Marcelin, G.; Stockhausen, N. J.; Post, J. F. M.; Schutz, A. *J. Phys. Chem*. **1989**, *93*, 4646.

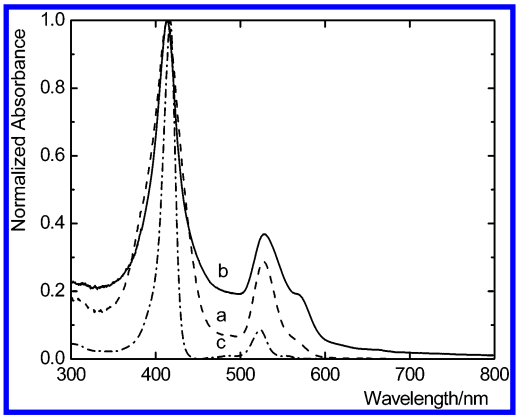

Figure 3. Normalized diffuse reflectance spectra of (a) Mg4Al2/PdTPPC-(10) and (b) Mg4Al2/PdTPPC(100) compared with (c) the absorption spectrum of 5 μM PdTPPC in a dimethylformamide solution. The solid samples were diluted with inert $BaSO_4$.

effect that we assign to a wide range of binding sites of the TPPS molecules. The absence of a splitting or a spectral shift of the Soret band in the TPPS-LDH samples allows us to rule out porphyrin aggregation known to occur for TPPS in solution and on solid hosts.[29]

Similar conclusions have been inferred from the comparison of the diffuse reflectance spectra of Mg4Al2/PdTPPC-(10) and Mg4Al2/PdTPPC(100), and the absorption spectrum of monomeric PdTPPC in solution depicted in Figure 3. Intercalation of the porphyrin molecules within the host matrix does not result in a splitting or a shift of the Soret band, which demonstrates that aggregation of intercalated PdTPPC does not occur. The Q bands exhibit a small red shift independent of the LDH loading. This behavior has also been observed for PdTPPC adsorbed on the LDH surface in Mg4Al2/PdTPPC(ads).

Although the intercalated porphyrin molecules are expected to be more dispersed than those bound on the surface, no significant differences in the diffuse reflectance spectra of intercalated- and surface-bound porphyrins have been observed. Therefore, we postulate that both sensitizers remain predominantly in their photoactive monomeric form in all porphyrin-LDHs.

Triplet States. The excited-state dynamics of the porphyrin molecules within the LDH hosts has been investigated in the solid state. Our attention was focused on the porphyrin-LDH samples with 10% AEC exchange (Mg4Al2/PdTPPC-(10) and Mg4Al2/TPPS(10)-Cl) because the samples with lower concentration of porphyrins (2% AEC) yielded small spectroscopy signals, and the samples with the highest loading (~80% AEC) were optically too dense. To explore the effect of the surrounding matrix on the triplet states of intercalated porphyrins, we have carried out transient absorption measurements on the Mg4Al2/PdTPPC(ads) and Mg4Al2/TPPS(ads) samples.

The transient difference absorption spectra of Mg4Al2/PdTPPC(10) and Mg4Al2/TPPS(10)-Cl (see the Supporting Information, Figure S10A) show the typical features of the porphyrin triplet states in solution,[30] i.e., a broad positive absorption band within ~400−550 nm arising from triplet−triplet absorption, which is partially depleted by the ground state absorption associated with the Soret (~400−420 nm) and Q-bands (~500−520 nm) (see Figure 3). Similar results were obtained for Mg4Al2/PdTPPC(ads) and Mg4Al2/TPPS-(ads). No transient signals were found for porphyrin-free LDHs. The transients of all porphyrin-LDHs decay in the microsecond scale in a nitrogen atmosphere (see the Supporting Information, Figure S10B), which supports their assignment to the porphyrin triplet states.[31] In contrast to Pd-5,10,15,20-tetraphenylporphyrin[32] and TPPS[31] in solution, the decay kinetics of transients in the solid LDHs are multiexponential. Experiments using different excitation power densities and the analysis of the ground state spectra allow ruling out the contribution of triplet−triplet annihilation[33] and porphyrin aggregation[31] to the multiexponential character. We ascribe the observed kinetics to the effect of the host resulting in (i) different intercalation and adsorption sites with distinct triplet state decay kinetics,[34] and (ii) conformational deformation of the porphyrin ring yielding two differently decaying triplet states.[35]

To analyze the kinetics of the multiexponential decays, we have employed a biexponential expression that assumes a mother−daughter kinetic pathway of two differently decaying triplet states. Although the differences between the triplet−triplet absorption spectra of these two states are minor (see the Supporting Information, Figure S11), the lifetimes of the short- and long-lived components are significantly distinct, as shown in Table 2. Comparison of the triplet state lifetimes retrieved for the porphyrin-LDH samples with those for free porphyrins in solution (τ = 65 μs for Pd-5,10,15,-20-tetraphenylporphyrin in pyridine[32] and τ = 2.50 ms for TPPS in water[31]) indicates triplet-state deactivation by interaction with the host, regardless of the location of porphyrins in the solid (intercalation or adsorption).

Table 2. Triplet and Singlet Oxygen Lifetimes of the Porphyrin-LDH Composites.

	triplet lifetimes[a]					
	N_2		air		$^1O_2$ lifetime[b]	
composite	τ_1 (μs)	τ_2 (μs)	τ_1 (μs)	τ_2 (μs)	τ_1 (μs)	τ_2 (μs)
Mg4Al2/PdTPPC(10)	3.1	50	0.96	14	15	64
Mg4Al2/PdTPPC(ads)	1.7	11	0.69	8.9	11	34
Mg4Al2/TPPS(10)-Cl	7.1	68	3.8	50	5.5	
Mg4Al2/TPPS(ads)	8.2	66		48		

[a] The triplet lifetimes are recovered from the global fit of the triplet−triplet absorption spectra. [b] The $^1O_2$ lifetime values are derived by a direct bi- or monoexponential fitting of the singlet oxygen decays within the range 5−300 μs. A more elaborate kinetic model can be used that assumes that the $^1O_2$ molecules produced by two different triplet states relax to its ground state with a single uniform rate (see the Supporting Information). Employing this model, we retrieve the following $^1O_2$ lifetimes: τ = 55 μs for Mg4Al2/PdTPPC(10) and 32 μs for Mg4Al2/PdTPPC(ads).

(29) Xu, W.; Guo, H.; Akins, D. L. *J. Phys. Chem. B* **2001**, *105*, 1543.
(30) Rodriguez, J.; Kirmaier, C.; Holten, D. *J. Am. Chem. Soc.* **1989**, *111*, 6500.
(31) García-Ortega, H.; Bourdelande, J. L.; Crusats, J.; El-Hachemi, Z.; Ribó, J. M. *J. Phys. Chem. B* **2004**, *108*, 4631−4639.
(32) Rogers, J. E.; Nguyen, K. A.; Hufnagle, D. C.; McLean, D. G.; Su, W. J.; Gossett, K. M.; Burke, A. R.; Vinogradov, S. A.; Patcher, R.; Fleitz, P. A. *J. Phys. Chem. A* **2003**, *107*, 11331−11339.
(33) Khairutdinov, R. F.; Hurst, J. K. *J. Phys. Chem. B* **1999**, *103*, 3682−3686.
(34) Levin, P. P.; Costa, S. M. B.; Lopes, J. M.; Serralha, F. N.; Ribeiro, F. R. *Spectrochim. Acta, Part A* **2000**, *56*, 1745−1757.
(35) Kyrychenko, A.; Andreasson, J.; Martennson, J.; Albinsson, B. *J. Phys. Chem B* **2002**, *106*, 12613.

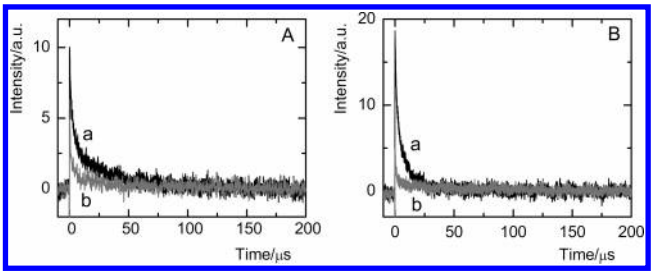

Figure 4. Decays of the triplet states of (A) Mg4Al2/PdTPPC(10) and (B) Mg4Al2/PdTPPC(ads); (a) in N_2 atmosphere and (b) in air ($\lambda_{exc} = 532$ nm, $\lambda_{abs} = 480$ nm).

The decay of the triplet states is accelerated in the presence of oxygen (Table 2). To demonstrate this well-known process,[31,34] Figure 4 shows the triplet decays of Mg4Al2/PdTPPC(10) and Mg4Al2/PdTPPC(ads) in a nitrogen atmosphere and in air. Similar data were found for the TPPS-doped samples (see the Supporting Information, Figure S12). The changes observed clearly demonstrate that the porphyrin molecules are accessible to oxygen even when intercalated into the solid matrix, i.e., O_2 diffuses into the LDH matrix. The fact that the triplet state decays in air are fairly fitted with a biexponential function also documents that the distinct triplet porphyrin states in the solids are quenched by O_2 differently. It is worth noticing that despite the identical experimental conditions and geometry used, the transient signals in air at $t = 0$ are lower than those under nitrogen (Figure 4 and the Supporting Information, Figure S12). Assuming that the same quantity of the triplet states is generated in both cases, it indicates that quenching by O_2 causes a significant population of the triplet states to decay within the time resolution of our instrument ($\approx$ 300 ns). Therefore, the τ_1 values recovered from the fit of the decays in air should be taken as the upper limit of the real lifetime. As expected, the fast decay is especially pronounced for Mg4Al2/PdTPPC(ads) and Mg4Al2/TPPS(ads) because of the better accessibility of the adsorbed porphyrin molecules to oxygen. Indeed, in the case of the Mg4Al2/TPPS(ads) sample in air, we assume that the short-lived triplet state decays so rapidly that only the long-lived component is detected.

Singlet Oxygen. The production of $^1O_2$ by the porphyrin-LDH composites is expected on the basis of the transient absorption measurements shown above. To assess the efficiency of the $^1O_2$ generation, we have measured its photoluminescence at $\lambda_{em} = 1270$ nm upon laser pulse excitation. Emission at this wavelength arises from relaxation of $^1O_2$ to the triplet ground state. Figure 5 depicts the time dependence of the $^1O_2$ luminescence intensity produced by the intercalated and adsorbed porphyrin molecules in air. Because porphyrin-free LDHs do not display any $^1O_2$ luminescence, we conclude that $^1O_2$ is generated by the porphyrin photosensitized reaction (see the Supporting Information, Figure S13). Adsorption of TPPS on LDHs led to tiny signals of $^1O_2$ (Figure 5B and the Supporting Inforamtion, Figure S14). We believe that this is due to the lower capability of TPPS to photoproduce $^1O_2$ and to the short lifetime of $^1O_2$ photogenerated by this sample with respect to the time resolution of the experiments ($\sim$5 μs).

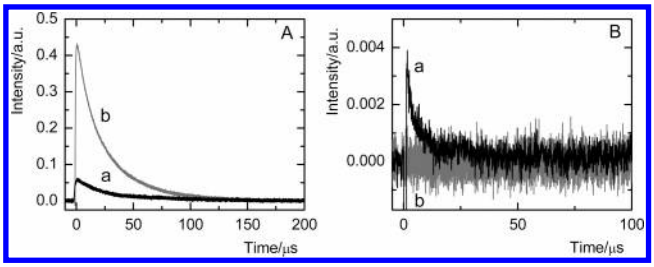

Figure 5. Time dependence of the $^1O_2$ luminescence signal at 1270 nm of Mg4Al2/PdTPPC(10) (A, a), Mg4Al2/PdTPPC(ads) (A, b), Mg4Al2/TPPS-(10)-Cl (B, a) and Mg4Al2/TPPS(ads) (B, b) in air (A, $\lambda_{exc} = 532$ nm; B, $\lambda_{exc} = 435$ nm).

From the results plotted in Figure 5, it is evident that the $^1O_2$ signals obtained for the solids containing PdTPPC are significantly larger than for those with TPPS. We ascribe it to the higher yield of triplet state formation of Pd(II) porphyrins (intersystem crossing yield is 1.0 for Pd-5,10,-15,20-tetraphenylporphyrin in ethanol solution[36] and 0.77 for TPPS in water[37]). Because the goal of this work is the development of efficient sources of $^1O_2$, most of the following discussion will be focused on the PdTPPC-doped samples. In this case, the adsorbed PdTPPC molecules (Mg4Al2/PdTPPC(ads)) produce a higher signal of $^1O_2$ than those intercalated (Mg4Al2/PdTPPC(10)). This can be explained by the limited penetration depth of the laser excitation pulse into the solid, hence only those sensitizer molecules intercalated into the more external layers of the LDH host can be excited. It is important to note, however, that leakage of the adsorbed sensitizer molecules will take place if the experiments are conducted in solid−liquid interfaces, a drawback overcome by intercalation into the host. Having proved the ability of the solid samples with intercalated photosensitizers to act as singlet oxygen sources, eventual application will depend on the lifetime of $^1O_2$, because the longer the lifetime, the more powerful the oxidative performance. Therefore, the analysis of the factors determining the singlet oxygen lifetime is of utmost importance.

The $^1O_2$ luminescence signals of PdTPPC-doped LDH in Figure 5A do not decay monoexponentially. This multiexponential feature is in agreement with the behavior of their triplet−triplet absorption signals in air. The $^1O_2$ lifetimes recovered from biexponential fits are about 10−50 μs longer than those for their precursor porphyrin triplet states (Table 2). This indicates that the $^1O_2$ decay kinetics measured in our experiments reflect both the duration of the triplet states and the intrinsic $^1O_2$ lifetime, i.e., τ(triplet) $\approx$ $\tau(^1O_2)$. Otherwise, a multiexponential $^1O_2$ signal reproducing the triplet-state decay kinetics (if τ(triplet) $\gg$ $\tau(^1O_2)$) or monoexponential $^1O_2$ decays (if τ(triplet) $\ll$ $\tau(^1O_2)$) would have been observed. Naturally, in all these three situations, an initial rise of the $^1O_2$ luminescence signal prior to the subsequent decay is obscured by the experimental uncertainty within first 5 μs. To estimate the intrinsic $^1O_2$ lifetimes, we fitted the singlet oxygen decay signals with a kinetic model

(36) Harriman, A.; Porter, G.; Wilowska, A. *J. Chem. Soc., Faraday Trans. 2* **1983**, *27*, 807.
(37) Goncalves, P. J.; Aggarwal, L. P. F.; Marquezin, C. A.; Ito, A. S.; De Boni, L.; Barbosa-Neto, N. M.; Rodrigues, J. J.; Zílio, S. C.; Borissevitch, I. E. *J. Photochem. Photobiol., A* **2006**, *181*, 378−384.

in which the singlet oxygen molecules were photogenerated from two different triplet states but decayed with the same rate (see the Supporting Information). The intrinsic lifetimes obtained are 55 μs for Mg4Al2/PdTPPC(10) and 32 μs for Mg4Al2/PdTPPC(ads).

To the best of our knowledge, no information on the singlet oxygen behavior within LDH hosts has been published so far. For comparison, reports on the $^1O_2$ lifetime in the interior of zeolites can be found in the literature.[9,10] Quenching of $^1O_2$ by aluminum, by cations associated with the matrix, and by adsorbed water was proposed, and the upper limits of the singlet oxygen lifetimes in the interior of supercages of zeolite Y suspended in perfluorohexane (7.5 μs)[9] and in porous silica with no aluminum content (64 μs)[10] were given. Earlier measurements on silica gel−solvent systems have shown that the OH groups of adsorbed water molecules and silanols can act as effective quenchers of $^1O_2$.[11] Consequently, we expect that the singlet oxygen decay kinetics measured in this work are affected by interaction of $^1O_2$ with the surrounding LDH matrix.

Two mechanisms might contribute to quenching of $^1O_2$: (i) Interaction of $^1O_2$ with parent or neighboring porphyrin molecules resulting in porphyrin degradation. Because evidence for porphyrin degradation as observed only at very high laser energies, we rule out the contribution of porphyrin-mediated $^1O_2$ deactivation at normal experimental conditions. (ii) Interaction of $^1O_2$ with the surrounding host matrix as it occurs in solution, where singlet oxygen quenching proceeds by a radiationless transfer of the electronic energy to vibrational modes of the terminal oscillators of the solvent molecules (X−Y atom pairs, e.g., C−H, O−H). Among several types of X−Y atom pairs, the O−H group is one of the most efficient quenchers of $^1O_2$. Because the OH groups coordinated around the Mg and Al centers in the LDH hosts point toward the interlayer space, the effect of these groups and of the water molecules confined in the space will be critical in determining the lifetime of $^1O_2$.

To explore further LDH effects on the singlet oxygen lifetime, we have investigated the $^1O_2$ decay kinetics for the Mg4Al2/PdTPPC(10) solid suspended in several solvents. In toluene suspensions, a monoexponential luminescence decay for $t > 5$ μs has been obtained with a characteristic lifetime of 10 μs (see the Supporting Information, Figure S15). Photoexcitation of Mg4Al2/PdTPPC(10) suspended in D_2O results in a multiexponential $^1O_2$ decay whose fit with a biexponential function yields lifetimes of 8 and 37 μs. Comparison of these results with the known $^1O_2$ lifetimes in pure toluene (29 μs) and D_2O (68 μs) confirms that the LDH matrix partially quenches the $^1O_2$ molecules photogenerated in its interior. It is clear, however, that the $^1O_2$ molecules also sense the surrounding solvent because their decay kinetics varies from toluene to D_2O. Hence, we can conclude that $^1O_2$ generated in the interior of the LDH hosts can actuate on an adjacent medium.

Effects of Subtle Structural Changes. As already mentioned, the potential application of sensitizer-doped solids as singlet oxygen sources depends both on the yield and on the lifetime of $^1O_2$. We have shown that the LDH host is not inert and influences the experimental lifetime of photo-

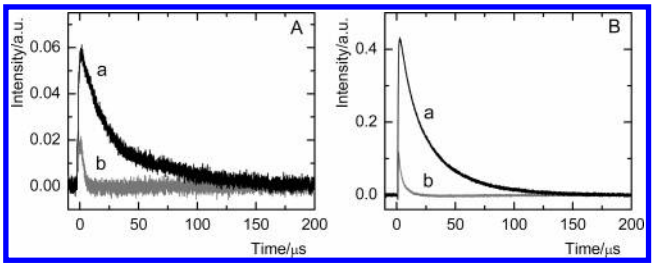

Figure 6. Time dependence of the $^1O_2$ luminescence signal at 1270 nm of (a) fresh and (b) dehydrated (A) Mg4Al2/PdTPPC(10) and (B) Mg4Al2/PdTPPC(ads) in air (λ_{exc} = 532 nm). The singlet oxygen decays of the dehydrated samples can be fitted with a monoexponential function, yielding the lifetimes of 2.7 μs for Mg4Al2/PdTPPC(10) and 3.8 μs for Mg4Al2/PdTPPC(ads).

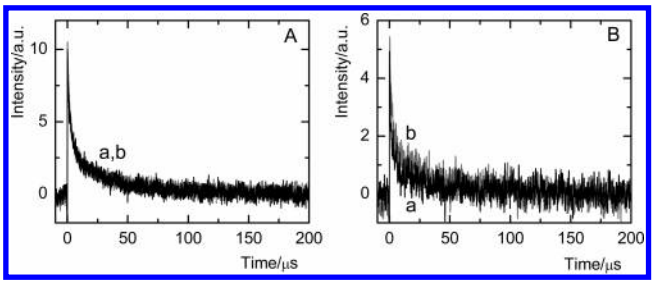

Figure 7. Decays of the triplet states of (a) fresh and (b) dehydrated Mg4Al2/PdTPPC(10) (A) under N_2 (the curves are fully overlapped) and (B) in air (λ_{exc} = 532 nm, λ_{abs} = 480 nm).

produced $^1O_2$, as previously observed for other inorganic hosts.[9−11] Therefore, structural and composition changes of the host may bring about significant variations of the $^1O_2$ activity. To pursue this issue, we have investigated the singlet oxygen signals produced by Mg4Al2/PdTPPC(10) and Mg4Al2/PdTPPC(ads) after evacuation and heating of the solids (∼ 70 °C) prior to feeding in dry air or O_2. We have shown above that such conditions decrease the interlayer distance in the LDH hosts owing to the removal of interlayer water. Because water is an efficient quencher of $^1O_2$, longer $^1O_2$ lifetimes can be expected for the dehydrated samples.

Nonetheless, an utterly opposite behavior was observed experimentally, as shown in Figure 6. Upon dehydration of the solid, a less intense and short-lived singlet oxygen signal was detected for both LDHs with intercalated and adsorbed PdTPPC. To rule out dehydration effects on the triplet state formation that might account for this result, we have also carried out transient difference absorption measurements on the dehydrated samples. Figure 7 compares the decays of the triplet states for hydrated and dehydrated Mg4Al2/PdTPPC(10) in air and under nitrogen at otherwise identical conditions. As observed also for Mg4Al2/PdTPPC(ads), the population and relaxation kinetics of the porphyrin triplet states are not significantly affected by the removal of interlayer water from the host. Consequently, dehydration of the sample directly influences the lifetime of photoproduced $^1O_2$.

Indeed, the release of interlayer water allows the $^1O_2$ molecules diffusing in the interior of the solid host to approach closer to the hydroxyl groups of the LDH matrix. Hence, the quenching activity of these groups induces the dramatic decrease in the singlet oxygen lifetime. The tentative fits of the luminescence decays in Figure 6 accounting for the triplet state and singlet oxygen relaxation

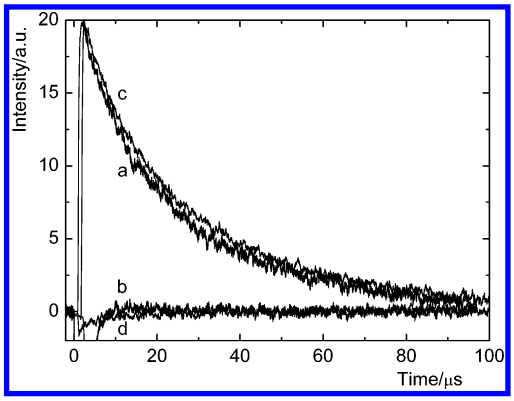

Figure 8. Time dependence of the $^1O_2$ luminescence signal at 1270 nm of the Mg4Al2/PdTPPC(10) sample in O_2 when (a) fresh, (b) dehydrated, (c) rehydrated by exposure to ambient air, and (d) dehydrated again (λ_{exc}= 425 nm, ~1 mJ/pulse).

kinetics render the following intrinsic $^1O_2$ lifetimes for the dehydrated samples: 2.7 μs for Mg4Al2/PdTPPC(10) and 3.8 μs for Mg4Al2/PdTPPC(ads). Obviously, the quenching efficiency of the surrounding matrix increases about 10-fold after the removal of adsorbed interlayer water. Similar effects were also observed for TPPS-LDHs. It manifests that subtle structural and composition changes may lead to striking variations of the $^1O_2$ lifetime and influence to a large extent the potential oxidative activity of the material.

The capability of dehydrated porphyrin-LDHs to photogenerate long-lived $^1O_2$ molecules was recovered after exposure to atmospheric humidity (Figure 8). In agreement with previous reports,[24] this indicates that the basal spacing characteristic of the hydrated layers is restored within several hours of exposition of dehydrated LDH to ambient atmosphere. We have further investigated the reversibility of this process by performing three consecutive cycles of dehydration−rehydration of the solids. Interestingly, the ability to produce $^1O_2$ remained unaltered (Figure 8). It confirms that evacuation and heating evidently does not induce irreversible changes of the matrix but only desorption of water. The LDH materials with the intercalated PdTPPC molecules can therefore be envisaged as an efficient source of $^1O_2$ with controlled oxidative activity that can be stopped and resumed by dehydration and rehydration of the host.

Conclusions

In this work, we describe the structural and optical properties of layered double hydroxides (LDHs) doped with porphyrin sensitizers. Powder X-ray diffraction and X-ray photoelectron spectroscopy demonstrated intercalation of TPPS and PdTPPC into LDHs by anion exchange when the LDH precursors with a suitable content of Al^{3+} and Mg^{2+} ions and monovalent interlayer counteranions were employed. Otherwise, the porphyrin molecules were adsorbed on the surface of the host. Diffuse reflectance UV−vis spectra show that neither intercalated nor adsorbed porphyrin molecules are prone to aggregate, but preserve their photoactive monomeric form. Likewise, the properties of their photoexcited triplet states do not seem to be critically altered by the surrounding matrix. The lifetime of these triplet states decreases in the presence of oxygen as a result of energy transfer to O_2 molecules and generation of $^1O_2$. This process is found to be very effective in case of the PdTPPC-doped samples. On account of the long lifetime of $^1O_2$ produced by this composite material, we conclude that the singlet oxygen molecules generated in the interior of the LDH matrix can diffuse out of the solid matrix and react with a substrate. Dehydration of these samples dramatically inhibits the production of long-lived $^1O_2$ molecules and thereby decreases the oxidative capacity of the composite material. Because this behavior can be reverted after exposure of the composite to atmospheric humidity, we envisage LDHs with the intercalated PdTPPC molecules as efficient, easy-to-use $^1O_2$ sources with directed oxidative activity.

Acknowledgment. The authors gratefully acknowledge the financial support from the Czech Science Foundation (203/06/1244, 203/07/1424), the Research Plan of the Academy of Sciences of the Czech Republic (AV0Z40320502), the Grant Agency of the Academy of Sciences of the Czech Republic (KAN 100500651), the Ministry of Education, Youth and Sports of the Czech Republic (MSM 6046137302), and the Ministry of Education and Science of Spain (CTQ2006-01040 and "Ramon y Cajal" program (J.H.)).

Supporting Information Available: Details on LDH preparation, powder X-ray diffraction, X-ray photoelectron and diffuse reflectance UV−vis spectroscopy experiments, XPS results (stoichiometry, core level group shifts, and binding energies E_b), powder XRD patterns in vacuo, at room and increased temperatures, diffuse reflectance spectra, decays of the triplet states, and $^1O_2$ luminescence signals at 1270 nm. This material is available free of charge via the Internet at http://pubs.acs.org.

CM070351D

Layered Double Hydroxides with Intercalated Porphyrins as Photofunctional Materials: Subtle Structural Changes Modify Singlet Oxygen Production

Kamil Lang, Petr Bezdička, José L. Bourdelande, Jordi Hernando*, Ivan Jirka, Eva Káfuňková, František Kovanda, Pavel Kubát, Jiří Mosinger, Dana M. Wagnerová*

Institute of Inorganic Chemistry v.v.i., Academy of Sciences of the Czech Republic, 250 68 Řež, Czech Republic; Departament de Química, Universitat Autonoma de Barcelona, Bellaterra, 08193 Barcelona, Spain; J. Heyrovský Institute of Physical Chemistry v.v.i., Academy of Sciences of the Czech Republic, Dolejškova 3, 182 23 Praha 8, Czech Republic; Department of Solid State Chemistry, Institute of Chemical Technology Prague, Technická 5, 166 28 Praha 6, Czech Republic, and Faculty of Sciences, Charles University in Prague, 2030 Hlavova, 128 43 Praha 2, Czech Republic

Corresponding authors:

Kamil Lang, Institute of Inorganic Chemistry, Academy of Sciences of the Czech Republic, 250 68 Řež, Czech Republic, e-mail: lang@iic.cas.cz

Jordi Hernando, Departament de Química, Universitat Autonoma de Barcelona, Bellaterra, 08193 Barcelona, e-mail: jordi.hernando@uab.es

I. Experimental

Sample Preparation. The LDH hosts in the nitrate and chloride forms were prepared by coprecipitation according to Miyata.[1] In both cases carbonate-free distilled water and nitrogen atmosphere were employed to avoid any contamination of the final product by carbonate anions. To prepare LDHs with nitrate counteranions, an aqueous solution (450 ml) of $Mg(NO_3)_2 \cdot 6H_2O$ and $Al(NO_3)_3 \cdot 9H_2O$ with a Mg/Al molar ratio of 2 or 4 and total metal ion concentration of 1.0 M were added into a 1000 ml reactor containing 200 ml of distilled water with a flow rate of 7.5 ml min^{-1}. Simultaneously, 3M aqueous solution of NaOH was also added to maintain the pH of the mixture at a constant value around 10.0 ± 0.1. Coprecipitation was carried out under vigorous stirring at 75 °C and the resulting suspension was further stirred for 1 h at this temperature. The product was filtered off, washed several times with distilled water and dried at 60 °C. The obtained LDHs were denoted by acronyms describing the elemental composition, molar ratios of the constituents and interlayer anions, i.e. Mg4Al2-NO_3 ($Mg_4Al_2(OH)_{12}(NO_3)_2 \cdot 4H_2O$) or Mg8Al2-$NO_3$ ($Mg_8Al_2(OH)_{12}(NO_3)_2 \cdot 4H_2O$). The LDHs with chloride counteranions, Mg4Al2-Cl ($Mg_4Al_2(OH)_{12}Cl_2 \cdot 4H_2O$), were prepared using $MgCl_2 \cdot 6H_2O$ and $AlCl_3 \cdot 6H_2O$ at the same conditions as described above. Similarly, carbonate LDH, Mg4Al2-CO_3 ($Mg_4Al_2(OH)_{12}CO_3 \cdot 4H_2O$), was prepared by coprecipitation of Mg and Al nitrates using aqueous alkaline solution of NaOH (3 M) and Na_2CO_3 (0.5 M).

Characterization Techniques. Powder X-ray diffraction patterns (XRD) were recorded from 2 to 80° 2Θ with a step size 0.02° (10 s/point) using a Siemens D5005 diffractometer (Bruker AXS, Germany, CuK_α radiation, 40 kV, 30 mA) equipped with a diffracted beam monochromator. The samples were pressed on a titanium holder and measured under air atmosphere. Diffraction patterns at elevated temperatures were collected with a PANalytical X´Pert PRO diffractometer equipped with a conventional X-ray tube (Co K_α radiation, 40 kV, 30 mA) and a multichannel detector X'Celerator with an anti-scatter shield and a high temperature chamber (HTK 16, Anton Paar, Graz, Austria). The experiments were performed in air atmosphere and in vacuum (5×10^{-3} Pa). Qualitative analysis of the measured data was performed with a HighScore software package

[1] Miyata, S. *Clays Clay Miner*. **1975**, *23*, 369.

(PANalytical, The Netherlands, version 1.0d), Diffrac-Plus software package (Bruker AXS, Germany, version 8.0) and JCPDS PDF-2 database.[2] The Diffrac-Plus Topas software (Bruker AXS, Germany, version 2.1) in combination with structural models based on the ICSD database was used for quantitative analysis of the XRD patterns.[3]

Photoelectron spectra were measured using a spectrometer ESCA 3 Mk 2 (VG) with a hemispherical analyzer operating with a constant pass energy of 50 eV in the low resolution mode (1000 eV scan, step 1 eV) and a pass energy of 20 eV in the high resolution mode (30 eV scan, step 0.1 eV) regimes. The non-monochromatized Al K $\alpha_{1,2}$ line was used to excite photoelectrons. The X-ray source was operated at 220 W and vacuum was typically ~1.10^{-9} Torr at the beginning of the experiment. The initial pressure increased to ~1.10^{-8} Torr after 30 minutes of X-ray irradiation. The samples were placed into the spectrometer on a double sided Scotch tape. The photoelectron spectra of pure TPPS, used as a standard for the calibration of the core level binding energies (E_b), were measured in a thin transparent layer prepared by evaporation of a drop of methanol solution on a stainless steel sample holder. The prepared layer was thin enough to eliminate charging during photoemission, and thick enough to avoid interferences of the sample holder lines with those of TPPS. The binding energies and intensities of the photoelectron lines were estimated by a curve fitting procedure using pseudo-Voight functions. The Shirley background was subtracted.[4] The Al 2p, Mg 2s, C 1s, N 1s, S 2p and O 1s photoelectron lines were measured in the high resolution regime. The atomic ratios were calculated from the intensities of the pertinent photoelectron lines corrected on the Wagner sensitivity factors.[5] The values of E_b were calibrated using E_b of the C 1s and N 1s photoelectron lines of the TPPS standard (E_b(C 1s) = 285.55 eV, E_b(N 1s) = 400.35 eV).

The simultaneous TGA/DSC/DTA QMS characterization of the samples (cca 20mg) was carried out on a NETZSCH apparatus STA 409 coupled with a quadrupole mass spectrometer Balzers QMG 420. The measurements were performed in air atmosphere (flow rate 75 ml/min) from laboratory temperature to 1000°C with a heating rate of 10K/min. Released gases were

2. JCPDS PDF-2 database, International Centre for Diffraction Data, Newtown Square, PA, U.S.A. release 54, 2004.
3. ICSD database, FIZ Karlsruhe, Germany, release 2006/1, 2006.
4. Shirley D. A. *Phys Rev* **B** 5 (1972) 4709.
5. Practical Surface Analysis by Auger and X-ray Photoelectron Spectroscopy (Eds. Briggs, D.; Seach, M.P.) J. Wiley, 1983.

transferred from the thermobalance to the quadrupole mass spectrometer (in the MID mode up to mass numbers of 100) using a heated stainless capillary coupling (up to 200°C).

The diffuse reflectance UV-vis spectra were recorded on a Perkin Elmer Lambda 35 spectrometer equipped with a Labsphere RSA-PE-20 integration sphere. A sample holder with a fused silica window was filled with the LDHs or $BaSO_4$, which was used as a white standard (Merck, white standard DIN 5033). If necessary the solid LDH composites were diluted with $BaSO_4$ prior to measurement. The recorded reflectance was converted to the Kubelka-Munk scale, and processed using OriginPro7.0 software (OriginLab Co., USA).

Table S1. Occurrence of the porphyrin intercalates in LDH.

Composite	Intercalation
Mg4Al2/TPPS(10)	Yes
Mg4Al2/TPPS(10)-Cl	Yes
Mg4Al2/TPPS(100)	Yes
Mg8Al2/TPPS(10)	No
Mg8Al2/TPPS(100)	Yes
Mg4Al2/TPPS(ads)	No
Mg4Al2/PdTPPC(10)	Yes
Mg4Al2/PdTPPC(ads)	No

Additional discussion of the XPS results - Core level group shifts (CLGS)

The intercalated molecules of TPPS can serve as an internal standard for description of the delicate framework properties. The effect of the charge in an inorganic framework on the core level binding energies E_b was applied on zeolites.[6] An excess of the negative charge in their lattice induces the so called core level group shifts (CLGS) of the elements constituting the framework. As a result, the binding energies E_b of Si 2p, Al 2p and O 1s photoelectron lines increase with decreasing concentration of zeolite aluminum. However, analogous CLGS with the opposite sign might be observed in the LDH framework. Since zeolites (like LDH) are insulators, the positive charge induced by emission of electrons during the measurement causes a systematic positive shift of the photoelectron lines to higher values. Hence, the evaluation of the absolute E_b values requires their proper calibration that eliminates the charging effects. Recently it was demonstrated[7] that the error of the E_b values determined using the calibration based on the E_b (C 1s) line of adventitious carbon may be greater than CLGS and reliability of this concept was questioned. The introduced error is due to the significantly variable character of carbon-containing contamination. To avoid this problem, we calibrated the spectra using the N 1s photoelectron line of the TPPS standard. The standard is well defined, stable under X-rays and no charging effects were observed during photoemission. As follows from Table S2, the E_b (C 1s) and E_b (S 2p) values are not affected while the E_b (Mg 2s) and E_b (Al 2p) values decrease by 0.75 and 0.60 eV, respectively, with the decreasing positive charge density in the LDH lattice. This finding supports reliability of the CLGS concept in the LDH frameworks for the first time and, in addition, it indicates high crystallinity of the sample interface region.

6. Barr, T.L.; Lishka, M.A. *J. Am. Chem. Soc*. **1986**,*108*, 3178.
7. Gijzeman, O.L.J.; Mens, A.J.M.; Lenthe, J.; Mortier, W.J.; Weckhuysen, B.M. *J. Phys. Chem.* B **2003**, *107,* 678.

Table S2. Binding energies E_b (eV) calibrated using E_b (N 1s) = 400.4 eV (TPPS).

Molar ratio	C 1s	Mg 2s	Al 2p	O 1s	S 2p
Mg:Al=4:2 [a]	285.45±0.25	89.85±0.15	75.3±0.20	532.65±0.25	168.8±0.00 (168.8±0.10)[b]
Mg:Al=8:2 [c]	285.2 (-0.25)	89.1 (-0.75)	74.7 (-0.60)	-	168.7 (-0.10)

[a] the mean values calculated from data of Mg4Al2/TPPS(100) and Mg4Al2/TPPS(ads)

[b] the standard film of TPPS

[c] the lines of Mg8Al2/TPPS(100); CLGS in parenthesis were obtained by subtracting E_b of the samples with Mg:Al=4:2

Figure S1. Powder XRD patterns of Mg4Al2-CO3 (a) and Mg4Al2/TPPS(ads) (b); the patterns are shifted for clarity.

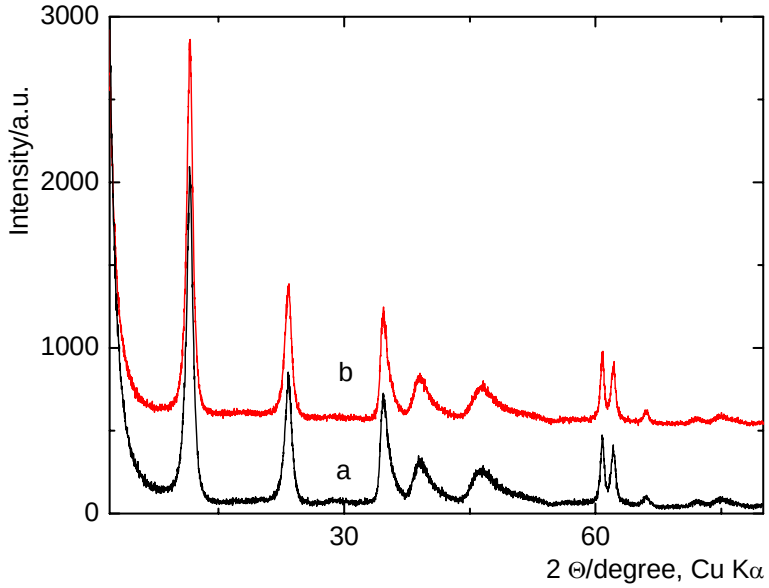

Figure S2. Powder XRD patterns of Mg8Al2-NO_3 (a) and Mg8Al2/TPPS(10) (b); the patterns are shifted for clarity.

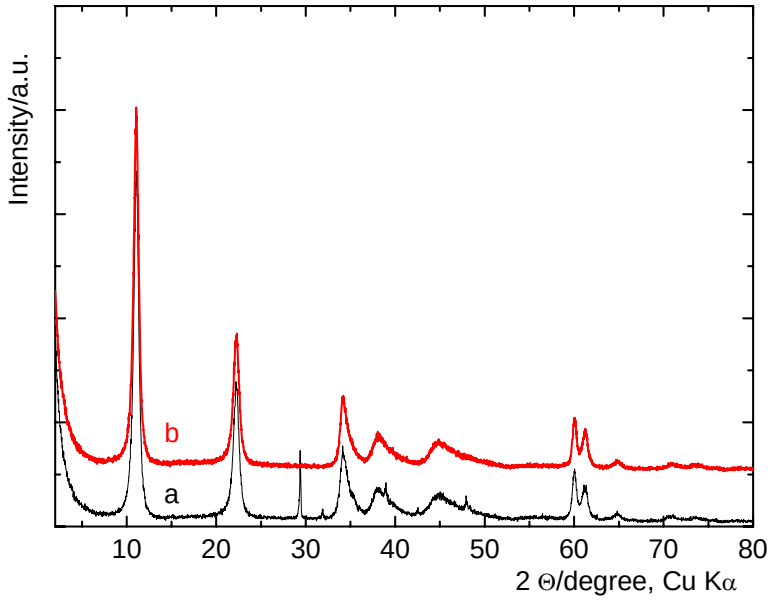

Figure S3: The N 1s photoelectron line of parent Mg4Al2-NO_3 (a), Mg4Al2/TPPS(100) (b), Mg8Al2-NO_3 (c) and Mg8Al2/TPPS(100) (d). The solid lines represent a least squares fit to the pseudo-Voight sum functions.

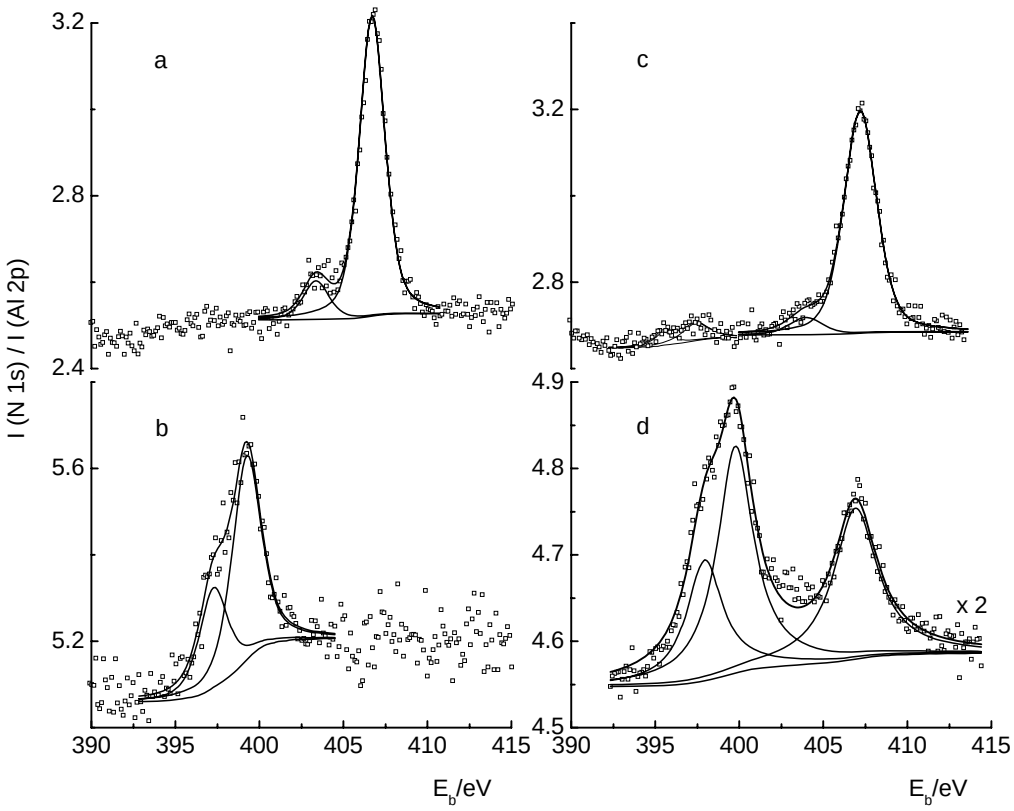

Figure S4. Temperature dependence of the powder XRD patterns of Mg4Al2-NO_3. The patterns are shifted for clarity.

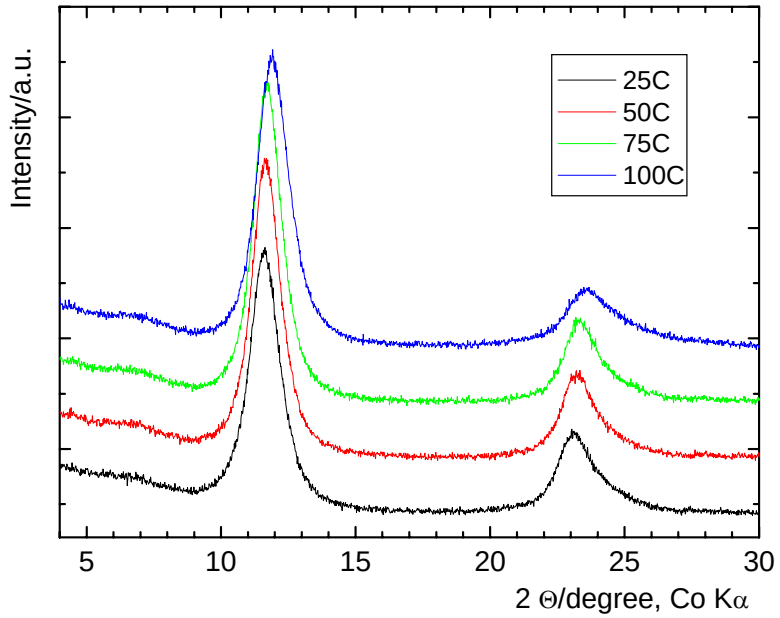

Figure S5. Temperature dependence of the powder XRD patterns of Mg4Al2/TPPS(100). The patterns are shifted for clarity.

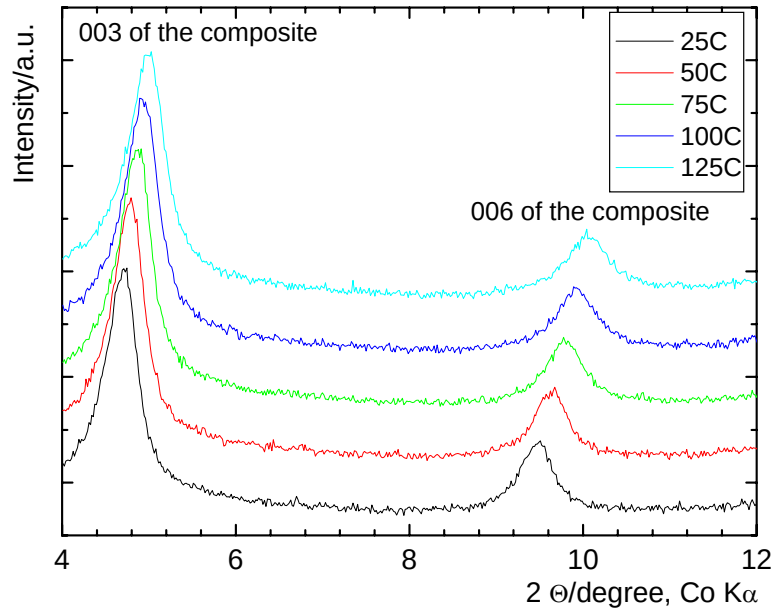

Figure S6. Temperature dependence of the diffraction line (003) of Mg4Al2/PdTPPC(10). The patterns are shifted for clarity. (The line belongs to the LDH phase)

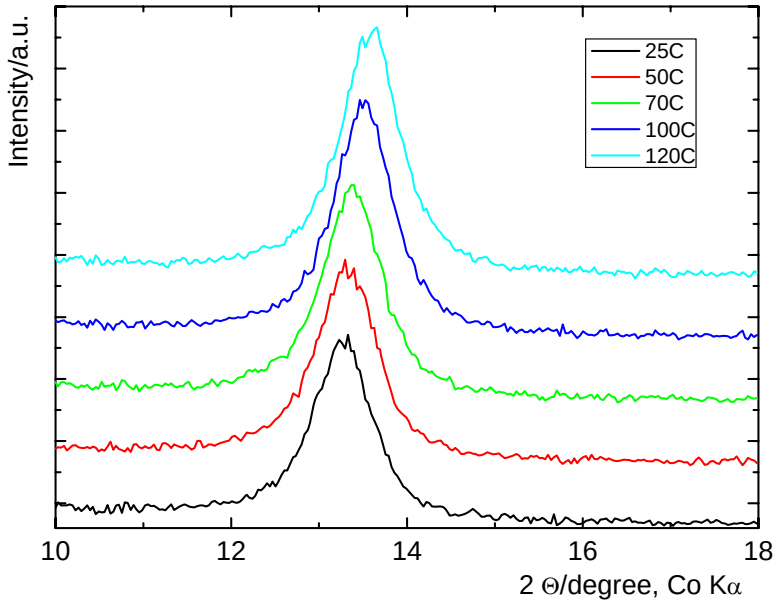

Figure S7. Temperature dependence of the powder XRD patterns of Mg4Al2/PdTPPC(10) under vacuum: a) air atmosphere at 22 ^{o}C; b) evacuation for 2 h to 5 × 10^{-3} Pa, 25 ^{o}C; c) annealing at 120 ^{o}C followed by cooling to 25 ^{o}C under vacuum. (The line belongs to the LDH phase; the lines within 2θ of 21.3-23.5 are due to an impurity on a sample holder).

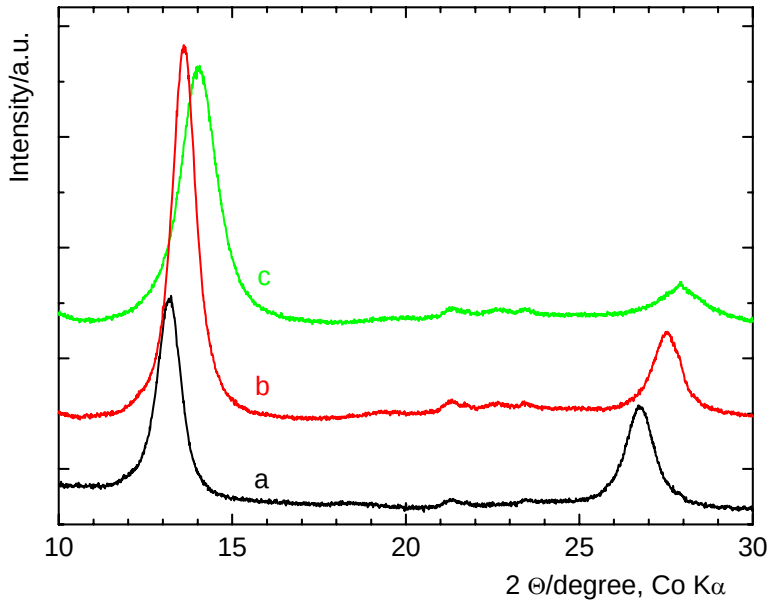

Figure S8. Normalized diffuse reflectance spectra of Mg4Al2/TPPS(10) (a), Mg4Al2/TPPS(ads) (b) and Mg8Al2/TPPS(10) (c) compared with the absorption spectrum of 1.4 μM TPPS in water (d). The solid samples were diluted with inert $BaSO_4$.

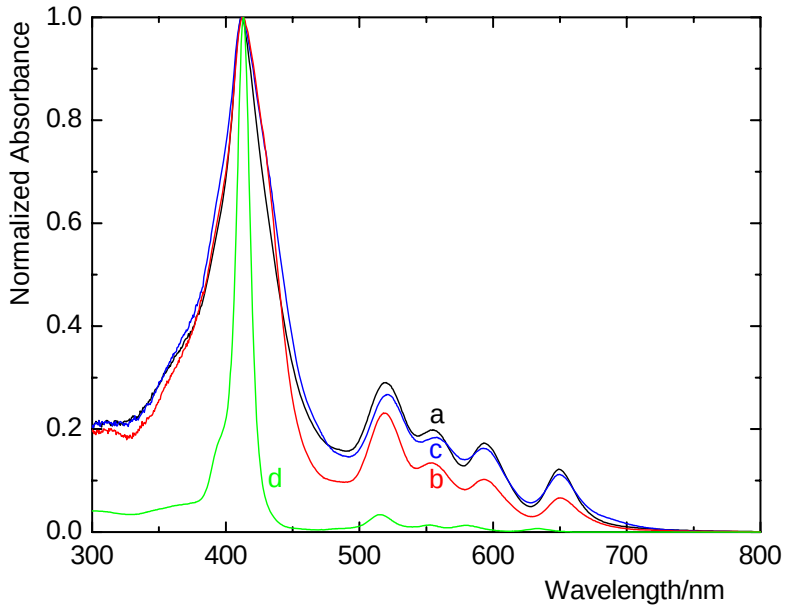

Figure S9. Normalized diffuse reflectance spectra of Mg4Al2/TPPS(2) (a), Mg4Al2/TPPS(10) (b) and Mg4Al2/TPPS(100) (c) compared with the absorption spectrum of 1.4 μM TPPS in water (d). The solid samples were diluted with inert $BaSO_4$.

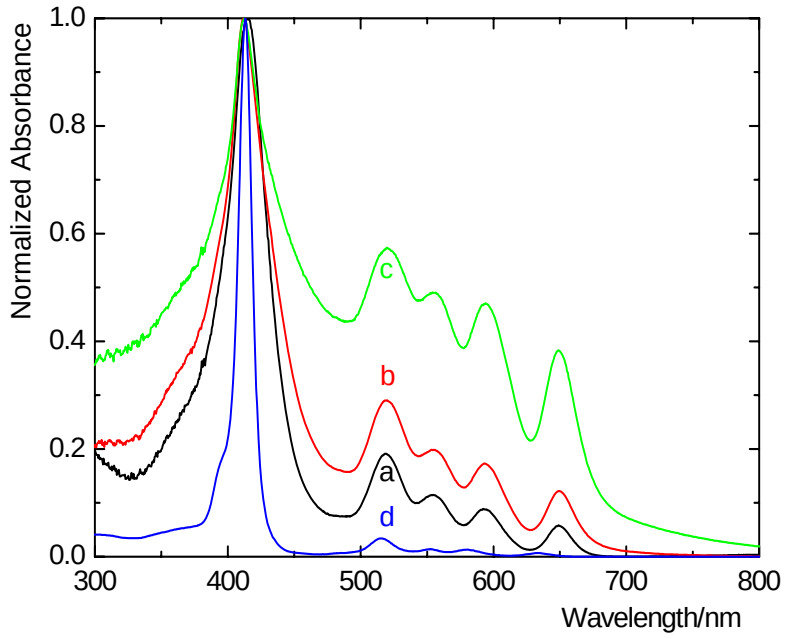

Figure S10. (a) Difference absorption spectra of the short- (solid line) and long-lived (dashed line) triplet states of Mg4Al2/PdTPPC(10) under N_2 atmosphere (λ_{exc}=532 nm) obtained by global analysis of the data.

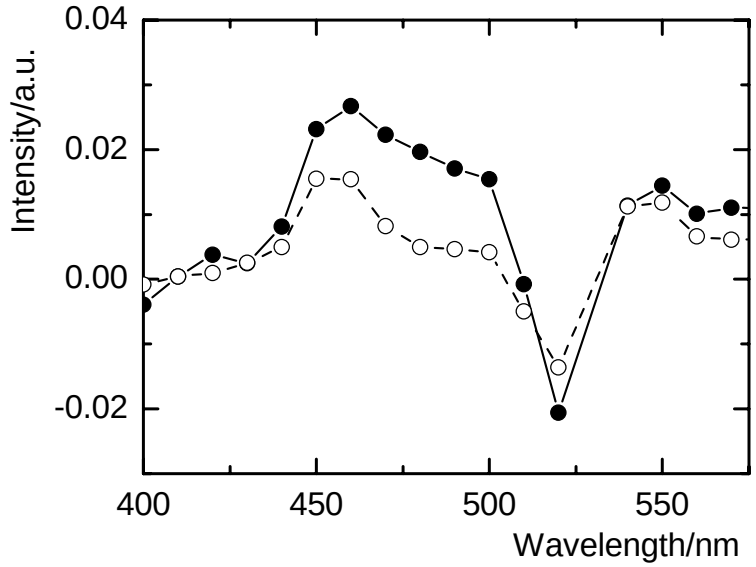

Figure S11. Decays of the triplet states of Mg4Al2/TPPS(10) (A) and Mg4Al2/TPPS(ads) (B) under N_2 atmosphere (black) and in air (red) (λ_{abs}= 485 nm, λ_{exc} = 450 nm).

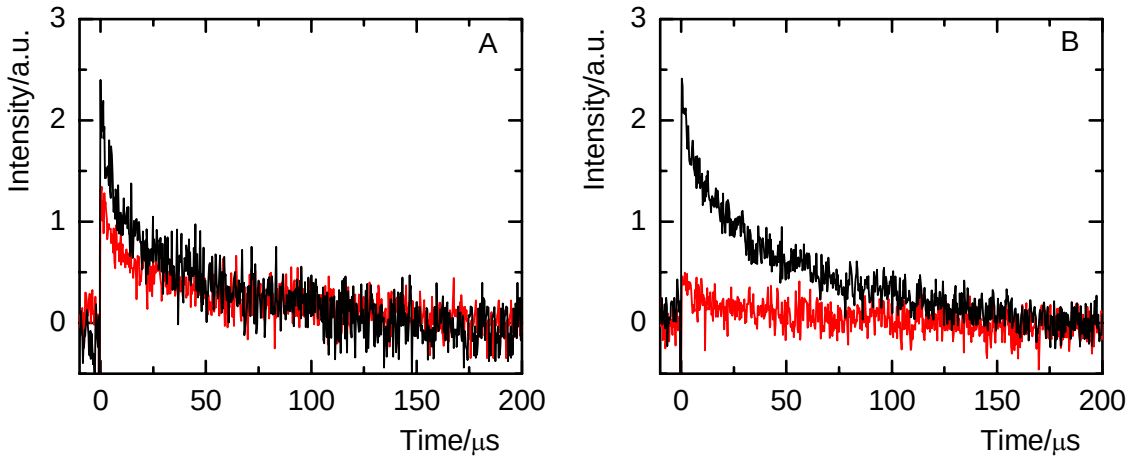

Figure S12. Time dependence of the $^1O_2$ luminescence signal at 1270 nm produced by Mg4Al2/PdTPPC(10) (black) and by the host Mg4Al2-NO_3 (blue). The luminescence signal of $^1O_2$ obtained in O_2 atmosphere contained a short-lived signal caused by scattering of excitation laser pulse. This signal was eliminated by exciting the sample in the absence of O_2 and by subtracting the obtained signal from the signal recorded in O_2 atmosphere. The smoothed line (red) is a least squares monoexponential fit of the pure luminescence signal of $^1O_2$. The same treatment with the porphyrin-free Mg4Al2-NO_3 sample gives a zero-line response documenting that the recorded luminescence signals are associated with the photofunction of the porphyrin molecules and that laser scattering is completely eliminated. (The solid was excited at 425 nm using 380 μJ/pulse and evacuated before saturation with O_2 and Ar).

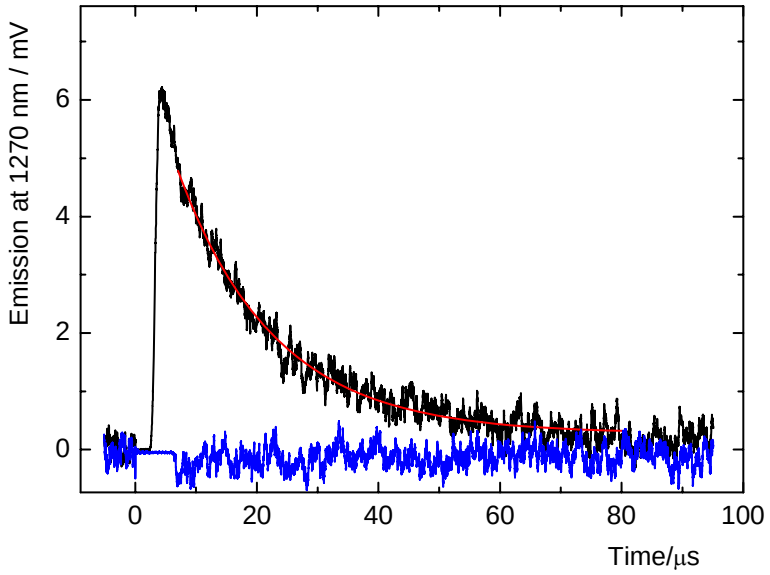

Figure S13. Qualitative comparison of the singlet oxygen productivity of the composites containing TPPS: Mg4Al2/TPPS(10) (black), Mg4Al2/TPPS(ads) (red) and Mg8Al2/TPPS(10) (blue). The solid was excited at 425 nm using ~ 1 mJ/pulse and evacuated before saturation with O_2 and Ar.

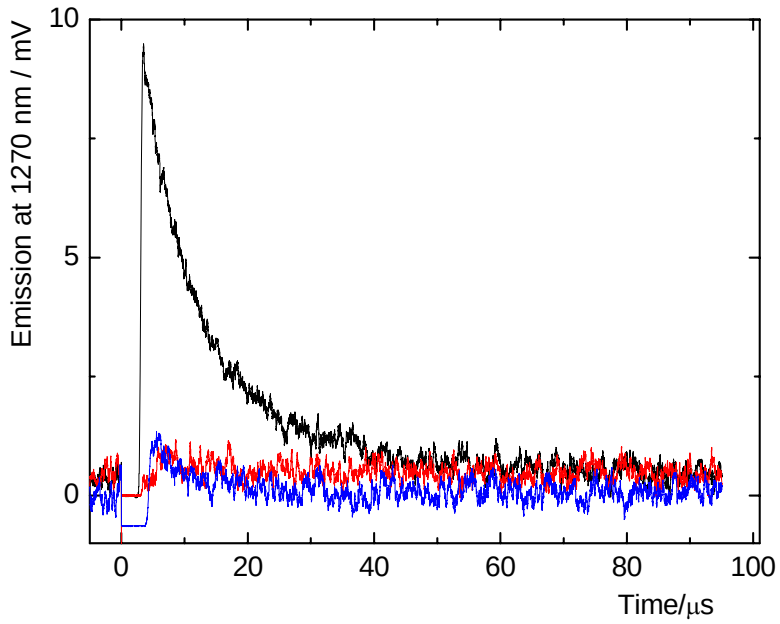

Figure S14: Singlet oxygen produced by a suspension of Mg4Al2/PdTPPC(10) in toluene saturated by O_2. The smoothed line (red) is a least squares monoexponential fit. Excitation at 425 nm, energy ~ 1 mJ/pulse.

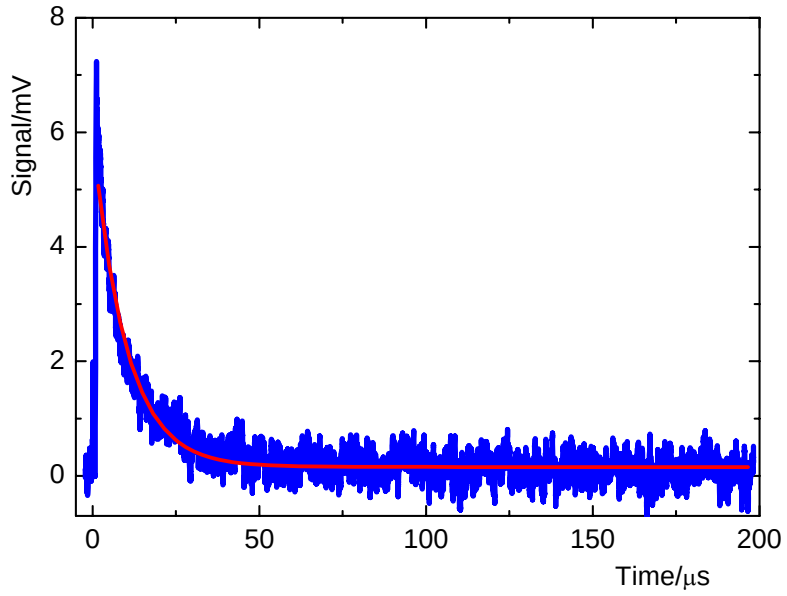

Appendix II

A. Píšková, P. Bezdička, D. Hradil, ***E. Káfuňková****, K. Lang, E. Večerníková, F. Kovanda, T. Grygar:*

High-temperature XRD as a tool for characterization of smectites, layered double hydroxides, and their intercalates with porphyrins

Applied Clay Science **2010**, 49, 363-371

Applied Clay Science 49 (2010) 363–371

Contents lists available at ScienceDirect

Applied Clay Science

journal homepage: www.elsevier.com/locate/clay

High-temperature X-ray powder diffraction as a tool for characterization of smectites, layered double hydroxides, and their intercalates with porphyrins

Anna Píšková [a,b,*], Petr Bezdička [a], David Hradil [a], Eva Káfuňková [a,c], Kamil Lang [a], Eva Večerníková [a], František Kovanda [d], Tomáš Grygar [a]

[a] Institute of Inorganic Chemistry ASCR, v.v.i., 250 68 Rez, Czech Republic
[b] Institute of Geochemistry, Mineralogy and Mineral Resources, Charles University in Prague, Albertov 6, 128 43 Prague, Czech Republic
[c] Department of Inorganic Chemistry, Faculty of Science, Charles University in Prague, Hlavova 2030, 128 43 Prague, Czech Republic
[d] Department of Solid State Chemistry, Institute of Chemical Technology, Prague, Technická 5, 166 28 Prague, Czech Republic

ARTICLE INFO

Article history:
Received 25 September 2008
Received in revised form 1 September 2009
Accepted 7 September 2009
Available online 24 September 2009

Keywords:
Smectite
Layered double hydroxides
Thermal decomposition
Dehydration
Decarbonation

ABSTRACT

We have analyzed expandable clay minerals and layered double hydroxides with different interlayer ions by high-temperature X-ray powder diffraction (HT-XRD) with comparison to thermal analysis (DTG/DTA) coupled with evolved gas analysis (EGA). We described in detail their thermal behaviour with emphasis to the differences among samples related to their crystallochemical characteristics. Porphyrin-intercalated smectites have a quite unique thermal behaviour as monitored by HT-XRD; the intercalates with tetrakis (1-methyl-4-pyridinio)porphyrin have a basal spacing of about 1.4 nm and are thermally stable up to ca. 600 °C. The resolution of the individual dehydration steps of smectites (from 2-layer hydrate *via* 1-layer hydrate to the anhydrous form) is much better in HT-XRD then in DTG/EGA curves. Layered double hydroxides (LDHs) have a varying thermal stability depending on their chemical composition and crystallinity. LDHs intercalated with porphyrin anions are thermally stable up to 350–400 °C.

1. Introduction

X-ray diffraction on a heated support (high-temperature X-ray diffraction, HT-XRD) is the *in-situ* measurement producing a set of diffractograms at each pre-set temperature. HT-XRD is a more reliable tool to study dehydration and decarbonation of crystalline solids than *ex-situ* diffraction, because HT-XRD eliminates the risk of reverse reactions after sample storage in air before the diffraction experiment. HT-XRD or high-temperature neutron diffraction is especially efficient if reactions induced by heating are directly related to well-defined changes of lattice parameters, such as dehydration and reorganization of interlayer space of layered structures of clay minerals (CMs) (e.g., Kawano and Tomita, 1991; Collins et al., 1992; Bérend et al., 1995; Bray et al., 1998) and layered double hydroxides (LDHs) (e.g., Kanezaki, 1998; Stanimirova et al., 2004). Originally, both *ex-situ* XRD during thermal decomposition and *in-situ* HT-XRD have served to study the reversibility and mechanism of thermal reactions. Later HT-XRD was used in identification of expandable clay minerals in mineral mixtures (Grygar et al., 2005), for characterization of LDHs and their decomposition products (Bellotto et al., 1996; Yang et al., 2002; Chmielarz et al., 2003; Kovanda et al., 2006; Zhang et al., 2008; Kovanda et al., 2009), organic intercalates of LDHs (Wei et al., 2004, 2005a,b, 2006; Yan et al., 2008) and discrimination between pillared CMs and mere ion-exchanged CMs (Grygar et al., 2007). The growing relevance of HT-XRD as an analytical tool can be expected because of growing popularity of materials obtained by intercalation of large ions into layered structures to produce novel sorbents, catalysts, and drug carriers (del Hoyo, 2007).

The most important obstacle in routine application of HT-XRD is the time necessary to acquire a diffraction pattern of a sufficient quality in the speed common in conventional thermal analysis. Reasonable solutions are based on application of a primary high-intensity beam, e.g., synchrotron X-ray sources (Huang et al., 1994; Artioli, 1997; Bray et al., 1998) or position-sensitive (multichannel) detectors in laboratory diffractometers (Grygar et al., 2005; Kovanda et al., 2006; Grygar et al., 2007; Kovanda et al., 2009). We have previously used HT-XRD for identification of a small amount of expandable CMs in a complex, non-separated mixture of minerals in lake sediments (Grygar et al., 2005) and also to distinguish pillared CMs and CMs intercalated by oligomeric Fe^{3+} cations (Grygar et al., 2007). In analogy, HT-XRD can be used also for analysis of various anions intercalated into LDHs. After the initial HT-XRD study of LDHs and the comparison of HT-XRD and TG/DTA/EGA (Kovanda et al., 2006, 2009) we continue the study of LDHs intercalated with porphyrin anions.

The aim of this work was to test HT-XRD as a routine analytical tool for identification and recognition of the degree and mode of intercalation of CMs and LDHs with small inorganic and large organic

* Corresponding author. Institute of Inorganic Chemistry ASCR, v.v.i., 250 68 Rez, Czech Republic. Tel.: +420 266 173 124; fax: +420 220 941 502.
E-mail address: gazanie@iic.cas.cz (A. Píšková).

0169-1317/$ – see front matter © 2009 Elsevier B.V. All rights reserved.
doi:10.1016/j.clay.2009.09.004

(porphyrin) ions in their interlayer space. We also aimed to study the possibilities of HT-XRD when discriminating between individual interlayer cations of CMs, the information hardly obtained by chemical analysis or other conventional analytical means for mixtures of CMs.

2. Experimental

2.1. Materials — clay minerals

We used the following expandable clay minerals supplied by the Source Clay Repository (Clay Mineral Society, USA): montmorillonites (STx-1, SWy-2, and SAz-1) and saponite (SapCa-2). All analyses were performed with <2 μm fractions prepared by standard laboratory procedures. The homoionic forms of various ions (K^+, Na^+, Li^+, Mg^{2+}, Fe^{3+}, Ni^{2+}, Ca^{2+}) were prepared by repeated saturation of clay minerals in 1 M chloride solutions followed by dialysing to remove the excess salts, drying, and homogenization. Li^+ homoionic forms were prepared from Na^+ forms. Porphyrin cation (5,10,15,20-tetrakis (1-methyl-4-pyridinio)porphyrin, TMPyP, Aldrich) (Fig. 1) was intercalated to the Mg^{2+} forms of STx-1 or SWy-2 by dropping a porphyrin solution into a vigorously stirred suspension of the clay mineral followed by centrifugation, drying, and homogenization of the product.

2.2. Materials — layered double hydroxides

Layered double hydroxides (LDHs) with general formula $M^{II}_{1-x}M^{III}_x(OH)_2A^{n-}_{x/n}\cdot yH_2O$ contain different M^{II} and M^{III} metal cations and A^{n-} anions were synthesized by methods suitable for individual anions A. LDH samples are labelled: M^{II} and M^{III} cations with their molar ratios and interlayer anions, e.g., nitrate form of Mg–Al LDH with the Mg/Al molar ratio of 2 is marked as Mg_4Al_2–NO_3.

Co–Al, Mg–Al, and Ni–Al LDHs in CO_3^{2-} forms were prepared by coprecipitation according to Miyata (1975). Procedure adjustment is described in detail in Kovanda et al. (2008). The nitrate and chloride forms of Mg–Al LDH were prepared under nitrogen atmosphere from carbonate-free solutions of Mg^{2+} and Al^{3+} nitrates or chlorides and 3 M NaOH. The products were precursors for preparation of Mg–Al LDHs intercalated with porphyrins.

Anion exchange (for Mg–Al–NO_3) and rehydration reactions were used for intercalation of porphyrin anions into Mg–Al LDH hosts (Lang et al., 2007). The following porphyrins were intercalated into Mg–Al LDHs: 5,10,15,20-tetrakis(4-sulfonatophenyl)porphyrin (TPPS), Aldrich; Pd(II)-5,10,15,20-tetrakis(4-carboxylphenyl)porphyrin (PdTPPC) and Zn(II)-5,10,15,20-tetrakis(4-carboxylphenyl)porphyrin (ZnTPPC), both Frontier Scientific Europe, Ltd., UK (Fig. 1). The samples are denoted by acronyms describing the Mg to Al molar ratios the LDH, intercalated porphyrin anion, its loading in percent, and the method used for the intercalation. The LDH host/porphyrin molar ratio was adjusted to achieve 10 and 100% porphyrin loading with respect to the theoretical anion exchange capacity of the LDH. The 10% excess of porphyrin was used when the samples with a theoretical load of 100% were prepared. The UV–VIS spectra of the residual filtrates document maximally 80% loading in the nominally 100% loading.

2.3. Thermal analytical experiments

HT-XRD was performed in an Anton Paar HTK16 high-temperature chamber with a PANalytical X'Pert PRO diffractometer ($Co_{K\alpha}$ radiation, X'Celerator multichannel detector). The heating program was composed of a repeated sequence of three steps: heating, delay, and diffraction experiment. Powder samples were gently ground in ethanol–water mixtures (CMs) or water (LDHs) and deposited on a Pt-plate using a micropipette to form a very thin layer upon drying. The Pt-plate serves as both the sample holder and the heating medium. The positions of diffraction lines were determined by fitting the smoothed (5 point FFT filter) diffraction patterns to Gaussian function using the OriginPro 7 (OriginLab, USA). Possible inaccuracy in the determination of the line position was less than 0.05 nm (randomly chosen curves were compared with fit of unsmoothed line and with respect to the peak asymmetry).

Conventional thermal analyses, thermogravimetry (TG), differential thermal analysis (DTA), and evolved gas analysis (EGA) were carried out using a Netzsch STA 409 instrument equipped with a QMS 403/4 quadrupole mass spectrometer (Balzers) to monitor gaseous reaction products.

3. Results

3.1. Performing HT-XRD experiment

The time necessary for HT-XRD analysis depends on the XRD angular range, number of temperature steps, and the time necessary to acquire an XRD pattern in each temperature step. Measuring programs used in this work and their total execution times are summarized in Table 1. Each program was selected to monitor certain XRD features, either only basal diffractions or basal and non-basal diffraction lines.

3.2. HT-XRD of expandable CMs

Fig. 2 represents an example of the HT-XRD scan of Mg^{2+} form of montmorillonite (MgSTx-1) showing complete dehydration of the interlayer Mg^{2+} cations in a two step collapse of the basal spacing to ~1.0 nm, i.e. formation of a mica-like structure with dehydrated interlayer cation denoted as M. Similarly to Bérend et al. (1995) and Bray et al. (1998) we use the denotation 2bLH and 2aLH, two-layer hydrates (1.5–1.4 nm), and 1LH, one layer hydrate (~1.2 nm), to assign the species responsible for the steps of the basal spacing changes induced by heating. Before the first dehydration step we detected by the removal of weakly bound water by HT-XRD as an intensity increase and a minor shift of the 001 basal diffraction line

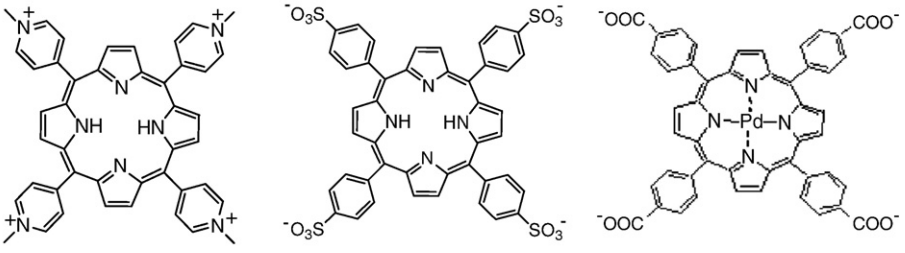

Fig. 1. Porphyrins used for intercalation to expandable CMs (TMPyP— left) and LDHs (TPPS — middle, PdTPPC — right). ZnTPPC is similar to PdTPPC but the former has Zn instead of Pd.

Table 1
Programs used in HT-XRD experiments.

	Samples (diffractions or reactions monitored)	Angular diffraction range [° 2Θ]	Temperature interval [°C]	Heating step [°C]	Total time [min]	Effective heating rate [°C/min.]
1	CMs (basal and non-basal diffractions)	4–40	25–300	5	1310	0.21
2	Porphyrin-intercalated	4–25	25–560	20	330	1.6
3	CMs (basal diffractions)		25–900	20	530	2.8
4	LDHs (*003* basal line)	11–18	25–450	10	90	5.5
5	LDHs (decomposition and crystallization of calcination products)	4–80	25–400 400–900	25 100	630	0.5 2.6
6	Porphyrin-intercalated LDHs (decomposition)	4–80	25–560	20	570	0.9

from initial 6.9 (2bLH) to 7.7° (2aLH) in the 2Θ scale (from $d = 1.50$ nm to $d = 1.42$ nm) up to 75 °C. 2LH structures with Mg^{2+} or Ca^{2+} dehydrates to M at temperatures above 200 °C. On the other hand, two-layer hydrates of alkaline metal ions are unstable under ambient conditions, and hence smectites with these ions produce single-step shrinkage of their basal spacing from 1LH to M at temperatures below 100 °C (Fig. 3). While in most cases the position of the 001 diffraction line changes gradually on dehydration, some irregularities appear in experiments with Li^+, Ca^{2+}, and Mg^{2+}. In these cases the clusters of 1LH structures are still visible in the diffraction pattern beside the major M structure that is obvious from "splitting" of the dependence of the basal diffraction line position on temperature (Fig. 3). The more detailed description of the smectite dehydration kinetics can be found in several past *ex-situ* and *in-situ* experiments (Kawano and Tomita, 1991; Collins et al., 1992; Bérend et al., 1995; Bray et al., 1998). With further temperature increase the neo-formed mica-like minerals with anhydrous metal cations in the interlayer space are decomposed *via* dehydroxylation of structural sheets leading to expulsion of interlayer cations from the interlayer space or their introduction into the structural sheets (Chorom and Rengasamy, 1996; Hrobáriková et al., 2001), and/or crystallization of new alumosilicates. However, the information most straightforward and specific to expandable CM structures can be obtained from the dehydration steps.

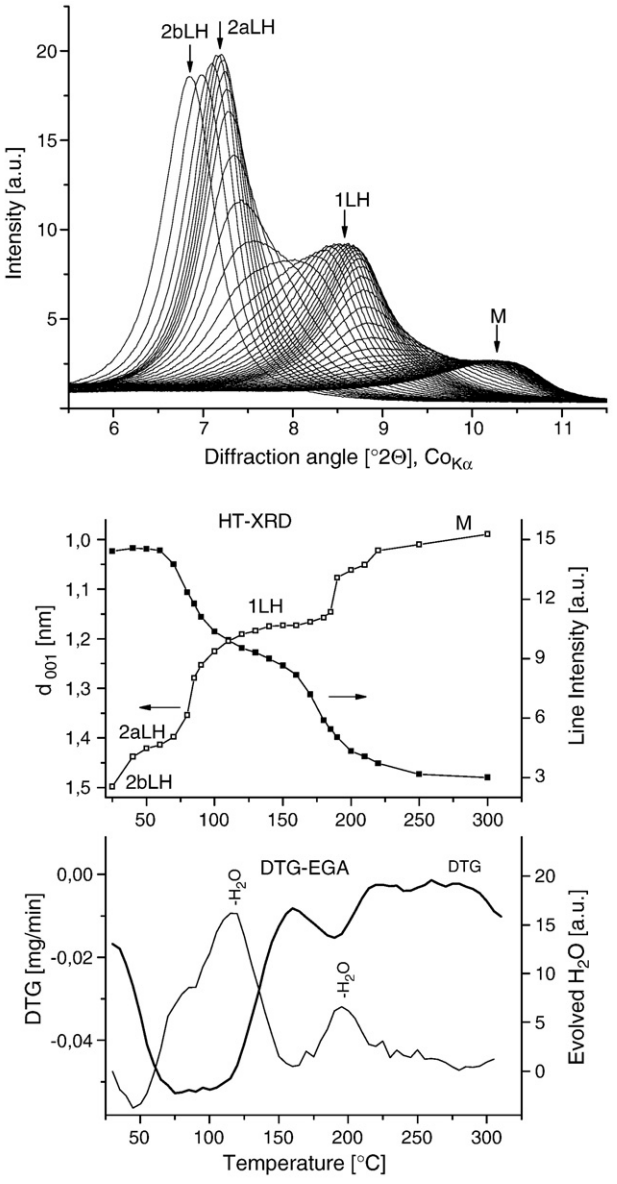

Fig. 2. HT-XRD (upper and central panels) and DTG-EGA (bottom panel) of Mg-saturated STx-1 montmorillonite. The "two-layer" hydrate 2aLH (basal spacing 7.2°, 1.42 nm) and the "one layer" hydrate 1LH (8.7°, 1.18 nm) predominate at 45 °C and 130 °C, respectively, and the anhydrous mica-like form (M) (10.3°, 0.99 nm) is formed at about 300 °C. 2bLH — original form, 2aLH — slightly dehydrated form. HT-XRD program 1 (Table 1).

The dehydration mechanism of a given interlayer cation is affected by the kind of the expandable clay mineral, as it is documented in Fig. 4. In the second stage of the dehydration, trioctahedral expandable CM (saponite) dehydrates at a higher temperature than dioctahedral expandable CMs (montmorillonites). The final dehydration temperature is higher also in the case of Li^+ or Na^+ forms of saponite if compared to the corresponding homoionic smectites (not shown).

The flat molecule of TMPyP is easily intercalated into the CMs structure. The intercalation causes a colour change from deep violet (solution of porphyrin) to greenish (suspension with porphyrin and CMs) due to changes in orientation of pyridinium substituents. Even partly TMPyP-exchanged expandable CMs have almost the same behaviour in HT-XRD experiment as samples with 100% ion exchange (Table 2). The actual interlayer spacing of porphyrin-intercalated CMs depends on the actual tilting of pyridyl rings and other factors (Carrado and Winans, 1990). The thermal stability of porphyrin-containing intercalates is much higher in the comparison with smectites with alkaline and alkaline earth metal cations (Table 2). At low temperatures (<100 °C), the basal spacing (forms of hydrated intercalate bHI and aHI) is slightly shifted similarly to pure montmorillonite (Fig. 5). Basal diffractions of aHI at ~1.35 nm remain almost constant between 100 and 350 °C and anhydrous intercalate (AI) at ~1.29 nm between 450 and 550 °C, and then gradually collapses to a mica-like structure M with basal spacing ~1.0 nm (Fig. 5). This collapse is related to the complete burning off of the organic intercalated cation.

3.3. HT-XRD of LDHs

The thermal decomposition of LDHs is initiated by dehydration and reorganization of the interlayer space with intercalated anions. The expulsion and decomposition of the interlayer anions and the

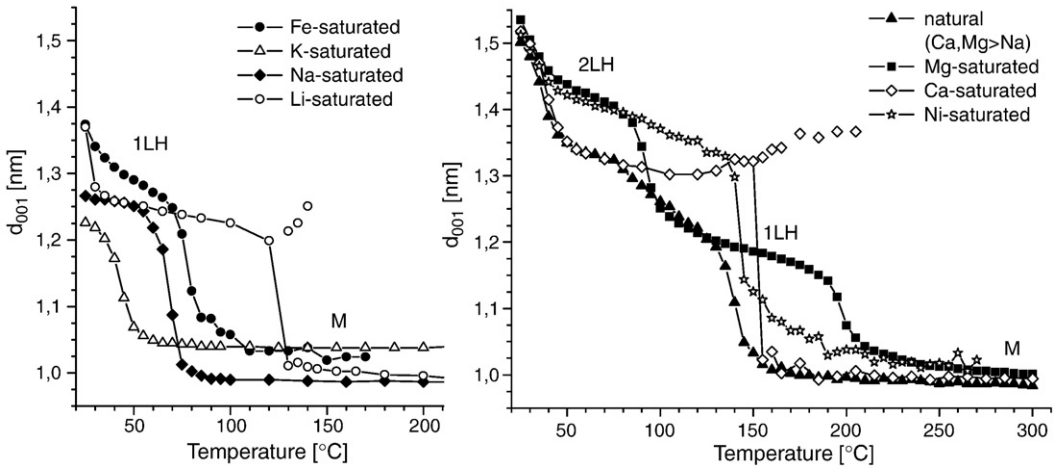

Fig. 3. The shift of the (001) basal diffraction line of smectite SAz-1 with different inorganic interlayer cations obtained by HT-XRD (program 1, Table 1).

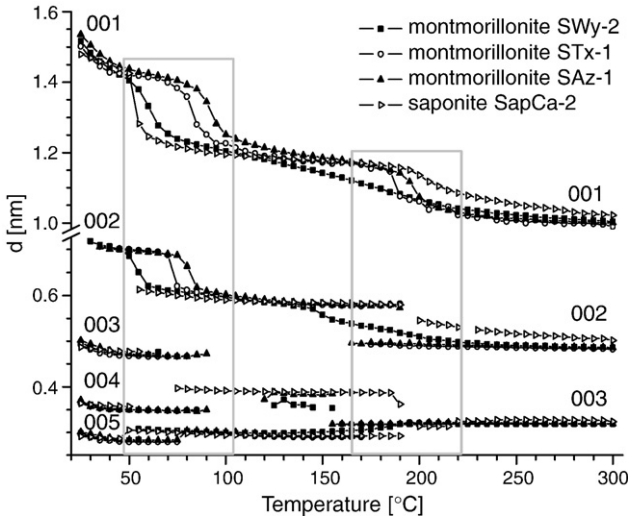

Fig. 4. Dehydration of different Mg-saturated smectites using program 1 (Table 1). Grey rectangles highlight major dehydration steps representing destruction of the hydrate layer. For the description of the dehydration the (001) diffraction line is typically used but the trend of contraction is also clearly visible from the shift of the other basal diffraction lines. The dehydration temperature of dehydration evaluated using the (002) line position is shifted toward lower temperatures when compared to that obtained using the (001) line position.

destruction of the layered structure occur at temperatures above 300 °C (Stanimirova et al., 2004). Both of these processes can be characterized by HT-XRD. An example, Co_4Al_2–CO_3 (Fig. 6) documents the shift of the 003 diffraction line of LDH from 0.75 nm at a room temperature (the original structural form is denoted LDH-1) to 0.67 nm at 190 °C (dehydrated and reorganized form is denoted LDH-2). A similar decrease of the basal spacing 003 from 0.76 to 0.66 nm was reported for Mg_4Al_2–CO_3 (Yang et al., 2002, Wei et al., 2004). Most studies including the thermal decomposition of LDHs have been focused on their carbonate forms; we compare the complete thermal behaviour of LDHs containing CO_3^{2-}, NO_3^-, Cl^- and porphyrin anions (Table 3).

The original basal spacings measured for the nitrate forms of LDHs (Table 3) are in good agreement with those reported by del Arco et al. (2000) (0.875 nm for Mg_4Al_2–NO_3 and 0.808 nm for Mg_8Al_2–NO_3) and Wang and Wang (2007) (0.900 for Mg_4Al_2–NO_3 and 0.804 nm for Mg_8Al_2–NO_3). Both original (LDH-1) and shrunk (LDH-2) form have larger basal spacings than corresponding carbonate forms. In contrast to the behaviour of the carbonate and nitrate form of LDHs, the LDH-2 basal spacing of the chloride form (Mg_6Al_2–Cl) decreases very little, only by 0.04 nm (Table 3). Therefore, while the original basal spacings of the chloride and carbonate forms of LDHs (LDH-1) are very similar, both samples are clearly discernible according to their LDH-2 forms. The thermal behaviour studied by HT-XRD hence allows identifying the actual anion form of LDHs.

The decomposition temperatures of LDHs varied from 270 °C (Co–Al LDH) to 400 °C (poorly crystalline Mg–Al LDH) (Table 3). The difference in the actual elemental composition of LDHs strongly influences their final thermal stability, e.g. lower charged Mg_8Al_2 is stable up to 300 °C whereas LDHs with a higher layer charge Mg_4Al_2 are stable to temperatures at least by 50 °C higher.

HT-XRD and TG/EGA results give comparable qualitative information. However, there is a systematic quantitative difference between temperatures of the water desorption (DTG minimum at 137 °C, maximum H_2O evolution at 150 °C) and the documented formation of LDH-2 (the lattice shrinkage had an inflex point at 100 °C, the diffraction lines of LDH-1 completely disappear at 150 °C). A similar difference is observed in the temperatures of the subsequent major process of LDHs thermal decomposition, the amorphization, dehydroxylation, and decarbonation. At 325 °C, the layered structure of LDH-2 is not discernible in HT-XRD. The inflex of the mass decrease is

Table 2
The dehydration of TMPyP intercalated and non-intercalated STx-1 montmorillonite.

Temperature [°C]	Position of diffraction line (001) [nm] at given temperature									Used program
	20	60	100	200	300	400	500	600	700	
MgSTx-1	1.50	1.42	1.23	1.06	0.99					1
MgSTx-1/TMPyP (50)	1.38	1.37	1.36	1.35	1.35	1.33	1.29			2
CaSTx-1	1.48	1.35	1.33	1.19	1.14					1
CaSTx-1/TMPyp (10)	1.49	1.33	1.29	1.31	1.31	1.29	1.25	1.22	0.99	3
CaSTx-1/TMPyp (30)	1.38	1.36	1.35	1.34	1.34	1.29	1.27	1.24	1.02	3
CaSTx-1/TMPyp (50)	1.38	1.36	1.35	1.35	1.35	1.34	1.29	1.28	1.01	3

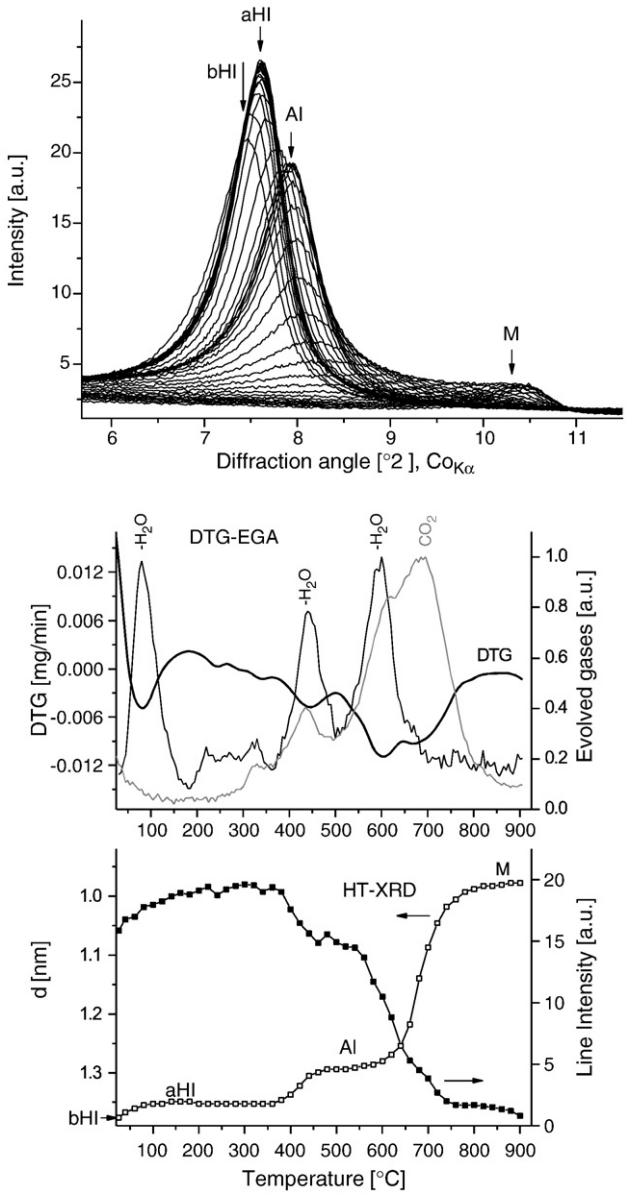

Fig. 5. The thermal analysis of CaSTx-1/TMPyP 50%, HT-XRD (the upper and bottom panels) evaluated using the (001) diffraction line and DTG/EGA (the central panel). bHI and aHI denote the hydrated intercalates, AI the anhydrous intercalate, and M the mica-like decomposition product. HT-XRD program 2 (Table 1).

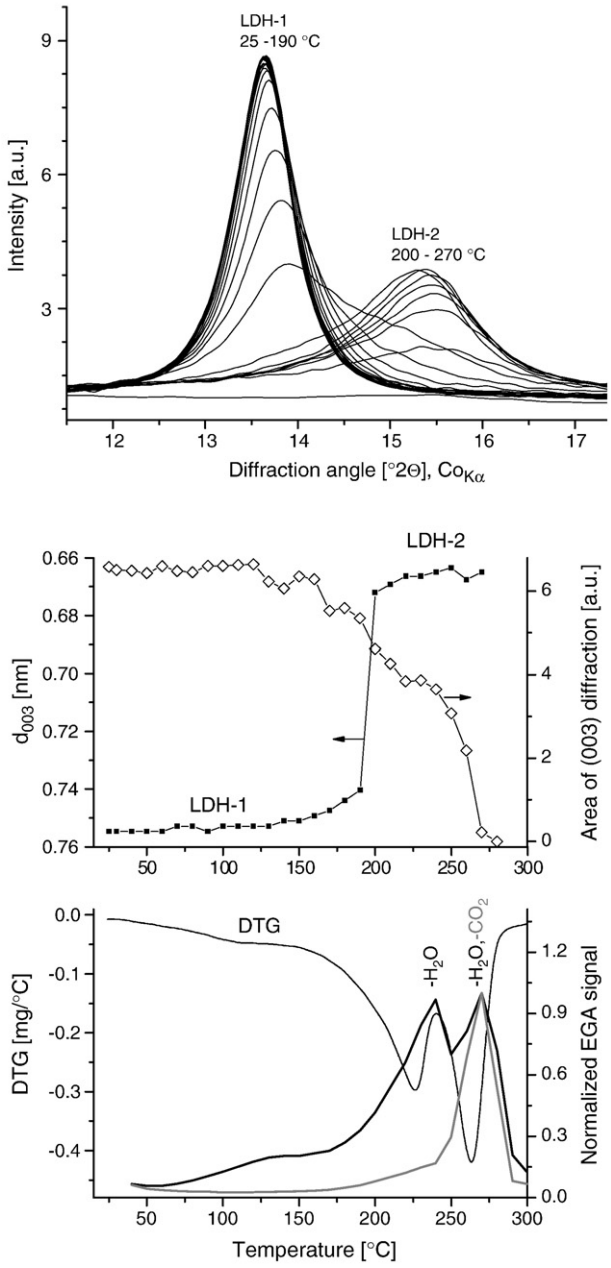

Fig. 6. The comparison of HT-XRD (the upper and central panels) and DTG/EGA (the bottom panel) of Co_4Al_2–CO_3. LDH-1 is the parent from and LDH-2 is the species formed after the partial dehydration and thermal reorganization of the interlayer anion. HT-XRD program 4 (Table 1).

at 330 °C in DTG and the peaks of the gas evolution are at 335 °C for H_2O and 425 °C for NO_2 in EGA. These temperature discrepancies between the two methods confirm our hypothesis that the gaseous reaction products escape from amorphous oxides after the complete destruction of the regular crystal structure of LDH-2 (Kovanda et al., 2006, 2009). The influence of different heating rates of HT-XRD and thermoanalytical methods on these discrepancies is insignificant, as it is demonstrated in Fig. 7, where HT-XRD scans at two different temperature rates are evaluated by the variation in the integral intensity of the basal diffraction lines. The intensity variations are accompanied by the changes of the lattice size. The decomposition (amorphization) is not postponed to higher temperatures with the increase of the effective heating rate from 0.5 to 5.5 °C/min. The heating rate of DTA (2 °C/min) was within the ranges of HT-XRD measurements, and hence we can neglect the kinetic effect on the results of these methods.

In comparison with conventional TG/DTA characterization, HT-XRD can bring additional information related to the actual crystallographic features of the individual structures. In Table 3, two different routes of thermal decomposition of Mg_4Al_2–CO_3 are shown depending on the LDH crystallinity. The well-crystalline LDH specimens (full width at half maximum (FWHM) of 003 diffraction line = 0.26° in the 2Θ scale) behaves in the same manner as the specimens described above and in literature (Yang et al., 2002). Contrarily, a poorly crystalline LDH specimen (FWHM of 003 diffraction line = 1.32° in the 2Θ scale) behaves in an opposite manner: the lattice expanded upon heating from 0.76 nm to 0.90 nm (Table 3). Such behaviour has not been described yet, probably because only well-crystalline LDHs were subjected to structural studies. Another effect of crystallinity on the thermal behaviour is a slower and less evident reorganization observed for Ni_4Al_2–CO_3 obtained by anion exchange in contrast to hydrothermally re-crystallized Ni_4Al_2–CO_3. The 003 diffraction line of the poorly crystalline specimen has FWHM of 2.9° (in the 2Θ scale) while the

Table 3
The positions of the (003) basal diffraction line of LDHs, temperatures of LDH crystal structure alteration, and temperature of LDH decomposition (disappearance of layered structure).

LDH stoichiometry and interlayer anion	(003) of LDH-1 [nm]	Temperature of change along *c* axis [°C]	(003) of LDH-2 [nm]	Temperature of LDH decomposition [°C]
Ni_4Al_2–CO_3, 20 h	0.757	210	0.66	350
Mg_4A_2–CO_3 poorly crystalline	0.761	150	0.90	400
$Mg_4Al_2CO_3$, 20 h	0.762	190	0.66	375
Co_4Al_2–CO_3	0.753	190	0.67	270
Mg_4Al_2–NO_3	0.884	140	0.76	350
Mg_8Al_2–NO_3	0.798	100	0.76	300
Mg_6Al_2–Cl	0.778	90	0.74	370
Porphyrin-intercalated LDH	(003) of intercalate [nm]		(003) before decomposition [nm]	
Mg_4Al_2/PdTPPC(100)R	2.25	140	2.05	400
Mg_4A_2/ZnTPPC(100)R	2.25	continuous broadening	2.06	400
Mg_4Al_2/TPPS(100)R	2.17		2.03	360
Mg_4Al_2/TPPS(100)AE	2.19		1.87	350
Mg_6Al_2/TPPS(100)AE	2.21		1.80	340
Mg_4Al_2/TPPS(10)AE	2.20		2.08	350

20 h marks 20 h of autoclave aging.

hydrothermally aged specimen has FWHM of 0.64°. The lattice shrinkage has a much sharper course in the latter specimen, but surprisingly, it occurred at lower temperature.

Our HT-XRD results (Table 3) cover LDHs differing in the porphyrin-intercalated (TPPS or TPPC complexes), the metal cation in the TPPC porphyrin structure (Zn, Pd), the layer charge of the host structure (Mg/Al molar ratio of 2, 3, and 4), and the method of their synthesis. The porphyrin intercalation changes the basal spacing of the LDH according to the porphyrin size, i.e., diffraction lines 003 shift to 2.25 and 2.17 nm for TPPC and TPPS, respectively. The typical thermal transformation has three stages similar to non-intercalated LDH. In the first one between room temperature and 125 °C, all the basal diffraction lines are shifted toward a lower *d*-spacing and the 003 line increases in the intensity due to an improved structure ordering after the release of weakly bounded interlayer water. The second stage, starting from 150 °C, represents reorganization specific for the type of the porphyrin. The basal diffraction lines of ZnTPPC intercalate move continuously toward lower *d*-spacing with a slightly decreasing intensity, whereas 003 of TPPS intercalate remains at its initial positions up to 225 °C and the intensity of the 006 line is increasing both indicating some structural reorganizations of the intercalates. Porphyrin PdTPPC intercalate had already significantly decreased intensities of all basal diffraction lines and on heating from 150 up to 380 °C their positions remain almost constant. The last stage of the thermal decomposition is the loss of crystallinity followed by a structure collapse, i.e., the continuous movement of the basal diffraction lines toward lower *d*-spacing with a significant line broadening at temperatures depending on the kind of intercalated porphyrin: it starts at 220 °C (Mg_4A_2/ZnTPPC(100)R), 300 °C (Mg_4Al_2/TPPS(100)AE) and 380 °C (Mg_4Al_2/PdTPPC(100)R). The structural collapse is accompanied by the complete disappearance of all basal diffraction lines at temperatures specified in Table 3. Wei et al. (2006) pointed out that these processes are connected not only with the decomposition of intercalated porphyrin and the co-intercalated anion, but also with the dehydroxylation of the host layers. According to our results, LDHs intercalated with TPPC are stable up to 400 °C and with TPPS up to 360 °C. The contraction of the structure between 25 and 200 °C for ZnTPPC-LDH is expressed by the change of the *d*-spacing values: 003 2.25–2.11 nm, 006 1.12–1.05 nm, 009 0.748–0.697 nm, and 00-12 0.559–0.523 nm.

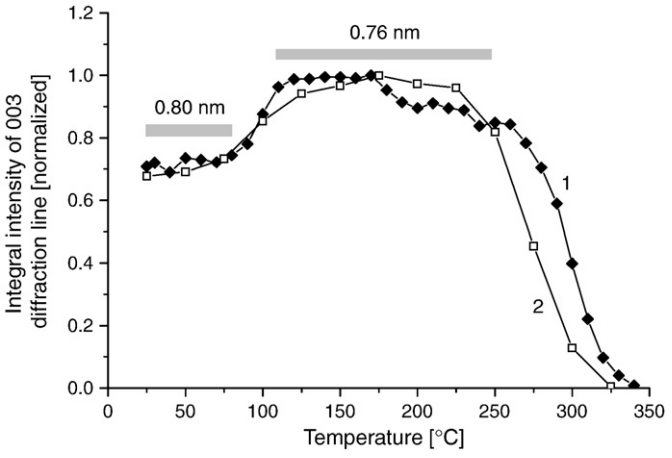

Fig. 7. The influence of the effective heating rate during HT-XRD measurements of Mg_4Al_2–NO_3. Curve 1: 0.85 °C/min (program 4, Table 1), curve 2: 5.6 °C/min (program 3, Table 1). Ranges of stability of original (LDH-1) and partly collapsed structures (LDH-2) are denoted by grey rectangles labelled by the corresponding *d*-spacing of the (003) diffraction line.

The complete (100%) porphyrin loading of LDHs has never been achieved in the performed syntheses. We always observed small remnants of non-intercalated LDH particles (Fig. 8), i.e., there is always a minor 003 diffraction line of the original host precursor at 0.76 nm. The non-intercalated LDH particles behave as poorly crystalline, which is proved by the appearance of a broad 003 diffraction line of LDH-2 at 0.90 nm instead of 0.66 nm after heating (Table 3, Fig. 8). The intercalates with low loading (10%) exhibited a broad 003 diffraction line at the same *d*-spacing (Table 3) as high-loaded LDHs, i.e., the porphyrin molecule has the same position irrespective of the loading. LDHs intercalate collapse was accompanied by the appearance of a broad diffraction line at the beginning of the diffraction patterns. The determination of an exact position of this diffraction was not possible due to limitations in the instrument geometry at $<4°$ 2θ).

4. Discussion

4.1. HT-XRD of clay minerals

The dependence of the dehydration mechanism on the interlayer cation allows distinguishing homoionic forms of a given expandable CM. This would not be possible in the case of a mixture of interlayer

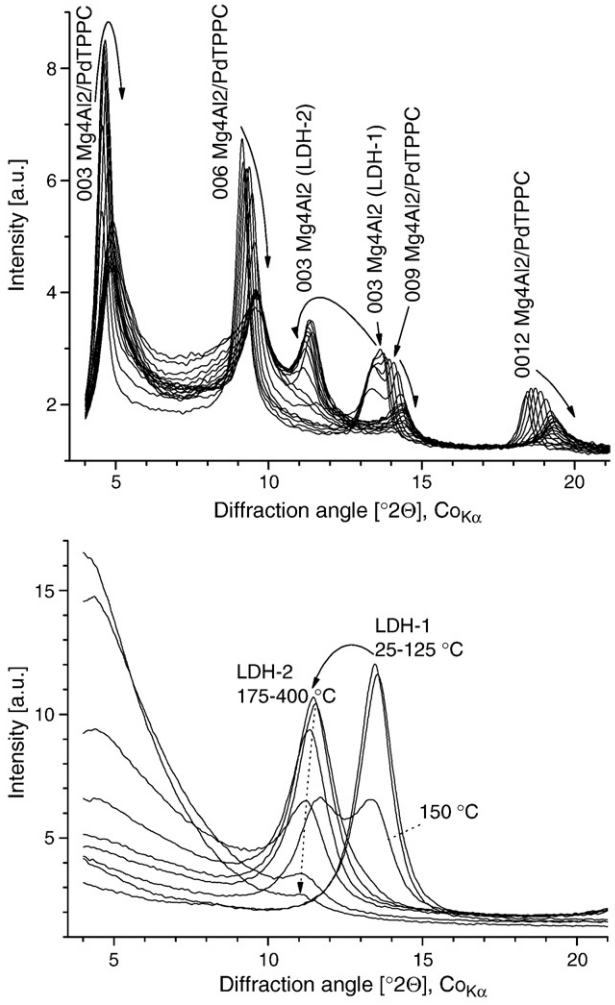

Fig. 8. HT-XRD of Mg_4Al_2/PdTPPC(100)R (the upper panel) using program 6 (Table 1) in comparison with poorly crystalline Mg_4Al_2–CO_3 (the bottom panel) using program 4 (Table 1). The mixture of intercalated Mg_4Al_2/PdTPPC and non-intercalated Mg_4Al_2 particles is well visible. The thermal behaviour of non-intercalated Mg_4Al_2 particles is identical with the poorly crystalline Mg_4Al_2–CO_3.

cations. For example, the natural form of smectite SAz-1 contains Ca^{2+}, Mg^{2+} and minor amount of Na^+, and its dehydration pattern is "in-between" Na- and Mg-homoionic forms (Fig. 3).

The "resistance" of homoionic smectites to the dehydration to the mica-like structure with ~1.0 nm basal spacing (Fig. 3) increases in the following order:

$$K^+ < Na^+ < Fe^{3+} < Li^+ < Ni^{2+} < Mg^{2+}, Ca^{2+} < Al^{3+}$$

The stability of smectite with Al^{3+} in the interlayer space was reported in Grygar et al. (2007). This order is in good agreement with *ex-situ* analysis (Casses et al., 1997; Bray et al., 1998; Bérend et al., 1995) except for Ca^{2+} forms. The dehydration temperature changes in a broad range of temperatures from less than 100 °C for monovalent cations to ~200 °C for Mg^{2+}, Ca^{2+} and >300 °C for Al^{3+}. The thermal stability of 1LH form of Ca-saturated smectites is rather surprising with respect to the previous report by Casses et al. (1997), who found that Ca-montmorillonite dehydrates easier than Mg-form. We checked the 'postponed' formation of the dehydrated M form of Ca-montmorillonites using several Ca-homoionic specimens and the higher temperature of 1LH to M transformation of Ca-saturated CMs with respect to Mg-saturated CMs was repeatedly confirmed. It is probable that rather specific properties of individual cations are responsible for their different stability in a hydrated form in the interlayer gallery, because there is seemingly no simple explanation of this order such as charge density or ionic radii. Additionally, it is not sure that all these cations are present in the purely ionic form in the interlayer space (Ferrage et al., 2005).

According to the thermal stability of Mg-exchanged expandable CMs toward dehydration from 2LH form (basal spacing ~1.5 nm) to 1LH form (basal spacing ~1.2 nm) (Fig. 4) the following order can be established

$$SapCa-1 < SWy-2 < STx-1 < SAz-1$$

However, there are significant differences in the CMs stability between the first and the second dehydration steps. SapCa-1 has the highest final dehydration resistance, probably due to its tetrahedral charge that produces higher charge density at the layer–interlayer interface and a stronger Coulombic interaction of H_2O dipoles and CM skeleton. Contrarily the other smectites–montmorillonites SWy-2, STx-1, SAz-1 with octahedral charge dehydrate at lower temperatures.

Kaufherr et al. (1971) and then Kosiur (1977) were the first authors who mentioned that porphyrin cations intercalated in the interlayer increase thermal stability of the expanded forms of CMs. The basal spacing of TMPyP intercalated smectite (about 1.35 nm) remains unchanged between 100 and 350 °C. Then, between 450 and 550 °C, there is a slight collapse of the intercalate basal spacing to about 1.3 nm probably due to a partial destruction of the porphyrin. Yermiyahu et al. (2005) reported formation of charcoal from a sulfonated azo dye intercalated in CM at about 480 °C. According to the results of DTA, TMPyP oxidation in air is completed at 630 °C, and correspondingly above 600 °C the intercalated CM is converted to the mica-like structure.

The porphyrin is a very efficient spacer of the clay structure: the basal spacing and thermal stability of the intercalates are almost the same even when ion exchange is only 10% (Table 2). The flat molecule of porphyrins is aligned parallel with the structural sheets of CMs (Constantino et al., 2000), and hence the height of the interlayer gallery cannot be controlled by the percentage of the porphyrin exchange, unless interstratified (mixed layer) structures were formed (it was not observed).

4.2. Layered double hydroxides

The observed dependence of the thermal stability of LDHs on the type of M(II) and M(III) cations and their ratio in the hydroxide layers has already been proved, mostly by TG/DTA/EGA analysis (Yun and Pinnavaia, 1995; Zhao et al., 2002; Chmielarz et al., 2003; Lin et al., 2005). HT-XRD can monitor the thermally induced reorganization of the interlayer space in CO_3^{2-} and NO_3^- forms. Well crystalline carbonate and nitrate forms show substantial decrease of the *d* values of the basal diffraction line upon heating, while the *d* value of the poorly crystalline carbonate form increases. del Arco et al. (2000) found that the decomposition temperature of LDHs with borate and silicate anions is higher than that with nitrate anions. In the case of non-volatile species, such as chlorite and silicate anions, XRD is the most versatile technique to monitor the course of the thermal reactions.

The knowledge of the thermal behaviour of LDHs can be used to identify various synthetic mixtures of intercalated and non-intercalated LDHs (Fig. 8). The analysis of the porphyrin intercalates is not a trivial task, because the mere fact of "immobilization" of porphyrin in the solid product does not necessarily mean their intercalation unless physical adsorption and aggregation of porphyrin on the external surface of LDH crystals is excluded. HT-XRD can hence serve as a specific and convenient tool for the description of the porphyrin anions in the solid products.

Wei et al. (2004, 2005a, 2005b, 2006) and Yan et al. (2008) recorded a small decrease of the diffraction 003 line intensity on

heating <100 °C in HT-XRD of organic intercalates of LDHs. We observe the same phenomenon in organic intercalates of CMs (Fig. 5). It is surprising that even removal of such a weakly bound water (DTG change below 100 °C) is reflected by a structural change, i.e., that even weakly bound interlayer water is not bound only on an external surface but crystallochemically. Thus HT-XRD allows specifically distinguishing between weakly chemically sorbed (structural) water intercalated in molecules and superficially bound water. The same effect was observed in a very mild dehydration of porphyrin-intercalated LDH where that weak dehydration substantially affected the photophysical behaviour of the intercalate (Lang et al., 2007).

LDHs intercalated with less stable organic molecules (methoxy-methyl-naphthaleneacetic acid or tyrosin) are decomposed to amorphous products at 350 °C (Wei et al. 2004, 2005a, 2006), i.e. at temperatures similar to the decomposition of LDH with common inorganic anions. Our results show similar temperature for the TPPS intercalate (Table 3) but intercalates with TPPC complexes are stable up to 400 °C, i.e. intercalation increased the thermal stability in comparison with the parent LDH precursor by about 50 °C. Wei et al. (2004) suggested that organic intercalate is more stable than free organic molecule. However, our DTA results of TPPS and TPPC anions show that the trend of increased stability is not as trivial. TPPC complex is stable up to 350 °C and its intercalate up to 400 °C, contrarily TPPS remains unchanged at least up to 500 °C whereas its intercalate has stability not more than 360 °C. These differences might be caused by the catalytic activity of finely dispersed metal oxides formed by decomposition of the LDH structural sheets, in certain cases the intercalates can be burnt out during the measurements easier than pure porphyrins.

The orientation of porphyrin molecules in the LDH interlayer gallery was suggested by Bonnet et al. (1996) and Constantino et al. (2000). They concluded that the porphyrin planes are oriented perpendicularly to the plane of the LDH layers and closely packed. This alignment corresponds to ca. 2.3 nm basal spacing (0.48 nm for brucite-like layers and 1.84 nm for the porphyrin anion), which is slightly higher than our results. It could indicate that the angle between the porphyrin plane and the LDH layer is slightly lower than 90°. This porphyrin alignment is similar in the partly loaded (10%) LDHs. The described behaviour is opposite to the behaviour of clay minerals (see above).

4.3. Comparison of HT-XRD vs. TG/DTA/EGA results

The main processes connected to the temperature increase including the removal of the interlayer water (dehydration), dehydroxylation of the layers and a loss of the interlayer cation are mirrored by structural changes observed by HT-XRD and by weight losses and evolved gases viewed by TG/DTA/EGA. The comparison of both methods is shown in Figs. 2, 5, and 6. While the dehydration of CMs with inorganic cations (Fig. 2) is easily traced by HT-XRD without TG/DTA analysis, the porphyrin intercalation in the case of CMs (Fig. 5) makes the situation more complicated: the thermal processes could be unambiguously identified only by using both methods. HT-XRD itself cannot distinguish dehydration, decarbonation (organic cation decomposition), and dehydroxylation.

In our previous report on Co–Al (Kovanda et al., 2006) and Ni–Al LDHs in carbonate forms (Kovanda et al. 2009) we described a significant difference in the estimated temperatures of thermal reactions as obtained by HT-XRD and by conventional thermal analysis. In particular, TG/DTA/EGA indicated that the decarbonation and sometimes the dehydration of LDHs follow the structural changes monitored by HT-XRD by a few tens °C. The "delayed" evolution of carbonates and nitrates (420 °C) after the amorphization (300 °C) of LDH-2 is also observed in Fig. 6, a clear example that TG/DTA/EGA can give discrepant estimates of the characteristic temperatures than HT-XRD because of the different physical–chemical nature of the processes monitored. This dissimilarity is likely caused by the chemisorption of molecular CO_2 and NO_2 on the surface of structurally amorphous metal oxides formed by the LDH decomposition.

That "delay" of thermoanalytical methods with respect to HT-XRD was not significant in the dehydration of interlayer cations in CMs. Although the heating rates in HT-XRD and TG/DTA/EGA varied between 1 and 6 °C/min), the resulting temperatures of the dehydration reactions shift within 10–20 °C and difference between dehydration temperatures of CMs estimated by HT-XRD and thermo-analytical methods are within the same range.

5. Conclusions

HT-XRD is a versatile tool for analysis of clay minerals and LDHs, because they both contain hydrated interlayer species producing typical dehydration/decomposition patterns on heating. In very specific reactions such as dehydration, HT-XRD easily distinguishes physically adsorbed water and intercalated water both evolving at temperatures below 100 °C. In LDHs, carbonate and nitrate anions show a structural reorganization typical for these anions while LDHs with chloride ions do not produce such changes.

We applied HT-XRD not only for the description of the dehydration steps or the detailed observation of layered structure collapse but also for distinguishing interlayer cation or anion. The results obtained by HT-XRD are rather specific for differently charged layered structures. Comparing thermal behaviour of porphyrin intercalated into positively charged CMs or negatively charged LDHs we can formulate general conclusions: Both structures can be easily intercalated with porphyrins, but a difference came with the partial loading and stability of intercalated structures. Whereas intercalated CMs with varying intercalation extent behave in the same way, because partially loaded CMs form interstratified or mixed structures, LDHs form physical mixtures of intercalated and non-intercalated host structures. Other difference originates from the relative thermal stabilities of the porphyrin intercalates. The porphyrin intercalation increases the stability of the expanded form of CMs toward their dehydration to mica-like structures from about 300 °C to 600 °C. There is a substantial dissimilarity in the thermal stability of intercalated LDHs related to the type of the intercalated porphyrin. However, LDHs never increased its thermal stability by more than 50 °C. The different behaviour can be explained by diverse porphyrin orientation in the interlayer space. The parallel alignment of the porphyrin molecules between the CM layers probably better shields the structure against oxidation.

Acknowledgements

This work was supported by the Czech Science Foundation (203/06/1244) and by the Grant Agency of the Academy of Science of the Czech Republic (IAA3032401, KAN100500651). The authors are grateful to Michaela Hrušková for preparing homoionic forms of clay minerals.

References

Artioli, G., 1997. In situ powder diffraction studies of temperature induced transformations in minerals. Nuclear Instruments and Methods in Physics Research B 133, 45–49.

Bellotto, M., Rebours, B., Clause, O., Lynch, J., Bazin, D., Elkaim, E., 1996. Hydrotalcite decomposition mechanism: a clue to the structure and reactivity of spinel-like mixed oxides. Journal of Physical Chemistry 100, 8535–8542.

Bérend, I., Cases, J.M., François, M., Uriot, J.P., Michot, L., Masion, A., Thomas, F., 1995. Mechanism of adsorption and desorption of water vapor by homoionic montmorillonites: 2. The Li^+, Na^+, K^+, Rb^+ and Cs^+- exchanged forms. Clays and Clay Minerals 43, 324–336.

Bonnet, S., Forano, C., de Roy, A., Besse, J.P., Maillard, P., Momenteau, M., 1996. Synthesis of hybrid organo-mineral materials: anionic tetraphenylporphyrins in layered double hydroxides. Chemistry of Materials 8, 1962–1968.

Bray, H.J., Redfern, S.A.T., Clark, S.M., 1998. The kinetics of dehydratation in Ca-montmorillonite: an in situ X-ray diffraction study. Mineralogical Magazine 62, 647–656.
Carrado, K.A., Winans, R.E., 1990. Interactions of water-soluble porphyrins and metaloporphyrins with smectite clay surfaces. Chemistry of Materials 2, 328–335.
Casses, J.M., Bérend, I., François, M., Uriot, J.P., Michot, L.J., Thomas, F., 1997. Mechanism of adsorption and desorption of water vapor by homoionic montmorillonite: 3. the Mg^{2+}, Ca^{2+}, Sr^{2+} and Ba^{2+} exchanged forms. Clays and Clay Minerals 45, 8–22.
Chmielarz, L., Kuśtrowski, P., Rafalska-Łasocha, A., Dziembaj, R., 2003. Influence of Cu, Co and Ni cations incorporated in brucite-type layers on thermal behaviour of hydrotalcites and reducibility of the derived mixed oxide systems. Thermochimica Acta 395, 225–236.
Chorom, M., Rengasamy, P., 1996. Effect of heating on swelling and dispersion of different cationic forms of a smectite. Clays and Clay Minerals 44, 783–790.
Collins, D.R., Fitch, A.N., Catlow, C.R.A., 1992. Dehydration of vermiculites and montmorillonites: a time-resolved powder neutron diffraction study. Journal of Materials Chemistry 2, 865–873.
Constantino, V.R.L., Barbosa, C.A.S., Bizeto, M.A., Dias, P.M., 2000. Intercalation compounds involving inorganic layered structures. Anais de Academia Brasileira de Ciências 72, 45–49.
del Arco, M., Gutiérrez, S., Martín, C., Rives, V., Rocha, J., 2000. Effect of the Mg: Al ratio on borate (or silicate)/nitrate exchange in hydrotalcite. Journal of Solid State Chemistry 151, 272–280.
del Hoyo, C., 2007. Layered double hydroxides and human health: an overview. Applied Clay Science 36, 103–121.
Ferrage, E., Tournassat, C., Rinnert, E., Charlet, L., Lanson, B., 2005. Experimental evidence for Ca-chloride ion pairs in the interlayer of montmorillonite. An XRD profile modeling approach. Clays and Clay Minerals 53, 348–360.
Grygar, T., Bezdička, P., Hradil, D., Hrušková, M., Novotná, M., Kadlec, J., Pruner, P., Oberhänsli, H., 2005. Characterization of expandable clay minerals in Lake Baikal sediments by thermal dehydration and cation exchange. Clays and Clay Minerals 53, 389–400.
Grygar, T., Hradil, D., Bezdička, P., Doušová, B., Čapek, L., Schneeweiss, O., 2007. Fe(III)-modified montmorillonite and bentonite: synthesis, chemical and UV–Vis spectral characterization, As sorption, and catalysis of oxidative dehydrogenation of propane. Clays and Clay Minerals 55, 165–176.
Hrobáriková, J., Madejová, J., Komadel, P., 2001. Effect of heating temperature on Li-fixation, layer charge and properties of fine fractions of bentonites. Journal of Materials Chemistry 11, 1452–1457.
Huang, W.-L., Bassett, W.A., Wu, T.-C.h., 1994. Dehydratation and hydratation of montmorillonite at elevated temperatures and pressures monitored using synchrotron radiation. American Mineralogist 79, 683–691.
Kanezaki, E., 1998. Direct observation of a metastable solid phase of Mg/Al/CO3 – layered double hydroxide by means of high temperature in situ powder XRD and DTA/TG. Inorganic Chemistry 37, 2588–2590.
Kaufherr, N., Yariv, S., Heller, L., 1971. The effect of exchangeable cations on the sorption of chlorophyllin by montmorillonite. Clays and Clay Minerals 19, 193–200.
Kawano, M., Tomita, K., 1991. Dehydration and rehydration of saponite and vermiculite. Clays and Clay Minerals 39 (2), 174–183.
Kosiur, D.R., 1977. Porphyrin adsorption by clay minerals. Clays and Clay Minerals 25, 365–371.
Kovanda, F., Rojka, T., Dobešová, J., Machovič, V., Bezdička, P., Obalová, L., Jirátová, K., Grygar, T., 2006. Mixed oxides obtained from Co and Mn containing layered double hydroxides: preparation, characterization, and catalytic properties. Journal of Solid State Chemistry 179, 812–823.
Kovanda, F., Káfuňková, E., Rojka, T., Lang, K., 2008. Intercalation of porphyrins into Mg–Al hydrotalcite. Materials Structure 15 (1), 28–32.
Kovanda, F., Rojka, T., Bezdička, P., Jirátová, K., Obalová, L., Pacultová, K., Bastl, Z., Grygar, T., 2009. Effect of hydrothermal treatment on properties of Ni–Al layered double hydroxides and related mixed oxides. Journal of Solid State Chemistry 182 (1), 27–36.
Lang, K., Bezdička, P., Bourdelande, J.L., Hernando, J., Jirka, I., Káfuňková, E., Kovanda, F., Kubát, P., Mosinger, J., Wagnerová, D.M., 2007. Layered double hydroxides with intercalated porphyrins as photofunctional materials: subtle structural changes modify singlet oxygen production. Chemistry of Materials 19, 3822–3829.
Lin, Y.-J., Li, D.-Q., Evans, D.G., Duan, X., 2005. Modulating effect of Mg–Al–CO_3 layered double hydroxides on the thermal stability of PVC resin. Polymer Degradation and Stability 88, 286–293.
Miyata, S., 1975. Synthesis of hydrotalcite-like compound and their structures and phydicochemical properties. 1. Systems Mg^{2+}–Al^{3+} NO_3^-, Mg^{2+}–Al^{3+}–Cl^-, Mg^{2+}–Al^{3+} ClO_4^-, Ni^{2+}–Al^{3+}–Cl^- and Zn^{2+}–Al^{3+}–Cl^-. Clays and Clay Minerals 23, 369–375.
Stanimirova, Ts, Piperov, N., Petrova, N., Kirov, G., 2004. Thermal evolution of Mg–Al–CO_3 hydrotalcites. Clay Minerals 39, 177–191.
Wang, S.L., Wang, P.C., 2007. In situ XRD and ATR-FTIR study on the molecular orientation of interlayer nitrate in Mg/Al-layered double hydroxides in water. Colloids and Surfaces A: Physicochemical and Engineering Aspects 292, 131–138.
Wei, M., Shi, S., Wang, J., Li, Y., Duan, X., 2004. Studies on the intercalation of naproxen into layered double hydroxide and its thermal decomposition by in situ FT-IR and in situ HT-XRD. Journal of Solid State Chemistry 177, 2534–2541.
Wei, M., Yuan, Q., Evans, D.G., Wang, Z., Duan, X., 2005a. Layered solids as a "molecular container" for pharmaceutical agents: L-tyrosine-intercalated layered hydroxides. Journal of Materials Chemistry 15, 1197–1203.
Wei, M., Wang, J., He, J., Evans, D.G., Duan, X., 2005b. In situ FT-IR, in situ HT-XRD and TPDE study of thermal decomposition of sulfated b-cyclodextrin intercalated in layered double hydroxides. Microporous and Mesoporous Materials 78, 53–61.
Wei, M., Xu, X., He, J., Yuan, Q., Rao, G., Evans, D.G., Pu, M., Yang, L., 2006. Preparation and thermal decomposition studies of L-tyrosine intercalated MgAl, NiAl and ZnAl layered double hydroxides. Journal of Physics and Chemistry of Solids 67, 1469–1476.
Yan, D.P., Lu, J., Wei, M., Li, H., Ma, J., Li, F., Evans, D.G., Duan, X., 2008. In situ polymerization of the 4-vinylbenzenesulfonic anion in Ni–Al-layered double hydroxide and its molecular dynamic simulation. Journal of Physical Chemistrt A 112, 7671–7681.
Yang, W., Kim, Y., Liu, P.K.T., Sahimi, M., Tsotsis, T.T., 2002. A study by in situ techniques of the thermal evolution of the structure of a Mg–Al–CO_3. Chemical Engineering Science 57, 2945–2953.
Yermiyahu, Z., Lapides, I., Yariv, S., 2005. Thermo-XRD-analysis of montmorillonite treated with protonated Congo-red. Curve fitting. Applied Clay Science 30, 33–41.
Yun, S.K., Pinnavaia, T.J., 1995. Water content and particle texture of synthetic hydrotalcite-like layered double hydroxides. Chemistry of Materials 7, 348–354.
Zhang, W.H., Guo, X.D., He, J., Qian, Z.Y., 2008. Preparation of Ni(II)/Ti(IV) layered double hydroxide at high supersaturation. Journal of the European Ceramic Society 28, 1623–1629.
Zhao, Y., Li, F., Zhang, R., Evans, D.G., Duan, X., 2002. Preparation of layered double-hydroxide nanomaterials with a uniform crystallite size using a new method involving separate nucleation and aging steps. Chemistry of Materials 14, 4286–4291.

Appendix III

***E. Káfuňková**, C. Taviot-Guého, P. Bezdička, M. Klementová, P. Kovář, P. Kubát, J. Mosinger, M. Pospíšil, K. Lang:*

Porphyrins Intercalated in Zn/Al and Mg/Al Layered Double Hydroxides: Properties and Structural Arrangement

Chemistry of Materials **2010**, *22*, 2481-2490

CHEMISTRY OF MATERIALS
Article

Chem. Mater. **2010,** *22,* 2481–2490 2481
DOI:10.1021/cm903125v

Porphyrins Intercalated in Zn/Al and Mg/Al Layered Double Hydroxides: Properties and Structural Arrangement

Eva Káfuňková,[†,§] Christine Taviot-Guého,[‡] Petr Bezdička,[†] Mariana Klementová,[†] Petr Kovář,[⊥] Pavel Kubát,[∥] Jiří Mosinger,[†,§] Miroslav Pospíšil,[⊥] and Kamil Lang*[,†]

[†]*Institute of Inorganic Chemistry, v.v.i., Academy of Sciences of the Czech Republic, 250 68 Řež, Czech Republic,* [‡]*Laboratoire des Materiaux Inorganiques, Universite Blaise Pascal, UMR-CNRS no. 6002, 63177 Aubiere Cedex, France,* [§]*Department of Inorganic Chemistry, Faculty of Science, Charles University in Prague, Hlavova 2030, 128 43 Praha, Czech Republic,* [⊥]*Faculty of Mathematics and Physics, Charles University in Prague, Ke Karlovu 3, 121 16 Praha 2, Czech Republic, and* [∥]*J. Heyrovský Institute of Physical Chemistry, v.v.i., Academy of Sciences of the Czech Republic, Dolejškova 3, 182 23 Praha 8, Czech Republic*

Received October 9, 2009. Revised Manuscript Received February 7, 2010

The arrangement of porphyrin molecules in the interlayer space of layered double hydroxides (LDH) has been studied by a combination of experimental techniques and molecular dynamics simulations. Intercalation of 5,10,15,20-tetrakis(4-sulfonatophenyl)porphyrins (TPPS) into Zn_RAl and Mg_RAl LDH hosts led to a gallery height of about 15.5 Å that is comparable with the size of the porphyrin molecules. The porphyrin sulfonate groups are located at about 4 Å from the center of the hydroxide layers that is consistent with hydrogen bonding interactions between the sulfonate groups and OH groups of the layers. The aromatic ring system in the middle of the gallery is rather disordered. A large number of in-plane diffraction lines suggests that the rigidity of the porphyrin framework has a beneficial effect on the layer ordering. Molecular dynamics simulations are in agreement with the experimental results showing that the interlayer space is filled with nearly parallel porphyrin units with a slightly inclined orientation of the porphyrin planes with respect to the normal of the hydroxide layers. The photophysical experiments proved that TPPS in Mg_2Al LDH hosts produce $O_2(^1\Delta_g)$ with long effective lifetimes. The LDH hybrids based on intercalated porphyrin sensitizers are suggested as new photofunctional materials.

Introduction

The prospect of obtaining novel materials gave impetus to studies of molecules immobilized in clays, layered double hydroxides (LDH), zeolites, or sol−gel derived matrices.[1−7] Layered solids are materials that can be functionalized by intercalation of active molecules with specific properties. In this case, layered structures act as hosts with a two-dimensional expandable interlayer space for the placement and organization of guest molecules. The intercalated solids not only provide an easy-to-apply transport material, but mostly increase chemical, photochemical, and thermal stability of guests including the control of their release during applications.[8,9] The constrained geometry, enforced by host−guest noncovalent interactions, is reflected in physicochemical and photophysical properties of guest molecules.[10]

LDH are nanostructured materials of the general formula $[M_{1-x}^{2+}M_x^{3+}(OH)_2]A_{x/m}^{m-}\cdot nH_2O$, abbreviated hereafter as $M_R^{2+}M^{3+}$−A, where M^{2+} and M^{3+} are divalent and trivalent cations, respectively, A is an anion of valence m and $R = (1 - x)/x$ is the M^{2+}/M^{3+} molar ratio. Their lamellar structure consists of brucite-like layers of positive charge counterbalanced by anionic species in the interlayer space together with water molecules.[11,12] LDH have attracted much attention owing to their ability to intercalate a wide variety of anions, either organic or inorganic. As a consequence, LDH have found potential applications in catalysis,[13] wastewater treatment,[14−16] electrochemical sensors,[17] or as fillers in polymers.[18] Furthermore, LDH are environmentally friendly, biocompatible

*Author to whom correspondence should be addressed. E-mail: lang@iic.cas.cz.

(1) Rives, V.; Ulibarri, M. A. *Coord. Chem. Rev.* **1999**, *181*, 61.
(2) Evans, D. G.; Duan, X. *Chem. Commun.* **2006**, 485.
(3) Ogawa, M.; Kuroda, K. *Chem. Rev.* **1995**, *95*, 399.
(4) Choy, J.-H.; Choi, S.-J.; Oh, J.-M.; Park, T. *Appl. Clay Sci.* **2007**, *36*, 122.
(5) Costantino, U.; Ambrogi, V.; Nocchetti, M.; Perioli, L. *Microporous Mesoporous Mater.* **2008**, *107*, 149.
(6) Takagi, S.; Eguchi, M.; Tryk, D. A.; Inoue, H. *J. Photochem. Photobiol. C* **2006**, *7*, 104.
(7) Wang, S.; Gao, R.; Zhou, F.; Selke, M. *J. Mater. Chem.* **2004**, *14*, 487.
(8) Laguna, H.; Loera, S.; Ibarra, I. A.; Lima, E.; Vera, M. A.; Lara, V. *Microporous Mesoporous Mater.* **2007**, *98*, 234.
(9) Wei, M.; Pu, M.; Guo, J.; Han, J.; Li, F.; He, J.; Evans, D. G.; Duan, X. *Chem. Mater.* **2008**, *20*, 5169.
(10) Lang, K.; Mosinger, J.; Wagnerová, D. M. *Coord. Chem. Rev.* **2004**, *248*, 321.
(11) Leroux, F.; Taviot-Guého, C. *J. Mater. Chem.* **2005**, *15*, 3628.
(12) Evans, D. G.; Slade, R. C. T. *Layered Double Hydroxides, Structural Bonding*; Duan, X., Evans, D. G., Eds.; Springer-Verlag: Berlin, Heidelberg, 2006; Vol. *119*; p 1−87.
(13) An, Z.; Zhang, W. H.; Shi, H. M.; He, J. *J. Catal.* **2006**, *241*, 319.
(14) Kovanda, F.; Kovácsová, E.; Koloušek, D. *Collect. Czech. Chem. Commun.* **1999**, *64*, 1517.

Published on Web 03/12/2010

materials with possible use as drug stabilizers and carriers.[19,20] The important features are the flexibility of the two-dimensional interlayer space and the variable charge density of the hydroxide layers (x usually lies between 0.20 and 0.35) allowing the incorporation of variable amounts of bulky guest molecules[21,22] including porphyrins and phthalocyanines.[1,23−27]

Porphyrins and related macrocycles are photosensitizers with rich fluorescence properties and the ability to produce singlet oxygen, $O_2(^1\Delta_g)$.[10] The photosensitized production of $O_2(^1\Delta_g)$ is based on excitation of a photosensitizer to the triplet states and energy transfer of this energy to the ground electronic state of oxygen that is excited to the lowest singlet state, $O_2(^1\Delta_g)$. The oxidative potential of $O_2(^1\Delta_g)$ can be exploited in chemical syntheses, photodynamic treatment of cancer, and disinfection. Planar porphyrin molecules tend to form stacked aggregates, in which absorbed excitation energy is dissipated through decay channels competing with desired photoinitiated reactions.[10,28] The aggregation can be eliminated by the immobilization of the individual molecules in inorganic hosts of ordered structures such as LDH or layered silicates.[3,6,11,24] In addition, the advantages are well-defined microscopic structures of the host matrices, specific organization, variability, and enhanced stability of the photoactive molecules. Recently, we have described the structural and photophysical properties of porphyrin−LDH hybrids prepared by ion exchange and shown that the porphyrin triplet states interact with oxygen molecules in the LDH interlayer to form $O_2(^1\Delta_g)$.[29] These hybrids can serve as handy sources of $O_2(^1\Delta_g)$ and in the form of films they are suitable, e.g., for the construction of bactericidal surfaces.[30]

Molecular dynamics simulations in combination with powder X-ray diffraction (XRD) provide new information on the structural features, dynamics, and arrangement of the interlayer water and anions, the properties mostly not available by direct measurements.[12,31,32] We recently modeled Mg_2Al LDH with 5,10,15,20-tetrakis(4-sulfonatophenyl)porphyrin (TPPS) in the interlayer and compared the measured XRD patterns of the sample prepared by anion exchange with simulated patterns.[33] The porphyrin units are horizontally shifted to each other, disordered, and inclined with respect to the hydroxide layers.

In the present work, we have investigated the intercalation of anionic TPPS and Zn(II)-5,10,15,20-tetrakis(4-sulfonatophenyl)porphyrin (ZnTPPS) into Zn_RAl and Mg_RAl LDH by the coprecipitation method. In general, Zn_RAl LDH hybrids exhibit higher crystallinity than corresponding hybrids based on Mg_RAl LDH. The gain in crystallinity was accompanied with the stabilization of a Zn^{2+}/Al^{3+} ratio equal to 2, and with the appearance of many in-plane diffraction lines in XRD that allowed us to propose, for the first time, a structural model of the interlayer space of Zn_RAl LDH hosts. Molecular dynamics simulations and XRD refinements indicate an inclined orientation of the porphyrin planes with respect to the hydroxide layers. The formation of $O_2(^1\Delta_g)$ by porphyrin−LDH hybrids is also presented.

Materials and Methods

Preparation. The tetrasodium salt of TPPS (Aldrich, Germany), $Al(NO_3)_3\cdot 9H_2O$, $AlCl_3\cdot 6H_2O$, $Zn(NO_3)_2\cdot 6H_2O$, $ZnCl_2\cdot 6H_2O$, $Mg(NO_3)_2\cdot 6H_2O$, $MgCl_2\cdot 6H_2O$, and NaOH (all by Acros Organics, France) were used as purchased. Deionized and decarbonated water was used throughout all experiments.

The LDH samples were prepared at constant pH using a coprecipitation technique adjusted to small quantities.[24,34] A solution of Zn^{2+} and Al^{3+} (3 mL, 0.2 M) in a variable molar ratio ($R = Zn^{2+}/Al^{3+} = 2-4$) was slowly added at a rate of 0.01 mL/min to 10 mL of an aqueous TPPS solution. TPPS was in a 2-fold molar excess over the stoichiometry. In some experiments, ZnTPPS obtained by stirring TPPS with an equimolar amount of Zn^{2+} for 1 h, was used instead of pure TPPS. The pH value was maintained constant at pH 7.5 for $R = 2$ and 3 and at pH 8.0 for $R = 4$ by the simultaneous addition of 0.4 M NaOH. Coprecipitation was carried out under vigorous stirring in a nitrogen atmosphere at room temperature in order to avoid dissolution of atmospheric CO_2 and subsequent contamination by carbonate anions. The addition of NaOH was completed after 5 h, and the resulting violet precipitate was aged for 24 h under stirring. The product was centrifuged, washed three times with water, and finally dried in air at room temperature. All

(15) Wang, Y. F.; Gao, H. Z. *J. Colloid Interface Sci*. **2006**, *301*, 19.
(16) Lakraimi, M.; Legrouri, A.; Barroug, A.; de Roy, A.; Besse, J. P. *Mater. Res. Bull*. **2006**, *41*, 1763.
(17) Mousty, C. *Appl. Clay Sci*. **2004**, *27*, 159.
(18) Taviot-Guého, C.; Leroux, F. *Layered Double Hydroxides, Structural Bonding*; Duan, X.; Evans, D. G., Eds.; Springer-Verlag: Berlin, Heidelberg, 2006; Vol. 119, p 121−159.
(19) (a) Khan, A. I.; O'Hare, D. *J. Mater. Chem*. **2002**, *12*, 3191. (b) Khan, A. I.; Ragavan, A.; Fong, B.; Markland, C.; O'Brien, M.; Dunbar, T. G.; Williams, G. R.; O'Hare, D. *Ind. Eng. Chem. Res*. **2009**, *48*, 10196.
(20) Del Hoyo, C. *Appl. Clay Sci*. **2007**, *36*, 103.
(21) Latterini, L.; Nocchetti, M.; Aloisi, G. G.; Costantino, U.; Elisei, F. *Inorg. Chim. Acta* **2007**, *360*, 728.
(22) Marangoni, R.; Taviot-Guého, C.; Illaik, A.; Wypych, F.; Leroux, F. *J. Colloid Interface Sci*. **2008**, *326*, 366.
(23) Ukrainczyk, L.; Chibwe, M.; Pinnavaia, T. J.; Boyd, S. A. *J. Phys. Chem*. **1994**, *98*, 2668.
(24) Bonnet, S.; Forano, C.; de Roy, A.; Besse, J. P.; Maillard, P.; Momenteau, M. *Chem. Mater*. **1996**, *8*, 1962.
(25) Wark, M. Porphyrins and Phthalocyanines in Inorganic Host Materials. *The Porphyrin Handbook*; Kadish, K. M., Smith, K. M., Guillard, R., Eds.; Elsevier Science: New York, 2003; Vol. *17*.
(26) Barbosa, C. A. S.; Ferreira, A. M. D. C.; Constantino, V. R. L. *Eur. J. Inorg. Chem*. **2005**, 1577.
(27) Halma, M.; de Freitas Castro, K. A. D; Taviot-Guého, C.; Prévot, V.; Forano, C.; Wypych, F.; Nakagaki, S. *J. Catal*. **2008**, *257*, 233.
(28) Sandanayaka, A. S. D.; Araki, Y.; Wada, T.; Hasobe, T. *J. Phys. Chem. C* **2008**, *112*, 19209.
(29) Lang, K.; Bezdička, P.; Bourdelande, J. L.; Hernando, J.; Jirka, I.; Káfuňková, E.; Kovanda, F.; Kubát, P.; Mosinger, J.; Wagnerová, D. M. *Chem. Mater*. **2007**, *19*, 3822.
(30) Lang, K.; Kubát, P.; Mosinger, J.; Bujdák, J.; Hof, M.; Janda, P.; Sýkora, J.; Iyi, N. *Phys. Chem. Chem. Phys*. **2008**, *10*, 4429.
(31) (a) Newman, S. P; Cristina, T. D.; Coveney, P. V.; Jones, W. *Langmuir* **2002**, *18*, 2933. (b) Yan, D.; Lu, J.; Wei, M.; Li, H.; Ma, J.; Li, F.; Evans, D. G.; Duan, X. *J. Phys. Chem. A* **2008**, *112*, 7671.
(32) (a) Lombardo, G. M.; Pappalardo, G. C.; Punzo, F.; Costantino, F.; Costantino, U.; Sisani, M. *Eur. J. Inorg. Chem*. **2005**, 5026. (b) Lombardo, G. M.; Pappalardo, G. C.; Costantino, F.; Costantino, U.; Sisani, M. *Chem. Mater*. **2008**, *20*, 5585.
(33) Kovář, P.; Pospíšil, M.; Káfuňková, E.; Lang, K.; Kovanda, F. *J. Mol. Model*. **2010**, *16*, 223.
(34) Miyata, S. *Clays Clay Miner*. **1975**, *23*, 369.

samples were then submitted to a hydrothermal treatment. Typically, about 20 mg of the solids was suspended in 25 mL of water in a 30 mL Teflon inner vessel in a stainless autoclave and treated at 120 °C for 72 h under autogenous pressure. Mg_RAl LDH hybrids were synthesized similarly.

The samples were labeled, e.g., as Zn_2Al-TPPS, Zn_2Al-(Zn)TPPS^H, and Zn_2Al-ZnTPPS where the molar ratio M^{2+}/Al^{3+} (R) used in the synthesis is given by subscript, the superscript H stands for hydrothermally treated samples, and the porphyrin used for the synthesis is expressed by TPPS or ZnTPPS. The fact that originally used TPPS was metalated to ZnTPPS during the hydrothermal treatment is indicated by (Zn). Zn_RAl-Cl LDH intercalated with chloride anions is used here as a reference.

Characterization Techniques. Powder X-ray diffraction (XRD) (see the Supporting Information) was performed on a PANalytical X'Pert PRO X-ray diffractometer in the Bragg−Brentano geometry. The sample Zn_2Al-ZnTPPS^H of high crystallinity was also analyzed in the Debye−Scherrer geometry equipped with a capillary sample holder and a hybrid mirror monochromator ($CuK\alpha_1$, λ = 1.540598 Å). In-situ high-temperature measurements were performed using a high-temperature Anton PAAR HTK-16 chamber.

The diffuse reflectance UV−visible spectra were acquired on a Perkin-Elmer Lambda 35 spectrometer equipped with a Labsphere RSA-PE-20 integration sphere. Thermogravimetric analyses (TG-DTA) were carried out on a Setaram SETSYS Evolution instrument in air. The gas emission analysis was performed using a Setaram SETSYS Evolution-16-MS coupled with a mass spectroscopy system. High-resolution transmission electron microscopy (HRTEM) was carried out on a JEOL JEM 3010 microscope operated at 300 kV (LaB_6 cathode, point resolution 1.7 Å). The time-resolved near-infrared luminescence of $O_2(^1\Delta_g)$ at 1270 nm was monitored using a Ge diode detector upon laser excitation by a Lambda Physik FL 3002 dye laser (λ_{exc} = 425 nm, incident energy ~ 1 mJ/pulse). The detailed description of all methods is given in the Supporting Information.

Molecular Modeling. Molecular mechanics and classical molecular dynamics[35] were carried out in the Cerius and Materials Studio modeling environment (see the Supporting Information).[36] The structure of ZnTPPS was optimized by the quantum-chemistry computational program Turbomole v5.9.[37] Zn_2Al−LDH is created as a trilayered structure with a trigonal cell in hexagonal axes.[33] The space group is $R\bar{3}m$, and the initial experimental cell parameters used were $a = b$ = 3.064 Å. The basal spacing d_{003} was 23.05 Å. A layer $[Zn_{64}Al_{32}(OH)_{192}]^{32+}$ was created by the linking of 96 individual cells to give the lattice parameters of A = 49.024 Å and B = 18.384 Å, with Al^{3+} cations distributed in the layers on the condition that the location of Al^{3+} in neighboring octahedra is excluded.[38] The total composition was $[Zn_{192}Al_{96}(OH)_{576}](ZnTPPS)_{24}\cdot 192\,H_2O$ with the space group set to P1. Charges were calculated by the Qeq method.[39] The initial models were minimized in the Universal force field, the electrostatic energy was calculated by the Ewald summation method,[40] and the van der Waals energy was calculated by the Lennard-Jones potential.[41] The dynamics simulations were carried out in an NVT statistical ensemble at 300 K. One dynamic step was 0.001 ps, and dynamics of 200 ps were carried out.

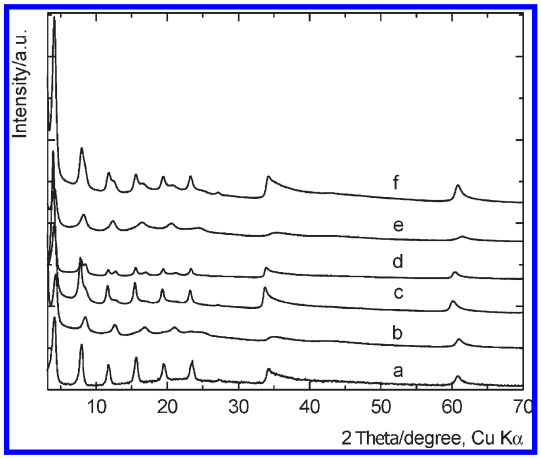

Figure 1. Powder XRD patterns of samples before hydrothermal treatment: Zn_2Al−ZnTPPS (a), Mg_4Al−TPPS (b), Zn_4Al−TPPS (c), Zn_3Al−TPPS (d), Mg_2Al−TPPS (e), and Zn_2Al−TPPS (f).

Results and Discussion

Characterization of LDH Intercalated with Porphyrins. The coprecipitation method facilitates the effective intercalation of bulky porphyrin anions to compensate for the positive charge of the layers. Furthermore, this method often viewed as a self-assembly process should permit an adjustment of the M^{2+}/M^{3+} ratio, i.e., to control the layer charge density and make it coincide with the charge *per* unit area for the intercalated anion. The composition based on Zn^{2+} and Al^{3+} is advantageous because Zn_RAl LDH hosts usually have higher crystallinity than Mg_RAl LDH. Here, we present the properties of both Zn_RAl and Mg_RAl LDH hybrids.

The XRD patterns of as-prepared samples were recorded in the Bragg−Brentano geometry and were all indexed in the rhombohedral space group $R\bar{3}m$, typical for LDH-based systems (Figure 1). A splitting of 003n basal lines of Zn_RAl LDH indicates two phases with close interlayer distances that are both consistent with the intercalation of the porphyrin molecules. The cell parameters, shown in Table 1, were obtained from the peak profile analysis, and it should be noted that the spherical harmonics correction for an anisotropic peak broadening[42] due to size effects was essential to reach a good fit. The molar ratios R_{calc} were derived from a relationship between the cell parameter a and the M^{2+}/M^{3+} molar ratio established for the Zn_RAl and Mg_RAl LDH series.[43] Both calculated, R_{calc}, and experimental, R_{exp}, values are comparable and in agreement with the initial molar ratios used for the synthesis (Table 1). The molar ratio

(35) Comba, P; Hambley, T. W. *Molecular Modeling of Inorganic Compounds*; VCH Verlagsgesselschaft mbH: Weinheim, 1995.
(36) Accelrys Software Inc. *Materials Studio Modeling Environment*; release 4.3 documentation, Accelrys Software Inc.: San Diego, 2003.
(37) Ahlrichs, R.; Bär, M.; Häser, M.; Horn, H.; Kölmel, C. *Chem. Phys. Lett*. **1989**, *162*, 165.
(38) Sideris, P. J.; Nielsen, U. G.; Gan, Z.; Grey, C. P. *Science* **2008**, *321*, 113.
(39) Rappe, A. K; Goddard, W. A.III *J. Phys. Chem*. **1991**, *95*, 3358.
(40) Karasawa, N; Goddard, W. A.III *J. Phys. Chem*. **1989**, *93*, 7320.
(41) Lennard-Jones, J. E. *Proc. R. Soc. London, Ser. A* **1925**, *109*, 584.
(42) Rodríguez-Carvajal, J. *Newslett. Powder Diff. Comm. Int. Union Crystallogr*. **2001**, *26*, 12.
(43) Leroux, F.; Adachi-Pagano, M.; Intissar, M.; Chauvière, S.; Forano, C.; Besse, J. P. *J. Mater. Chem*. **2001**, *11*, 105.

Table 1. Refined Cell Parameters of Porphyrin−LDH Hybrids and the Molar M^{2+}/M^{3+} Ratios Obtained from XRD (R_{calc}) and Elemental Analysis (R_{exp})

samples	a/Å	c/Å	d_{003}/Å	R_{calc}	R_{exp}
Mg_2Al−TPPS	3.0300(3)	65.093(9)	21.70	1.5	
Mg_2Al−$TPPS^H$	3.0351(2)	69.105(5)	23.03	1.8	1.73
Zn_2Al−TPPS	3.0548(2)	68.856(3)	22.95	1.8	1.94
	3.0548(2)	64.332(9)	21.44		
Zn_2Al−(Zn)$TPPS^H$	3.0568(4)	68.702(9)	22.90	1.7	1.90
Zn_2Al−ZnTPPS	3.0621(2)	69.215(7)	23.07	1.8	
Zn_2Al−$ZnTPPS^H$	3.0625(3)	69.090(1)	23.03	1.8	1.91
Zn_4Al−TPPS	3.0859(3)	68.909(9)	22.97	4.1	3.60
	3.0859(3)	63.740(3)	21.25		
Zn_4Al−(Zn)$TPPS^H$	3.0667(2)	69.047(4)	23.01	2.1	3.05

sulfur/Al^{3+} suggests that over 80% of hydroxide positive charges were compensated by the sulfonated groups of the porphyrin molecule. An explanation for the origin of the two interlayer distances can be deduced from the absorption spectra and thermal behavior. The absorption spectrum of pure TPPS displays the Soret band at 412 nm and four Q bands at 516, 550, 590, and 647 nm, while ZnTPPS shows the intensive Soret band at 424 nm and only two Q bands peaking at 561 and 603 nm due to the increase of the porphyrin symmetry (Figure 2). The spectra of Zn_RAl−TPPS differ from those of pure TPPS showing a red-shifted Soret band of 423 nm and more intensive absorptions at 560 and 600 nm, while the spectra of Mg_RAl−TPPS and TPPS have the same features. This documents a partial metalation of TPPS by Zn^{2+} during the Zn_RAl LDH synthesis. This is further corroborated by Zn_2Al−ZnTPPS, prepared using ZnTPPS, whose spectrum equals that of pure ZnTPPS (Figure 2) and the XRD patterns are not split as in the case of Zn_2Al−TPPS (Figure 1). Evidently, Mg_2Al−TPPS is characterized by a single basal spacing of 21.70 Å, while two phases containing either TPPS or ZnTPPS within the Zn_2Al LDH interlayer space result in two different basal spacings of 21.44 and 22.95 Å, respectively.

Although the absorption spectra clearly show the presence of both TPPS and ZnTPPS in Zn_RAl−TPPS, one must check whether the variations of the interlayer water content might also contribute to the two distances observed by XRD. Hence, the thermal behavior of Zn_4Al−TPPS

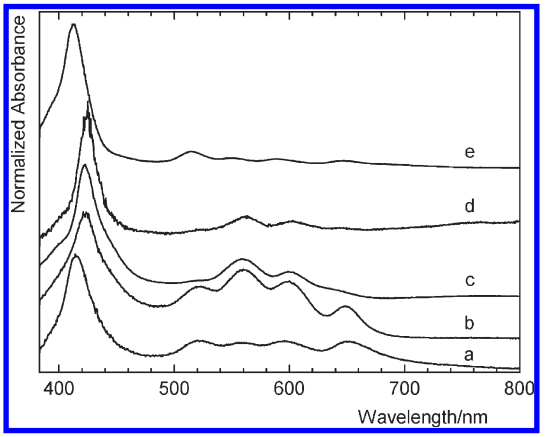

Figure 2. Normalized diffuse reflectance spectra before hydrothermal treatment: Mg_2Al−TPPS (a), Zn_2Al−TPPS (b), and Zn_2Al−ZnTPPS (c) compared with ZnTPPS (d) and TPPS (e).

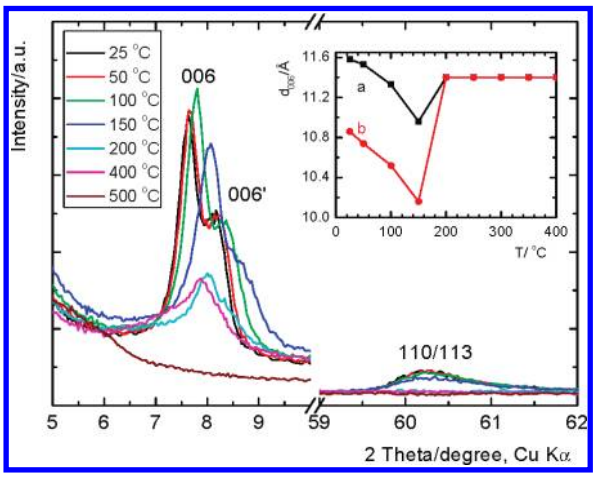

Figure 3. In-situ high-temperature XRD patterns of Zn_4Al-TPPS. The inset shows the relationship between the d_{006} (a) and $d_{006'}$ (b) basal spacings and temperature.

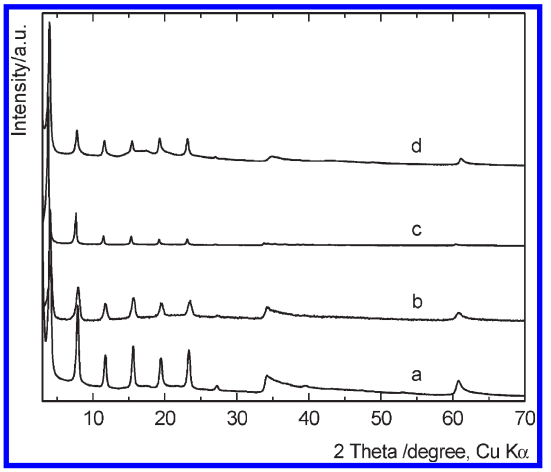

Figure 4. Powder XRD patterns of Zn_2Al−(Zn)$TPPS^H$ (a), Zn_2Al−ZnTPPS (b), Zn_2Al−$ZnTPPS^H$ (c), and Mg_2Al−$TPPS^H$ (d).

was examined by *in situ* high-temperature XRD (Figure 3). A gradual shift of the 006 double line toward higher 2θ values after increasing temperature from 50 to 150 °C indicates a decrease of the interlayer distance due to the removal of interlayer water. This was also confirmed by mass spectroscopy during thermogravimetric analysis (see below). The intensity of the 006 lines reaches a maximum at 100 °C suggesting a maximal ordering of the interlayer at this temperature. At 200 °C, dehydroxylation of the hydroxide layers is evidenced by the collapse and disappearance of the 006 and 110/113 lines, respectively. The fact that the 006 double line does not merge into a single line, even at 150 °C, supports the existence of two distinct phases that differ in the nature of intercalated porphyrin. Indeed, if these two basal lines were due to the different interlayer water content, we would have expected the two peaks to fuse into a single peak during interlayer dehydration.

The hydrothermal treatment causes a net increase of crystallinity of all samples (Table 1, Figure 4). The disappearance of the two-phase XRD patterns (Figures 1 and 4) and corresponding absorption spectra document that originally intercalated TPPS in Zn_RAl

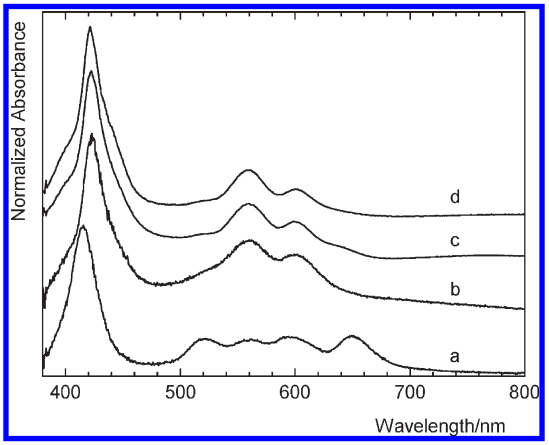

Figure 5. Normalized diffuse reflectance spectra of $Mg_2Al-TPPS^H$ (a), $Zn_2Al-(Zn)TPPS^H$ (b), and $Zn_2Al-ZnTPPS$ (c) compared with $Zn_2Al-ZnTPPS^H$ (d).

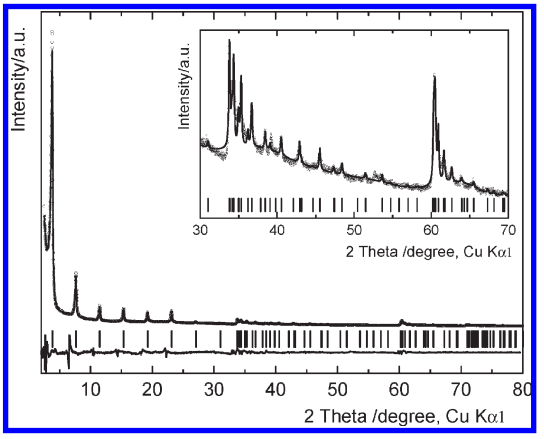

Figure 6. Profile analysis of the XRD pattern of $Zn_2Al-ZnTPPS^H$ recorded in the Debye–Scherrer geometry: experimental X-ray diffraction (circles), calculated (line), Bragg reflections (ticks), and difference profiles. Refined unit cell parameters: $a = 3.0604(6)$ Å and $c = 69.01(1)$ Å. $R_{Bragg} = 0.08\%$. (inset) Extended region $30-70°/2\theta$.

LDH is completely metalated to ZnTPPS, while intercalated TPPS in Mg_RAl LDH remains unchanged (Figure 5). It is worth noting that TPPS metalation is not unexpected due to the high affinity of TPPS toward free Zn^{2+} in solution. The XRD patterns of $Zn_3Al-(Zn)TPPS^H$ and $Zn_4Al-(Zn)TPPS^H$ newly show the diffraction lines of ZnO that is accompanied by a decrease of the Zn^{2+}/Al^{3+} ratio (R_{calc}) within the hydroxide layers to 2 as deduced from the decrease of the cell parameter a (Table 1). It can be attributed to a dissolution/decomposition of Zn-based LDH during the hydrothermal treatment in conjunction with the low octahedral crystal field stabilization energy of Zn^{2+} ions.[44] In contrast, the metal ratio in Zn_2Al LDH host remains unchanged with no signs of the ZnO presence. The stability of Zn_2Al LDH under specific hydrothermal conditions indicates that the most energetically favorable host–guest charge and structure alignment are reached at this molar ratio.

The absorption spectra (Figure 5) and XRD patterns of $Zn_2Al-ZnTPPS$ and $Zn_2Al-ZnTPPS^H$ (Figures 4 and 6) document the stability of ZnTPPS in the interlayer space and very high crystallinity after the hydrothermal treatment. This is indicated by not only the very narrow 003n basal lines, but also by the appearance of many 10n and 01n in-plane lines at high 2θ angle values. One must say that the observation of the in-plane reflections is quite rare in LDH. The high crystallinity of $Zn_2Al-ZnTPPS^H$ allowed us to extract additional information on the intercalate structure (see below).

Thermal Behavior. The amount of physisorbed and interlayer/structural water molecules can be determined using thermogravimetric analyses (Table 2). The TG-DTA curves, describing the general thermal behavior of hybrids, have similar features (Supporting Information Figure S1). The amount of physisorbed water was determined by evacuating the samples at 50 °C for 5 h. The thermal processes are characterized by three weight loss steps. Depending on sample crystallinity, all these thermal events are either well-separated or superimposed phenomena. The loss between 50 and 150 °C, accompanied by a decrease of the interlayer spacing (Figure 3), is attributed to the removal of interlayer water molecules. The results show that 40–75% of total water belongs to physisorbed water molecules. The number of intercalated water molecules is close to that reported for LDH, i.e., about two water molecules per Zn_2Al formula unit. In the case of Mg_2Al LDH, the obtained number is less accurate because of less defined weight losses related to their lower crystallinity. The second step (150–400 °C) involves two simultaneous processes, dehydroxylation of the brucite-like layers, and decomposition of interlayer anions, while the third step above 400 °C is a consequence of decomposition and combustion of intercalated anions.

The thermal stability of the porphyrin molecules intercalated between the hydroxide layers was investigated by TG-DTA in conjunction with mass spectroscopy. Pure porphyrins and their intercalated phases exhibit complex thermal behavior (Supporting Information Figures S2–S5); therefore, the most sensitive measure of thermal behavior appears to be the evolution of gases due to porphyrin decomposition, namely SO_2 and NO_2. While the onset of the evolution of NO_2 is not affected by intercalation, the evolution of SO_2 starts at lower temperature for both pure porphyrins. Thus, ZnTPPS starts to decompose at ca. 340 °C and the onset is shifted to nearly 465 °C after intercalation. In the case of the Mg_2Al LDH hybrid, the onset is shifted from ca. 310 to 480 °C. These results indicate that host–guest interactions thermally stabilize the porphyrin molecules similarly to other intercalated molecules.[45–47]

XRD Analysis. $Zn_2Al-ZnTPPS^H$ displays very narrow 003n diffraction lines which are characteristic of high coherency materials and a large number of the 10n and 01n in-plane diffraction lines. The latter observation is

(44) Britto, S.; Radha, A. V.; Ravishankar, N.; Kamath, P. V. *Solid State Sci.* **2007**, *9*, 279.
(45) Vaysse, C.; Guerlou-Demourgues, L.; Demourgues, A.; Delmas, C. *J. Sol. State Chem.* **2002**, *167*, 59.
(46) Zhang, X.; Wei, M.; Pu, M.; Li, X.; Chen, H.; Evans, D. G.; Duan, X. *J. Sol. State Chem.* **2005**, *178*, 2701.
(47) Wang, Z.-L.; Kang, Z.-H.; Wang, E.-B.; Su, Z.-M.; Xu, L. *Inorg. Chem.* **2006**, *45*, 4364.

Table 2. Thermogravimetric Data of Porphyrin−LDH Hybrids

samples	weight loss/% < 150 °C	150−400 °C	400−800 °C	nH_2O physisorbed	nH_2O interlayer
Mg_2Al−TPPS	2.6	8	19.1	1.89	0.61
Mg_2Al−$TPPS^H$	6.1	11.3	26.5	2.32	1.48
Zn_2Al−TPPS	5.6	10.2	27	1.33	1.67
Zn_2Al−(Zn)$TPPS^H$	6.2	10.2	22.7	1.13	1.87
Zn_4Al−TPPS	5.7	10.6	22.4	[a]	[a]
Zn_4Al−(Zn)$TPPS^H$	6.1	10.3	23.1	[a]	[a]

[a] Not determined because of the formation of ZnO.

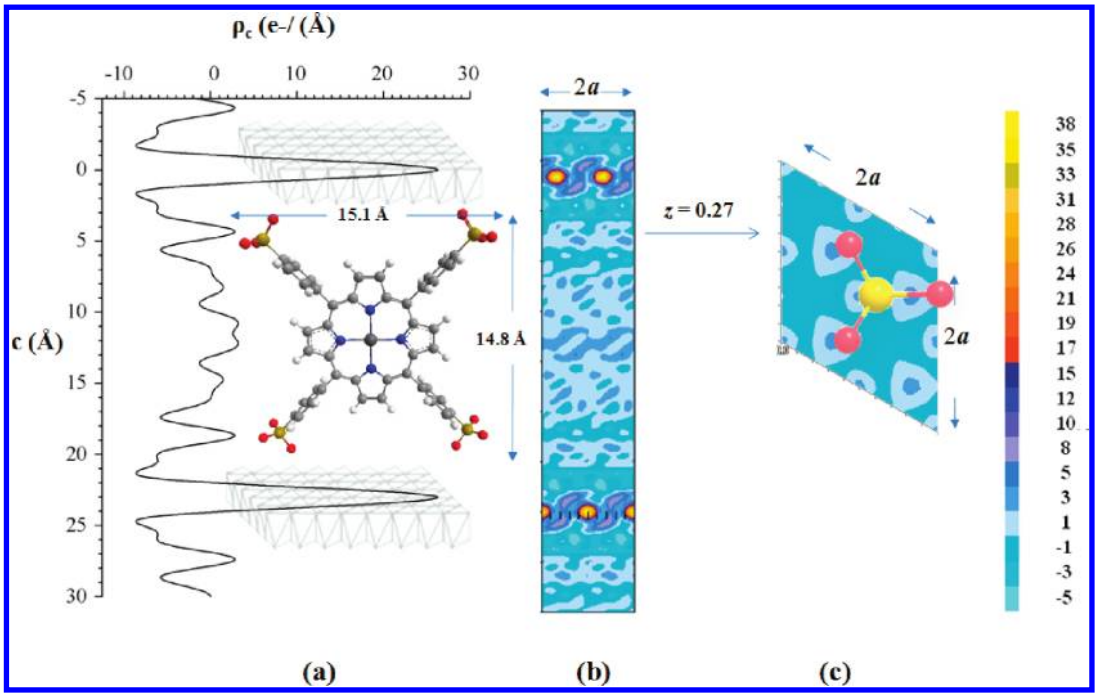

Figure 7. Structure model of Zn_2Al−$ZnTPPS^H$: (a) one-dimensional electron density determined from the Debye−Scherrer data projected along the *c*-stacking axis; (b) contoured Fourier map of the (*x*0*z*) plane (summed from 0 to 1 along the *b*-axis); (c) contoured Fourier map of the (*xy*0) plane ($z = 0.27$). The sulfonate group is overlaid on the (*xy*0) plane to show the matching with the density spots observed at $z = 0.27$ (and $z = 0.07$). The electron density scale (e^-/Å) is given on the right.

quite rare in LDH-based materials because these materials are known to be low crystalline, especially hybrid LDH, due to anisotropic size effects (i.e., platelet morphology), microstrains, and stacking faults. Besides, owing to the small difference between the Zn^{2+} and Al^{3+} X-ray atomic scattering factors and the low contribution expected from light atoms such as C, O, N, S, and H forming the skeleton of the porphyrin guest molecule, it would be too tentative to attribute the in-plane diffraction lines to either a cation ordering of Zn^{2+} and Al^{3+} within the hydroxide layer or to an ordering of the porphyrin molecules in the interlayer space. As the in-plane diffraction lines are expected for a 3R polytype without stacking faults, we can reasonably assume a nearly perfect 3R stacking of the hydroxide layers. It may be attributed to the rigidity of the porphyrin framework.

The large number of 003n diffraction lines (up to seven harmonics) related to the large size of the intercalated porphyrin molecule allows probing the structure of the interlayer space projected on the *c*-axis via the Fourier transformation.[48] The one-dimensional (1D) electron density map for Zn_2Al−$ZnTPPS^H$, determined from Debye−Scherrer data, can be calculated using the known structure of a hydroxide layer, assuming a weak contribution from the interlayer part to total scattering (Figure 7a). The corresponding plots for Mg_2Al−$TPPS^H$ and Zn_2Al−$ZnTPPS^H$ determined using the Bragg−Brentano XRD data are compared in Supporting Information Figure S6A. The difference between the 1D plots for Zn_2Al−$ZnTPPS^H$ displayed in Figures 7a and S6A is due to resolution differences between the two XRD data sets; the high-resolution data obtained in the Debye−Scherrer mode gives the 1D plot with a better resolution.

The 1D electron density map of Zn_2Al−$ZnTPPS^H$ (Figure 7a) displays two strong maxima at 0 and 23 Å corresponding to the metal containing hydroxide layers. The five additional peaks of lower electron densities located in between can be attributed to the intercalated porphyrin and water molecules. Upon comparison with the dimensions of the porphyrin molecule (~ 15/4.3 Å), a

(48) Whittingham, M. S.; Jacobson, A. *Intercalation Chemistry*; Academic Press: New York, 1982.

perpendicular arrangement of the porphyrin plane against the hydroxide layer can be proposed in agreement with previous study.[24] The sulfonate groups cause maxima at the outer parts of the interlayer space at about 4 Å from the center of the hydroxide layers that is consistent with hydrogen bonding interactions between the sulfonate groups and OH groups of the layers. These interactions along with Coulombic interactions dictate the orientation of the anions with respect to the LDH surface.[49] The central maxima and the two peaks on each side arise from the porphyrin ring. The splitting of the central maxima indicates an orientation disorder of the porphyrin molecules around a given central site (see below). If we assumed a perpendicular orientation, the porphyrin molecule would fill a surface area of 16.2 $Å^2/e^-$ that is largely compensated with the surface area of 23.5 $Å^2/e^-$ of the hydroxide layer. A far better accordance could certainly be obtained by slightly inclined molecular planes resulting in an increase of the surface required by the porphyrin molecule. Yet, the present data do not allow distinguishing between a perpendicular and inclined orientation. On the other hand, this result can be compared with the calculation of the interlayer space available for intercalated anions that is often applied in hybrid LDH:[50] 23.03 Å (d_{003}) − 2.10 Å (i.e., hydroxide layer thickness) − 2 × 2.70 Å (i.e., hydrogen bonding) = 15.5 Å. The gallery height thus obtained is comparable with the size of the porphyrin molecule and again indicates a perpendicular or nearly perpendicular orientation of the porphyrin units between the hydroxide layers.

The electron-density distributions on the (*x0z*) and (*xy0*) planes, plotted with the GFourier program,[51] are presented in the form of contour plots in Figure 7b and c. In the same way as for the 1D projection, the phases and structure factors were computed from the known configuration of the hydroxide layer part of the structure. Note that the differences in the electron density between spots in the interlayer space are quite small, preventing us from a detailed description of the interlayer structure. Nevertheless, four important points can be drawn. (i) The highest density peaks observed at $z \sim 0.27$ and 0.07, i.e., 4 Å from the center of the hydroxide layers, are localized vertically to metal cations and can be reasonably assigned to the sulfonate groups. This does not mean that the distance between sulfonate groups is equal to the distance between metal cations within the hydroxide layer, i.e., ~3 Å. Indeed, one must keep in mind that equivalent positions that are too close to one another are only partially occupied by the sulfonate groups, in agreement with the $Zn_2Al-ZnTPPS^H$ chemical formula. The distances around 1.6 Å between density peaks observed at $z \sim 0.27$ (and ~0.07) are consistent with an S−O bond length. (ii) The aromatic ring system gives rise to a rather disordered electron density in the middle of the gallery. Such disorder suggests a low contribution, if any, of a superstructure based on regularly aligned porphyrin units. (iii) Assuming the $R\bar{3}m$ space group, metal ions of two successive hydroxide layers are shifted by 1/3 in the [110] direction, then the sulfonate groups located at the outer parts of the interlayer space exhibit the same shift, leading to a slightly inclined orientation of the porphyrin plane with an angle of ca. 8° with respect to the normal of the hydroxide layer. (iv) The decrease of the electron densities attributed to the sulfonate groups, after a thermal treatment at 100 °C under vacuum, is indicative of the presence of water molecules located nearby the sulfonate groups (Supporting Information Figure S6B).

Comparison of the less resolved one-dimensional plots of $Zn_2Al-ZnTPPS^H$ and $Mg_2Al-TPPS^H$ calculated from the Bragg−Brentano XRD data is valuable since these two samples display the same M^{2+}/M^{3+} molar ratio according to the chemical analysis; hence, they are intercalated with the same amount of porphyrin (Supporting Information Figure S6). The 1D plots show differences in the electron densities at the hydroxide layers and porphyrin ring positions. The lower electron density observed for the Mg_2Al hydroxide layers is due to the difference between Zn ($Z = 30$) and Mg ($Z = 12$) atomic numbers. In addition, the presence of Zn^{2+} in the middle of the porphyrin unit explains the higher electron density in the interlayer central plane of $Zn_2Al-ZnTPPS^H$.

The studies show that ordering of some organic anions within the interlayer galleries is relatively common, in contrast to the generally disordered interlayers filled with inorganic anions.[12] In this respect, we might speculate on the ordering of the porphyrin units. They are bulky and rigid, and the final arrangement is governed by the interplay of the Coulombic interactions of porphyrin anions with the positively charged layers, interactions between neighboring anions, and the hydrogen bonding interactions among the hydroxyl groups, porphyrin sulfonate groups, and water. The indexing calculations either using DiffracPlus Topas (v. 4.1) or Dicvol 2006 give a trigonal cell well-described by $a = 3.0625(3)$ Å, $c = 69.090(1)$ Å, and $\gamma = 120°$. If one assumes that intercalated porphyrin units are ordered and create a superstructure, such an *a* parameter would not allow accommodating the porphyrin molecule with a size of ca. 15 Å. The simplest model that would permit the ordering of ZnTPPS anions within the $R\bar{3}m$ unit cell is the multiple application of the unit cell transformation (IIc, $a' = -2a, b' = -2b$)[52] yielding a new *a* parameter of 24.5 Å. This parameter is comparable with the size of the porphyrin molecule; however, no additional diffraction lines allow this indexing of the XRD patterns. In fact, these additional lines are expected to be very weak, if any, because experimental electron density maps indicate some disorder in the middle of the

(49) Cai, H.; Hillier, A. C.; Franklin, K. R.; Nunn, C. C.; Ward, M. D. *Science* **1994**, *266*, 1551.
(50) Ennadi, A.; Khaldi, M.; de Roy, A.; Besse, J. P. *Mol. Cryst. Liq. Cryst.* **1994**, *244*, 373.
(51) Roisnel, T.; Rodriguez-Carvajal, J. WinPLOTR: a Windows tool for powder diffraction patterns analysis, Materials Science Forum. Proceedings of the Seventh European Powder Diffraction Conference (EPDIC 7), Barcelona, Spain, May 20−23, 2000; Delhez, R., Mittemeijer, E. J., Eds.; Trans Tech Publications Inc.: Switzerland, 2001; p 118−123.
(52) *International Tables for Crystallography*, 5th ed.; Hahn, Th.; Ed.; Springer: Dordrecht, The Netherlands, 2005; Vol. *A*, p 546.

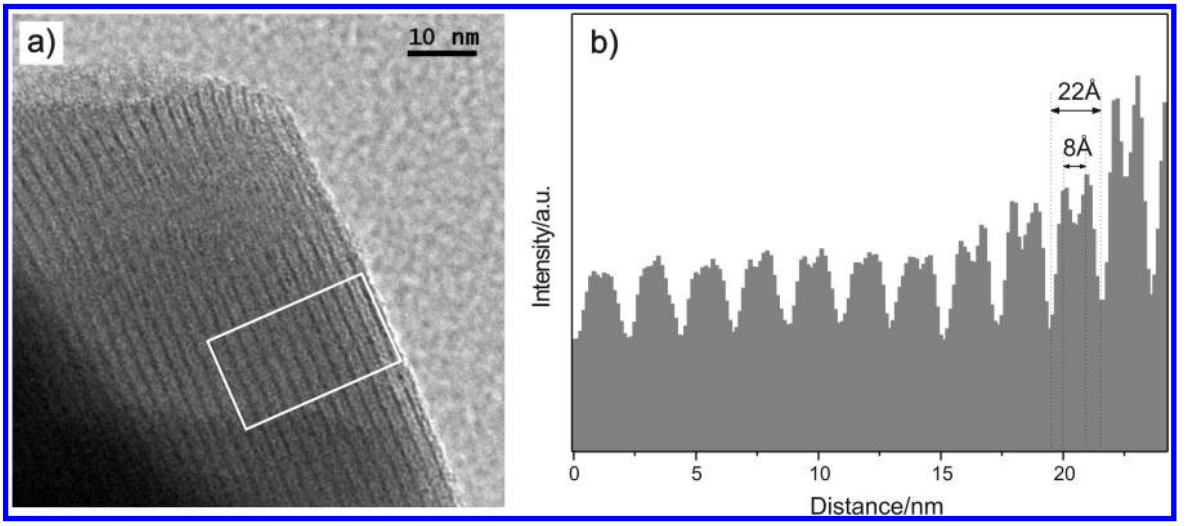

Figure 8. HRTEM observation of $Zn_2Al-ZnTPPS^H$: (a) high-resolution micrograph, (b) intensity histogram of the area marked in part a.

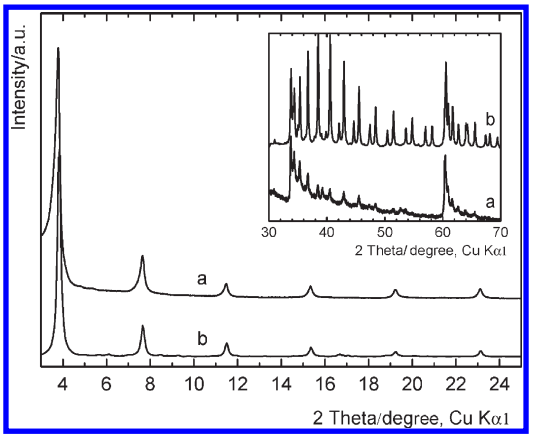

Figure 9. Experimental (a) and calculated (b) XRD basal diffraction lines of $Zn_2Al-ZnTPPS^H$ hybrid. (inset) Corresponding experimental (a) and calculated (b) XRD nonbasal diffraction lines.

interlayer and because of small differences between the atomic scattering factors of hydroxide metals.

Transmission Electron Microscopy. The HRTEM micrographs of original and porphyrin-intercalated LDH were recorded to observe the changes of the layered structure upon intercalation. The particles of original LDH, Zn_2Al-Cl^H, have a typical hexagonal shape; sometimes slightly irregular with the unequal length of sides (Supporting Information Figure S7). The size of the crystals is below 1 μm. The basal spacing of Zn_2Al-Cl^H, measured as a distance between the intensity minima, is about 8 Å (Supporting Information Figure S8), which corresponds to 7.75 Å obtained from the XRD patterns. The distance between the parallel fringes in $Zn_2Al-ZnTPPS^H$ is about 22 Å (Figure 8), which is in good agreement with the d_{003} value of 23.03 Å determined by XRD. Moreover, the HRTEM micrographs reveal additional lattice fringes with a fringe separation of about 8 Å indicating an increase of electron density in the middle of the interlayer space (Figure 8b). In agreement with information obtained from XRD, this suggests that the metal centra of the porphyrin units are aligned in the middle of the interlayer space.

Molecular Modeling. The experimentally accessible XRD patterns bear important structural information. We constructed a structural model using the molecular simulations approach taking the van der Waals dimension of the porphyrin guest and by assuming that the intercalation process does not change measurably the structure of the hydroxide layers. The calculated XRD patterns of the optimized $Zn_2Al-ZnTPPS^H$ structure and the experimental XRD are compared in the 2θ scale in Figure 9. The patterns exhibit typical features of a layered structure, i.e., basal lines 003n. The measured basal spacing (Table 1), line positions, and intensities of diffraction lines are very similar. Some intensity differences might be due to the crystallite morphology and roughness of the sample surface.[53] The calculated XRD has additional very low intensity lines between 5 and 6° and 16 and 18° of the 2θ scale, which appear due to the forced periodicity of the model. In the calculation, the supercell is treated as a structural element, which is infinitely repeated in all directions forming an infinite and perfectly periodic 3D crystal. The forced repeating of the structural elements imposes the periodicity of central zinc atoms of ZnTPPS leading to the appearance of these lines. Indeed, once Zn atoms are removed from the model, the low intensity lines disappear. However, intensities of these diffraction lines are very low and it is difficult to differentiate them from possible imperfections and small amounts of impurities in the real sample.

The observation of the nonbasal lines and their comparison with calculated XRD bring additional information on the layer ordering (Figure 9). The experimental line positions are best reproduced by a model with a = 3.063 and d_{003} = 23.05 Å, the values that correspond well to the experimental ones (Table 1). The higher intensities of some calculated lines are imposed by the perfect layer periodicity of the model. The host layers were kept in the same layer stacking order as in the original nitrate form

(53) Kovář, P.; Pospíšil, M.; Nocchetti, M.; Čapková, P.; Melánová, K. *J. Mol. Model.* **2007**, *13*, 937.

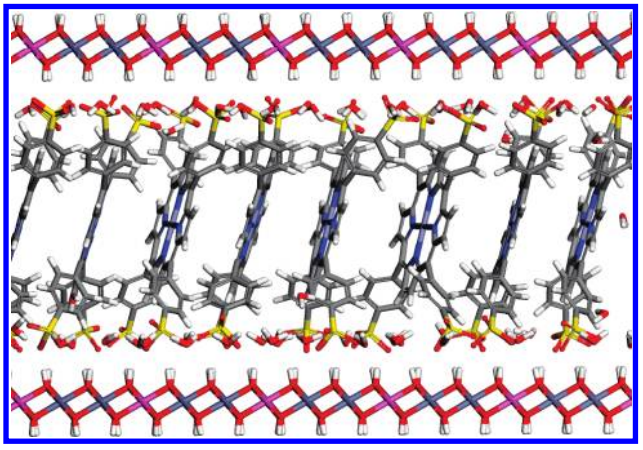

Figure 10. Interlayer space of the Zn_2Al LDH lattice filled with ZnTPPS.

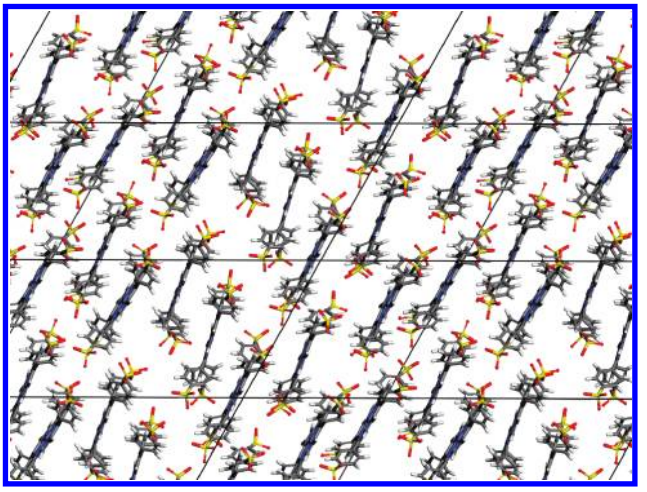

Figure 11. Top view of linked supercells containing ZnTPPS anions in the interlayer space.

(polytype 3R), therefore, the consistence between the calculated and experimental patterns indicates that the original symmetry is a good approximation for the layer stacking of the investigated intercalate. This is also corroborated by the fact that a horizontal shift of the layers violating the $R\bar{3}m$ symmetry induces many additional diffraction lines in the calculated XRD in disagreement with the experimental diffraction data. Because exchanging the Zn and Al atomic positions within the hydroxide layers does not affect the calculated diffraction patterns, an order/disorder arrangement of Al/Zn atoms is not distinguishable, and the nonbasal diffraction lines are governed only by a translation of atomic positions. Some layer nonperiodicity can be reproduced by the reoptimization of the final model with variable cell parameters (c, α, and β) used in step 2 (see the Supporting Information). It slightly changes the cell angles (0.3° at maximum) with only minor deviations of the layer stacking order, and as a result, the intensities of the calculated and experimental nonbasal diffraction lines are more similar.

The interlayer space in the minimized model (Figure 10) is filled with nearly parallel porphyrin units with a dihedral angle varying between 0 and 10°. The porphyrin planes are not perpendicular to the hydroxide layers. Instead, angle variations between the porphyrin plane and the layer normal satisfy the Gaussian distribution with the average angle of ca. 14° (Supporting Information Figure S9). In agreement with the HRTEM micrographs (Figure 8), porphyrin zinc atoms of ZnTPPS are in the middle of the interlayer space, i.e., 11.525 ± 0.300 Å with respect to the neighboring (003) basal plane (basal spacing is 23.05 Å). Due to a horizontal shift of the porphyrin units, their central Zn atoms are horizontally disordered (Figure 11). The distance between two neighboring porphyrin centra defined as a line connecting Zn atoms varies from 6 to 9 Å. The top view shows that the porphyrin molecules are horizontally shifted by a distance varying from one-third to one-half of the porphyrin size, thus homogeneously occupying the interlayer space (Figure 11). The pyrrole rings of the porphyrin molecule impose a hydrophobic region in the midplane of the interlayer causing that the most of interlayer water molecules are located close to the hydrophilic hydroxide layers together with the sulfonate groups of ZnTPPS (Figure 10) as documented by the XRD analysis. In this region, water molecules, oxygen atoms of the sulfonate groups, and the hydroxide surface are in close contacts indicating hydrogen bonding interactions. The hydrogen-bond donor is a surface OH group and the acceptors are oxygen atoms of a water molecule or sulfonate group. Only several water molecules (1−2 molecules per interlayer) are close to porphyrin zinc atoms among the porphyrin units (Figure 10). The modeled structural arrangement documents disorder of the central part of the interlayer that is in agreement with the XRD analysis. The TPPS molecules in the Mg_2Al LDH hosts are aligned similarly; however, the TPPS units can slightly deviate from the planarity.[33]

To complement the model description, the atom concentration profile of the optimized interlayer was compared with the experimental electron density map (Supporting Information Figure S10). The concentration profile is derived from the atomic densities assuming the equivalence of all atoms. While the electron density peaks of the hydroxide layers (d = 0 and 23 Å) and water molecules together with the sulfonate groups ($d \sim 4$ and 19 Å) are well-reproduced by the concentration profile, the concentration of porphyrin zinc atoms in the middle of the interspace is expectantly of very low intensity. The electron density peaks of pyrrole atoms located near 8 and 15 Å are shifted by about 0.8 Å to the middle of the interspace. It might indicate that central zinc atom attracts nitrogen and carbon electrons toward the porphyrin center.

Photophysical Properties. The results document that LDH hosts are well suited for accommodating the porphyrin molecules. The absorption spectra enable the characterization of the molecular state of porphyrins because their aggregation is accompanied by considerable spectral changes. Comparing the absorption spectra of monomeric porphyrin solutions with those of TPPS and ZnTPPS intercalated in LDH, it is evident that the intercalation does not significantly alter the shape of the Soret band but only broadens it, an effect that we assign

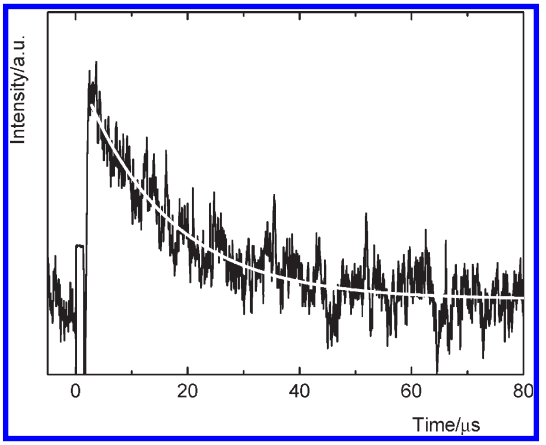

Figure 12. Time dependence of the $^1O_2$ luminescence signal of Mg_2Al−TPPS (λ_{exc} = 425 nm, ~ 1 mJ, oxygen atmosphere, recorded at 1270 nm). The smoothed line is a least-squares monoexponential fit.

to a range of binding sites of the porphyrin molecules. Thus, extensive porphyrin aggregation, a process that often occurs in solutions and on solid templates, is ruled out.[10,54] This is consistent with the molecular modeling results showing that the distance between two neighboring central atoms varies between 6 and 9 Å. The distance is considerably larger than the typical van der Waals separation of about 3.5 Å observed in π stacking of aromatic compounds.

Recently, we have described the photophysical properties of Mg_RAl hybrids containing intercalated porphyrin molecules.[29,30] The production of $O_2(^1\Delta_g)$ was predicted on the basis of quenching of the porphyrins triplet states by molecular oxygen and directly evidenced using time-dependent luminescence spectroscopy at 1270 nm. The same approach was applied here on Zn_RAl and Mg_RAl LDH hybrids prepared by the coprecipitation method. Figure 12 depicts the $O_2(^1\Delta_g)$ luminescence intensity recorded after excitation of Mg_2Al−TPPS hybrid. The effective lifetime of $O_2(^1\Delta_g)$ recovered from the monoexponential fits is 16 μs. Since pure LDH hosts do not exhibit any $O_2(^1\Delta_g)$ luminescence, it is evident that $O_2(^1\Delta_g)$ is generated solely by the porphyrin photosensitized reaction. Surprisingly, the formation of $O_2(^1\Delta_g)$ was observed only for the hybrids based on Mg_RAl LDH hosts practically not depending on the sample crystallinity, while Zn_RAl LDH-based hybrids do not produce any measurable amount of this species. The explanation is not clear because both TPPS and ZnTPPS are effective sensitizers with high quantum yields of $O_2(^1\Delta_g)$ in aqueous solutions.[55] We suppose that the lifetimes of the porphyrin triplet states and $O_2(^1\Delta_g)$ are considerably affected by Zn- and Al-coordinated OH groups oriented toward the interlayer space. Evidently, the best photosensitizing LDH materials studied in this paper are based on the Mg_RAl LDH hosts.

(54) Xu, W.; Guo, H. Q.; Akins, D. L. *J. Phys. Chem. B* **2001**, *105*, 1543.
(55) (a) García-Ortega, H.; Bourdelande, J. L.; Crusats, J.; El-Hachemi, Z.; Ribó, J. M. *J. Phys. Chem. B* **2004**, *108*, 4631. (b) Mosinger, J.; Micka, Z. *J. Photochem. Photobiol. A* **1997**, *107*, 77.

Conclusions

LDH are suitable hosts of porphyrin sensitizers. Porphyrin TPPS is intercalated in Mg_RAl LDH (R = 2−4) to give the hybrids with a characteristic basal spacing of about 23 Å. Similar results are obtained for ZnTPPS within the Zn_RAl LDH interlayer space (R = 2−4). The hydrothermal treatment increases crystallinity of the hybrids and originally intercalated TPPS in Zn_RAl LDH is metalated to ZnTPPS, while intercalated TPPS in Mg_RAl LDH remains unchanged.

The presented results can be summarized as follows. (i) The rigid framework of ZnTPPS has a benefical effect on the ordering of the hydroxide layers. (ii) The diffraction patterns are well characterized by the $R\bar{3}m$ rhombohedral space group, typical of LDH-based systems. (iii) Intercalated porphyrins do not aggregate, which is a prerequisite of effective photosensitization of $O_2(^1\Delta_g)$. The distance between two neighboring central atoms varies from 6 to 9 Å that is much longer than that of about 3.5 Å typical in parallel stacking of aromatic compounds. (iv) The gallery height of 15.5 Å is filled with nearly parallel porphyrin units. The porphyrin units are inclined with respect to the hydroxide layers with the average angle between the porphyrin plane and the layer normal of about 14°. Central zinc atoms of ZnTPPS are in the middle of the interlayer space. (v) The sulfonate groups are about 4 Å from the center of the hydroxide layers indicating the hydrogen bonding interactions between the sulfonate groups and OH groups of the layers with the contribution of water molecules. (vi) The disorder in the middle of the gallery suggests a low contribution, if any, of a superstructure based on regularly aligned porphyrin units. (vii) Mg_RAl−TPPS hybrids produce $O_2(^1\Delta_g)$, while no measurable amount of this species was found for Zn_RAl LDH-based hybrids.

Acknowledgment. This work was supported by the Czech Science Foundation (Nos. P207/10/1447, 203/07/1424), the Ministry of Education, Youth and Sports of the Czech Republic (Nos. MSM 0021620835, MSM 0021620857), and the French National Center of Scientific Research CNRS (No. 22538). The authors thank Zdeněk Futera (Faculty of Mathematics and Physics, Charles University in Prague) for ab initio calculations of the ZnTPPS porphyrin geometry.

Supporting Information Available: Details of characterization techniques and molecular modeling; TG-DTA curves, one-dimensional electron densities; HRTEM micrographs; angle distributions; experimental electron density vs atom concentration profiles. This material is available free of charge via the Internet at http://pubs.acs.org/.

PORPHYRINS INTERCALATED Zn/Al and Mg/Al LAYERED DOUBLE HYDROXIDES: PROPERTIES AND STRUCTURAL ARRANGEMENT

Eva Káfuňková,[1,3] Christine Taviot-Guého,[2] Petr Bezdička,[1] Mariana Klementová,[1] Petr Kovář,[4] Pavel Kubát,[5] Jiří Mosinger,[1,3] Miroslav Pospíšil,[4] and Kamil Lang[1*]

[1]*Institute of Inorganic Chemistry, v.v.i., Academy of Sciences of the Czech Republic, 250 68 Řež, Czech Republic*
[2]*Laboratoire des Materiaux Inorganiques, Universite Blaise Pascal, UMR-CNRS no. 6002, 63177 Aubiere Cedex, France*
[3]*Department of Inorganic Chemistry, Faculty of Science, Charles University in Prague, Hlavova 2030, 128 43 Prague, Czech Republic*
[4]*Faculty of Mathematics and Physics, Charles University in Prague, Ke Karlovu 3, 121 16 Prague 2, Czech Republic*
[5]*J. Heyrovský Institute of Physical Chemistry, v.v.i., Academy of Sciences of the Czech Republic, Dolejškova 3, 182 23 Praha 8, Czech Republic*

*** Corresponding authors:**

Kamil Lang, Institute of Inorganic Chemistry v.v.i., Academy of Sciences of the Czech Republic, 250 68 Řež, Czech Republic, e-mail: lang@iic.cas.cz

Content

Characterization Techniques

Powder X-ray diffraction (XRD) was performed on a PANalytical X'Pert PRO X-ray diffractometer. In the Bragg-Brentano geometry, incident X-ray radiation produced from a line-focused PW3373/10 Cu X-ray tube operating at 40 kV and 30 mA beam (CuKα_1/Kα_2, λ = 1.540598/1.544426 Å) passed through a 0.04 rad Soller slit, a 1/2° divergence slit, a 10 mm fixed mask, and a 1° fixed antiscatter slit. The diffracted beam was detected by an X'Celerator RTMS detector. In front of the detector a β filter, a 0.04 rad Soller slit and an antiscatter slit of 5.5 mm were used. The detector was set in the scanning mode with an active length of 2.122° *(2θ)*. In order to minimize preferred orientation effects, the powders were lightly pressed in a back loaded sample holder and were rotated with a spinning rate of 1 rotation/second. The acquisitions were performed at room temperature over a range of 2-90° *(2θ)* with a step size of 0.0167° *(2θ)* and counting time 100 s/step.

The sample Zn_2Al-ZnTPPS^H of high crystallinity was also analyzed in the Debye-Scherrer geometry equipped with a capillary sample holder and a hybrid mirror monochromator (CuKα_1, λ = 1.540598 Å), which gives the monochromatic parallel beam geometry. The diffracted beam with the X'Celerator configuration had an antiscatter shield and a Soller slit (0.04 rad). The powder was introduced in a glass capillary (outside diameter 0.3 mm, Hilgenberg GmbH) mounted on a goniometric head, which is screwed on a rotary sample stage with the spinning rate of 4 rotations/s. The high-resolution powder X-ray diffraction patterns were collected in the range 2-110° *(2θ)* with a step size of 0.0167° *(2θ)* and counting time 7300 s/step at room temperature.

In-situ high-temperature measurements were performed using a high-temperature Anton PAAR HTK-16 chamber installed on a PANalytical X'Pert PRO X-ray diffractometer, in the Bragg-Brentano geometry. The powders were spread on a 10-mm heating platinum ribbon and the powder patterns were collected at different temperatures between 25 and 700°C in air; in the range 2-70° (2θ) with a step size of 0.0167° (2θ) and 100 s/step. The heating rate was 5°C/min, which was identical to that applied in the thermogravimetric measurements.

All samples were analyzed using a sample holder exactly in the reference plane. For some of the samples, the powders were mixed with silicon in order the check the cell parameters and there was no difference between the cell parameters obtained with and without silicon.

The lattice parameters were determined by the full pattern matching analysis of the XRD diagrams obtained in the Bragg-Brentano geometry using the Fullprof suite.[1] The pseudo-Voigt profile function of Thompson, Cox and Hastings was used to generate the peak shapes of the simulated diffraction lines. To treat anisotropic size effects, the Lorentzian part of the peak broadening was modeled with linear combinations of spherical harmonics. In a second step, the integrated intensities of the 003n diffraction lines were used to calculate one-dimensional profiles along the c-stacking axis *via* the Fourier transformation.[2] The phases and structure factors were computed from the known configuration of the hydroxide layers[3] assuming a weak contribution from the interlayer part to the total scattering. For the analysis of Zn_2Al-$ZnTPPS^H$ recorded in the Debye-Scherrer geometry, the Rietveld refinement of the partial structure by considering only the hydroxide layers, was performed followed by the Fourier map calculation and visualization using the Gfourier software.[4]

Diffuse reflectance spectra were acquired on a Perkin Elmer Lambda 35 spectrometer equipped with a Labsphere RSA-PE-20 integration sphere. A sample holder with a fused silica window was filled with hybrid powder or $BaSO_4$ (Merck), which was used as a white standard. LDH powders were diluted with $BaSO_4$ prior to the measurements. The spectra were converted from reflection to absorbance by the Kubelka–Munk method and processed using the OriginPro7.5 software (OriginLab Co., USA).

Thermogravimetric analyses (TG-DTA) were carried out on a Setaram TGA 92 instrument in air. The measurements were conducted in three steps: (i) evacuation at 50°C during 5 hours in order to remove physisorbed water, (ii) temperature increase up to 200°C with a heating rate of 1°C/min, and (iii) temperature increase up to 800°C with a heating rate of 5°C/min. The gas emission analysis was performed using a Setaram SETSYS Evolution-16-MS coupled with a mass spectroscopy system.

Chemical analysis (H, Mg, Al, S and Zn) was performed by inductively coupled plasma atomic emission spectroscopy at the Vernaison Analysis Center of CNRS (France).

High-resolution transmission electron microscopy (HRTEM) was carried out on a JEOL JEM 3010 microscope operated at 300 kV (LaB_6 cathode, point resolution 1.7Å). Images were recorded on a CCD camera (1024x1024 pixels resolution) using the Digital Micrograph software package. Powder samples were dispersed in hexane and the suspension was treated in ultrasound for 10 minutes. A drop of very dilute suspension was placed on a holey-carbon-coated copper grid and allowed to dry in air at ambient temperature.

Time-resolved near-infrared luminescence of $O_2(^1\Delta_g)$ at 1270 nm was monitored using a Ge detector (1270 nm interference filter, Judson J16-8SP-R05M-HS Ge diode) upon

laser excitation by a Lambda Physik FL 3002 dye laser (λ_{exc} = 425 nm, incident energy ~1 mJ/pulse). The signal-to-noise ratio of the signals was improved by averaging of 100 to 500 individual traces. The short-lived signal produced by the scattering of excitation laser pulse and/or by red fluorescence was eliminated by exciting the sample in argon atmosphere, and subtracting the obtained signal from the signal recorded in oxygen atmosphere. The solid samples were equilibrated in a selected atmosphere by evacuating the cell and filling it with Ar or O_2. The treatment was repeated three times to ensure the desired atmosphere.

Molecular modeling

Porphyrin ZnTPPS was built in the 3*D* - Sketcher module.[5] The structure was further optimized by the quantum-chemistry computational program Turbomole v5.9 using the RI-DFT method with B-P86 functional.[6] A small def-SV(P) basis set and ECP on zinc (28 core electrons) and sulfur (10 core electrons) atoms were used because of the large size of the molecule (89 atoms). Several initial structures were optimized in order to find the global minimum with no symmetry restrictions. The optimized molecule was used in the following calculations.

Molecular mechanics and classical molecular dynamics[7] were carried out in the Cerius and Materials Studio modeling environment. The Zn_2Al LDH host with a Zn^{2+}/Al^{3+} molar ratio of 2 is a trilayered structure with a trigonal cell in hexagonal axes.[8] The space group is $R\bar{3}m$, initial experimental cell parameters were $a = b$ = 3.064 Å, and the basal spacing d_{003} was 23.05 Å. A layer $[Zn_{64}Al_{32}(OH)_{192}]^{32+}$ was created by the linking of 96 individual cells to give the following lattice parameters: A = 49.024 Å and B = 18.384 Å, with Al^{3+} cations distributed in the layers on condition that the location of Al^{3+} in neighboring octahedra is excluded.[9] Based on experimental results, ZnTPPS anions saturate over 80% of anion exchange capacity (AEC). The model structure was approximated by 100% AEC saturation assuming various orientations of guest anions with respect to the hydroxide layers and with respect to each other. The number of intercalated water molecules was estimated using thermal analysis giving the total composition of $[Zn_{192}Al_{96}(OH)_{576}][(ZnTPPS)_{24}\cdot 192\ H_2O]$ with the space group set to P1. Charges were calculated by the Qeq method (charge equilibrium approach).[10] The initial models were minimized in the Universal force field, the electrostatic energy was calculated by the Ewald summation method,[11] and the van der Waals energy was calculated by the Lennard-Jones potential.[12]

The best agreement between the experimental and calculated XRD was achieved by the following strategy. After varying the d_{003} basal spacing to obtain agreement within 3 - 25° (2θ), the positions of the diffraction lines ranging from 30 to 70° were optimized by varying the a cell parameter. After obtaining the initial a and d_{003} values, minimization in the Minimizer module was carried out iteratively in two steps. Step 1: The positions of Zn, Al and O atoms in the hydroxide layers were kept fixed. The porphyrin pyrrole units were kept rigid in their planar geometry, while all phenyl and SO_3^- atoms were variable together with the positions of water molecules and hydrogen atoms of the hydroxide layers. Step 2: The hydroxide layers were kept as rigid units, the pyrrole units were constrained as in Step 1, and the cell parameters c, α and β were variable. This procedure enabled to estimate the angle between the guest molecular planes and the host layers. Thus, a new value of the angle was estimated and the Step 1 and Step 2 were repeated until the calculated d_{003} value was in good agreement with the experimental one.

The geometry of the minimized models was further refined by quench dynamics. After a given number of dynamics steps, elucidation of the total crystal energy in dependence on the geometry and arrangement of the guest helps to determine the most probable interlayer arrangement. The dynamics simulations were carried out in an NVT statistical ensemble (N - constant number of atoms, V - constant volume, T - constant temperature) at 300 K. One dynamic step was 0.001 ps and dynamics of 200 ps were carried out. During quench dynamics, porphyrin pyrroles were kept fixed, while the other atomic positions in the interlayer space together with hydrogen atoms of the LDH hydroxide groups were variable. After quench dynamics, the partially minimized structures were again minimized by Step 1 and Step 2 to obtain the final structure models.

Figure S1. Thermogravimetric curves of Mg_2Al-TPPS, Mg_2Al-$TPPS^H$, Zn_2Al-TPPS, Zn_2Al-(Zn)$TPPS^H$, Zn_4Al-TPPS, Zn_4Al-(Zn)$TPPS^H$.

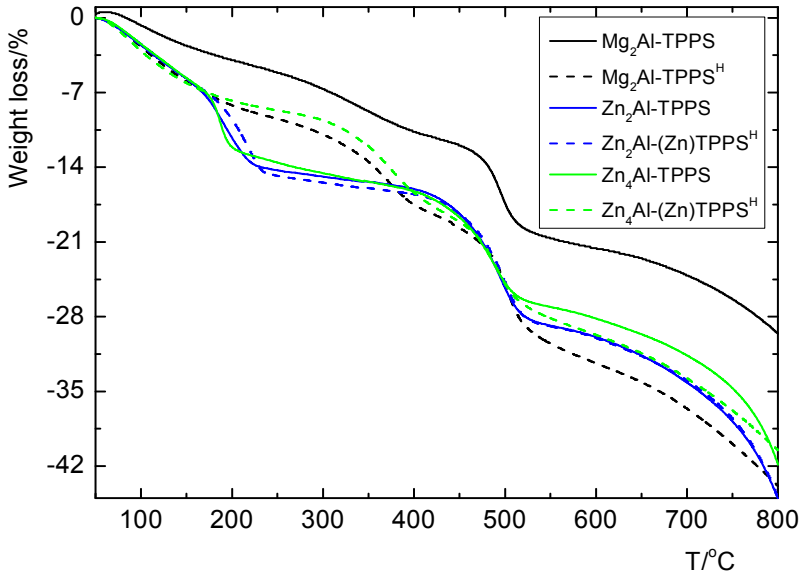

Figure S2. TG-DTA curves and the evolution of gases for ZnTPPS.

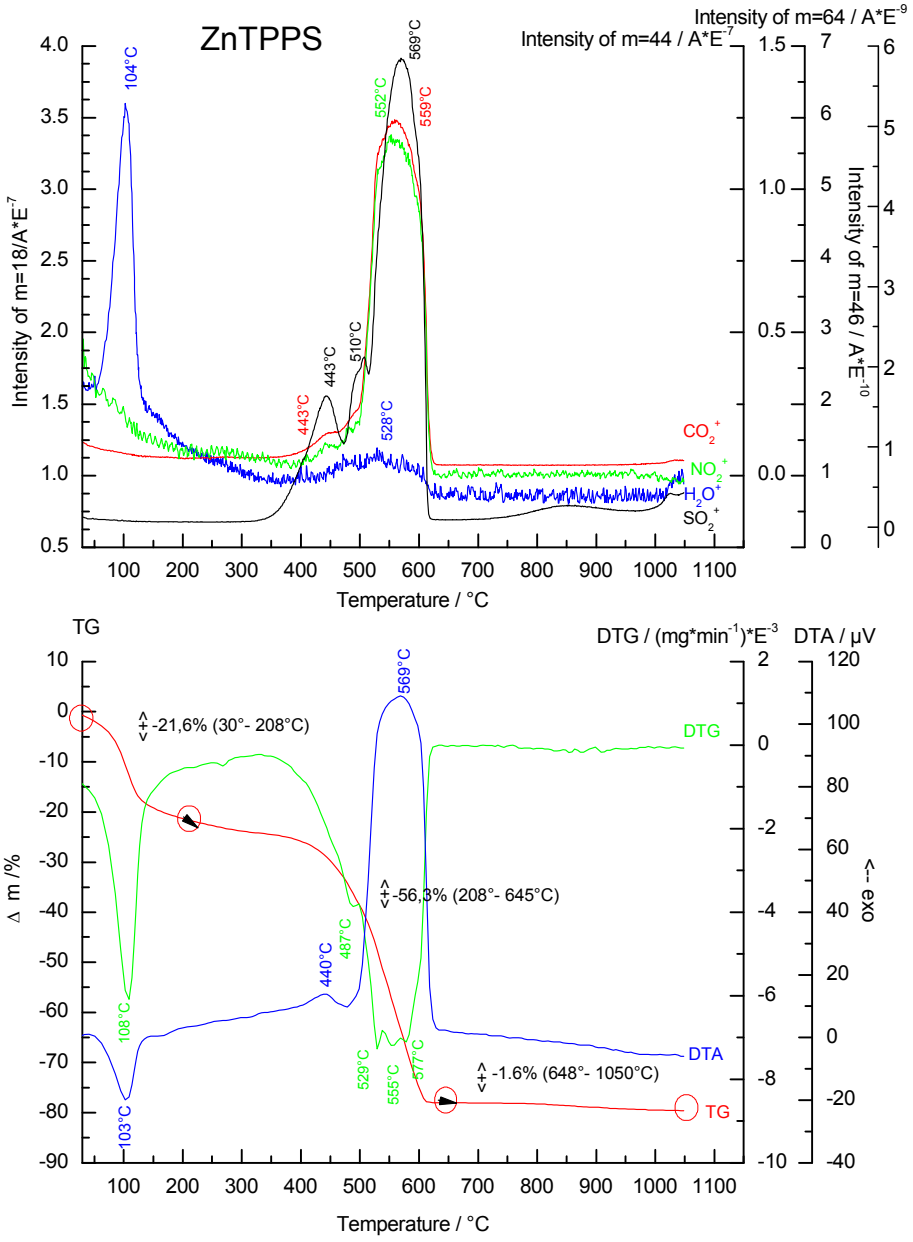

SETARAM Instrumentation		ZnTPPS	17.81mg
		Carrier gas	Air Synthetic 30ml/min.
		Crucible	Al_2O_3 100µl
SETSYS EVOLUTION-1750			Zone : 1 : 1050°C/5°C

Figure S3. TG-DTA curves and the evolution of gases for Zn_2Al-ZnTPPS^H.

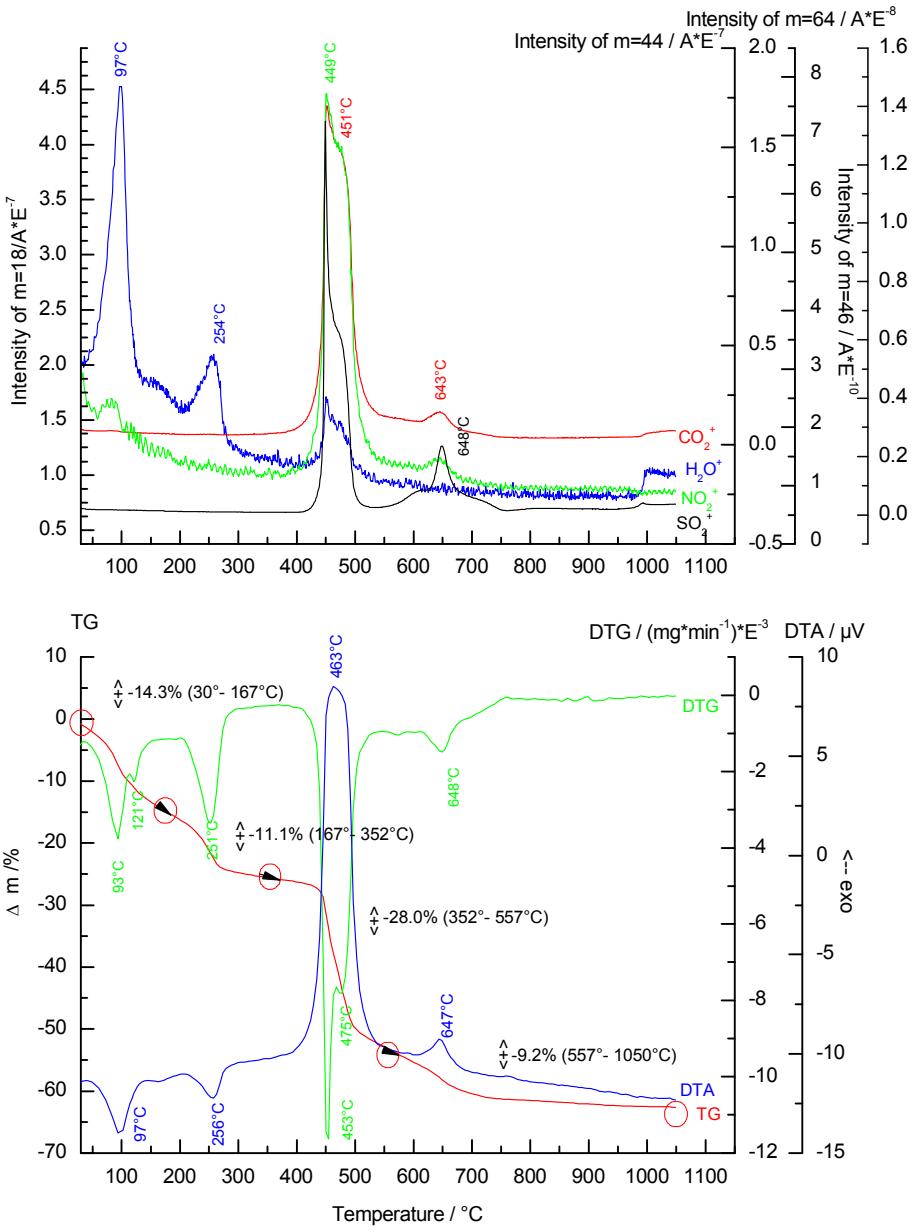

SETARAM Instrumentation		Zn_2Al-ZnTPPS^H	19.91mg
		Carrier gas	Air Synthetic 30ml/min.
		Crucible	Al_2O_3 100µl
SETSYS EVOLUTION-1750			Zone : 1 : 1050°C/5°C

Figure S4. TG-DTA curves and the evolution of gases for TPPS.

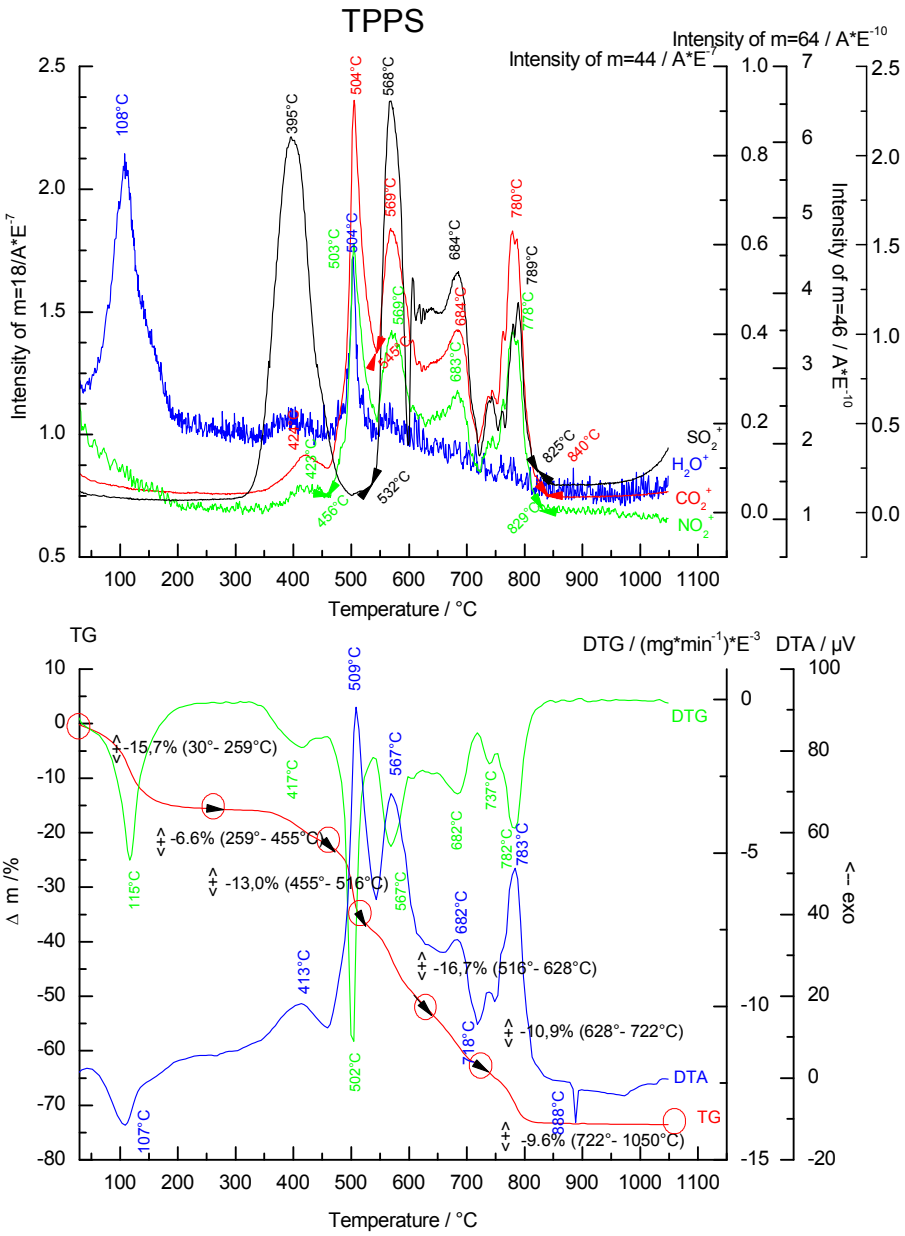

SETARAM Instrumentation		TPPS	20.64mg
		Carrier gas	Air Synthetic 30ml/min.
		Crucible	Al_2O_3 100µl
SETSYS EVOLUTION-1750			Zone : 1 : 1050°C/5°C

Figure S5. TG-DTA curves and the evolution of gases for Mg_2Al-TPPS^H.

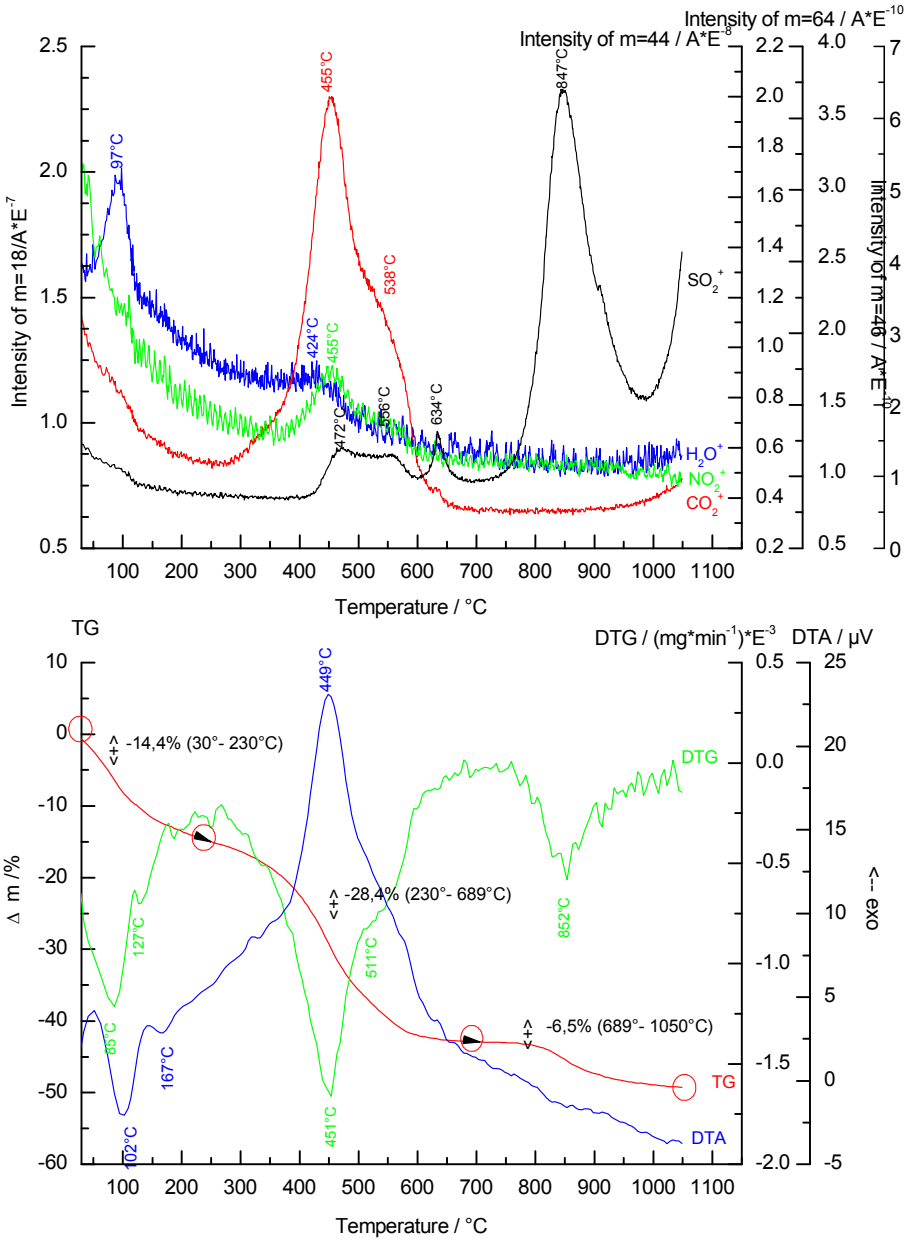

SETARAM Instrumentation	Experiment	Mg_2Al-TPPS^H	9.91mg
		Carrier gas	Air Synthetic 30ml/min.
		Crucible	Al_2O_3 100µl
SETSYS EVOLUTION-1750			Zone : 1 : 1050°C/5°C

Figure S6A. One-dimensional electron density of Zn_2Al-ZnTPPS^H (a, black line) and Mg_2Al-TPPS^H (b, red line) projected along the *c*-stacking axis. The densities were calculated from the Bragg-Brentano XRD data recorded at room temperature.

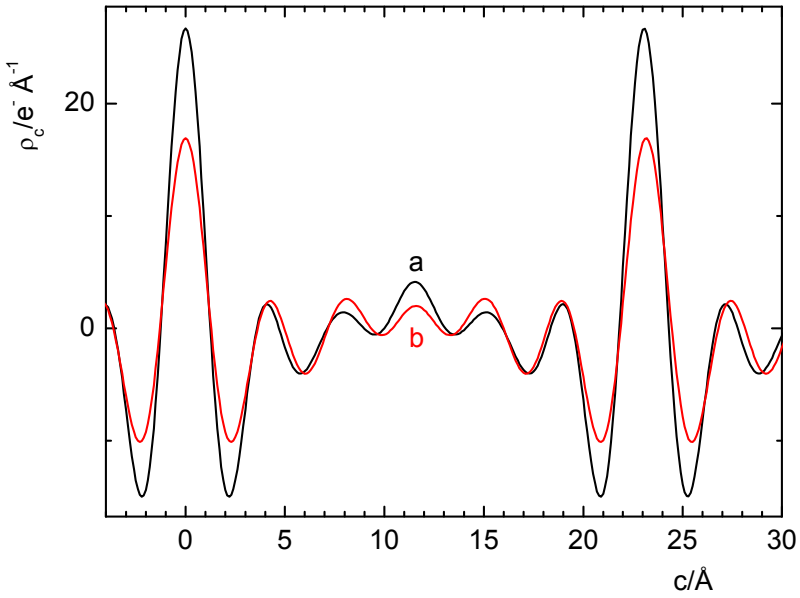

Figure S6B. One-dimensional electron density for Zn_2Al-ZnTPPS^H projected along the c-stacking axis and determined from the Bragg-Brentano data recorded at room temperature (black line) and at 100°C under vacuum (grey line).

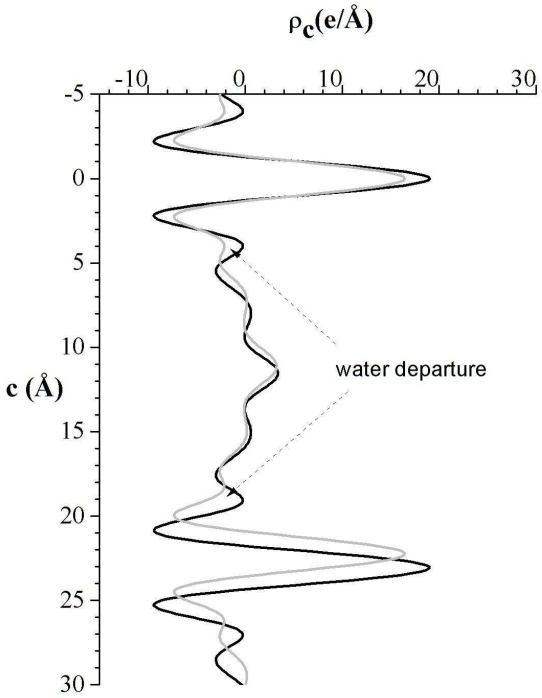

Figure S7. HRTEM observations of $Zn_2Al\text{-}Cl^H$: a) bright-filed image of typical hexagonal crystals, b) electron diffraction along [001].

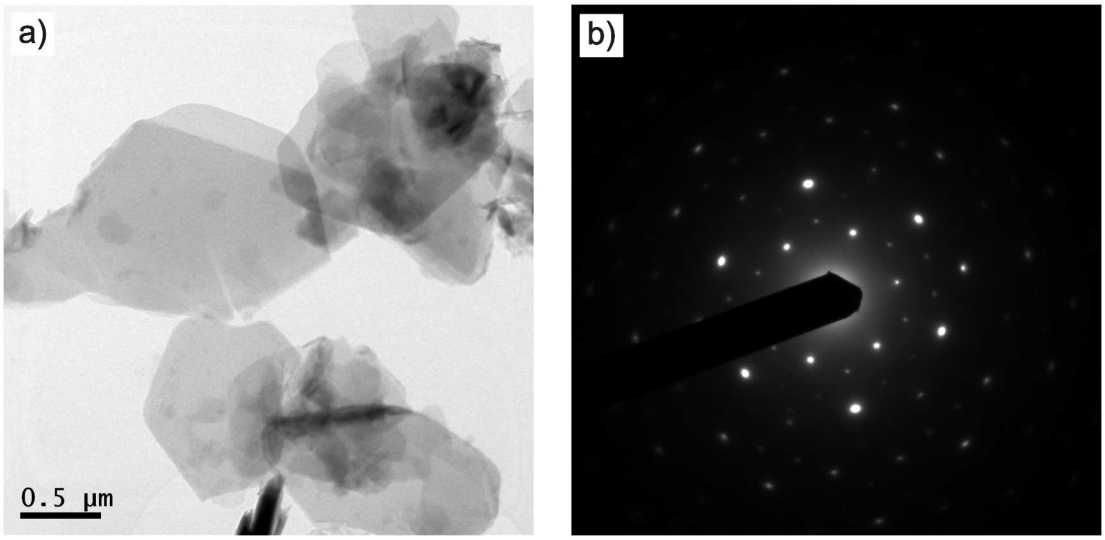

Figure S8. HRTEM observation of $Zn_2Al\text{-}Cl^H$: a) high-resolution micrograph, b) intensity histogram of the area marked in a).

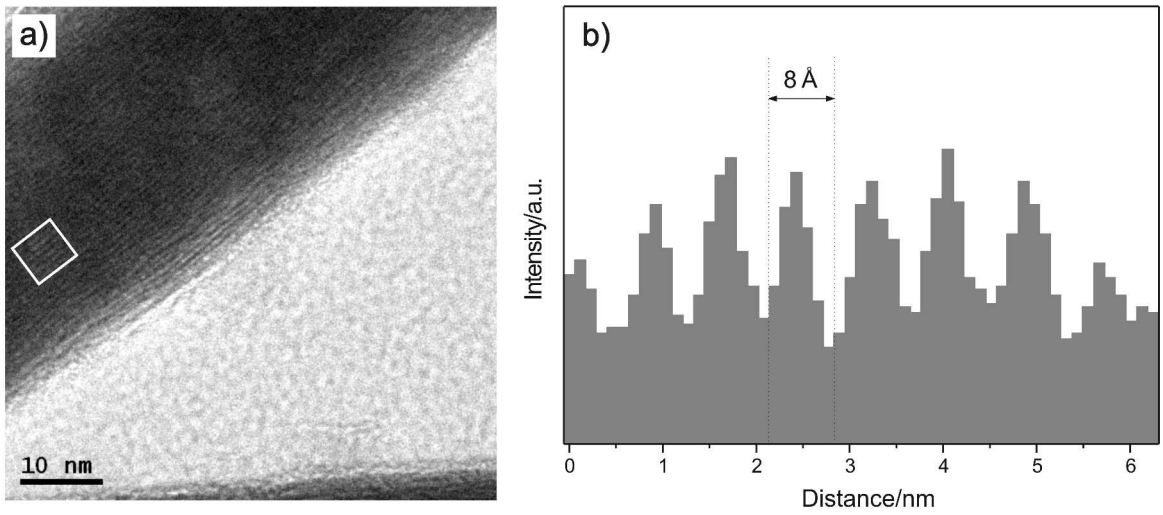

Figure S9. Distribution of angles between the porphyrin plane and hydroxide layer normal.

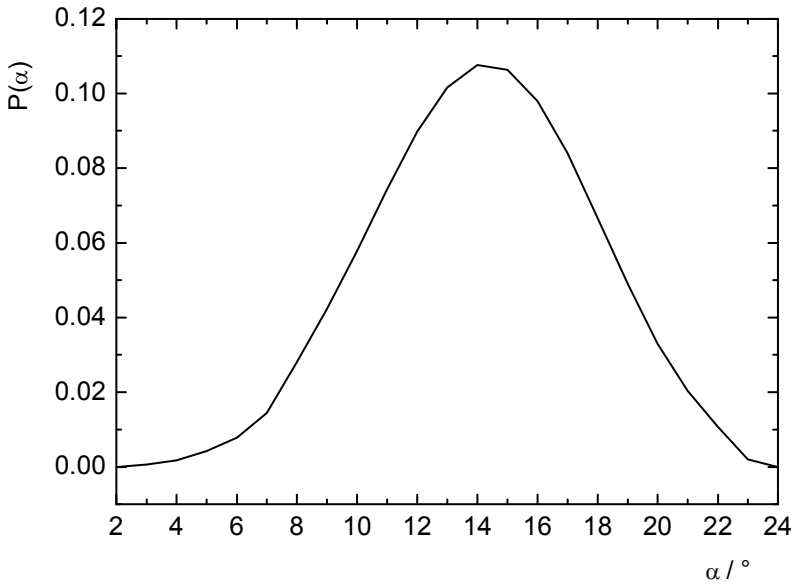

Figure S10. Comparison of the experimental electron density (a) with calculated atom concentration (b) profiles of Zn_2Al-ZnTPPS^H. The electron density was calculated from the Bragg-Brentano XRD data.

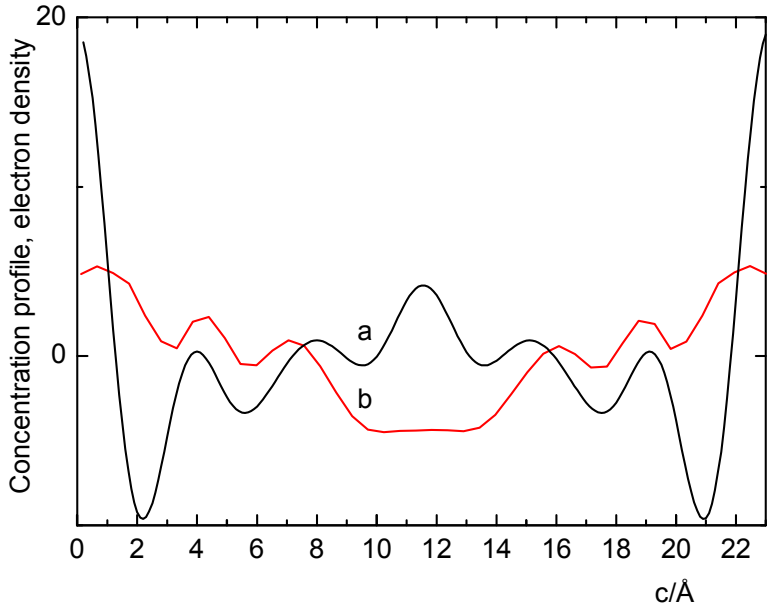

(1) Rodríguez-Carvajal, J. Recent Developments of the Program FULLPROF, in Commission on Powder Diffraction (IUCr). Newsletter **2001**, *26*, 12-19. The software is downloadable at http://www.ill.eu/sites/fullprof/.

(2) Whittingham, M. S.; Jacobson, A. Intercalation Chemistry; Academic Press, New York, 1982.

(3) Ennadi, A.; Legrouri, A.; de Roy, A.; Besse, J. P. *J. Mater. Chem.* **2000**, *10*, 2337.

(4) Roisnel, T.; Rodríguez-Carvajal, J. WinPLOTR: a Windows tool for powder diffraction patterns analysis, Materials Science Forum, Proceedings of the Seventh European Powder Diffraction Conference (EPDIC 7) **2000**, 118-123, Delhez, R.; Mittenmeijer, E. J. (Eds.).

(5) Accelrys Software Inc. (2003), Materials Studio Modeling Environment, Release 4.3 documentation. Accelrys Software Inc., San Diego.

(6) Ahlrichs, R.; Bär, M.; Häser, M.; Horn, H.; Kölmel, C. *Chem. Phys. Lett.* **1989**, *162***,** 165.

(7) Comba, P; Hambley, T. W. (1995) Molecular Modeling of Inorganic Compounds. VCH Verlagsgesselschaft mbH, Weinheim.

(8) Kovář, P.; Pospíšil, M.; Káfuňková, E.; Lang, K.; Kovanda, F. *J. Mol. Model*. **2010**, *16*, 223.

(9) Sideris, P. J.; Nielsen, U. G.; Gan, Z.; Grey, C. P. *Science* **2008**, *321*, 113.

(10) Rappe, A. K; Goddard, W. A. III *J. Phys. Chem*. **1991**, *95*, 3358.

(11) Karasawa, N; Goddard, W. A. III *J. Phys. Chem*. **1989**, *93*, 7320.

(12) Lennard-Jones, J. E. *Proc. Royal Society London*, series A **1925**, *109*, 584.

Appendix IV

***E. Káfuňková**, K. Lang, P. Kubát, M. Klementová, J. Mosinger, M. Šlouf, A. L. Troutier-Thuilliez, F. Leroux, V. Verney, C. Taviot-Guého:*

Porphyrin-Layered Double Hydroxides/Polymer Composites as Novel Ecological Photoactive Surfaces

Journal of Materials Chemistry **2010**, DOI: 10.1039/C0JM00746C

Porphyrin-layered double hydroxide/polymer composites as novel ecological photoactive surfaces†‡

Eva Káfuňková,[ab] Kamil Lang,*[a] Pavel Kubát,[c] Mariana Klementová,[a] Jiří Mosinger,[ab] Miroslav Šlouf,[d] Anne-Lise Troutier-Thuilliez,[e] Fabrice Leroux,[e] Vincent Verney[f] and Christine Taviot-Guého*[e]

Received 18th March 2010, Accepted 27th May 2010
DOI: 10.1039/c0jm00746c

Nanocontainer and nanofiller aspects of layered double hydroxides (LDH) were combined to prepare porphyrin-LDH/polymer composites for photoactive coatings. The suggested properties are derived from cytotoxicity of singlet oxygen, $O_2(^1\Delta_g)$, produced by interaction of molecular oxygen with excited porphyrin molecules located within the interlayer space of Zn_RAl and Mg_RAl LDH. Porphyrins, Pd(II)-5,10,15,20-tetrakis(4-carboxyphenyl) porphyrin (PdTPPC) and 5,10,15,20-tetrakis(4-sulfonatophenyl) porphyrin (TPPS) photoproducing $O_2(^1\Delta_g)$, were successfully intercalated into LDH hosts using the co-precipitation procedure and then used as fillers in two eco-friendly polymers, namely polyurethane (PU) and poly(butylene succinate) (PBS). Porphyrin-LDH/polymer composites were prepared either by the solvent cast/cross-linking technique or melt-compounding with different porphyrin-LDH filler loadings (up to 1.3 wt%). Both X-ray diffraction and transmission electron microscopy measurements indicate a good dispersion of porphyrin-LDH fillers into the polymer matrices and that the porphyrin molecules remain intercalated within LDH layers. The polymers do not block the diffusion of oxygen and the triplet states of the intercalated porphyrins in the composite films have enough long lifetimes to produce $O_2(^1\Delta_g)$ upon irradiation by visible light. The present composites allow the elaboration of photoactive surfaces with a precise control of the $O_2(^1\Delta_g)$ concentration depending on porphyrin-LDH filler loadings.

1. Introduction

In the last decade, the research on layered double hydroxides (LDH) as nanostructured hybrid materials has developed considerably.[1] Also known as hydrotalcite-like materials, LDH are generally described by the formula $[M^{2+}_{1-x}M^{3+}_x(OH)_2]A^{m-}_{x/m}\cdot nH_2O$, abbreviated hereafter as $A–M^{2+}_RM^{3+}$, where M^{2+} and M^{3+} are divalent and trivalent cations within the hydroxide layers, A^{m-} an interlayer anion of valence m, and $R = (1-x)/x$ is the M^{2+}/M^{3+} molar ratio. The lamellar structure of LDH, the wide range of cationic compositions of the hydroxide layers, and the ease with which various inorganic and organic anions can be accommodated into the interlayer space of LDH bring these materials at a high level of interest for the development of advanced nanostructured materials with potential applications in catalysis,[2] waste water treatment,[3] as electrochemical sensors,[4] fillers in polymers,[5] and in drug/gene delivery systems.[6] According to the classification stated by C. Sanchez for hybrid organic-inorganic materials,[7] LDH belong to class I where organic and inorganic components are linked together through interactions like hydrogen, van der Waals, or ionic bonding. Because of these interactions, synergy effects are less pronounced than for materials of class II, in which the two phases are linked together through covalent bonds. However, as discussed below, the properties of guest species can be affected by a geometrically constrained environment supplied by the LDH hosts and the properties of hybrid LDH materials generally differ from those of pure guest species. Furthermore, embedding an active species within the LDH host may also retard its degradation and minimize an eventual leakage.

A promising field of hybrid LDH applications is that of optical devices and pigments. The literature already offers several examples where the combination of organic chromophores with inorganic matrices has synergistic effects.[8] Porphyrin-LDH hybrids are particularly interesting in this respect as handy sources of singlet oxygen, also offering potential applications in catalysis and as electrochemical microsensors.[9,10] Indeed, the LDH host, with a two-dimensional space of a flexible height and variable layer charge density, allows the incorporation of large guest molecules such as porphyrins with a control of their

[a]*Institute of Inorganic Chemistry of the AS CR, v.v.i., 250 68 Husinec-Řež, Czech Republic. E-mail: lang@iic.cas.cz*
[b]*Department of Inorganic Chemistry, Faculty of Science, Charles University in Prague, Hlavova 2030, 128 43 Praha, Czech Republic*
[c]*J. Heyrovský Institute of Physical Chemistry of the AS CR, v.v.i., Dolejškova 3, 182 23 Praha 8, Czech Republic*
[d]*Institute of Macromolecular Chemistry of the AS CR, v.v.i., Heyrovského náměstí 2, 162 06 Praha 6, Czech Republic*
[e]*CNRS, UMR 6002, LMI, F-63177 Aubiere - Clermont Université, Université Blaise Pascal, Laboratoire des Matériaux Inorganiques, BP 10448, F-63000 Clermont-Ferrand, France. E-mail: Christine.Taviot-Gueho@univ-bpclermont.fr*
[f]*CNRS, UMR 6505, LPMM, F-63177 Aubiere - Clermont Université, Université Blaise Pascal, LPMM, BP 10448, F-63000 Clermont-Ferrand, France*

† Electronic Supplementary Information (ESI) available: Porphyrin-LDH reference materials - refined cell parameters and powder XRD patterns; TEM/EDX spectra; singlet oxygen luminescence signals generated by the references. See DOI: 10.1039/c0jm00746c/

‡ This paper is part of a *Journal of Materials Chemistry* themed issue on Advanced Hybrid Materials, inspired by the symposium on Advanced Hybrid Materials: Stakes and Concepts, E-MRS 2010 meeting in Strasbourg. Guest editors: Pierre Rabu and Andreas Taubert.

distribution and orientation. Furthermore, it has been shown that the relatively long-lived triplet states of intercalated porphyrin molecules in LDH can be involved in photochemical reactions.[10,11] The nanometre-sized dispersion of LDH fillers in polymers improves performances of the polymer matrix with positive effects on key properties such as thermal, mechanical, barrier, and even flame-retardant properties.[5] LDH fillers can also bring additional functionalities such as optical and antioxidant properties, depending on interlayer anions properties, leading to multifunctional polymer composites with interesting applications.[12,13]

The immobilization of porphyrin by polymers has already been proposed to create solid surfaces with potential applications in water disinfection,[14] electrochemical sensing,[15] sensing of toxic gases,[16] and for photobactericidal surfaces.[17] In the present work, we aimed to combine two aspects of LDH chemistry, *i.e.*, nanocontainer and nanofiller function, to prepare photobactericidal surfaces based on porphyrin-LDH/polymer composites. The intercalation of porphyrin into the LDH host may overcome porphyrin leaching problems, increase thermal stability, and can also prevent porphyrin aggregation. Two kinds of eco-friendly polymer were thus investigated, namely polybutylene succinate (PBS) and waterborne polyurethane (PU). PBS is a biocompatible linear aliphatic polyester,[18] synthesized by polycondensation of 1,4-butanediol with succinic acid. It is commercially available as a thermoplastic polyester with many interesting properties, including biodegradability, melt processability, thermal and chemical resistance.[19] However, practical applications of PBS have been limited so far because of its softness and low gas barrier properties. PU can be made from bio-derived polyols combined with petro-derived isocyanates. A waterborne PU dispersion is a binary colloidal system, in which PU particles are dispersed in a water phase. Since aqueous dispersions of PU are non-toxic, non-flammable, and do not pollute the air, PU is considered to be eco-friendly and has been widely used in coatings and adhesives for textile, leather, paper, wood, and glass fibers.[20]

The intercalation of 5,10,15,20-tetrakis(4-sulfonatophenyl)porphyrin (TPPS) and Pd(II)-5,10,15,20-tetrakis(4-carboxyphenyl)porfyrin (PdTPPC) into Zn_RAl and Mg_RAl LDH hosts can be achieved by the coprecipitation method.[21] In this paper, we describe the preparation of the porphyrin-LDH/polymer composites with different porphyrin-LDH filler loadings from 0.4 to 1.3 wt%. The LDH fillers and corresponding polymer composites were characterized by a combination of techniques: powder X-ray diffraction and absorption, transmission electron microscopy, viscoelasticity, and transient spectroscopy (triplet states, singlet oxygen). In the case of the PU composites, a good dispersion of porphyrin-LDH fillers leads to transparent and colored films. The intercalated porphyrin-LDH structure is preserved. Photophysical experiments proved that the triplet states of porphyrins in porphyrin–LDH/polymer composites are quenched by oxygen to produce singlet oxygen. In addition, the varying concentration of porphyrin-LDH fillers allows the modulation of the amount of cytotoxic singlet oxygen at the composite surface.

2. Experimental

Materials

The tetrasodium salt of 5,10,15,20-tetrakis(4-sulfonatophenyl)porphyrin (TPPS) (Aldrich, Germany), Pd(II)-5,10,15,20-tetrakis(4-carboxyphenyl)porphyrin, PdTPPC, (Frontier Scientific Europe, Ltd., UK), and $Al(NO_3)_3\cdot 9H_2O$, $AlCl_3\cdot 6H_2O$, $Zn(NO_3)_2\cdot 6H_2O$, $ZnCl_2\cdot 6H_2O$, $Mg(NO_3)_2\cdot 6H_2O$, $MgCl_2\cdot 6H_2O$ and NaOH (all supplied by Acros Organics, France) were used as purchased. An aqueous polyurethane (PU) dispersion Daotan VTW 1225 (Solutia Inc., St. Louis, MO) contains hydroxyl functionalities (the hydroxy value of 47 mg KOH/g as indicated by the supplier) available for crosslinking with methylated melamine formaldehyde resin Maprenal MF 900 (INeos Melamines GmbH, Frankfurt, Germany). Poly(butylene succinate) (PBS) (EnPol G4560) was supplied by IRe Chemical Limited (South Korea).

Preparation of porphyrin-LDH reference materials and fillers

The synthesis of porphyrin-LDH materials was carried out using the coprecipitation method at constant pH and adjusted to small quantities as reported elsewhere.[21] Typically, a metal-salt solution at a concentration of 0.2 M containing $MCl_2\cdot 6H_2O$ (M^{2+}: Zn or Mg) and $AlCl_3\cdot 6H_2O$ in a variable molar ratio ($R = M^{2+}/Al^{3+}$ ranging from 2 to 4) and 0.4 M NaOH solution were added dropwise, under a nitrogen atmosphere and vigorous stirring, to an aqueous porphyrin solution in a concentration representing a twofold excess over the stoichiometry amount (given by the Al^{3+} content). The pH value was maintained constant at pH 7.5 for $R = 2$ and 3 and at pH 8.0 for $R = 4$. In the case of the reference samples, resulting violet precipitates were aged for 24 h under stirring at room temperature, afterwards centrifuged and washed three times with water and finally dried at room temperature.

Table 1 Experimental conditions for the preparation of the porphyrin-LDH/polymer composites

Samples	Code	Ageing[a]	Sonication	LDH wt%[b]	Melamine wt%[c]
PdTPPC-Zn_2Al/PU	B1	—	x	1.0	24
PdTPPC-Zn_2Al/PU	B2	—	x	1.0	16
PdTPPC-Zn_3Al/PU	A	x	—	0.75	24
PdTPPC-Mg_2Al/PU	B4	x	x	0.5	16
TPPS-Mg_2Al/PU	B5	x	x	0.4	16
PdTPPC-Zn_2Al/PBS		x	—	1.3	—

[a] LDH precipitates were aged for 12 h under stirring at room temperature. [b] Amount of dried LDH related to the amount of PU dispersion and melamine. [c] Melamine related to the amount of PU dispersion.

In order to improve the crystallinity of the reference samples, they were submitted to a post-synthesis hydrothermal treatment. Typically, about 20 mg of the solids were suspended in 25 mL of water, in a 30 mL Teflon inner vessel inside a stainless autoclave, and treated at 120 °C for 72 h under autogeneous pressure. The powder reference samples were labeled as, *e.g.*, PdTPPC-M_RAl^H where *R* subscript gives the M^{2+}/Al^{3+} molar ratio used in the synthesis and H exponent stands for hydrothermally treated samples (Table S1, see ESI†). TPPS is metallated by Zn^{2+} during the synthesis of Zn_RAl LDH hybrids,[21] therefore the product is labelled as ZnTPPS-Zn_RAl^H. Since PdTPPC-Zn_4Al^H displays the highest crystallinity, most of the structural information on PdTPPC intercalation were obtained with this sample.

In the case of fillers, *i.e.*, PdTPPC-Zn_RAl ($R = 2, 3$), PdTPPC-Mg_2Al and TPPS-Mg_2Al, precipitates after centrifugation and washing steps were kept in a desiccator under nitrogen atmosphere as a paste. LDH fillers were used without ageing treatment (B1, B2 composites), while the others were aged for 12 h (Table 1).

Preparation of porphyrin-LDH/polymer composites

Porphyrin-LDH/PU composites were obtained by mixing fillers as pastes (0.4, 0.5, 0.75, and 1 wt% of dried LDH related to the amount of PU dispersion and melamine) and PU dispersion. In the case of the composites denoted by "B", these mixtures were then subjected to sonication (2.5 s pulses followed by 1 s breaks, Vibra Cell, Bioblock Scientific, 750 W) for 10 min. On the contrary, the "A" composite was not sonicated. Dispersions were stirred for 12 h at room temperature under air in a closed container. Afterwards, melamine formaldehyde cross-linker agent was added in two different amounts (16 or 24 wt%). Then, the three-component suspensions were poured onto polypropylene plates and a thickness was adjusted to 100 or 200 μm using a box bar. Finally, PU cross-linking was performed by heating covered polypropylene plates at 140 °C for 20 min in an oven, in air. The composites thus obtained and preparation conditions are gathered in Table 1.

PdTPPC-Zn_2Al/PBS composite was prepared through the melt-extrusion technique using a twin rotor thermohaake-mixer (Haake Force Feeder Minlab system) operating at 140 °C with a rotor speed of 100 rpm for 5 min. PBS in a pellet form and PdTPPC-Zn_2Al as a powder (obtained by drying a paste) were alternately thrown batch-wise inside the mixer. The dried samples were then converted into sheets by pressing at 140 °C for 30 s.

Characterization techniques

The chemical compositions of porphyrin-LDH reference materials (R_{exp}) were determined by inductively coupled plasma emission spectroscopy on an IRIS Intrepid II XPS spectrometer (ICP-EOS) using the axial plasma view and cyclone type nebulizer.

Powder X-ray diffraction (XRD) experiments were performed on a PANalytical X'Pert PRO diffractometer using Cu $K\alpha_1/K\alpha_2$ radiation in two different geometries. The reference and filler powder materials were analyzed in the reflection mode (divergence slit ½, mask 10 mm). The diffracted beam was detected by an X'Celerator RTMS detector over a range 2–90° (2θ) with a step size of 0.0167° (2θ) and counting time 100 s/step. The composites (PU composites were placed on a Mylar foil) were analyzed in the transmission mode with an elliptical focusing mirror in the primary beam (divergence slit ½, mask 20 mm). The diffracted beam was detected by an PIXcel detector over a range 1–85° (2θ) with a step size of 0.007° (2θ) and counting time 510 s/step.

Extended X-ray absorption fine structure (EXAFS) spectra at the Pd K-edge (24350.3 eV) were recorded on a SAMBA beamline (SOLEIL) in the transmission mode at 77 K with a nitrogen cryostat.[22] The powders were mixed with boric acid (the sample mass was adjusted to obtain an absorption jump of 1 at the Pd K-edge) and sandwiched between Kapton tapes. A Si (220) sagitally focusing double-crystal monochromator was used for scanning the energy from 24 100 to 24 300 eV with an energy step of 5 eV and 1 s of integration time, and from 24 300 to 24 400 eV with an energy step of 0.5 eV and 2 s of integration time. EXAFS data were recorded in the ***k*** space with a constant step of 0.05 $Å^{-1}$ using 24 350 eV as threshold energy. Three spectra were recorded for each sample. A Pd coated collimating mirror and a Pd coated focusing mirror with a grazing incidence of 2 mrad were used for harmonic rejection. The spot size at the sample position was 3 mm in the horizontal plane and 0.25 mm in the vertical plane. Extraction and analysis of EXAFS data was performed following standard procedures as reported elsewhere.[23]

Small-angle X-ray scattering (SAXS) experiments were performed using a pinhole camera (Molecular Metrology SAXS System) attached to a microfocused X-ray beam generator (Osmic MicroMax 002) operating at 45 kV and 0.66 mA (30 W). The camera was equipped with a multiwire, gas-filled area detector with an active area diameter of 20 cm (Gabriel design). Two experimental setups were used to cover the *q* range of 0.005–1.1 $Å^{-1}$ ($q = (4\pi/\lambda)\sin\Theta$, where $\lambda = 1.54$ Å is the wavelength and 2Θ is the scattering angle). The scattering intensities were put on an absolute scale using a glassy carbon standard.

High-resolution transmission electron microscopy (HRTEM) was carried out on a JEOL JEM 3010 microscope operated at 200 kV (LaB_6 cathode, point resolution 1.7 Å). Micrographs were recorded on a CCD camera (1024 × 1024 pixels resolution) using the Digital Micrograph software package. Powder samples were dispersed in hexane and the suspension was treated in ultrasound for 10 min. A drop of very dilute suspension was placed on a holey-carbon-coated copper grid and allowed to dry in air at ambient temperature. A TEM microscope Tecnai G2 Spirit Twin 12 (FEI, Czech Republic), equipped with an energy dispersive X-ray microanalysis system (EDAX, USA), was employed for the morphology analysis of prepared hybrid films. Ultrathin sections (*ca* 50 nm) were cut using an ultra microtome UCT (Leica, Germany) at cryo conditions (sample temperature −90 °C, knife temperature −50 °C) and transferred to a Cu microscopic grid. Standard bright field (TEM/BF) images were obtained at 120 kV. The EDX spectra were collected from several locations with a diameter around 100 nm.

Molecular changes for PdTPPC-Zn_2Al/PBS were monitored by melt viscoelasticity experiments in the oscillatory shear mode using a rotational strain controlled rheometer (ARES) equipped with a parallel plate geometry (plate diameter 25 mm, gap 1.0 mm). The values of the strain amplitude were checked to

ensure that all measurements were conducted within the linear viscoelastic domain. A frequency sweep extending from 0.01 to 100 rad s^{-1} was performed at different temperatures 120, 140, and 160 °C. Temperature 120 °C was considered as a reference to generate master curves by the time-temperature superposition using the Innovative Rheological Interface Software (IRIS 2006). In the case of porphyrin-LDH/PU composites, such rheological approach would not distinguish between either melamine cross-linking or platelet reinforcing effects and, for this reason, no measurements were performed.

The diffuse reflectance absorption spectra were recorded on a Perkin Elmer Lambda 35 spectrometer equipped with a Labsphere RSA-PE-20 integration sphere. A sample holder with a fused silica window was filled with an LDH powder or $BaSO_4$ (Merck), which was used as a white standard. The spectra were converted from reflection to absorbance by the Kubelka–Munk method and processed using the OriginPro7.5 software (OriginLab Co., USA). The films were measured in the transmittance mode. The luminescence spectra of $O_2(^1\Delta_g)$ were monitored on a Fluorolog 3 spectrometer (Horiba Jobin Yvon). Emitted light was filtered by a Shott RG 830 glass filter to eliminate scattered light and detected using a Hamamatsu H10330-45 photomultiplier.

The time-resolved near-infrared luminescence of $O_2(^1\Delta_g)$ at 1270 nm was monitored using a Ge detector upon laser excitation by a Lambda Physik FL 3002 dye laser ($\lambda_{exc} = 425$ nm, incident energy ~1 mJ/pulse). The signal-to-noise ratio of the signals was improved by averaging of 100 to 500 individual traces. The short-lived signal produced by the scattering of an excitation laser pulse and/or by red fluorescence was eliminated by exciting the sample in argon atmosphere, and subtracting the obtained signal from the signal recorded in oxygen atmosphere. The powders and films were equilibrated in selected atmosphere by evacuating a cell and filling it with Ar or O_2. The treatment was repeated three times to ensure the desired atmosphere.

Nanosecond transient absorption experiments were performed with a Lambda Physik FL 3002 dye laser (425 nm, incident energy ~1 mJ/pulse) pumped with a Lambda Physik COMPEX 102 excimer (308 nm, pulse width 28 ns). Transient absorption spectra of the triplet states in polymer films were measured within 450–600 nm on a laser kinetic spectrometer (Applied Photophysics, U.K.). The time profiles were recorded using a 250 W Xe lamp equipped with a pulse unit and a R928 photomultiplier (Hamamatsu).

3. Results and discussion

3.1. Characterization of porphyrin-LDH reference and filler materials

This part is focused on the preparation and characterization of the porphyrin-LDH hybrids. The coprecipitation method, often viewed as a self assembly process, was used for the synthesis. Zn_RAl LDH hosts were chosen because Zn_RAl-based hybrids have usually a better crystallinity than hybrids derived from Mg_RAl LDH. All the as-prepared samples exhibit XRD patterns typical of LDH. The M^{2+}/Al^{3+} molar ratios (R_{exp}), given in Table S1 (see ESI†), were obtained by the chemical analysis of the powders and are consistent with the component concentrations

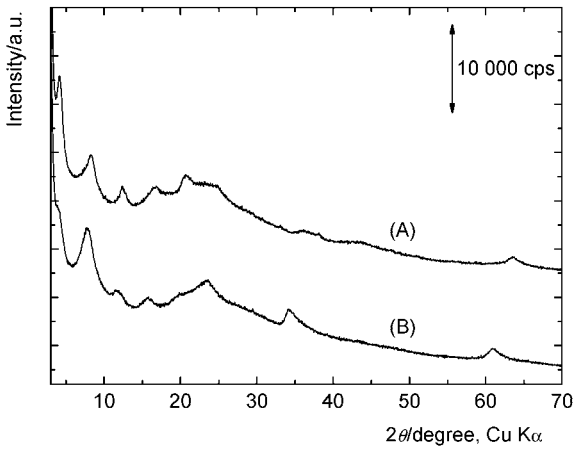

Fig. 1 Powder XRD patterns of porphyrin-LDH filler materials: (A) PdTPPC-Mg_2Al, aged for 12 h; (B) PdTPPC-Zn_2Al, no aging. The curves are shifted for clarity.

set for the preparation. Diffraction peaks are indexed in the rhombohedral space group $R\bar{3}m$ often reported for LDH (Fig. S1, see ESI†). The sharp diffraction lines between 2 and 25° of the 2θ scale, correspond to diffractions on (00*l*) planes (l = 3,6.) and the interlayer distance d_{003} is given by the position of the first peak of this series. The values thus calculated are all around 23 Å and are consistent with the interlayer distance expected for porphyrins intercalated into LDH, resulting from a slightly inclined orientation of the porphyrin plane with respect to the normal of the hydroxide layers.[21,24] In order to avoid extensive aggregation of porphyrin-LDH particles and get a good dispersion within the polymer matrix, either no aging or 12 h ageing time was applied for the preparation of fillers. Accordingly, the crystallinity of fillers (Fig. 1) was found poorer than that of the reference materials (Fig. S1, see ESI†). Yet, from the positions of the diffraction lines, the formation of porphyrin-intercalated LDH phases was confirmed in all cases.

As usually observed, the application of a post-synthesis hydrothermal treatment has a beneficial effect on the LDH crystallinity with the *00l* peaks becoming narrower, as well leading to a better signal to noise ratio. In addition, the formation of the ZnO phase in a small amount was observed in PdTPPC-Zn_3Al^H and PdTPPC-Zn_4Al^H (Fig. S1, see ESI†) that can be assigned to a dissolution/decomposition of Zn-based LDH during the hydrothermal treatment.[25] The decrease of the zinc content within the hydroxide layers, concomitant with the formation of ZnO, was also reported for hydrothermally treated ZnTPPS-Zn_4Al^H hybrids.[21] The *a* and *c* cell parameters gathered in Table S1 (see ESI†) were calculated from the peak profile analysis of the XRD patterns for hydrothermally treated samples using the Fullprof suite;[26] the interlayer distances d_{003} for the other samples of lower crystallinity were estimated from the position of the *00l* diffraction peaks.

The good crystallinity of PdTPPC-Zn_4Al^H allowed us going further in the structural characterization of PdTPPC-LDH assemblies. First, the structure of the interlayer space was probed *via* the Fourier transform of the *00l* X-ray reflection intensities giving a one-dimensional electron-density distribution along the *c*-stacking axis. The 1-*D* plots thus obtained are compared for

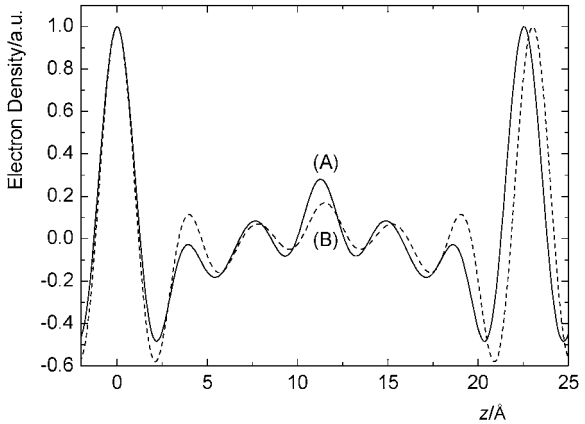

Fig. 2 One-dimensional electron-density distribution along the *c*-stacking axis determined by the Fourier transformation of the *00l* XRD patterns for (A) PdTPPC-Zn_4Al^H and (B) ZnTPPS-Zn_4Al^H.

PdTPPC-Zn_4Al^H and ZnTPPS-Zn_4Al^H in Fig. 2. The most intense peaks correspond to the electron densities of the hydroxide layers. Note that the distance between consecutive hydroxide layers is slightly larger in ZnTPPS-Zn_4Al^H than in PdTPPC-Zn_4Al^H in agreement with the interlayer distances d_{003} reported in Table S1 (see ESI†). The carboxylate and sulfonate groups of PdTPPC and ZnTPPS, respectively, together with water molecules, are responsible for the smaller maxima located at the outer parts of the interlayer space; the difference in electron densities between carboxylate and sulfonate groups explains the lower intensity observed with PdTPPC. On the other hand, the higher maximum in the centre of the interlayer space with PdTPPC is attributed to the presence of heavy Pd atoms.

The EXAFS technique was employed to better characterize the local structure of PdTPPC intercalated into the Zn_2Al-LDH host. As can be seen in Fig. 3, the modulus of the Fourier transform at the Pd K-edge for Zn_2Al-PdTPPC is identical to that of pure PdTPPC indicating that PdTPPC retains its molecular structure once intercalated into the LDH host.

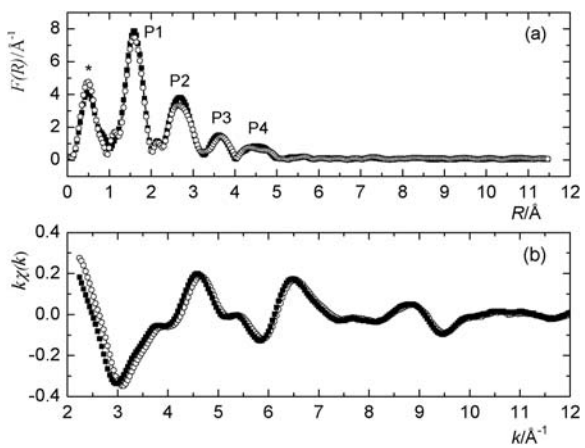

Fig. 3 (a) Fourier transform magnitude of the Pd K-edge EXAFS spectra measured on PdTPPC free porphyrin (■) and PdTPPC-Zn_2Al (○) and (b) corresponding $k\chi(k)$ signals. Only experimental data are displayed. The distances are not corrected for the phase shift. The noise peak labeled by * is due to the Fourier extraction.

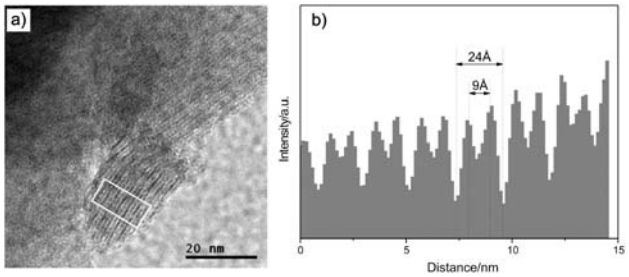

Fig. 4 HRTEM observation of PdTPPC-Zn_4Al^H: (a) high-resolution micrograph; (b) electron density histogram of the area marked in (a).

Although distances were not corrected for the phase shift, using the crystallographic data reported for PdTPPC one can easily ascribe the first peak P1 to the Pd–N distance at 2.02 Å and P2/P3/P4 peaks to Pd–C correlations.[27] Because the EXAFS technique is a local probe, we were not able to observed Pd–Pd contacts expected at a distance of 11.1 Å according to the structure of PdTPPC salt,[27] in spite of the high back-scattering power of Pd atoms. This result also indicates that intercalated porphyrins are spaced apart from each other by at least ~6 Å.

The structure on the nanometre scale of PdTPPC-Zn_4Al^H was also investigated by HRTEM. The micrograph presented in Fig. 4(a) shows a well-developed layered structure with a distance between the parallel fringes of about 24 Å in good agreement with the d_{003} value determined by XRD (Table S1†). It gives explicit evidence that the porphyrin molecules are distributed within the interlayer space of LDH. Indeed, this distance is comparable with the size of the porphyrin molecule and indicates an inclined orientation of the porphyrin planes with respect to the normal of the hydroxide layers similarly to other porphyrins.[9,10,21,24] Moreover, the micrographs reveal additional lattice fringes indicating an increase of the electron density in the middle of the interlayer space (Fig. 4(b)). It suggests that the Pd centra of the porphyrin units are aligned in the middle of the interlayer space. The same was observed for the zinc metal centra of ZnTPPS.[21]

3.2. Porphyrin-LDH/polymer composite films

Porphyrin-LDH fillers were elaborated for M^{2+}/Al^{3+} (M^{2+} = Mg^{2+}, Zn^{2+}) molar ratios equal to 2 and 3, for which a high concentration of the intercalated porphyrin molecules is expected (Table 1). In addition, we concentrated on two photosensitizers, PdTPPC and TPPS, because they produce $O_2(^1\Delta_g)$ even when intercalated into LDH hosts.[10] Because different prepared composites display comparable photophysical properties, it was decided to present here representative composites PdTPPC-Zn_RAl/PU (R = 2, 3), TPPS-Mg_2Al/PU and PdTPPC-Zn_2Al/PBS (Table 1).

The XRD patterns of porphyrin-LDH/polymer films show poor signals likely to be due to the low concentration of porphyrin-LDH fillers (Fig. 5). The amorphous like-halo between 15–30° (2θ) and the diffraction line at about 42.8° observed for the PU composites are ascribed to the polymer itself. Semi-crystalline PBS gives sharp diffractions between 18–50° (2θ). For PdTPPC-Zn_3Al/PU, the *00l* diffraction peaks at low 2θ angles expected for a porphyrin-LDH intercalated

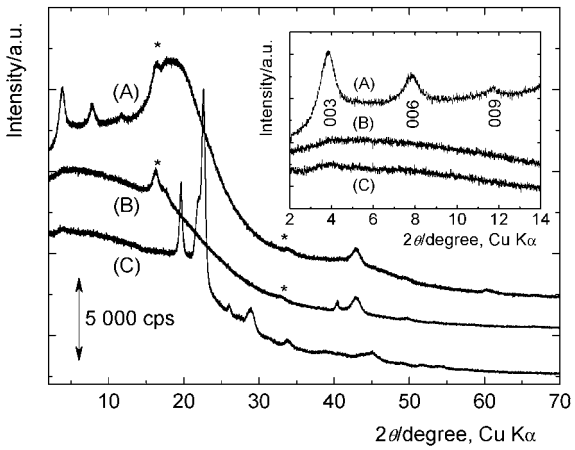

Fig. 5 Powder XRD patterns of representative porphyrin-LDH/polymer composites: (A) PdTPPC-Zn_3Al/PU, A; (B) TPPS-Mg_2Al/PU, B5; (C) PdTPPC-Zn_2Al/PBS. The peaks labeled as * are due to a Mylar foil used as a support. Inset shows the *00l* diffraction peaks at low 2θ angles. The curves are shifted for clarity.

structure are clearly visible, while for TPPS-Mg_2Al/PU and PdTPPC-Zn_2Al/PBS the *003* diffraction is hardly visible. It is worth noting that only the intercalated structures give rise to coherent diffraction while disordered and exfoliated structures having no periodic stacking remain XRD silent. We must also say that exfoliation of LDH is difficult to achieve due to a high layer charge density of hydroxide layers resulting in strong electrostatic interactions between the layers and interlayer anions. In the present case, the XRD analysis indicates that PdTPPC-Zn_3Al/PU filler retains its layered structure with intercalated porphyrins whereas TPPS-Mg_2Al/PU and PdTPPC-Zn_2Al/PBS display partially exfoliated and/or disordered structures (see below).

In order to better characterize the nanostructure of the composites, SAXS experiments were performed. Fig. 6 summarizes the SAXS patterns taken for PdTPPC-Zn_3Al/PU (A), TPPS-Mg_2Al/PU (B5) and PdTPPC-Zn_2Al/PBS. The results comply with those obtained by XRD. The two scattering maxima observed at $q \sim 0.28$ Å^{-1} and 0.55 Å^{-1} for PdTPPC-Zn_3Al/PU (A) giving d-spacings of ~22.4 and 11.4 Å, respectively, are ascribed to the PdTPPC-LDH layered structure. PdTPPC-Zn_2Al/PBS composite shows similar peaks and TPPS-Mg_2Al/PU (B5) gives faint diffractions at the same positions. The composites B1, B2 and B4 show only a faint peak at 0.54 Å^{-1}, *i.e.*, 11.6 Å, of unknown origin that may indicate a partial decomposition of the LDH filler during the composite preparation. Only for PdTPPC-Zn_2Al/PU (B2) is the intensity *vs.* scattering vector curve close to the q^{-2} dependence and this can be linked to the bidimensional nature of scattering objects. Indeed, the intense sonication applied in the case of PdTPPC-Zn_2Al/PU (B2) is likely to favor the dispersion of thin LDH platelets (only a few layers thick). In contrast, an exponent of 2.6 is obtained for PdTPPC-Zn_2Al/PBS and values ranging from 2.0 to ~3.5. are observed for the other composites. These values indicate that LDH fillers are mostly in the form of particles (see below for TEM results) sufficiently large to allow coherent diffraction and the appearance of the Bragg peaks expected for intercalated porphyrins as can be seen in Fig. 6. The average thickness of scattering particles of these three LDH fillers, estimated from the width of the Bragg peaks, is about 10–15 nm. Although the melt-compounding method used for the preparation of the PBS composite is less suitable for a good dispersion of a LDH filler than the solvent-casting/cross-linking technique used for PU composites, results show a similar dispersion in both polymers. In the case of PBS the driving force for dispersion might be positively affected by the linear structure of the polymer.

The morphology of LDH fillers in PU composites was also examined by TEM/BF. All PU composites exhibited a flake structure as illustrated in micrographs presented in Fig. 7. Dark areas in the micrograph (flakes) are filled with loose aggregates of LDH particles, while the light areas (matrix) are composed of pure polymer (see below for EDX results). Although LDH fillers and PU are partially phase separated, their compatibility is quite good as the matrix tends to encapsulate single LDH particles

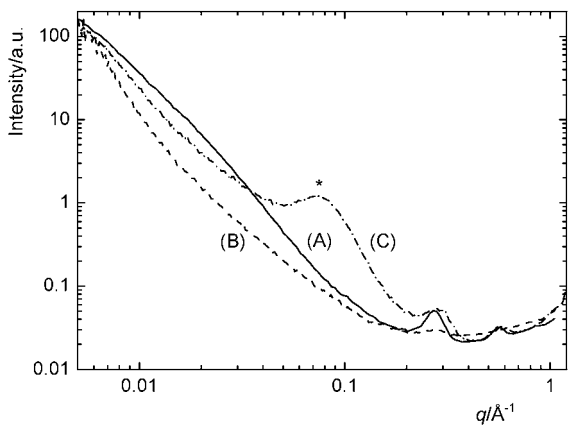

Fig. 6 SAXS of representative porphyrin-LDH/polymer composites: (A) PdTPPC-Zn_3Al/PU, A; (B) TPPS-Mg_2Al/PU, B5; (C) PdTPPC-Zn_2Al/PBS. The peak labeled as * on (C) belongs to PBS.

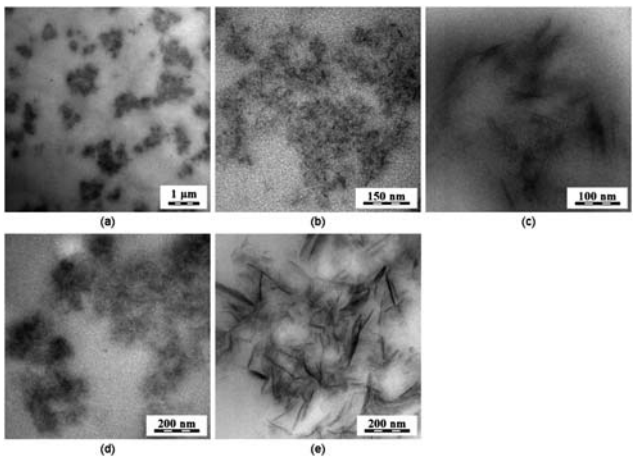

Fig. 7 TEM/bright field micrographs of composites (a) PdTPPC-Zn_2Al/PU, B1; (b) PdTPPC-Zn_2Al/PU, B2; (c) PdTPPC-Mg_2Al/PU, B4; (d) TPPS-Mg_2Al/PU, B5; (e) PdTPPC-Zn_3Al/PU, A.

and/or sheets, which is clearly observed at higher-magnification micrographs (Fig. 7(c), (e)). The micrographs of the samples that were subjected to intensive sonication (Fig. 7(a)–(d)) show smaller LDH particles and a more diffuse interface when compared with the other composites (Fig. 7(e)). The image analysis of the TEM/BF micrographs of composites A and some PdTPPC-Zn_2Al/PU for which the layered structure of nanoparticles is clearly visible, gives a periodic distance between the hydroxide layers of *ca* 2.5 nm. This distance is in agreement with the interlayer distance obtained by XRD for references and fillers (Table S1, see ESI†) and confirms that porphyrin remains intercalated when dispersed in PU.

The composition of PU composites was assessed by TEM/EDX measurements (Fig. S2, see ESI†). Comparison of the EDX spectra from darker flakes and lighter matrix documents that the flakes contain LDH fillers, as the Al and Zn peaks or Al and Mg peaks are always present in the flakes and never in the matrix. Second, the EDX analysis proves that porphyrins are located only in the flakes because characteristic elements of porphyrin-LDH fillers, such as Pd, Zn, Al or Mg, Al, S were present in the flakes and not in the matrix. It again confirms that the porphyrin molecules are in LDH nanoparticles.

The rheological properties of PdTPPC-Zn_2Al/PBS were examined and compared to filler-free PBS. As can be seen, the master curves (Fig. 8) are quite similar and superimposed in the high frequency domain, which is relevant for polymer–polymer interactions, while at low frequencies, a slight increase in G' is observed for the composite. It is, however, associated with a slight decrease in the loss modulus G''. Indeed, both the damping coefficient ($\tan\delta = G''/G'$) and the complex viscosity curves ($|\eta^*|$ as a function of ω) give similar curvatures than for PBS itself. In a low ω domain, $|\eta^*|$ tends to a frequency power law, ω^n with $n \rightarrow 0$, indicating that both composite and PBS have the quasi Newtonian behavior. It can be explained by freely relaxing PBS polymer and by the fact that the presence of the LDH filler does not obstruct chains motion as was surmised from the loading much lower than an expected percolative network coming from the 2D-filler. Yet, the description of a mechanical reinforcement is beyond the scope of the study.

3.3. Absorption spectra

The results presented above show that Zn_RAl LDH-based fillers can be considered as suitable hosts for accommodating PdTPPC porphyrin molecules. PdTPPC, similarly to TPPS, acts as a photosensitizer of cytotoxic $O_2(^1\Delta_g)$.[10,11,28] PdTPPC-Zn_RAl reference materials ($R = 2, 3, 4$), as-prepared or hydrothermally-treated, have the same absorption spectra documenting that the spectral properties are not affected by the metal ratio in the hydroxide layers and post-synthesis treatment (Fig. 9). The spectra show two Q-bands, at 526 and *ca.* 565 nm, of electronic transitions from the ground state to the first excited state of the porphyrin molecule. The Soret band is at 416 nm. These spectra are similar to those of monomeric aqueous solutions of PdTPPC having bands at 412, 521 and 555 nm. In general, the absorption spectra of porphyrins provide important information for studying their photosensitizing activity because the spectral features allow specifying the molecular state.[29] Hence, the aggregation of porphyrins usually leads to a fast competitive relaxation of the excited states associated with the decrease of the quantum yields of the triplet states and $O_2(^1\Delta_g)$ formation. The mutual arrangement of porphyrin units in aggregates generally falls into two types: (i) J-aggregates (edge-to-edge) characterized by a red shift of the Soret band, while (ii) the formation of H-aggregates (face-to-face) is accompanied by a blue shift. As shown in Fig. 9, the intercalation of PdTPPC into LDH hosts does not significantly alter the spectral features; it only broadens the peaks, an effect that can be assigned to a range of binding sites. These results are similar to those reported for TPPS-LDH intercalates.[10] Thus, one can say that extensive porphyrin aggregation, a process that often occurs in solutions and on solid templates,[30] does not take place within the LDH interlayer space. This is also confirmed by the EXAFS results. The exclusion of porphyrin aggregation is a good prerequisite for the fabrication of photoactive polymer composites.[31]

The absorption spectra of composites confirm the identity of intercalated porphyrins. The Q-bands of PdTPPC-Zn_RAl/PU ($R =$ 2, 3) at 524 and 555 nm are slightly shifted, better resolved, and narrower than those of the PdTPPC-Zn_RAl references (Fig. 9). This can be attributed to the effect of the PU matrix with well

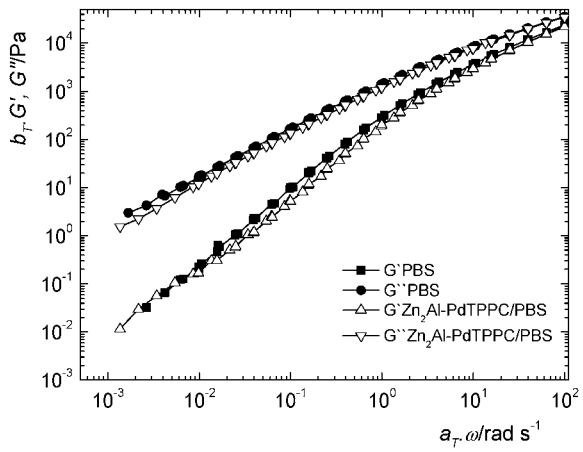

Fig. 8 Master curves expressed as elastic and loss modulus (G', G'') *vs.* the frequency for PdTPPC-Zn_2Al/PBS composite. The shift factors a_T and b_T were normalized for reference temperature of 120 °C.

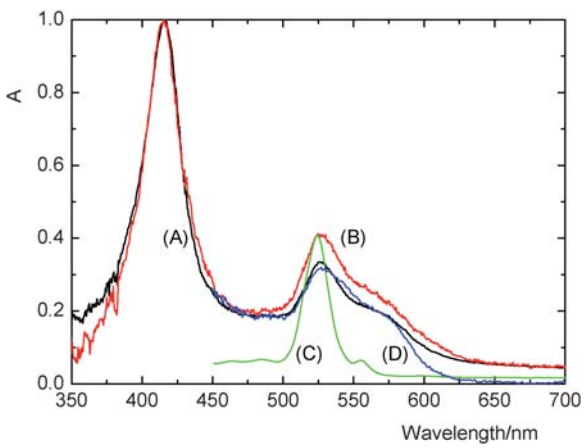

Fig. 9 Normalized absorption spectra: (A) PdTPPC-Zn_2Al (black); (B) PdTPPC-Zn_2Al^H (red); (C) PdTPPC-Zn_2Al/PU, B2, only the Q-region (green); (D) PdTPPC-Zn_2Al/PBS, only the Q-region (blue).

dispersed LDH fillers. On the contrary, PdTPPC-Zn_2Al/PBS is spectrally similar to references (Fig. 9).

3.4. Photophysical properties

We have already described the photophysical properties of TPPS intercalated into Mg_RAl LDH.[10,11] These results were based on the direct measurements of the porphyrin triplet state formation and their interaction with molecular oxygen. The production of $O_2(^1\Delta_g)$ was suggested on the basis of quenching of the corresponding triplet states by oxygen and directly evidenced by time-resolved luminescence of $O_2(^1\Delta_g)$ at 1270 nm. Emission at this wavelength arises from relaxation of $O_2(^1\Delta_g)$ to the triplet ground state. On the contrary, the same approach applied on ZnTPPS-Zn_RAl, intercalated with ZnTPPS, proved that these materials are uneffective.[21]

We combine PdTPPC having high $O_2(^1\Delta_g)$ quantum yields with the ability of Zn_RAl LDH hosts to intercalate porphyrins and act as well-defined and stable fillers for polymers.[13] Since the post-synthesis hydrothermal treatment does not appear to affect the $O_2(^1\Delta_g)$ formation, the use of less crystalline fillers is a good choice for obtaining well-dispersed LDH in the polymer matrix (see above), while keeping high $O_2(^1\Delta_g)$ yields. Indeed, the reference samples containing PdTPPC show intense signals of photoproduced $O_2(^1\Delta_g)$ (Fig. S3, see ESI†). It is evident that $O_2(^1\Delta_g)$ is generated by the photosensitized reaction of PdTPPC because pure LDH hosts do not exhibit any $O_2(^1\Delta_g)$ luminescence. Since longer lifetimes of $O_2(^1\Delta_g)$ increase the probability of $O_2(^1\Delta_g)$ reactions with an outside substrate, the lifetime is an important parameter. For example, PdTPPC-Zn_2Al^H luminescence curves (Fig. S3, ESI†) give two lifetimes of 6 and 21 μs. These results might indicate at least two distinguishable populations of the porphyrin triplet states differing in an oxygen accessibility and are comparable to the previously reported results on Mg_2Al LDH.[10]

The excited state dynamics of porphyrin molecules in prepared polymer composites was probed by nanosecond laser flash photolysis. The measured transient spectra show broad absorption bands in a 440–550 nm range, which are typical features of the porphyrin triplet states in solution. The decay of the triplet states is accelerated in the presence of oxygen and this well-known process is illustrated in Fig. 10 for TPPS-Mg_2Al/PU (B5). The triplet state lifetimes of TPPS decrease from 1.4–3.0 ms in vacuum to 60–100 μs in oxygen atmosphere. A similar behaviour is observed for PdTPPC-based PU composites, however, the kinetic traces are more complex in oxygen atmosphere to give two lifetimes of about 30 and 120 μs with a nearly equivalent contribution. The porphyrin triplet states in PdTPPC-Zn_2Al/PBS are well characterized by a lifetime of 0.5 ms in the absence of oxygen, while two lifetimes of about 10 and 200 μs describe the kinetic traces in oxygen atmosphere. Observed oxygen quenching indicates that porphyrin molecules imbedded in the polymer composites behave similarly to those in Mg_RAl LDH hosts. Intercalated molecules are accessible to oxygen although the accessibility is lower than in a solution.

The production of $O_2(^1\Delta_g)$ in polymer composites was evidenced by the appearance of the emission band peaking at 1275 nm (Fig. 11, inset). The emission intensities, related to the $O_2(^1\Delta_g)$ concentration, are larger for PdTPPC-based composites than for TPPS-Mg_2Al/PU meaning that the formers are better producers of $O_2(^1\Delta_g)$. It can be ascribed to the higher yield of the triplet state formation of Pd porphyrins.[10] The $O_2(^1\Delta_g)$ luminescence intensity decays monoexponentially giving an effective $O_2(^1\Delta_g)$ lifetime between 30–80 μs in oxygen atmosphere (Fig. 11). The fact that these lifetimes are comparable with the lifetimes of the parental triplet states indicates that the intrinsic lifetime of $O_2(^1\Delta_g)$ is shorter since the measured (effective) lifetime is controlled by the decay of the triplet states. Otherwise, the lifetime of the triplet states would have been much shorter than that of $O_2(^1\Delta_g)$. The rise of the luminescence signal is related to the lifetime of the triplet states in a given atmosphere. The precise analysis of this part of the curve is obscured by strong scattering of the excitation pulse.

The intrinsic lifetime of $O_2(^1\Delta_g)$ can be affected by interactions of $O_2(^1\Delta_g)$ with the surrounding LDH and/or polymer matrix. To explore the effect of the polymer matrix, the polymers with dissolved porphyrins PdTPPC/PU and TPPS/PU were analyzed. The lifetimes of the triplet states and of $O_2(^1\Delta_g)$ in PdTPPC/PU

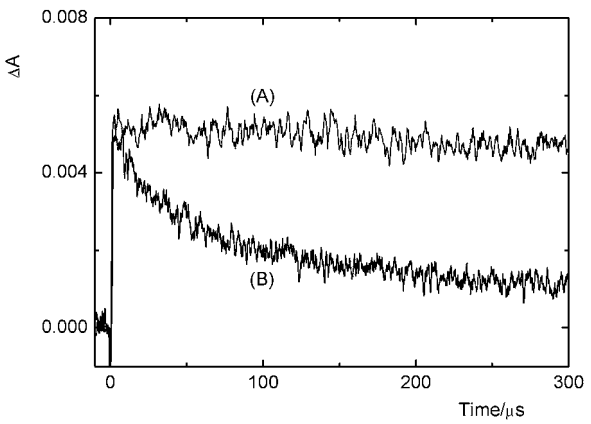

Fig. 10 Decay curves of the triplet states of TPPS in TPPS-Mg_2Al/PU, B5, recorded in (A) vacuum and (B) in oxygen atmosphere. Conditions: 425 nm excitation, ~1 mJ/pulse, pulse width ~28 ns, recorded at 480 nm, average of 50 traces.

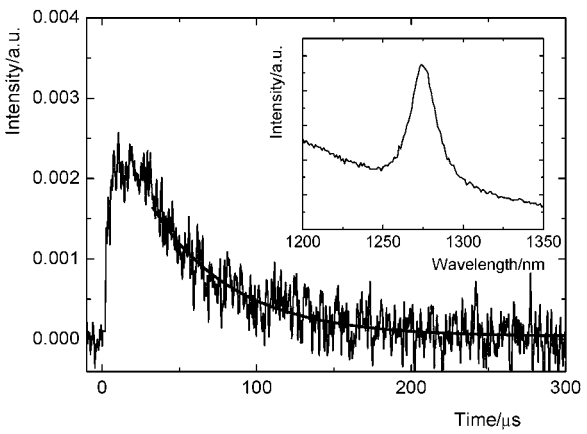

Fig. 11 The $O_2(^1\Delta_g)$ luminescence signal generated by TPPS-Mg_2Al/PU, B5, upon 425 nm excitation (~1 mJ/pulse, pulse width ~28 ns, oxygen atmosphere, recorded at 1270 nm). The smoothed line is a least-squares monoexponential fit. Inset: Luminescence spectrum of $O_2(^1\Delta_g)$.

are similar to those measured in corresponding polymer composites. It can be interpreted so that the $O_2(^1\Delta_g)$ lifetime in composites is governed mostly by the polymer itself, while LDH can be viewed as a passive carrier of the photoactive porphyrin molecules. The polymers affect the overall process by restricting diffusion of oxygen in the bulk and by possible quenching of $O_2(^1\Delta_g)$. As a consequence, the suggested cytotoxic effect on the composite surface would be predominantly induced by $O_2(^1\Delta_g)$ molecules produced in a narrow surface layer. From a practical point of view, the thickness of coatings should be at least in the order of tens of μm to keep the coating effective. As mentioned above, TPPS-Mg_2Al/PU composite (B5) being less effective producers of $O_2(^1\Delta_g)$ are expected to be more sensitive to the effects of the polymer matrix. Indeed, the signals of $O_2(^1\Delta_g)$ in TPPS/PU appear very low, if any, when compared with the intensities recorded for B5 composite (Fig. 11). It strongly suggests that LDH layers shield the excited states from the polymer bulk and positively affect the $O_2(^1\Delta_g)$ productivity. Summing up, the surface and the bulk of the composite films contain $O_2(^1\Delta_g)$ molecules under light irradiation. Therefore, one can say that the photosensitizing activity is affected by the polymers, while LDH hosts behave as passive containers of the photoactive porphyrin molecules.

Conclusions

Layered double hydroxides are relevant nanocontainers and nanofillers for the fabrication of functional polymer composite coatings. First, the intercalation into LDH host allows to avoid porphyrin aggregation and to keep the photophysical properties of porphyrins, namely the formation of cytotoxic $O_2(^1\Delta_g)$. The intercalation also increases the thermal stability of porphyrins as demonstrated in our previous work[21] and may prevent leaching problems. Second, porphyrin-LDH fillers can be well dispersed into PBS and PU polymers as isolated LDH platelets of a few layers or as larger particles, while keeping the rheological properties of the polymer intact as shown in the case of PBS composite. In all the composites examined here, the porphyrin intercalated structure of LDH fillers is maintained once dispersed into the polymer matrices. From the measurements of $O_2(^1\Delta_g)$ luminescence signals, it is inferred that the surface and the bulk of composite films contain $O_2(^1\Delta_g)$ molecules under visible light irradiation. We surmise that the polymers affect the overall process by restricting diffusion of oxygen in the bulk and by partial quenching of $O_2(^1\Delta_g)$. Therefore, the cytotoxic effect on the composite surface is predominantly governed by $O_2(^1\Delta_g)$ molecules produced in a narrow surface layer. In view of the application as photoactive coatings, the thickness in the order of tens of μm is suggested to be enough to keep the coating effective. Another interesting aspect is the possibility to finely tune the amount of cytotoxic $O_2(^1\Delta_g)$ at the composite surface by varying porphyrin-LDH filler loading and the amount of intercalated porphyrin within LDH hosts. These porphyrin-LDH/polymer composites provide a platform for the fabrication of bactericidal surfaces under visible light.

Since the bench-scale feasibility of such nanocomposites capable of producing singlet oxygen under visible light as well as the processability by preliminary rheological measurements have been here demonstrated, we intend in a next step to perform a pilot-scale study to further investigate the mechanical properties of the corresponding bulk nanocomposites.

Acknowledgements

We are grateful to Petr Bezdička (IIC, ASCR) for some XRD and fruitful discussion, Josef Pleštil (IMC, ASCR) for measurement and discussion on SAXS, and Branislav Husar for kind discussion on the preparation of porphyrin-LDH/PBS composites. This work was supported by the Czech Science Foundation (P207/10/1447) and the French National Center of Scientific Research CNRS (No. 22538).

References

1 D. G. Evans and R. C. T. Slade, in *Layered Double Hydroxides, Struct. Bond.* 2006, 119, 1–87, ed. X. Duan and D. G. Evans, Springer-Verlag, Berlin, Heidelberg 2005; A. I. Khan, A. Ragavan, B. Fong, C. Markland, M. O'Brien, T. G. Dunbar, G. R. Williams and D. O'Hare, *Ind. Eng. Chem. Res.*, 2009, **48**, 10196–10205.
2 A. Vaccari, F. Basile and G. Fornasari, in *Encyclopedia of Surface and Colloid Science*, ed. P. Somasundaran and A. Hubbard, Taylor & Francis, 2nd edn, 2006, pp. 1169–1189.
3 K. H. Goh, T. T. Lim and Z. Dong, *Water Res.*, 2008, **42**, 1343–1368.
4 D. Shan, S. Cosnier and C. Mousty, *Anal. Chem.*, 2003, **75**, 3872–3879.
5 F. Leroux, *J. Nanosci. Nanotechnol.*, 2006, **6**, 303–315.
6 C. Del Hoyo, *Appl. Clay Sci.*, 2007, **36**, 103–121.
7 C. Sanchez and F. Ribot, *New J. Chem.*, 1994, **18**, 1007–1047.
8 L. Latterini, M. Nocchetti, G. G. Aloisi, U. Costantino and F. Elisei, *Inorg. Chim. Acta*, 2007, **360**, 728–740.
9 T. J. Pinnavaia, M. Chibwe, V. R. L. Constantino and S. K. Yun, *Appl. Clay Sci.*, 1995, **10**, 117–129; S. Bonnet, C. Forano, A. de Roy, J. P. Besse, P. Maillard and M. Momenteau, *Chem. Mater.*, 1996, **8**, 1962–1968; M. Wark, in Porphyrins and Phthalocyanines in Inorganic Host Materials in *The Porphyrin Handbook*, ed. K. M. Kadish, K. M. Smith and R. Guillard, Elsevier Science, USA, 2003, Vol 17, pp. 247–283; C. A. S. Barbosa, A. M. D. C. Ferreira and V. R. L. Constantino, *Eur. J. Inorg. Chem.*, 2005, 1577–1584; M. Halma, K. A. D. de Freitas Castro, C. Taviot-Guého, V. Prévot, C. Forano, F. Wypych and S. Nakagaki, *J. Catal.*, 2008, **257**, 233–243.
10 K. Lang, P. Bezdička, J. L. Bourdelande, J. Hernando, I. Jirka, E. Káfuňková, F. Kovanda, P. Kubát, J. Mosinger and D. M. Wagnerová, *Chem. Mater.*, 2007, **19**, 3822–3829.
11 K. Lang, P. Kubát, J. Mosinger, J. Bujdák, M. Hof, P. Janda, J. Sýkora and N. Iyi, *Phys. Chem. Chem. Phys.*, 2008, **10**, 4429–4434.
12 Y. N. Chan, T. Y. Juang, Y. L. Liao, S. A. Dai and J. J. Lin, *Polymer*, 2008, **49**, 4796–4801; U. Costantino, V. Bugatti, G. Gorrasi, F. Montanari, M. Nocchetti, L. Tammaro and V. Vittoria, *ACS Appl. Mater. Interfaces*, 2009, **1**, 668–677; A. L. Troutier-Thuilliez, C. Taviot-Gueho, J. Cellier, H. Hintze-Bruening and F. Leroux, *Prog. Org. Coat.*, 2009, **64**, 182–192; C. Taviot-Guého, A. Illaik, C. Vuillermoz, S. Commereuc, V. Verney and F. Leroux, *J. Phys. Chem. Solids*, 2007, **68**, 1140–1146; A. Illaik, C. Taviot-Guého, J. Lavis, S. Commereuc, V. Verney and F. Leroux, *Chem. Mater.*, 2008, **20**, 4854–4860.
13 R. Marangoni, C. Taviot-Guého, A. Illaik, F. Wypych and F. Leroux, *J. Colloid Interface Sci.*, 2008, **326**, 366–373.
14 R. Bonnett, M. A. Krysteva, I. G. Lalov and S. V. Artarsky, *Water Res.*, 2006, **40**, 1269–1275.
15 L. Wang and M. E. Meyerhoff, *Anal. Chim. Acta*, 2008, **611**, 97–102.
16 Y. Itagaki, K. Deki, S.-I. Nakashima and Y. Sadaoka, *Sens. Actuators, B*, 2005, **108**, 393–397.
17 J. Mosinger, O. Jirsák, P. Kubát, K. Lang and B. Mosinger, *J. Mater. Chem.*, 2007, **17**, 164–166; C. Xing, Q. Xu, H. Tang, L. Liu and S. Wang, *J. Am. Chem. Soc.*, 2009, **131**, 13117–13124; M. Krouit, R. Granet and P. Krausz, *Eur. Polym. J.*, 2009, **45**, 1250–1259; M. Krouit, R. Granet, P. Branland, B. Verneuil and P. Krausz, *Bioorg. Med. Chem. Lett.*, 2006, **16**, 1651–1655.

18 H. Li, J. Chang, A. Cao and J. Wang, *Macromol. Biosci.*, 2005, **5**, 433–440.
19 T. Fujimaki, *Polym. Degrad. Stab.*, 1998, **59**, 209–214.
20 B. K. Kim and J. C. Lee, *J. Polym. Sci., Part A: Polym. Chem.*, 1996, **34**, 1095–1104; S. A. Chen and J. S. Hsu, *Makromol. Chem.*, 1992, **193**, 423–434.
21 E. Káfuňková, C. Taviot-Guého, P. Bezdička, M. Klementová, P. Kovář, P. Kubát, J. Mosinger, M. Pospíšil and K. Lang, *Chem. Mater.*, 2010, **22**, 2481–2490.
22 S. Belin, V. Briois, A. Traverse, M. Idir and T. Moreno, *Phys. Scr.*, 2005, 980–983.
23 F. Leroux, M. El Moujahid, C. Taviot-Guého and J. P. Besse, *Solid State Sci.*, 2001, **3**, 81–92.
24 P. Kovář, M. Pospíšil, E. Káfuňková, K. Lang and F. Kovanda, *J. Mol. Model.*, 2010, **16**, 223–233.
25 S. Britto, A. V. Radha, N. Ravishankar and P. V. Kamath, *Solid State Sci.*, 2007, **9**, 279–286.
26 J. Rodríguez-Carvajal, *Newsletter of the Powder Diffraction Commission of the International Union of Crystallography*, 2001, **26**, 12.
27 S. Lipstman, S. Muniappan, S. George and I. Goldberg, *CrystEngComm*, 2006, **8**, 601.
28 K. Lang, J. Mosinger and D. M. Wagnerová, *Coord. Chem. Rev.*, 2004, **248**, 321–350.
29 P. Kubát, K. Lang, K. Procházková and P. Anzenbacher, Jr., *Langmuir*, 2003, **19**, 422–428; K. Procházková, Z. Zelinger, K. Lang and P. Kubát, *J. Phys. Org. Chem.*, 2004, **17**, 890–897.
30 W. Xu, H. Q. Guo and D. L. Akins, *J. Phys. Chem. B*, 2001, **105**, 1543–1546.
31 F. Kovanda, E. Jindová, K. Lang, P. Kubát and Z. Sedláková, *Appl. Clay Sci.*, 2010, **48**, 260–270.

Supplementary Material (ESI) for Journal of Materials Chemistry

Electronic Supplementary Information

Porphyrin-Layered Double Hydroxides/Polymer Composites as Novel Ecological Photoactive Surfaces

Eva Káfuňková,[ab] Kamil Lang,[a]* Pavel Kubát,[c] Mariana Klementová,[a] Jiří Mosinger,[ab] Miroslav Šlouf,[d] Anne-Lise Troutier-Thuilliez,[e] Fabrice Leroux,[e] Vincent Verney[f] and Christine Taviot-Guého[e]*

[a] *Institute of Inorganic Chemistry of the AS CR, v.v.i., 250 68 Husinec-Řež, Czech Republic*

[b] *Department of Inorganic Chemistry, Faculty of Science, Charles University in Prague, Hlavova 2030, 128 43 Praha, Czech Republic*

[c] *J. Heyrovský Institute of Physical Chemistry of the AS CR, v.v.i., Dolejškova 3, 182 23 Praha 8, Czech Republic*

[d] *Institute of Macromolecular Chemistry of the AS CR, v.v.i., Heyrovského náměstí 2, 162 06 Praha 6, Czech Republic*

[e] *CNRS, UMR 6002, LMI, F-63177 Aubiere - Clermont Université, Université Blaise Pascal, Laboratoire des Matériaux Inorganiques, BP 10448, F-63000 Clermont-Ferrand, France*

[f] *CNRS, UMR 6505, LPMM, F-63177 Aubiere - Clermont Université, Université Blaise Pascal, LPMM, BP 10448, F-63000 Clermont-Ferrand, France*

*Corresponding authors: lang@iic.cas.cz (Kamil Lang), Christine.Taviot-Gueho@univ-bpclermont.fr,

Content

Table S1 Porphyrin-LDH reference materials: M^{2+}/Al^{3+} molar ratios (R_{exp}) of the hydroxide layers and refined cell parameters.

Samples	R_{exp} [a]	*a*/Å [c]	*c*/Å [c]	d_{003}/Å
PdTPPC-Zn_2Al	-	3.1	68.6	22.9
PdTPPC-Zn_2Al^H	2.04	3.0672(3)	68.38(1)	22.8
PdTPPC-Zn_3Al	2.83	3.1	68.0	22.6
PdTPPC-Zn_3Al^H	[b]	3.0685(4)	67.51(2)	22.5
PdTPPC–Zn_4Al	3.72	3.1	67.6	22.5
PdTPPC-Zn_4Al^H	[b]	3.0707(5)	67.61(2)	22.5
ZnTPPS-Zn_4Al^H	[b]	3.0667(2)	69.047(4)	23.0
PdTPPC–Mg_2Al	-	-	65.1	21.7
PdTPPC-Mg_2Al^H	-	3.042(1)	67.59(1)	22.5
TPPS-Mg_2Al	-	3.0	65.1	21.7
TPPS-Mg_2Al^H	1.73	3.0351(2)	69.105(5)	23.0

[a] Deduced from elemental analysis; [b] Owing to the formation of ZnO during the post-synthesis hydrothermal treatment, it was not possible to determine R_{exp}; [c] Cell parameters were determined from the peak profile analysis of XRD data for hydrothermally treated samples and from the positions of the *00l* and *110* diffraction lines for as-prepared samples.

Figure S1 Powder XRD patterns of porphyrin-LDH reference materials aged for 24 h (as-prepared samples) followed by the hydrothermal treatment (labeled with superscript H).

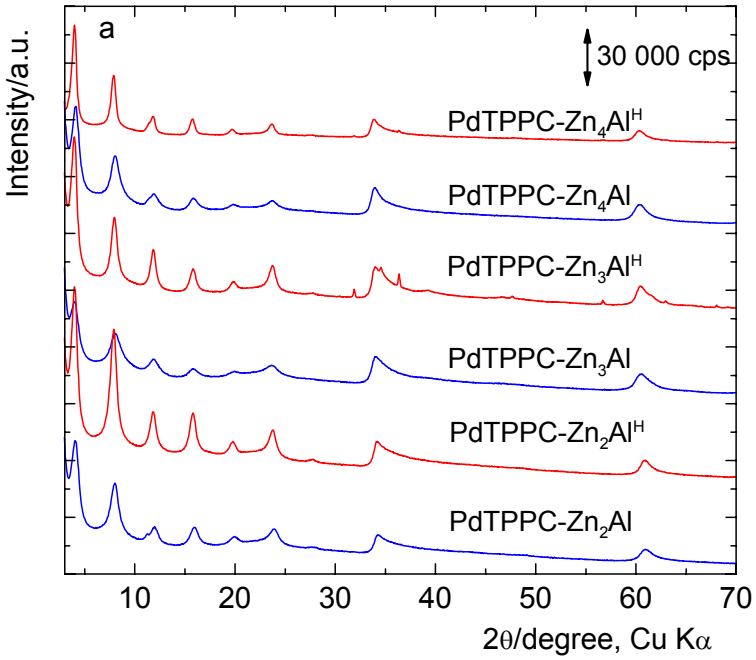

Figure S2 TEM/EDX spectra of (a) samples B1, (b) B2 and (c) B5. In each image, the upper spectrum was measured from dark areas (flakes) and the lower spectrum from light areas (matrix). Peaks corresponding to Cu come from a microscopic support copper grid; peaks of Si are probably due to a glassware used for the filler synthesis in basic media; oxygen peak is also present.

(a)

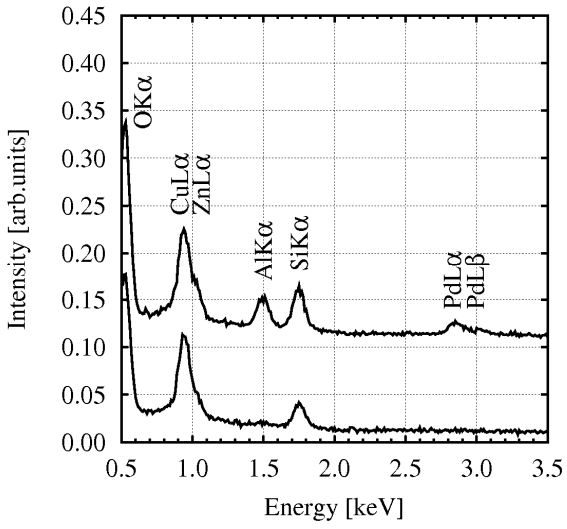

(b)

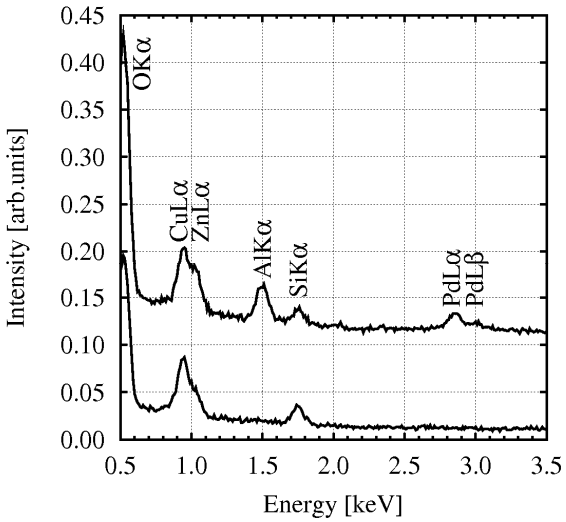
Intensity [arb.units]
Energy [keV]
OKα
CuLα
ZnLα
AlKα
SiKα
PdLα
PdLβ

(c)

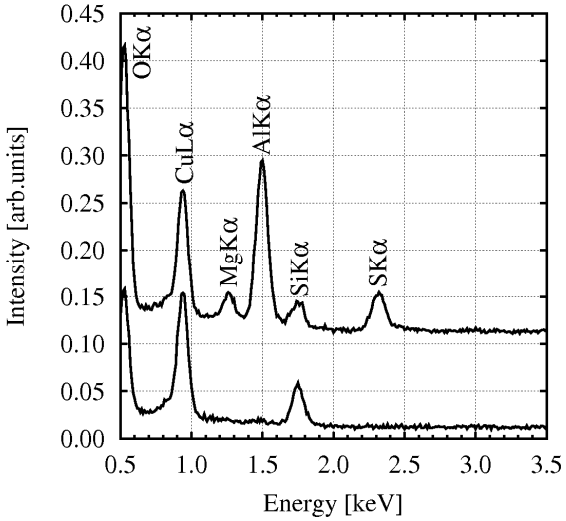
Intensity [arb.units]
Energy [keV]
OKα
CuLα
MgKα
AlKα
SiKα
SKα

Figure S3 Singlet oxygen luminescence signal generated by the PdTPPC-Zn_2Al^H reference upon 425 nm excitation (~0.9 mJ/pulse, pulse width ~ 28 ns, oxygen atmosphere, recorded at 1270 nm). The smoothed line (red) is a least squares fit and the quality of the fit is shown by residuals as the difference between the experimental curve and the fit (green).